DOCTOR OF PHILOSOPHY

The Development and Anatomy of the Sacrum in relation to the Ilium and the Sacroiliac Joint

Yusof, Nurul Asyiqin

Award date:
2013

DOCTOR OF PHILOSOPHY

The Development and Anatomy of the Sacrum in relation to the Ilium and the Sacroiliac Joint

Nurul Asyiqin Yusof

2013

University of Dundee

CONTENTS

Tables

Figures

Acknowledgements

I would like to express my sincere and humble gratitude to my three supervisors, Professor Roger Soames, Professor Sue Black and Dr Craig Cunningham for without their continuous guidance and support, I could not have achieved this stage. Professor Soames has guided me throughout this PhD journey with his experience, patience and wisdom that I adore so much and my gratitude couldn't be completely expressed here. Professor Black's expertise and enthusiasm for knowledge and research has always inspired me from the day I met her and I really appreciate her constant encouragement to me. The continuous training that Dr Craig Cunningham taught me has helped me tremendously and made me realise that he is wise beyond his years. I am forever indebted to my three supervisors and very honoured to be their PhD student. Indeed, the Centre for Anatomy and Human Identification (CAHId) is very fortunate to have these three great people.

The research culture in this department, this university, as well as in this country has definitely opened my eyes. I will bring this experience and the attitude back to my country as a lecturer in Malaysia, and hopefully for a future collaboration with the University of Dundee and across the UK.

I would also like to thank the following people who have directly aided in the data collection and analysis and played a vital role in completion of this thesis:

Prof Michael Fagan and Ms Sue Taft, Centre for Medical Engineering and Technology, University of Hull, for providing micro-computed tomography facilities.

Ms Margaret Low, for assistance with radiographic procedures.

Additionally, I would like to thank the following people for helpful discussions and suggestion at various stages throughout this research and directly or indirectly involved in the finishing of the thesis:

Dr Andrew O'Malley, Dr Chris Rynn, Dr Lucina Hackman, Dr Paul Felts, Dr Clare Lamb, Dr Catherine Carr, Professor Caroline Wilkinson, Mrs Vivienne McGuire, Miss Gillian Malone, Professor Rami Abboud and Mr Sadiq Nasir. I thank all my friends and staff in CAHId and Malaysian Dundee Community for their warm friendship and assistance throughout my life in Dundee.

Thank you to my dear parents, siblings and family. To my adorable and cheeky son, Zayd and my caring daughter, Maryam thank you for your good behaviour especially during my final stage of PhD. Finally, I would like to thank my beloved husband, Nizam for pulling out all the stops that he could to ensure my PhD journey was as smooth as possible especially when things did not appear to be progressing well. He supports me in every way that a person can be supported, and I dedicated this work for him.

Declaration

The candidate is the author of this thesis. Unless otherwise stated, all references cited have been consulted by the candidate. The work, of which the thesis is a record, has been completed by the candidate. No portion of the work referred to in this thesis has been submitted in support of an application for another degree or qualification of this or any other university, or other institute of learning.

Nurul Yusof

Copyright

Statement

I certify that Nurul Yusof has spent four years of research under our supervision. Nurul has fulfilled the conditions of Ordinance 39 and is qualified to submit the accompanying thesis in application for the degree of Doctor of Philosophy.

Professor Roger Soames

Professor Sue Black

Dr Craig Cunningham

Summary

The juvenile sacrum is a unique bone which starts as approximately 21 separate osseous components at birth. It eventually fuses throughout development into a single mature sacrum at adulthood. Despite the unfused nature of these ossified structures in early life, its location between the axial and lower appendicular skeleton and function in transmitting stresses are undeniably crucial. During gross physical developmental milestones, a child experiences locomotive and postural changes from sitting, to crawling, and then standing and walking especially during the first 8 years of life. Additionally, the pelvis undergoes functional changes where pelvic viscera descend into the pelvic cavity, together with fusion of the ischiopubic ramus before the age of 6 – 8 years, stabilizes the maturing pelvic complex. During this critical period, the body weight is reported to be transferred through the weight-bearing bones and joints related to body posture via the sacrum, through the sacroiliac joint and the innominate.

Recent investigations of trabecular bone architecture that reflect the routes of weight transmission were based on Wolff's law and bone functional adaptation theory. This is defined as the bone morphological response to mechanical strains and loading that is influenced by the genetic, nutritional status and general mechanical environment, where this response is reported to be higher during the juvenile period. The advancement of non-invasive, non-destructive imaging techniques has led to extensive research on this subject. However, studies on juvenile skeletal remains are insufficient, especially pertaining to trabecular pattern analysis, and can most probably be attributed to the limited availability of juvenile specimens compared to the adult. Additionally, the

constant change in growth of the juvenile age group make it more difficult to study compared to the adult group.

This research was divided into three different studies; the first and second studies were conducted on the juvenile sacrum, and the third on the juvenile ilium. The first was a preliminary study using qualitative radiographic analysis of the juvenile sacral microarchitecture, followed by the second study, a detailed trabecular microarchitecture quantification based on the reconstructed micro-CT images of S1 vertebra. The third study was conducted using a different approach, where a photographic image of the pelvic surface of the juvenile ilium was evaluated. Although not directly similar in terms of the methodological approach on both sacrum and ilium due to time constraints and uneven growth of the juvenile ilium, these studies were compared as the two bones meet at the sacroiliac joint.

In contrast to the juvenile ilium that showed most of the characteristic features of the adult bone at birth, the study of the juvenile sacrum pose considerable difficulties as it appears as multiple separated bones at birth with different times of fusion, thus providing until now, no available literature on the trabecular pattern of the juvenile human sacrum has been conducted. Thus the current research aims to fill this gap and to highlight the possible route of weight transmission of the juvenile sacrum during the critical developmental years of a child, especially in the first 8 years of life.

The result of the qualitative radiographic analysis of the juvenile sacrum revealed consistent and well-defined high intensity patterns of cortical and trabecular bone organisation in the sacrum from birth until late adolescence concentrating at the uppermost and centremost region of the sacrum. These high intensity areas reduce in the more distal sacral vertebra. The auricular area in contrast, largely exhibits low intensity areas suggesting minimal weight passes through this region.

Subsequently, the quantification results of the reconstructed micro-CT sacral images revealed high bone volume, thick trabecular bones at the central part of the juvenile S1 vertebra. This region exhibits the most robust and remodeled area, especially at the anteromedial sacral ala, persistently throughout the first 8 years of life, with increasing absolute values for all bone parameters. In contrast, the auricular area representing the sacral part of the sacroiliac joint exhibit a sparse, low bone volume area with very little remodeling activity reflected in this region.

The quantification study on the pelvic surface of the juvenile ilium revealed that post-auricular growth is always in advance of the auricular surface throughout development. Thus, from the three studies it can be inferred that the body weight that passes from L5 vertebra to S1 is most likely being transferred via the soft tissue structures that are in a close vicinity to the sacroiliac joint. These soft tissue structures are mainly formed by the strong and abundant posterior sacroiliac and interosseous ligaments that bind the post-auricular surfaces of the sacrum with the ilium. In the erect posture, the sacrum is suspended by these posterior ligaments and supported by the anterior sacroiliac ligaments creating constant tensile forces on these soft tissues. The body weight that passed via the S1 vertebra is postulated to be transmitted to the ilium via these ligaments by virtue of these tensile forces. The vertically-oriented sacroiliac joint that previously was suggested to play an important role in transmitting the body weight is not supported in these studies.

CHAPTER 1

Introduction

1.1 Thesis outline

This study focused on the developmental and biomechanical adaptation of the juvenile sacrum and ilium, with some reference to the sacroiliac joint. It consists of two studies on the sacrum and one study on the ilium. The first study is a preliminary qualitative study on the cortical and trabecular pattern of the juvenile sacrum, followed by a quantitative study on the trabecular microarchitecture of the juvenile sacrum. The third study is a quantitative study on the growth of the juvenile ilium.

The thesis consists of 8 chapters; the first three chapters address the literature surrounding the anatomy, embryology and biomechanics of the pelvis, sacrum, ilium and sacroiliac joint. The fourth chapter discusses the materials and methods used in this study with the aid of illustrative figures. The fifth chapter addresses the qualitative preliminary study on the cortical and trabecular architecture of the juvenile sacrum, followed by Chapter 6, a definitive and detailed quantification analysis on the trabecular arrangement of the sacrum. Chapter 7 is an independent quantitative study on the growth of the pelvic surface of the juvenile ilium from birth to adolescence. Finally, Chapter 8 is the discussion section which brings together the results of the three studies.

1.2 Rationale for research

The motivation for this study was to enlighten the debate on the influence of body weight transfer at the junction between the axial and appendicular skeleton: namely the sacrum and ilium at the sacroiliac joint. Study of the sacroiliac joint *per se* is not complete without analysing the sacrum and the load trajectory passing through it. This posterior pelvic region is influenced by the day-to-day biomechanical activity of the musculoskeletal system in humans, yet the definitive route of weight transfer through this area has been poorly understood and remains controversial. In addition, research on the sacrum with particular reference to its developmental perspective is inadequate, most probably due to limited access to juvenile samples.

Thus, the availability of juvenile skeletal material in the Centre for Anatomy and Human Identification, University of Dundee has inspired this study to explore the relationship between the trabecular arrangement in the sacrum with load distribution via the universally acknowledged Wolff's Law and Bone Functional Adaptation theory (Lee and Taylor, 1999; Pearson and Lieberman, 2004; Ruff *et al*, 2006). While there are many methodologies for evaluating the biomechanics of the sacrum and the pelvis, the non-invasive, non-destructive two-dimensional and three-dimensional (3D) imaging investigation combined with software analysis of the cortical and trabecular architecture was undertaken to aid the understanding of sacral weight transfer.

The techniques have already been tested and published in the study of the cortical and trabecular arrangement of the juvenile ilium (Cunningham and Black, 2009a, 2009b, 2009c). Even though the juvenile ilium has been analysed with this method, ilial specimens will also be included in this study using different quantification approaches to study the growth of the surface areas of the developing ilium. The results of these studies were compared at a particular reference point; the sacroiliac joint, which is

generally accepted to be the prime location of weight transfer between the axial and lower appendicular skeleton.

It is hoped that the findings from these studies will assist not only biomechanical engineers in a better understanding of the biomechanics of the juvenile sacrum and ilium, and forensic anthropologists in recognition of the important phases of sacral and iliac developments, but also clinicians in deciding the management of pelvic fracture or pathologies involving the pelvic region especially at the sacrum, ilium and the sacroiliac joint.

1.3 Objectives

The objectives for this research are:

1. To study, qualitatively, the cortical and trabecular arrangements of the juvenile sacrum from the fetal period to late adolescence.
2. To investigate, quantitatively, the internal microarchitecture of the juvenile sacrum and determine the pathway of likely weight transmission through it.
3. To study the growth of the juvenile ilium with reference to its pelvic surface areas.
4. To establish the relationship between the sacrum and the ilium at the sacroiliac joint.

1.4 The anatomy of the human pelvis

When discussing the sacrum, ilium and sacroiliac joint, the importance of the anatomy of the pelvis as a whole must be considered. The human pelvis is a unique structure comprising a junction between the appendicular (innominate) with the axial skeleton (sacrum) that meet at the sacroiliac joints. The pelvis creates a hollow passage that not only protects the pelvic viscera but also transmits weight from the axial skeleton to the lower limbs, and at the same time allows delivery of the fetus in the female. It has therefore evolved as a compromise between efficient and stable bipedalism, as well as safe parturition (Brooke, 1924; Sashin, 1930; Palastanga and Soames; 2012).

Shape of the pelvis

The shape of the pelvic complex is unique compared with other human bones. It has an inverted funnel shape with the base facing anteriorly and the apex posteriorly. The pelvis is formed by the two innominate bones articulating anteriorly at the symphysis pubis and posteriorly with the sacrum at the sacroiliac joint (Snell, 2008). The innominate consists of three bones fused at the acetabulum in the adult, superiorly is the ilium, posteroinferiorly is the ischium and anteroinferiorly the pubis.

Pelvic wall and floor

The wall of the pelvis is formed by bones, joints and ligaments covered by muscles and fascia. The rounded wall of the pelvis is bounded posteriorly by the sacrum and coccyx that accommodates an abundance of ligamentous attachments, while the anterior and lateral walls are formed by the ilium, ischium, and pubis.

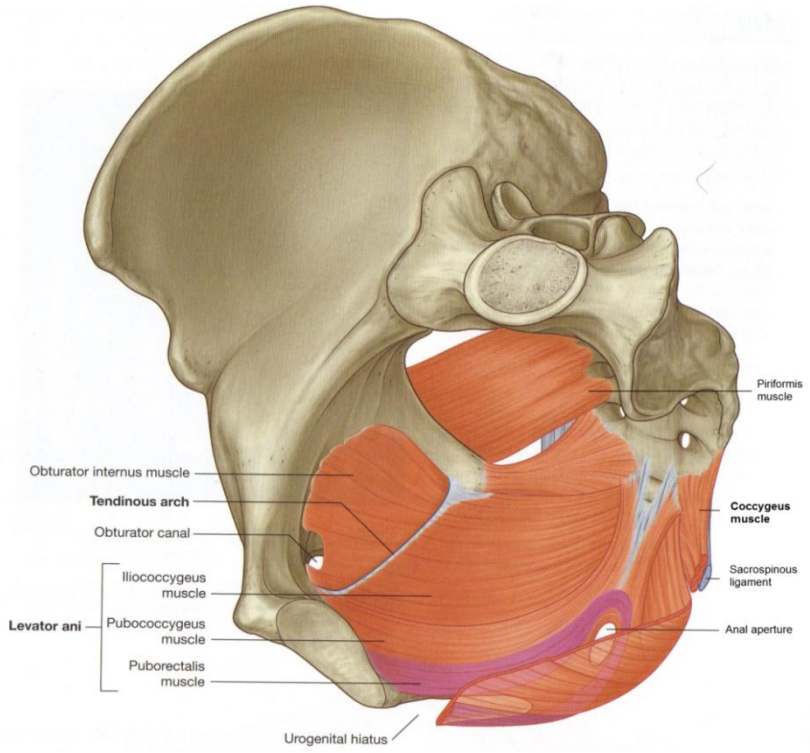

Figure 1.1: Pelvic wall and floor (taken from Drake *et al,* 2005).

The joints of the pelvis are the sacroiliac, sacrococcygeal, hip joints, and the symphysis pubis (Sinnatamby, 2006). The muscles that line the pelvic wall are mainly the piriformis posterolaterally and obturator internus anterolaterally (Figure 1.1).

The floor of the pelvis is formed by the pelvic diaphragm (levator ani and coccygeus muscles) (Figure 1.1), and in the anterior midline, the perineal membrane and muscles of the deep perineal pouch (Drake *et al,* 2005; Snell 2008).

Pelvic cavity

The pelvic cavity contains the bladder anteriorly and the rectum posteriorly in males, while in females, the uterus is located between these two structures. There are rich and abundant neurovascular bundles that lie particularly at the posterior pelvic region, close to the sacrum, ilium and the sacroiliac joint.

Differences between the true and false pelvis

The pelvis is divided into the false (greater) pelvis above and the true (lesser) pelvis below (Snell, 2008; Moore *et al*, 2013). This terminology arises as the structure of the pelvis has two passages; superior and inferior to the pelvic brim.

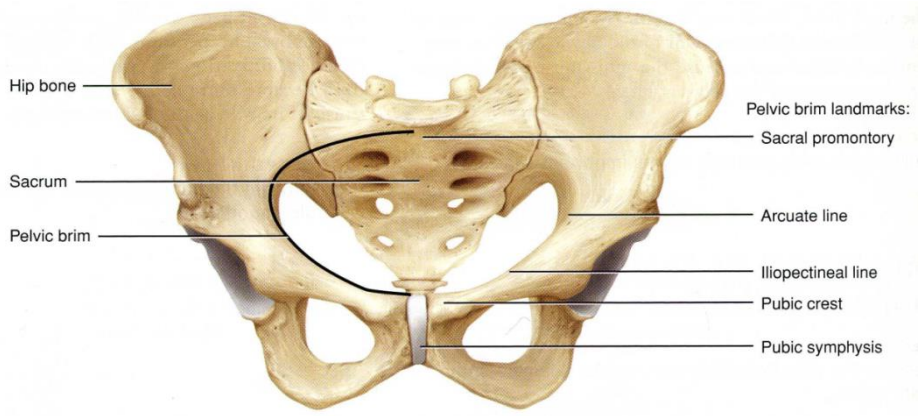

Figure 1.2: Anteroposterior view of the pelvic girdle (taken from Tortora and Nielsen, 2009).

This passage is divided by a boundary called the pelvic brim or pelvic inlet (Tortora and Nielsen, 2009), which is formed by the sacral promontory, alae of the sacrum, sacroiliac joints, arcuate lines, pectineal lines, pubic crests and symphysis pubis (Figures 1.2 and 1.3). The arcuate and pectineal lines and the pubic crest are referred to as the linea terminalis.

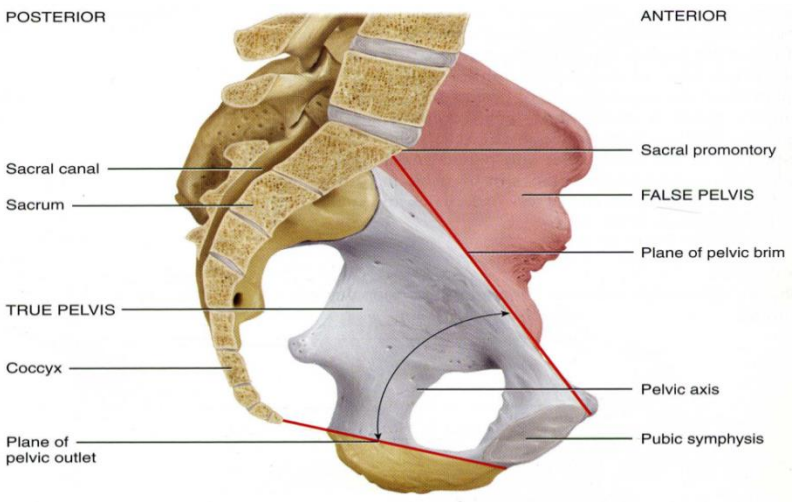

Figure 1.3: Midsagittal section indicating locations of true and false pelvis (taken from Tortora and Nielsen, 2009).

The pelvic outlet is a diamond-shape opening bounded by bones and ligaments, at its anterior and posterior aspects, respectively. On both sides, the inferior ischiopubic ramus projects posteriorly and laterally to end at the ischial tuberosity (Figure 1.4): this form the pubic arch, the margin of the anterior half of the pelvic outlet. The posterior half of the pelvic outlet is formed by the sacrotuberous ligament and the tip of the coccyx (Snell, 2008). As the posterior half of the pelvic outlet is bounded by ligaments, the size increases during the later stage of pregnancy due to laxity of the pelvic ligaments in response to the release of the hormone relaxin (Moore *et al,* 2013).

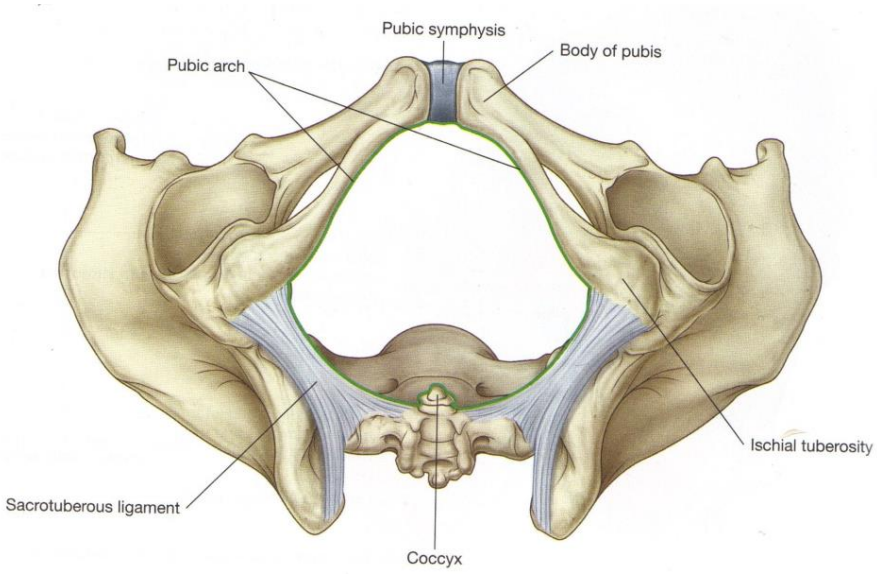

Figure 1.4: Pelvic outlet (taken from Drake *et al*, 2005).

The relaxation of pelvic ligaments in relation to hormones released in pregnancy has been suggested by many studies (Calguneri *et al*, 1982; Kristiansson *et al*, 1996; Albert *et al*, 1997). Although estradiol, progesterone and cortisol may play a part in the need for 'lax ligaments' in pregnancy, the hormone relaxin was reported to increase up to 10-fold during pregnancy and achieved its maximum concentration at 38-42 weeks (Calguneri *et al*, 1982).

Differences between male and female pelves

The differences between male and female pelves have a fundamental importance in obstetrics for the requirements of childbirth. Other factors contributing to the disparity are the greater weight and muscularity of males compared to females. These result in more robust markings of the pelvic bone in males as the bones become heavier. The female characteristics are more related to the increasing shape and size of the pelvic inlet and outlet. The sex-related steroids released at puberty bring about a remodeling of the pelvic openings by increasing the transverse diameter and outward projection of the acetabular wall from the pelvic canal (Greulich and Thoms, 1944) which facilitates the changes required for final adult pelvic morphology.

The pelvis can be classified according to the shape of the brim, either round, triangular, anteroposteriorly oval or transversely oval (Figure 1.5). The terms used are gynaecoid, android, anthropoid and platypelloid, respectively (Caldwell and Moloy, 1938).

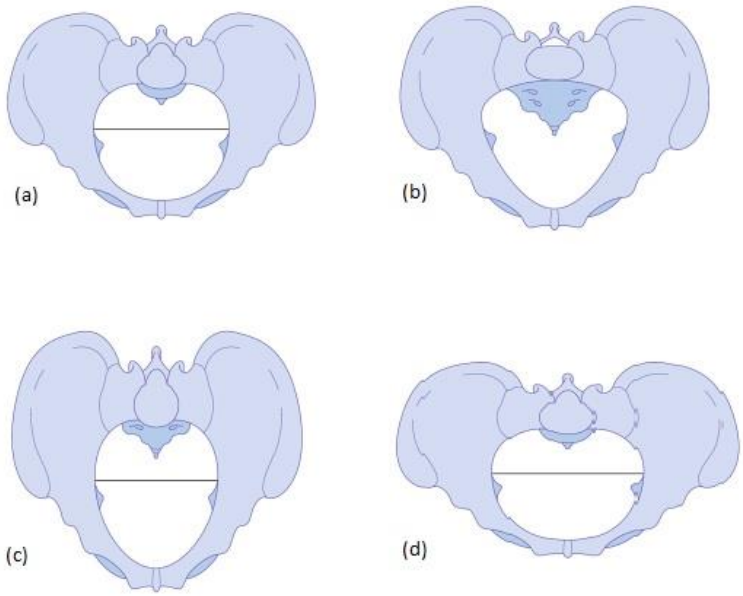

Figure 1.5: The four different types of pelvis, (a) gynaecoid, (b) android, (c) anthropoid, and (d) platypelloid (modified from Baker and Kenny, 2011).

In general, the male pelvic cavity is longer and narrower than the female pelvic cavity. The pelvic inlet in the male is triangular/heart shaped while in the female it is more circular. The more circular shape in the female is due partly to the less distinct sacral promontory and broader sacral alae (Drake *et al,* 2005).

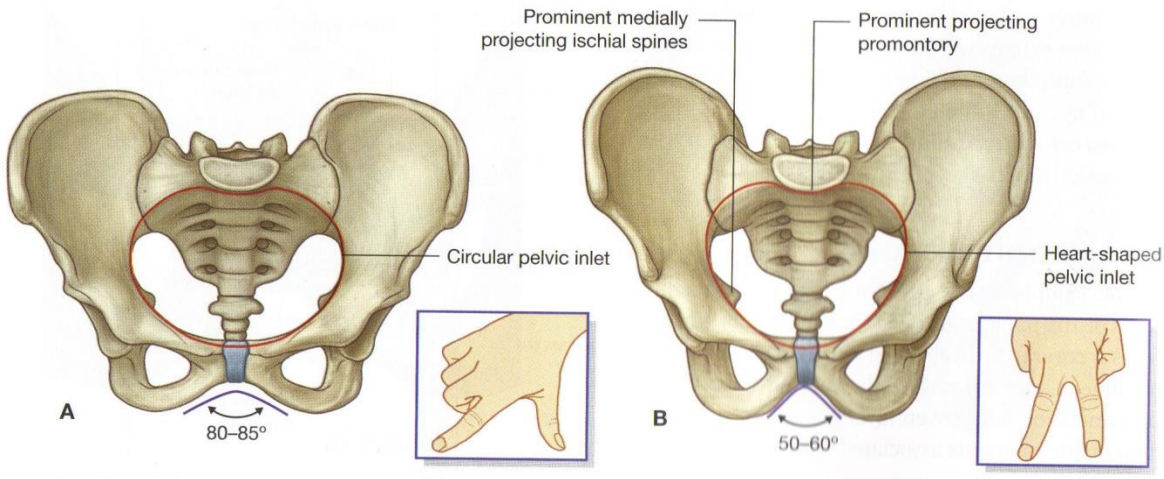

Figure 1.6: Structure of the bony pelvis in females (A) and males (B). The angle formed by the pubic arch can be approximated by the angle between the thumb and index finger for women and the angle between the index finger and middle finger for men (taken from Drake *et al*, 2005).

Other differences between male and the female pelves include the subpubic angle (Figure 1.6), which in females has a greater angle (>80º) than in males (50-60°); the diameter of the acetabulum is larger in males than females (Brothwell, 1981; Drake *et al,* 2005); the angle of the greater sciatic notch in females is larger (almost 90°) compared to that in males (approximately 70°) (Moore *et al,* 2013).

1.5 Biomechanics of the human pelvis and gait analysis

Biomechanics is a branch of physics using the applications of mechanics into the analysis of biological and physiological systems in the living

Forces acting on the skeleton are complex, including compression, tension, shear, bending and torsion (Figure 1.7). In long bones, compression stresses occurr when two opposing forces are applied to the bone in directions towards each other, while in tension, the two forces act away from each other. Shear stress take place when two parallel forces simultaneously displace one part of the bone in a direction opposite to the other part of the bone. Bending occurs when two forces acting at the end of the bone producing tension and compressive stresses on opposite sides of the mid bone. Torsion is two rotational forces acting in opposite directions, around the longitudinal axis of the long bone.

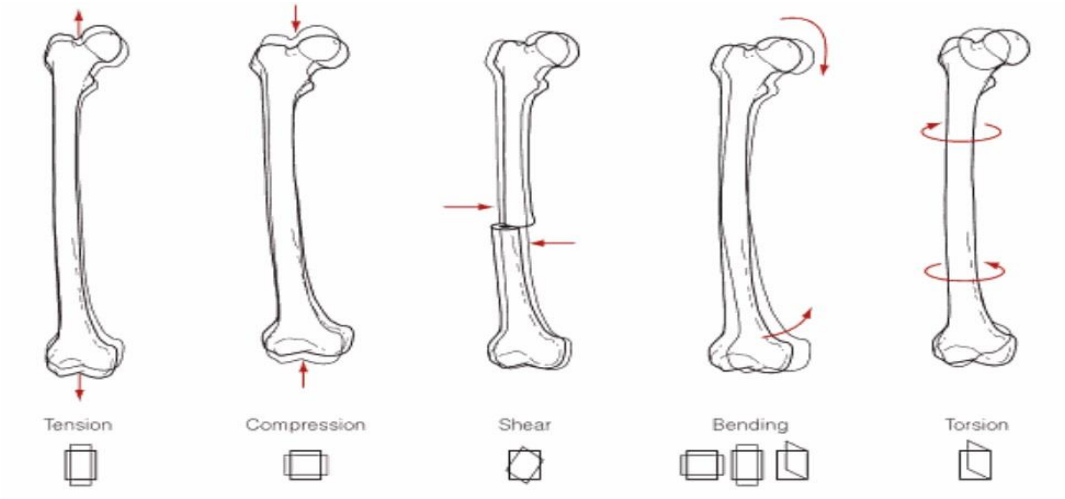

Figure 1.7: Example of tension, compression, shear, bending and torsion forces on the long bone (modified from MacLester and St. Pierre, 2008).

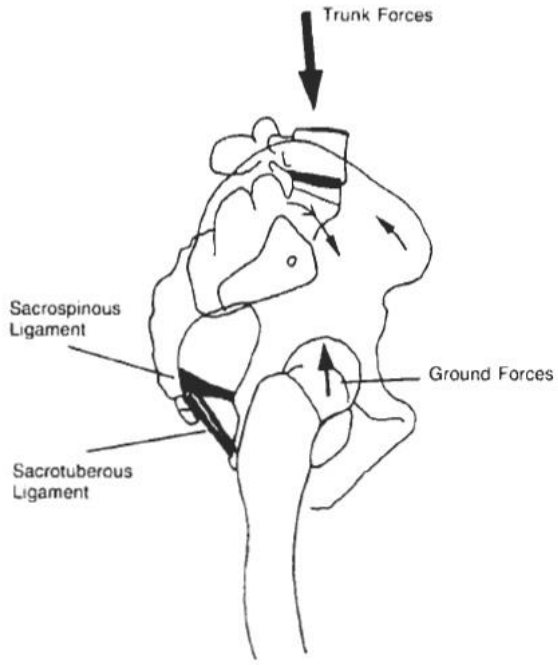

Figure 1.8: Example of forces transmitted through the lumbopelvic region from the trunk and the ground, with nutation of the sacrum resisted by the sacrotuberous and sacrospinous ligaments (taken from Alderink, 1991).

The biomechanics of the musculoskeletal system is the study of the forces exerted by body weight, muscles and gravity on skeletal structure. The primary function of the pelvis is to transmit weight from the upper limbs and the trunk to the lower limbs and to resist the ground forces from below (Alderink, 1991). It also provides an attachment site for powerful muscle groups which control the rotational degrees of freedom of the hip joint. During standing, a substantial weight from the upper limbs, trunk and head with the vertebral curvature stresses the base of the sacrum to nutate (downward movement of the sacral promontory) forward approximately 30º to the transverse plane as the centre of gravity lies anterior to the promontory (Figure 1.8), essentially locking the pelvis by the lumbopelvic ligamentous complex (Kapandji, 1974; Alderink, 1991; Nordin and Frankel, 2001; Palastanga and Soames, 2012).

Additionally, the strong and well-developed muscles supporting the pelvis and the sacrum contribute significantly to the stability of the pelvic region by virtue of a self-bracing mechanism, in response to the high shear forces between the sacrum and the innominates due to the almost vertically-oriented sacroiliac joint surfaces that inhibit significant weight transfer from the axial to the appendicular skeleton (Solonen, 1957; DonTigny, 1993; Snijders *et al*, 1993a).

In the pelvic region during standing, the main load transfer occurs around the area of the greater sciatic notch, and in the superior region of the acetabulum (Figure 1.9) that is buttressed by the iliac bone (Dalstra and Huiskes, 1995; Widmer *et al*, 2002).

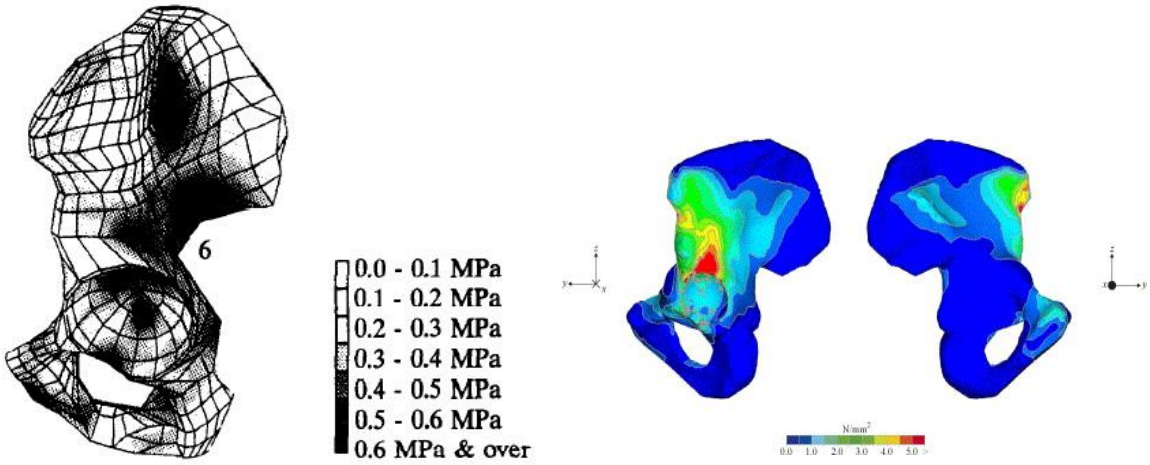

Figure 1.9: The lateral view (left) of the three-dimensional finite element stress distribution in the trabecular bone of the innominate during standing (modified from Dalstra and Huiskes, 1995), with (right) a recent FE model (Philips *et al*, 2007).

The narrow area of the anterosuperior acetabular region transferring the hip joint force results in a highly stressed region resulting in an increase in thickness of the trabecular region in nearby areas, particularly the greater sciatic notch area (Dalstra and Huiskes, 1995), which is also the site with highest trabecular density in the non-weight bearing ilium (Cunningham and Black, 2009a, 2009b).

Biomechanics of developing pelvis

Humans undergo tremendous changes associated with physical developmental milestones where early neuromotor maturation is initiated by suppression of primitive reflexes, such as the grasping and sucking reflex present during infancy (Keen, 1993; Schott and Rossor, 2003). These gross motor developments are summarized in Table 1.1.

Motor Milestones	**Average Age of Attainment**
Head control	2 months
Rolls to spine	4 months
Maintains sitting	6-7 months
Rolls to prone	7 months
Creeps on all fours	10 months
Stands momentarily	10 months
Cruises	10 months
Walks independently	12-14 months
Begins to run	2 years
Walks up and down stairs	2 years
Runs well	3 years
Walks up stairs alternating feet	3 years
Walks down stairs alternating feet	4 years
Hops on one foot	4 years
Skips	5 years
Walks with mature, adult gait	7-9 years

Table 1.1: The normal gross motor developmental milestones (modified from Keen, 1993).

The pelvis adjusts its position according to body weight transmission, which is governed largely by gravity (Kapandji, 1974). During the neonatal period, the child is predominantly supine, leading to insignificant demands from the influences of direct stance related locomotion (Thelen, 1981). Subsequently, when the child begins to sit up around six months to one year (Keen, 1993; Carruth and Skinner, 2002), axial weight is reportedly transferred via the first sacral vertebra, through the sacroiliac joints to the

ischial tuberosities (Aiello and Dean, 1990). At around 8-10 months, the child usually begins to crawl, thereby imposing a transitional form of quadrupedal locomotion on the pelvic complex, placing the centre of gravity perpendicular to the abdomen (Adolph *et al,* 1998; Carruth and Skinner, 2002). The centre of gravity again changes during standing, when it comes to lie in the midline just anterior to the second sacral vertebrae (Aiello and Dean, 1990). When a child starts to walk around 12 – 18 months of life, the demand placed on the pelvis by bipedal movement alters an almost flat neonatal ilium (Scheuer and Black, 2000) into an 'S'-shaped curved bone and iliac crest with a characteristic concavity and convexity of the gluteal and pelvic surfaces for muscle attachment (Aiello and Dean, 1990). In addition, the iliac blade changes its morphology by bending forward, around two years of age in response to the altered load transfer associated with the development of upright posture and bipedal locomotion (Scheuer and Black, 2000). This changing role from crawling to standing and then walking has a significant influence on the growth of the bony pelvis: it must adopt a stable and well-developed structure quickly that is able to withstand the stresses associated with body weight and gravity during bipedal locomotion.

These important milestones translate into alterations of both the internal and external pelvic morphology (Aiello and Dean, 1990). The pelvic complex witnesses other functional changes prior to full maturation of gait around eight years of age, including visceral descent into the pelvis and fusion at the ischiopubic ramus (Inman *et al,* 1981; Keen, 1993; Scheuer and Black, 2000; Kubo and Ulrich, 2006). Secondary sexual skeletal changes start to become evident at around ten years in females and twelve years in males (Scheuer and Black, 2000), although there is much variability within and between the sexes (Papadimitriou and Chrousos, 2005; Slyper, 2006). The pelvis is the area of the skeleton that displays the greatest degree of sexual dimorphism, primarily in preparation for the requirements of parturition (Walker, 2005).

Gait and mechanism of walking

The pelvis also plays an important role in normal gait. A normal gait consists of cyclical and repeated movements of two phases; the stance phase and the swing phase (Keen, 1993; Magee, 2008).

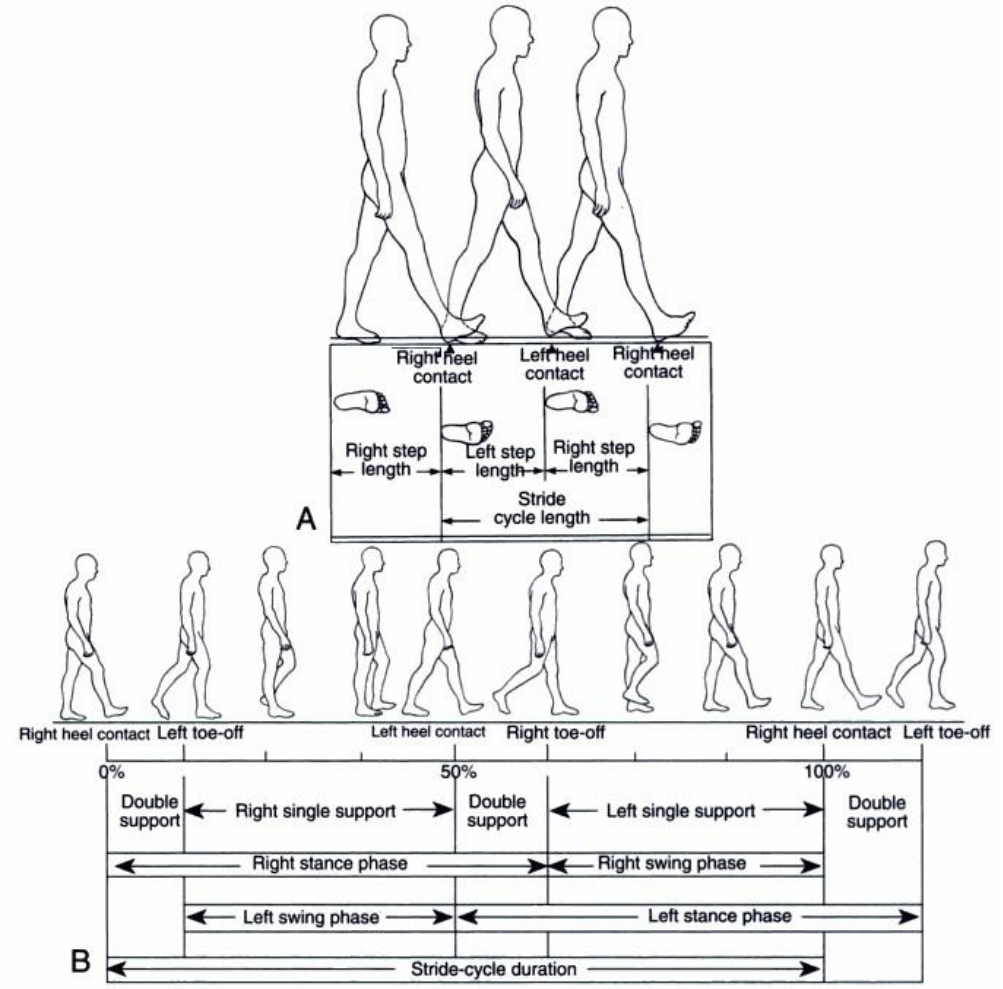

Figure1.10: The gait cycle (taken from Karageanes, 2005).

The stance phase consists of 5 subphases; heel strike - foot flat - single leg stance - heel off - toe off, and constitutes 60-65% of the total gait cycle, while the swing phase, which involves acceleration - mid-swing - deceleration, consists of 35-40% of the gait cycle (Magee, 2008).

The gait pattern (Figure 1.10) begins with heel strike of the foot and lasts until the same foot contacts the ground again with around 10% of it consisting of double support, where heel strike of one foot and toe off on the opposite foot overlap with both limbs being in contact on the ground (Aiello and Dean, 1990; Karageanes, 2005). The centre of gravity is at its highest at mid-stance phase when the supporting limb is fully extended and at its lowest when both feet are in contact with the ground (Aiello and Dean, 1990).

There are numerous muscular involvements during walking especially at the pelvic and hip joint area. Among the muscles acting during walking are the three gluteus muscles, semimembranosus, semitendinosus and biceps femoris (Dalstra and Huiskes, 1995). These muscles were thought to help in keeping the changes in the stress distribution on the pelvic area during walking to a minimum.

During walking, the trunk load passes through the lumbar vertebrae and the sacroiliac joint to the innominates, and subsequently to each leg alternately while the body sways from side to side where the centre of gravity is alternately over the right and left feet (Martin and Hurwitz, 1962). It was reported that SI joint can withstand medial forces 6 times greater than the axial compressive load, but only half torsion and $1/20^{th}$ of axial compression load, most probably due to the vertical position of this joint, albeit its primary function is to provide stability (Cohen, 2005).

1.6 Relationship between loading mechanism and trabecular pattern in bone

Many experimental and observational studies have reported that cortical and trabecular bone adapts in response to changes in biomechanical loading (Rubin and Lanyon, 1985; Forwood and Burr, 1993; Goldstein *et al*, 1993; Robling *et al*, 2002; Ruff *et al*, 2006; Shaw and Ryan, 2012). The extracellular matrix produced by the connective tissues has the ability to sustain functional loading at an "optimum customary" window without damage while regulating the orientation and physical properties of the matrix in relation to the loading area (Rubin and Lanyon, 1985). Bone tissue is selectively mechanosensitive with the adaptive response of bone to mechanical loading being highly site-specific (Figure 1.11). It is only the loading regions within a bone that experience sufficient strain to cause it to remodel (Warden *et al*, 2005).

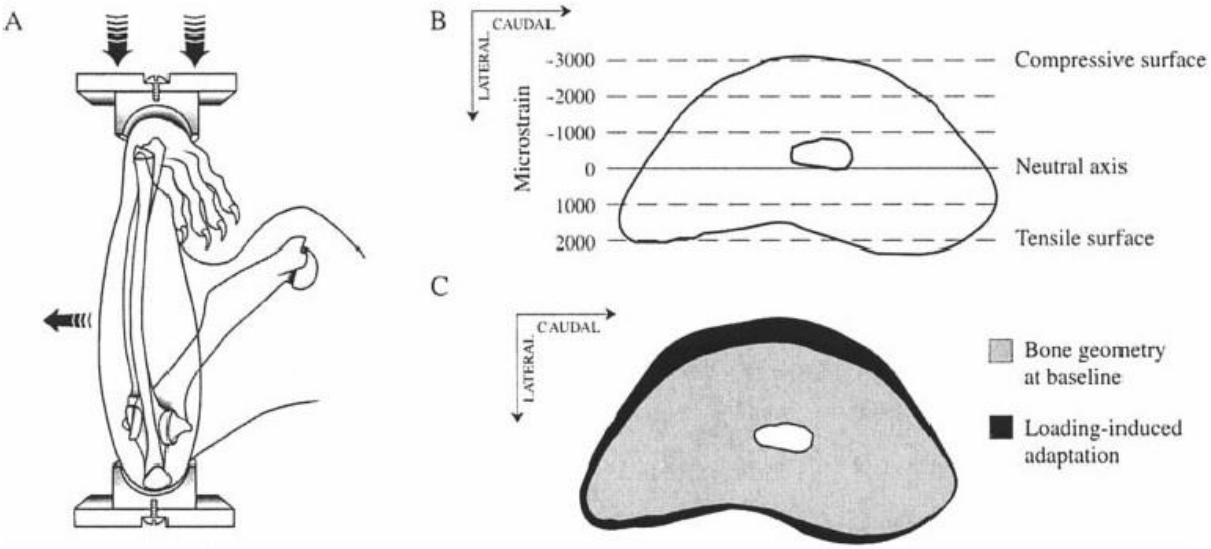

Figure 1.11: In vivo experiment of overloading of rat ulna (Robling *et al*, 2002). (A) The compressive (medial) and tension (lateral bending) loading on the ulna. (B) Cross-section of the ulna midshaft showing the strain distribution and (C) post 16-weeks intermittent loading shows the new bone formation particularly at the compressive site (modified from Warden *et al*, 2005).

The stimulus for this bone remodeling depends on the strain rate, magnitude and frequency of loading; hence bone structure is closely related to activity, where strenuous activity is far more osteogenic than a sedentary state (Ruff *et al*, 2006).

Under mechanical loading, the trabecular bone will increase in stiffness by increasing the bone per unit volume or adjusting the arrangement of the individual trabeculae to accommodate the pressure (Doube *et al*, 2011). The projection of the trabeculae appear to be aligned along the direction of the principal stress exerted by functional loading (Figure 1.12), as suggested by Culmann and von Meyer's mathematically-constructued stress trajectories of a crane-line beam (Skedros and Baucom, 2007).

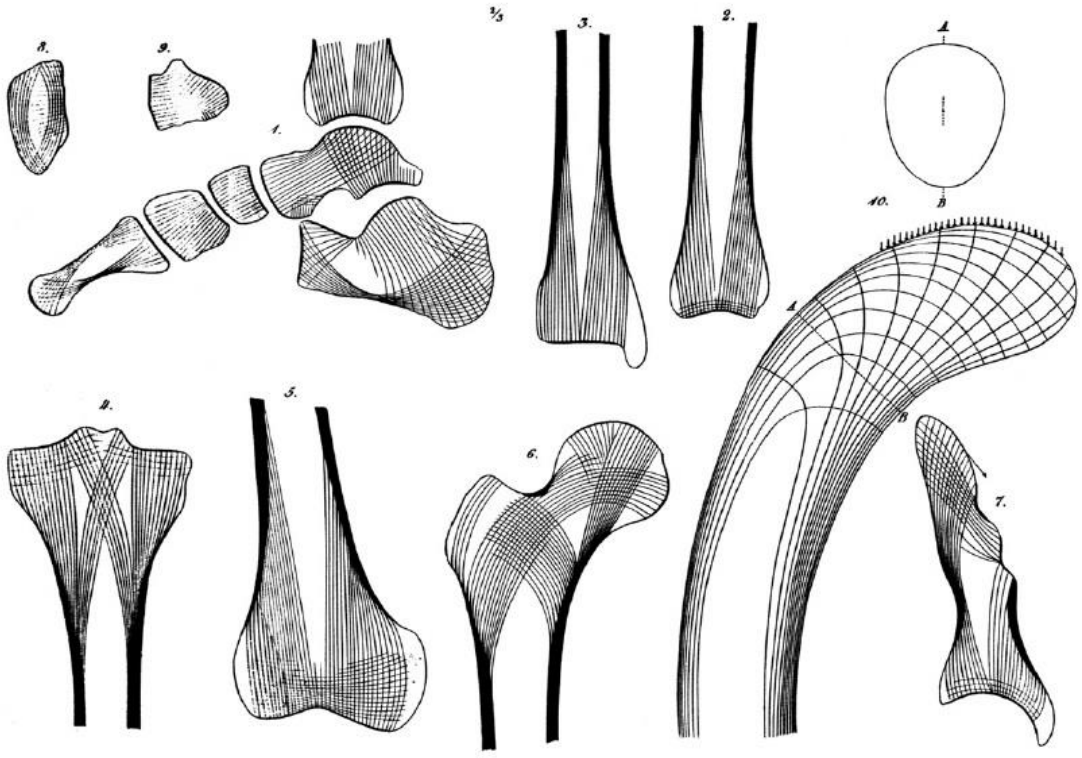

Figure 1.12: Illustration of Culmann 'crane' in comparison with various sections of human bones (taken from Skedros and Baucom, 2007).

One important factor that determines the effectiveness of bone response to mechanical loading is age, where juvenile bone is more responsive to mechanical stimuli, although genetics, hormonal status and disease should also be considered (Forwood and Burr, 1993; Keaveny *et al*, 2001; Ruff *et al*, 2006). In addition, studies on oestrogen receptors (ER) in mice report that skeletal response to loading around puberty is due to a direct regulation of mechanotransduction pathways by ER in concert with cell activation through the hypothalamic-pituitary axis (Forwood, 2008). Further details on bone physiology are discussed in the next chapter.

It can be summarized that the properties of trabecular bone are heterogeneous (varies with age, genetic, wellbeing), anisotropic (in response to the loading direction or multi-axial loading) and asymmetric according to the mode of loading (tension, compression or shear forces) (Figure 1.13).

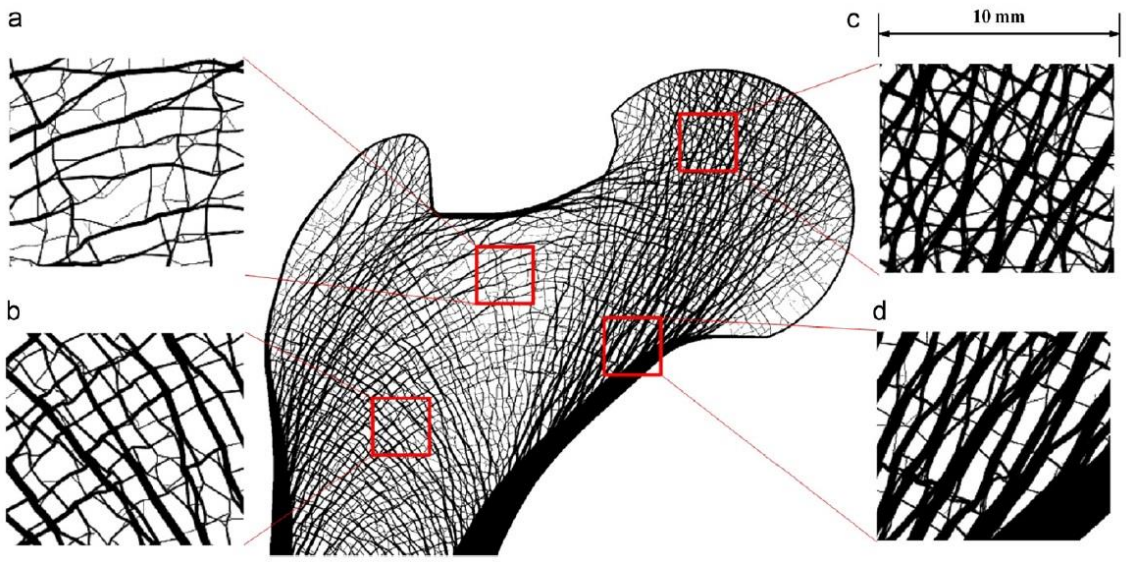

Figure 1.13: The different properties of trabecular architecture depending on the mode of loading obtained by simulation topology optimization. (a) Principal tensile group in Ward's triangle, (b) Intertrochanteric arches, (c) Principal compressive group in epiphysis, and (d) Principal compressive group in metaphysis (taken from Jang and Kim, 2008).

Despite the multifactorial source that determine the properties of trabecular bone, many studies have focused on the trabecular architectural properties of long bones, such as the femur and humerus (Fajardo and Muller, 2001; Skedros and Baucom, 2007; Jang and Kim, 2008; Doube *et al,* 2011; Shaw and Ryan, 2012) and recently reported femoral trabecular architectural density significantly more than that of the humeral heads (Shaw and Ryan, 2012) most likely in response to locomotion. Pelvic biomechanical studies have been mainly based on the acetabular region, ilium and the symphysis pubis (Dalstra *et al,* 1993; Anderson *et al*, 2005), and to some degree the sacrum (Ebraheim *et al,* 2000), in which it was reported that the adult S1 body is significantly denser than the adjacent alae (Figure 1.14) (Peretz *et al*, 1998).

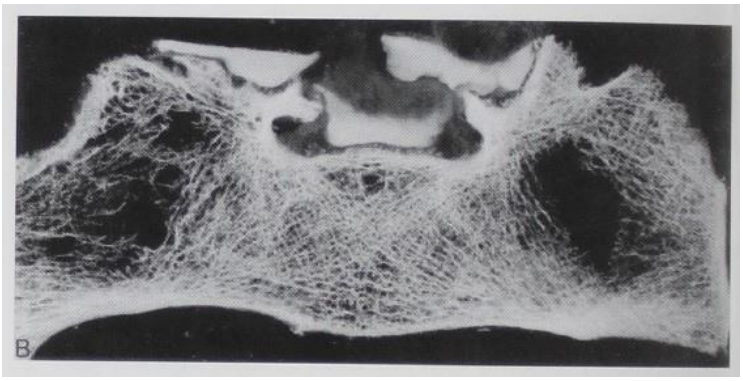

Figure 1.14: Axial section of an adult sacrum scanned by CT showing dense trabeculae in S1 body and sparse trabeculae in the ala regions (modified from Peretz *et al,* 1998).

Studies on the biomechanics of juvenile skeletal remains are particularly limited (Ivarsson *et al*, 2013), however, recently, a number of studies directed towards the pattern of trabecular bone ontogeny have emerged to enlighten understanding of this particular area (Ryan and Krovitz, 2006; Cunningham and Black, 2009b; Gosman and Ketcham, 2009). It has been reported that throughout development, the human proximal femur and proximal tibial at both medial and lateral condyles undergo reorganization by the process of functional adaptation, as well as growth and development into a

structurally adult pattern. The initially dense, numerous, and well organised trabecular pattern at birth becomes markedly reduced in the first year of life (Figure 1.15). Following onset of bipedalism to 8 years, the trabecular reorganisation resulted in increased bone volume and thickness with a greater degree of anisotropy with a concurrent decrease in the number of trabeculae (Ryan and Krovitz, 2006; Gosman and Ketcham, 2009). Additionally, it was found that the arrangement of the trabecular network in the non-weight bearing juvenile ilium resembles the adult pattern possibly suggesting a predetermined genetic template for its future role and functional intrauterine ligamentous interactions (Cunningham and Black, 2009b).

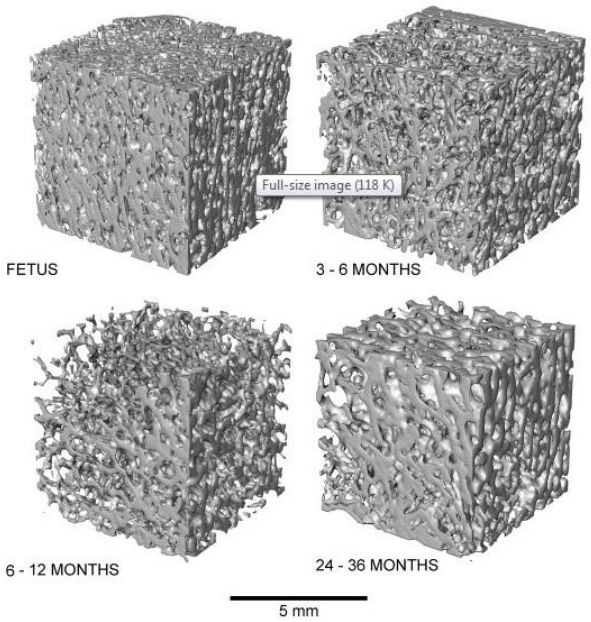

Figure 1.15: Three-dimensional reconstruction of the juvenile proximal femur from different individuals (modified from Ryan and Krovitz, 2006).

Despite studies on long bones and the ilium, little is known about the trabecular ontogeny of the sacrum. Thus, the current study aims to determine the trabecular organisation, through structural analysis, of the pelvic area with particular reference to the developing sacrum, before and after the commencement of independent stance and bipedality, to aid in the understanding of biomechanical properties of the posterior human pelvis.

CHAPTER 2

The sacrum and the ilium

2.1 Introduction

Chapter 2 discusses the basic component structure of bone: from its microstructure comprising the organic and non-organic materials to the macrostructure, which comprises the osseous materials. This chapter will also discuss the physiological processes and regulatory mechanism controlling bone development and how it is modulated to achieve optimum biomechanical adaptation throughout life.

In addition, the gross anatomy and embryology of the sacrum and ilium, along with the associated joints and soft tissues associated with these two bony structures is addressed comprehensively. The sexual disparity between the male and female sacrum is explained. The similarities and differences between the embryological origins of the sacrum and the ilium are reviewed and compared.

2.2 Basic structure of bone, bone modelling and remodelling

Bone

Bone is a protein-mineral composite living tissue and is generally categorised on the basis of its macrostructure and microstructure (Ji and Gao, 2004; Wang and Puram, 2004). The macrostructure of bone is divided partly on the basis of porosity into two categories; cortical and trabecular bone. Cortical bone, also known as compact bone, is dense and found primarily in the shafts of long bones (Figure 2.1) and the outer covering shell of all bones: it provides mechanical strength and protection (Bilezikian *et al,* 1996). Trabecular bone, also known as cancellous or spongy bone, consists of bony trabecular struts and marrow-filled cavities and is organised for load-bearing. It is more active metabolically than cortical bone and remodels more frequently (Rho *et al,* 1998; Huiskes, 2000; Wang and Puram, 2004).

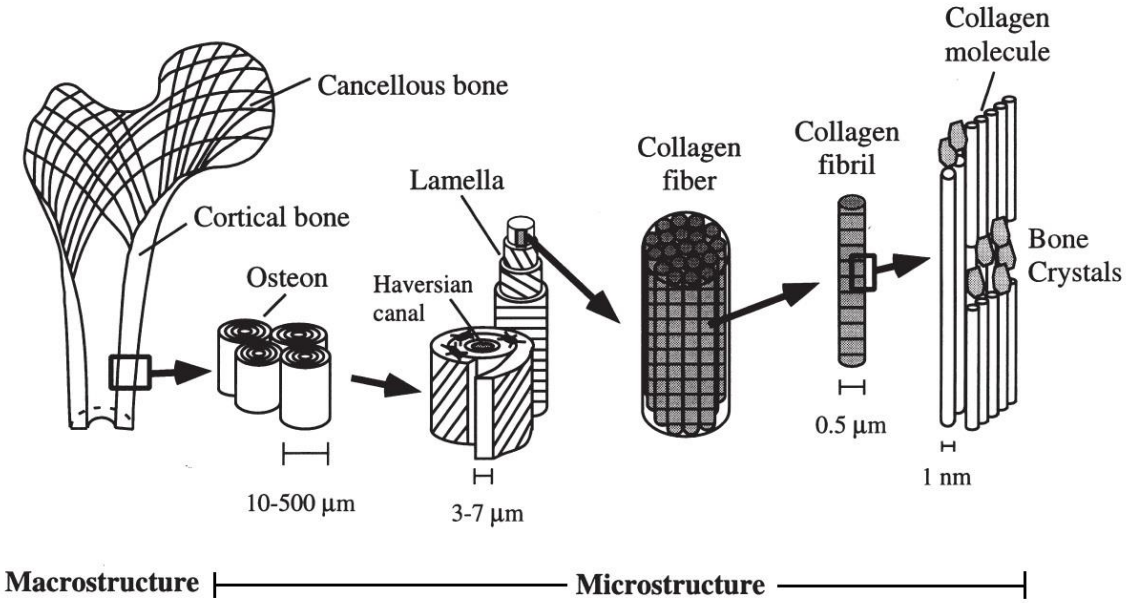

Figure 2.1: The hierarchical organisation of macrostructure and microstructure of bone (modified from Rho *et al,* 1998).

The macrostructure of bone is based upon its microstructure and consists of a hierarchical structure of osteons (Haversian systems), lamellae, collagen fibers, embedded minerals and non-collagenous organic proteins (Figure 2.1). The major difference between cortical and trabecular bone is the arrangement of trabecular bone into struts of rods and plates interspersed with marrow (Rho *et al,* 1998).

The human skeletal system develops from mesenchymal cells derived from neural crest cells and the mesoderm. The embryonic mesodermal layer is the middle germ layer. Mesodermal derivatives comprise the paraxial mesoderm, lateral plate mesoderm, and intermediate mesoderm which connects the medial paraxial and the lateral plate mesoderm (Sadler, 2010).

Paraxial mesoderm forms somitomeres (cranial region) and somites (post-cranial region), with the latter differentiating into a ventromedial (sclerotome) part and a dorsolateral (dermomyotome) part. The sclerotomes will eventually form the fibroblasts, chondroblasts, or osteoblasts forming the vertebrae. The lateral plate mesoderm, specifically at the parietal layer, will eventually form the bones of the shoulder and pelvic girdles, limbs and sternum, while the neural crest cells form the mesenchymal tissues that differentiate into bones of the face and skull, sensory ganglia of the cranial and spinal nerves, suprarenal glands and neurolemma sheaths of peripheral nerves (Sadler, 2010; Moore *et al,* 2011).

The ossification process transforms mesenchymal cell derivatives into osseous material and is divided into two types: intramembranous ossification and endochondral ossification. Intramembranous ossification is a process whereby mesenchymal cells mainly of dermal origin, differentiate directly into bone, usually found in the flat bones of the skulls, the mandible and the clavicle. Additionally, it is involved in periosteal apposition to increase the diameter of the diaphysis of long bones forming the external

covering of all bones as well as being involved in bone remodelling. The second type of ossification is the differentiation of mesenchymal cells into chondrocytes which then gradually ossifies by endochondral ossification following penetrating osteogenic-carrying vessels, usually found in the long bones of the limbs and any skeletal region that displays a considerable amount of trabecular bone (Bilezikian *et al,* 1996; Scheuer and Black, 2000; Sadler, 2010).

Bone has various functions and appears in many forms. It is a living connective tissue that collectively forms an organ and is part of the musculoskeletal system. Mechanically, bone acts as an anchor for muscles and ligaments to enable them to perform their functions optimally, protect internal organs and bear the forces transmitted through it, especially at weight-bearing regions, in addition to facilitating locomotion. Physiologically, the majority of bone acts as a site for haematopoiesis and to provide storage for fat and minerals. Biochemically, it increases its mineralization with the help of vitamin D (calcitriol) and along with the parathyroid hormone (PTH) and calcitonin regulates calcium-phosphate metabolism for optimal mineral homeostasis (Bilezikian *et al,* 1996; Lombardi *et al*, 2011).

Despite the multifunction and great strength of bone, it is a very lightweight material, with the skeleton only constituting around 20% of total body weight (White and Folkens, 2005). This lightweight yet resilient design optimizes the mechanical function of the skeleton without compromising the functional requirements of the material. The stiffness and strength of bone are determined by the content and quality of its components: approximately 70% minerals (mainly hydroxyapatite), 22% proteins (90% type I collagen) and 8% water (Currey, 2003; Wang and Puram, 2004). How the resulting materials are arranged with minor constituents of non-collagenous proteins are thought to play an important role in bone formation (Olszta *et al,* 2007).

The basic cellular components of bone comprise four different cell types; the matrix-producing osteoblasts, tissue-resorbing osteoclasts, osteocytes (highly-specialised, mature osteoblasts) and bone lining cells (Bilezikian *et al*, 1996; Manolagas, 2000; Sommerfeldt and Rubin, 2001). The osteoblasts, osteocytes and the bone lining cells are derived from local osteoprogenitor cells, while the osteoclasts are the haematopoietic descendants from the fusion of mononuclear precursors (Bilezikian *et al*, 1996).

The interaction and coordination between the bone-forming and bone-resorbing cells are modulated by osteoprotegerin (OPG), which is secreted by the osteoblasts and inhibits osteoclast formation. RANK (Receptor Activator of Nuclear Factor-Kappa B), a transmembrane receptor on the osteoclast precursor for osteoclast activation (Aubin and Bonnelye, 2000; Hofbauer *et al*, 2000), produces dynamic and regulated bone formation: woven and lamellar bone.

Woven bone is characteristic of embryonic and fetal development and is found at ligament and tendon insertions in the adult or associated with a healing fracture or bone metastasis. Lamellar bone is mature bone found in normal cortical or trabecular bone (Sommerfeldt and Rubin, 2001). The structural subunit of lamellar bone is the lamella, arranged parallel to the trabeculae in cancellous bone, or parallel with the Haversian system in cortical bone, around a central capillary canal. Haversian systems can be further subdivided into primary (from woven bone consolidation), and secondary, by the resorption of pre-existing bone (Albright and Skinner, 1987; Currey, 2002).

The human skeleton grows and matures at different rates in different individuals, with many factors contributing to the variation seen (Sinclair and Dangerfield, 1998). Diet and nutritional status, genetics, physical activity, disease and hormonal factors all play an important role in influencing the growth of bone (Tanner *et al*, 1971; Sinclair and Dangerfield, 1998; Rogol *et al*, 2000). Among all these influences, nutritional status is a

substantial factor in the growth and skeletal maturity in infants and children (Hoppa, 1992). It is reported that these gene-environment interactions act in a large part to determine the ultimate morphology and size of adult bone (Sinclair and Dangerfield, 1998; Ruff *et al,* 2006). Recent study suggests that the importance of a high-quality diet in the first trimester of pregnancy influences infant growth and future health (Lanham *et al*, 2010).

Bone dynamics: Bone modelling and remodelling

Bone is a dynamic tissue which has the ability to adapt its internal microarchitecture and external shape through its viscoelastic properties and resistance to fracture by actively undergoing modelling and remodelling activities (Rho *et al,* 1998; Lanyon and Skerry, 2001). This is influenced by feedback mechanisms (Figure 2.2). There should be a balance between bone formation and resorption in the modelling and remodelling processes (Scheuer and Black, 2000).

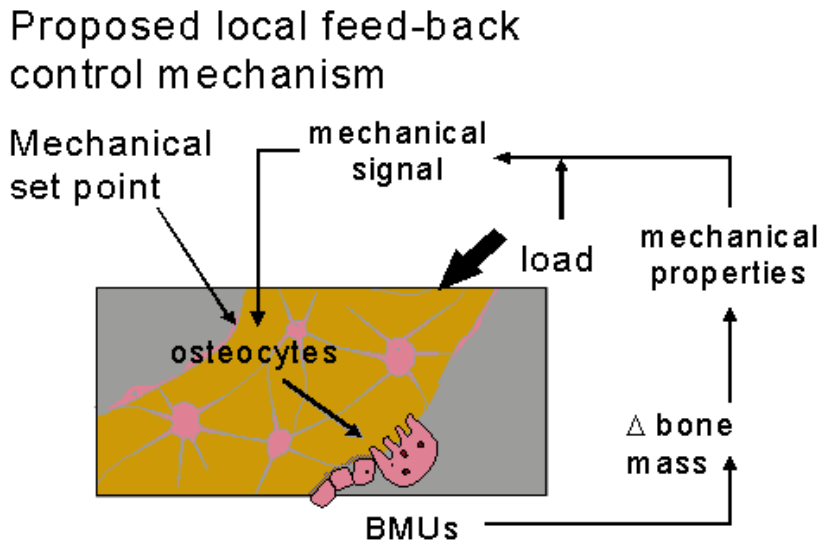

Figure 2.2: A schematic diagram of the regulatory process of bone remodelling based on a feedback-control mechanism until equilibrium is reached. The basic multicellular

units (BMUs) consist of osteoblasts and osteoclasts which regulate net bone formation or resorption (taken from Huiskes, 2000).

Bone modelling is the ability of bone to adapt to mechanical loads by balanced bone resorption and formation with morphological changes occurring according to bone location: it is markedly reduced after skeletal maturity (Frost, 1990; Seeman, 2009). Bone remodeling is simply a 'reparative procedure', replacing old bone with new osseous material to ensure mechanical integrity of the bone, but largely without inducing morphological changes (Seeman, 2009).

The dynamic adaptability of bone in the living has been observed since the time of Galileo with the assumption that its characteristic architecture is determined by the influences of mechanical stresses and strains imposed during normal functional activities (Einhorn, 1996).

A well-established law on basic bone biomechanics (Figure 2.3) is Wolff's law proposed by the German anatomist and orthopaedic surgeon Julius Wolff (1836-1902) which stated 'Every change in the form and function of bones or their function alone is followed by certain definite changes in their internal architecture, and equally definite secondary alterations in their external conformation, in accordance with mathematical laws'.

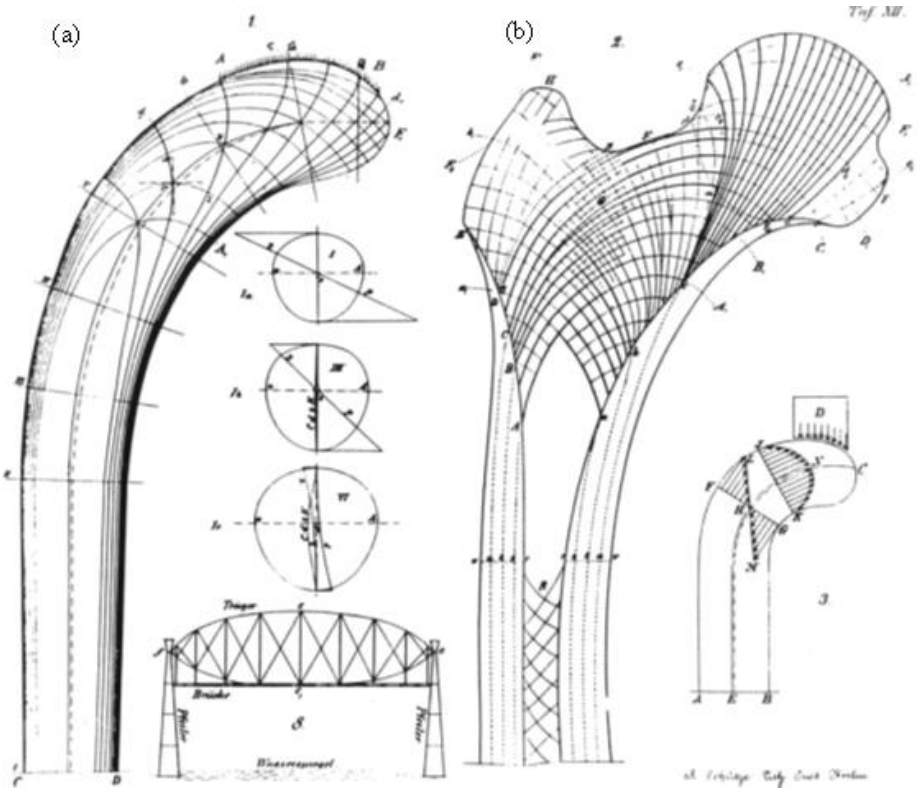

Figure 2.3: The static principal of (b) Wolff's Law of the trabecular arrangement of the proximal human femur with reference to the (a) Culmann crane (taken from Lee and Taylor, 1999).

Wolff's Law, although based on the principle of static force, served as a fundamental idea of bone as a mechanotransducer and has contributed to numerous subsequent studies, many of which disagree and challenge the law (Pearson and Lieberman, 2004; Ruff *et al*, 2006) by suggesting a more dynamic concept of 'Bone Functional Adaptation' to mechanical loading as a self-regulating mechanism proposed by Wilhelm Roux in the early 1880s (Lee and Taylor, 1999).

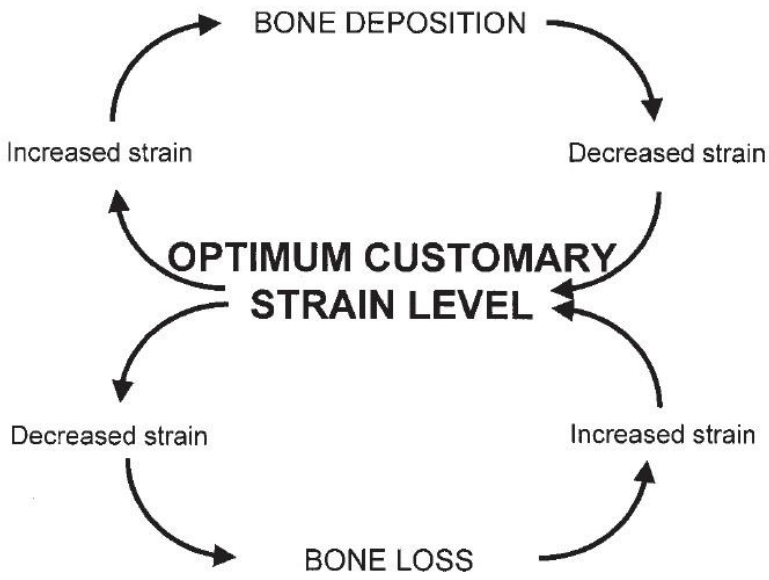

Figure 2.4: Bone functional adaptation model as a simple feedback mechanism (taken from Lanyon, 1982).

Bone functional adaptation is a complex process of bone tissue remodeling (Figure 2.4) induced primarily by mechanical demands and representing different interactions between genotype, systemic metabolic conditions, and local tissue interactions to stimulate a mechanotransducer reaction for the maintenance of bone tissue (Lanyon *et al,* 1982; Beauprê *et al,* 1990). The mechanosensory role played by the osteocytes is as sensor cells, and osteoblasts or osteoclast as effector cells, regulating cell-to-cell signaling to ensure a balance between bone formation and resorption in response to mechanical loading (Lanyon, 1993).

Frost (1987) proposed a detailed theory on load-bearing bones that adapt to different mechanical environments where bone tissue has an intrinsic ‘mechanostat’ that regulates bone functional adaptation. He suggests that below a certain threshold of mechanical use, bone resorption occurred to remove the excess material, while above a certain threshold level where it is exposed to higher than its normal peak mechanical loads, bone formation took place to increase its mechanical strength (Frost, 1987, 1990, 1996; Hughes and Petit, 2010).

In addition to the intrinsic regulatory mechanism of bone, externally bone formation and resorption are controlled by the hypothalamic-pituitary axis. The hypothalamus releases stimulating and inhibiting hormones particularly thyroid releasing hormone (TRH), gonadotropin releasing hormone (GnRH), and growth hormone releasing hormone (GHRH) to the anterior pituitary to release the thyroid-stimulating hormone (TSH) (Figure 2.5), adrenocorticotropic hormone (ACTH), growth hormone (GH), follicle-stimulating hormone (FSH) and luteinizing hormone (LH).

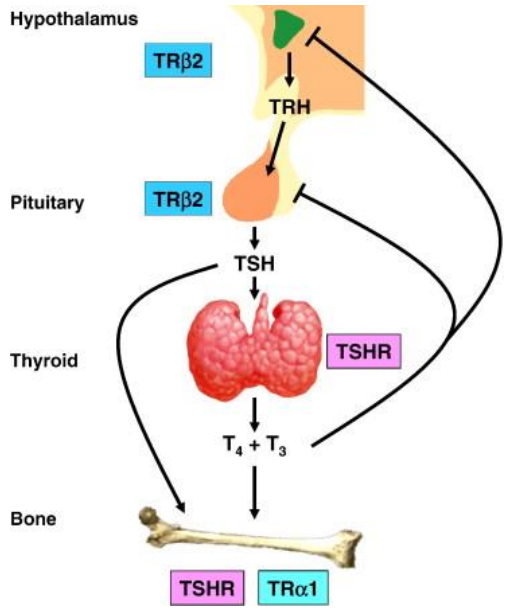

Figure 2.5: Hypothalamic-pituitary-thyroid axis effect on skeletal development via the stimulation of thyroid hormone and thyroid stimulating hormone (TSH) on the thyrotropin receptor (TSHR) and bone maintenance with negative feedback mechanism (modified from Bassett and Williams, 2008).

These hormones released from the anterior pituitary target organs such as bone (by GH) and the gonads (by FSH, LH) to produce sex hormones to stimulate bone formation, while in the thyroid (by TSH) to produce thyroid hormones and calcitonin. Studies have shown that normal thyroid hormone regulation is essential for skeletal growth while in the juvenile hypothyroidism results in delayed ossification, hyperthyroidism results in accelerated growth and advance skeletal development (Bassett and Williams, 2008; Sherwood, 2010).

2.3 Anatomy and embryology of the sacrum

Anatomy of the vertebral column and typical vertebra – cervical, thoracic and lumbar

Although the sacrum comprises one of the elements of the bony pelvis along with the innominates, it is categorised as part of the vertebral column. The vertebral column comprises approximately 33 vertebrae in humans within five regions; cervical, thoracic, lumbar, sacral and coccygeal (Figure 2.6). Each of the five regions has specific characteristics and comprises seven cervical, twelve thoracic and five lumbar vertebrae that constitute the moveable vertebrae, with five sacral and four coccygeal vertebrae representing the fused vertebrae which form part of the bony pelvis. Up to 10% from the overall population may vary in the number of vertebrae in each region (White and Folkens, 2005; Snell, 2008). The segmented vertebral column is flexible by virtue of the numerous facets, muscles and ligamentous attachments as well as the intervertebral disc that forms one quarter of the length of the column (Snell, 2008; Moore *et al*, 2013).

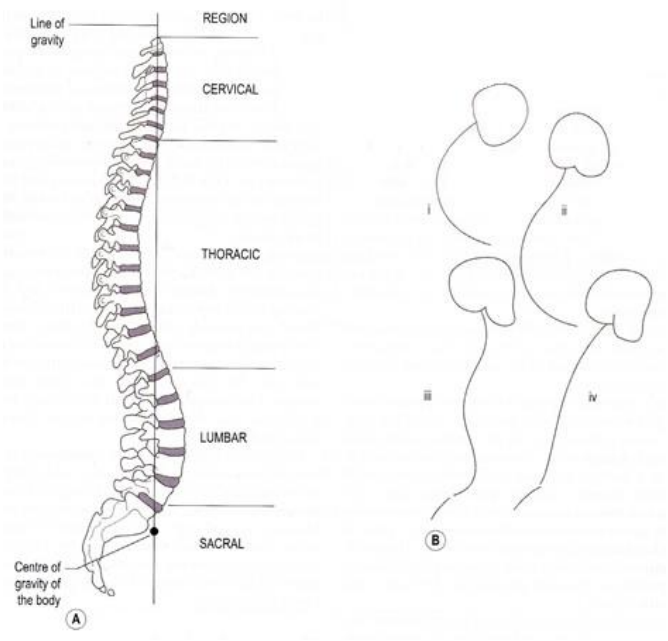

Figure 2.6: The (A) vertebral skeleton with the line and centre of gravity in lateral view. The differences in the curvatures in human (B) (i) at birth, (ii) 6 months, (iii) adult, and (iv) old age (taken from Palastanga and Soames, 2012).

The vertebral column consists of four curvatures: two primary and two secondary (Figure 2.6). The cervical and lumbar anterior convexities are the secondary curvatures acquired during development, while the thoracic and sacrococcygeal anterior concavities are primary curvatures retained since intrauterine life (Drake *et al*, 2005; Snell, 2008).

Around 3 months postnatal, the secondary cervical curvature begins to appear as the infant starts to hold up its head, and the lumbar lordosis commences when the child sits up at around 6 months becoming more established during standing and bipedal walking (Palastanga and Soames, 2012). Alterations can also occur in adults, such as during the later stage of pregnancy in which the lumbar anterior convexity increases to accommodate the change in the centre of gravity, while in old age, a gradual return of the vertebral column to a single continuous anterior concavity may occur mainly due to atrophy of the intervertebral discs (Snell, 2008).

The vertebral column functions:

1. as protection for the spinal cord, roots of the spinal nerves and the meninges.
2. as shock absorber mainly through the intervertebral discs and the curvature.
3. an attachments for muscles of the pectoral and pelvic girdles as well as muscles that maintain the erect posture of humans.
4. to produce, accumulate and transmit forces to other parts of the body (Snell, 2008; Palastanga and Soames, 2012).

A typical vertebra (Figure 2.7) consists of eight areas: (i) vertebral body, (ii) vertebral foramen, (iii) 2 pedicles, (iv) 2 laminae, (v) spinous process, (vi) 2 transverse processes, (vii) 2 superior articular facets, and (viii) 2 inferior articular facets. In short, a typical vertebra comprises a large weight-bearing body anteriorly, a vertebral arch posteriorly and a number of bony processes for muscles and ligamentous attachments (Sadler, 2010; Moore *et al*, 2013).

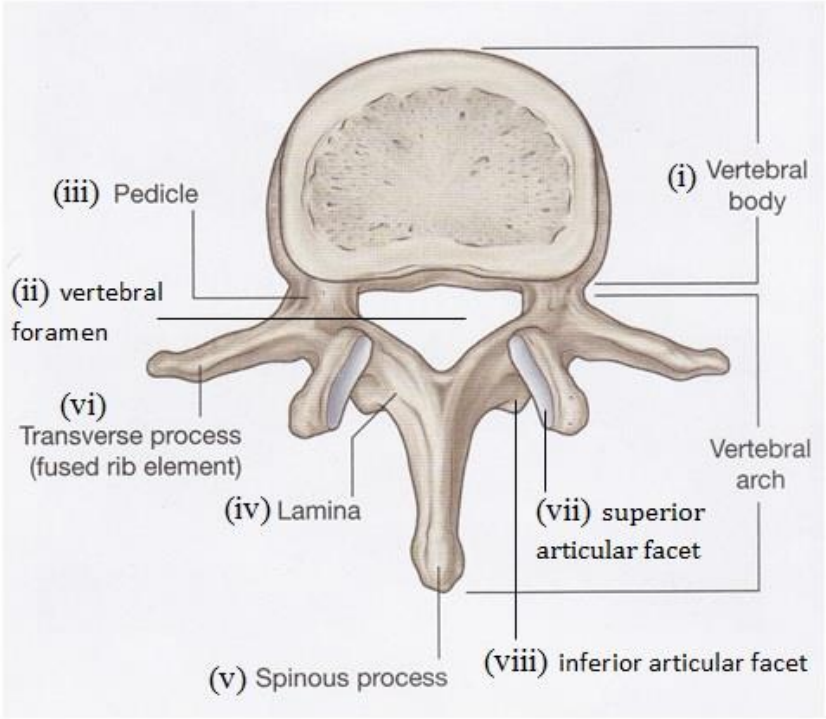

Figure 2.7: Anatomy of a typical vertebra (modified from Drake *et al*, 2005).

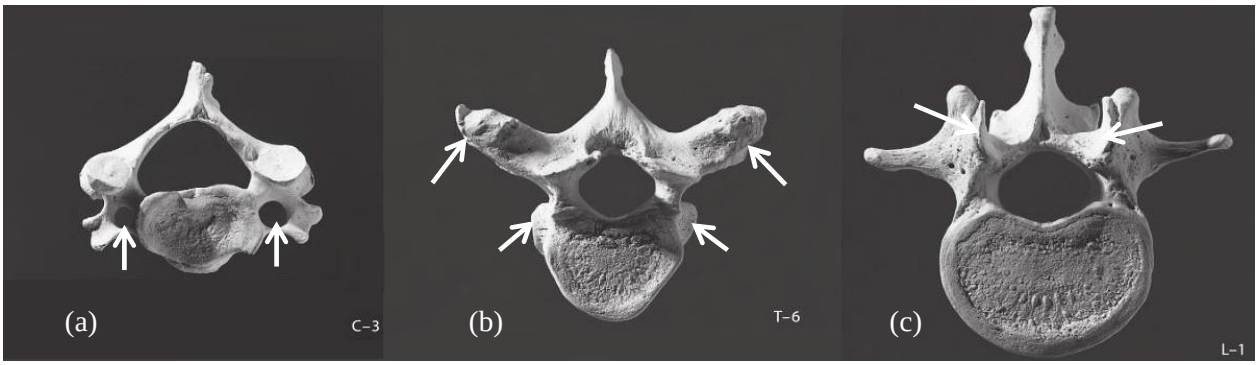

Figure 2.8: An example of three vertebrae in superior view from three different regions, (a) cervical (C3), (b) thoracic (T6) and (c) lumbar (L1). The cervical (a) vertebra has foramina transversaria (white arrows), The thoracic (b) has costal facets (white arrows), and lumbar (c) vertebra has prominent curved superior articular process (white arrows). Although the appearances of the three vertebrae are not identical, the main characteristic of having a vertebral body anteriorly and a vertebral arch posteriorly are present (modified from White and Folkens, 2005).

The cervical vertebrae have a special characteristic feature compared to the rest of the vertebrae by having bifid spinous processes and a foramen transversarium in each of the transverse processes shown by the white arrows in Figure 2.8 (a). This foramen transmits the vertebral artery and vein. The thoracic vertebrae (white arrows in Figure 2.8 (b)) are distinguished by the presence of articular (costal) facets on the body and the transverse processes for articulation with the head and tubercle of the ribs, respectively. The lumbar vertebrae possess neither a foramen transversarium, nor costal facets; however the body is very large and the superior (white arrow in Figure 2.8 (c)) and inferior articular processes are very prominent, with reciprocal curvatures of the concave upper facets and convex lower facets.

The bodies of the vertebrae are bound together by intervertebral discs forming symphyseal joints. Synovial zygapophyseal joint are formed between the inferior articular facet of the upper vertebra and the superior articular facets of the lower vertebra. These joints are reinforced mainly by the surrounding anterior and posterior

longitudinal ligaments on the anterior and posterior surface of the vertebral bodies respectively, the ligamentum flavum in between the laminae, the supraspinous and interspinous ligaments on the spinous process (Figure 2.9), and by the erector spinae and transversospinales muscles (Drake *et al*, 2005; Snell, 2008; Palastanga and Soames, 2012).

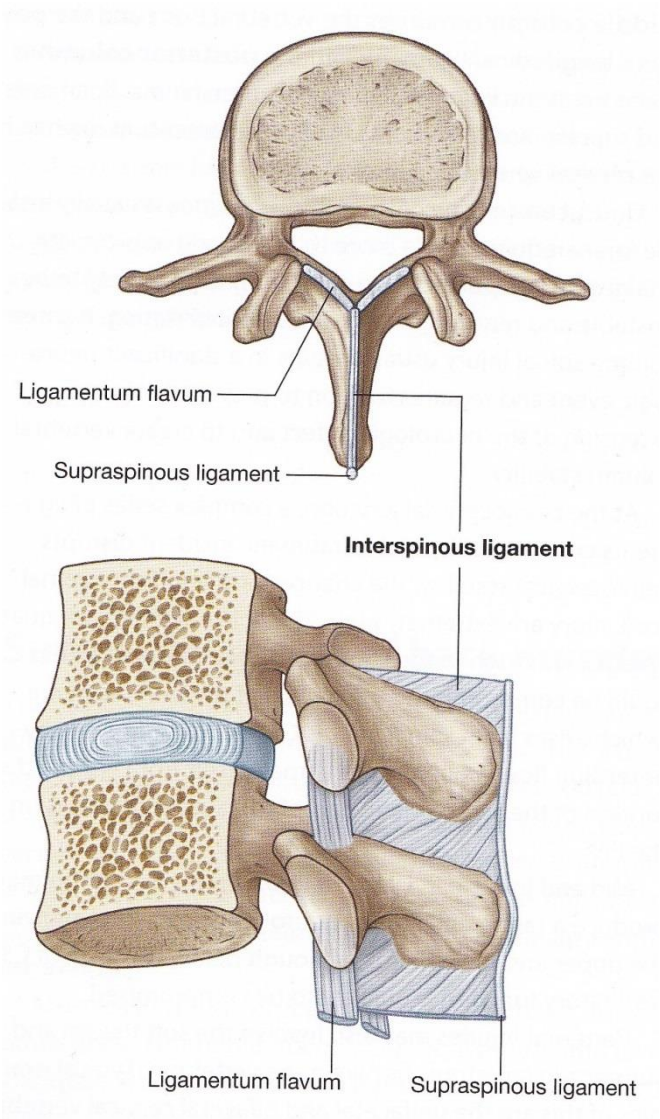

Figure 2.9: The supraspinous, interspinous and ligamentum flavum associated with the vertebrae (modified from Drake *et al*, 2005).

Anatomy of sacrum

Although the sacrum is a part of the vertebral column, the adult appearance is somewhat atypical, resulting from complete fusion of the five sacral vertebrae after the age of 25 years (Frazer, 1965; Scheuer and Black, 2000). Among the major differences between the sacral vertebra and the cervical, thoracic and lumbar vertebrae are the shape of the individual sacral vertebra and the presence of the costal (lateral) elements.

Figure 2.10: The S1 vertebra in superior view. The black arrows pointed at the sacral alae (costal) area.

The S1 vertebra (Figure 2.10) appears roughly rectangular in shape. Although the vertebral arch and the vertebral body are present in all of the four vertebral regions, the large costal (alae) elements (black arrows in Figure 2.10) are incorporated with the transverse processes of the neural arch and are broadened to form the lateral part of the sacrum (Palastanga and Soames, 2012). The coccyx on the other hand, is a vestigial tail with three to five (most frequently four) fused vertebrae, with prominent cornua seen on the first coccygeal vertebra (Snell, 2008). The coccyx decreases in size inferiorly as does the sacrum.

The adult sacrum is curved and triangular in shape, with a base that faces superiorly and an apex that faces inferiorly. It forms the posterosuperior wall of the pelvic cavity. It provides strength and stability to the pelvis and transfers body weight to the innominates (Moore *et al*, 2013). The sacrum has anterior and posterior surfaces

(Figures 2.11 and 2.12) and lateral parts. The sacrum articulates superiorly with the fifth lumbar vertebra at the lumbosacral angle, inferiorly with the first coccygeal segment at the coccygeal cornua and laterally with the innominate at the sacroiliac joints. The individual sacral vertebral segments decrease in size inferiorly as the influence of body weight diminishes after the S1-S2 vertebral segments (Pal, 1989).

Anterior part of sacrum

The anterior surface of the sacrum is concave superoinferiorly and mediolaterally. The anterior surface is smooth (Figure 2.11) and faces anteroinferiorly in the pelvic cavity. The median part represents the fused sacral vertebral bodies and is crossed by four transverse lines/ridges (marking the fusion of the sacral bodies): these may persist until old age (Scheuer and Black, 2000; Martini *et al*, 2006).

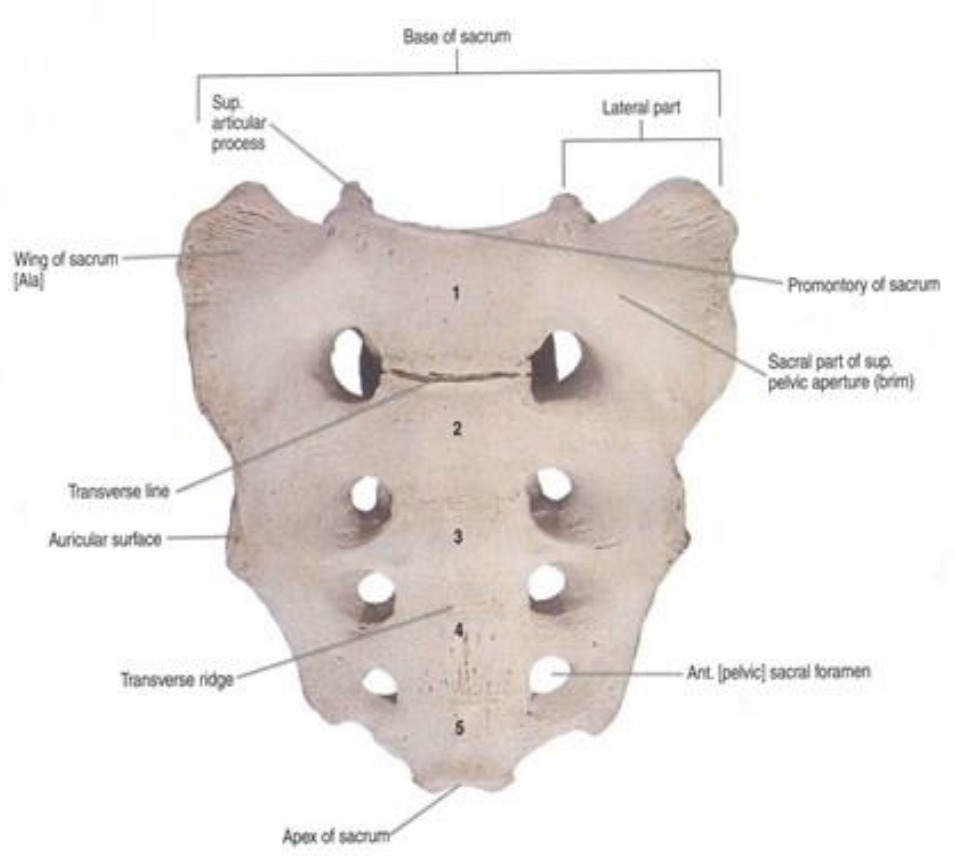

Figure 2.11: Anterior view of pelvic surface of sacrum (taken from Olson, 1996).

There are four pairs of anterior sacral foramina (Figure 2.11) which transmit the ventral rami of the first four sacral nerves and accompanying vessels. The broad sacral alae (wings) at the superolateral portion of the sacrum indicate the site of fusion of the costal/rib processes of the upper sacral vertebrae (Scheuer and Black, 2000).The sacral promontory, marked by the projecting border at the base of the sacrum, is a prominent landmark in females during pelvic examination, during labour and delivery.

Posterior part of sacrum

Posteriorly, the sacrum assumes a convex shape superoinferiorly corresponding to its concave anterior surface (Figure 2.11). This surface is rough, faces posterosuperiorly and has several bony landmarks (Whelan and Gold, 1982). In the midline, there is a series of elevations known as the median sacral crest, which represents the fused spinous processes, and paired lateral elevations termed the lateral sacral crest, which represents the fused transverse process of the sacral vertebrae (Figure 2.11).

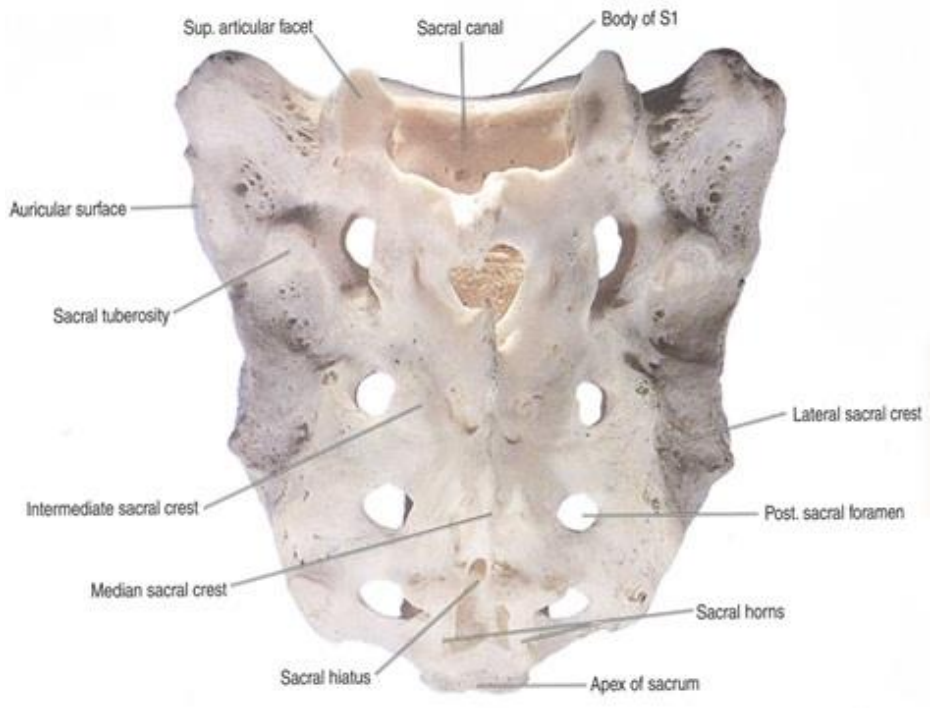

Figure 2.12: Posterior view of sacrum (taken from Olson, 1996).

O'Rahilly *et al* (1969) mentioned that the laminae were fused together to form the sacral groove, which is on each side of the median sacral crest, while lateral to the groove is the intermediate sacral crest (Figure 2.12), which represents the fused articular processes. The intermediate sacral crest projects downward to form the sacral cornua or horns, which mark the articular process of the 5^{th} sacral vertebra. The sacral cornua are formed by failure of the laminae of the 5^{th} sacral vertebrae to contact one another in the midline along with the spinous process which results in the formation of the sacral hiatus (Martini *et al,* 2006). This hiatus is an inverted 'V' just below the median sacral crest at the inferior opening of the sacrum: it is continuous with the sacral canal superiorly. The four paired posterior sacral foramina, which are smaller than the anterior sacral foramina (Whelan and Gold, 1982; Moore *et al*, 2013), transmit the dorsal rami of the S1 – S4 sacral nerves and corresponding vessels, and replace the intervertebral foramina which have been enclosed by fusion of the sacral vertebrae.

Lateral part of sacrum

The lateral surface of the sacrum is lateral to the posterior sacral foramina. It is bounded medially by the lateral sacral crest and laterally by a roughly L-shaped auricular surface that articulates with the innominate forming the sacroiliac joint (Brooke, 1924; Sashin, 1930). The cranial limb of the joint faces superodorsally and the caudal limb faces inferodorsally. The number of sacral segments involved in the auricular surface of the sacrum varies from S1 to S2, sometimes down to S3 especially in males probably due to more weight and forces transmitted through the sacroiliac articulation (Brothwell, 1981; Bellamy *et al,* 1983; Mahato, 2011).

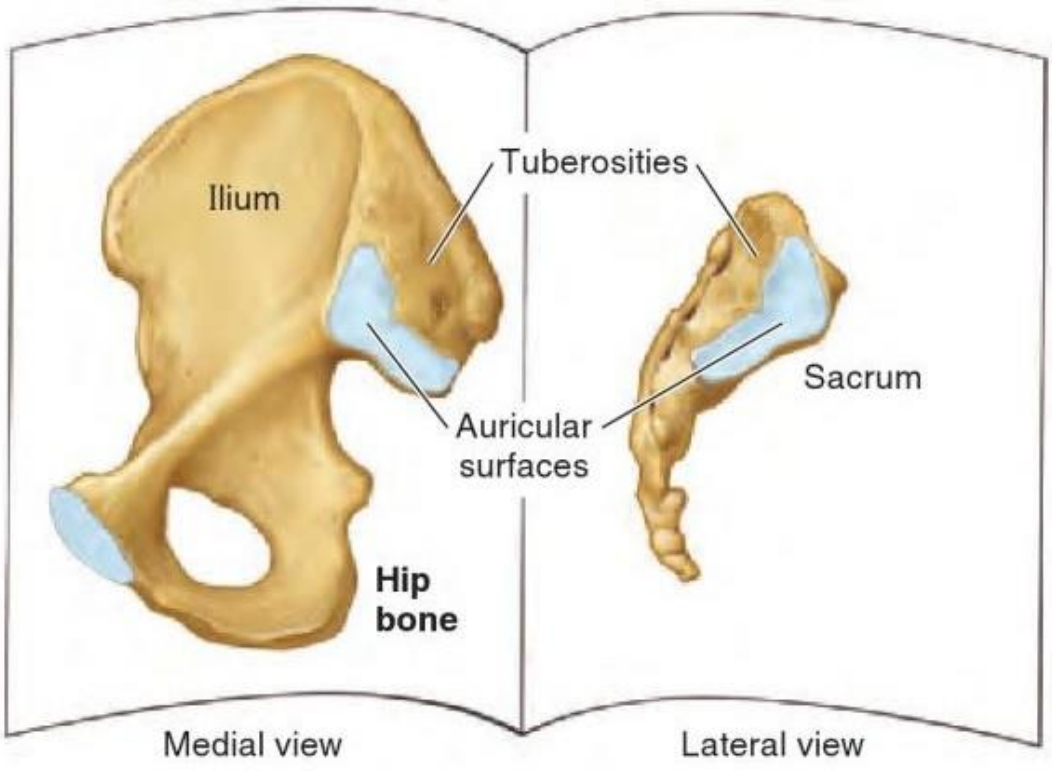

Figure 2.13: The lateral part of the sacrum consists of the auricular surface and the sacral tuberosities, with corresponding iliac counterpart (taken from Moore *et al*, 2013).

In between the lateral sacral crest and the auricular surface is the sacral tuberosity (Figure 2.13), a roughened surface containing depressions mainly for the insertion of ligaments. The sacral tuberosity is another surface of the sacrum that approximates with the ilium to form part of the sacroiliac joint (Tortora and Nielsen, 2009).

Apex of the sacrum

The apex is the narrow, caudal portion of the sacrum. This flattened surface marks the articulation of the sacrum with the first coccygeal segment, which fuses later in life (White and Folkens, 2005).

Base of the sacrum

The base of the sacrum consists of both sacral alae and the body of the 1st sacral vertebra (Figure 2.10) that articulates with the 5th lumbar vertebra to form the lumbosacral joint. In the general population, occasionally there is sacralisation of the L5 vertebra, where L5 is incorporated with the S1 vertebra especially in males, either completely or unilaterally (Mahato, 2010a) and often contributes to the formation of the auricular surface of the sacrum. This is possibly due to the 'heavier' male axial skeleton with more load 'forcing' the L5 to fuse with S1 and contribute in the formation of a larger auricular surface, while in females, lumbarisation of S1 (S1 incorporated into the L5 vertebra), is more common where S1 is not involved in the formation of the sacral auricular area (Mahato, 2011).

Posterior to the base of the sacrum is the sacral canal, which is a continuation of the vertebral canal and contains the nerve roots of the *cauda equina*, which arise inferior to the L1 vertebra. Specifically, this includes the anterior and posterior roots of the sacral and coccygeal nerves, the filum terminale and the lower part of the subarachnoid space down to the lower border of the S2 vertebra (Drake *et al*, 2005; Snell, 2008).

Lateral to this foramen are the paired superior articular processes (facets) which articulate with the inferior articular processes of the L5 vertebra, allowing weight transmission from the upper vertebrae at the lumbosacral junction (Davis, 1961; Pal,

1989; Mahato, 2010b). In the presence of rudimentary or abnormal orientation of the articular facets unilateral or bilaterally, lower back pain and spondylolisthesis is reported to be one of the results of disproportionate load transmission through the sacrum (Dai, 2001), resulting in compensatory secondary accessory lumbosacral articulations (Pal, 1989; Mahato, 2010b).

The associated vessels and nerves surround the sacrum

The blood supply to the vertebral bodies originates from three arteries: the nutrient artery forming the innermost supply, followed by metaphyseal arteries, and finally the arteries of the peripheral region of the vertebral body (Palastanga and Soames, 2012). These three arteries arise from the lateral sacral arteries (Figure 2.14), originating from the posterior branch of the internal iliac artery.

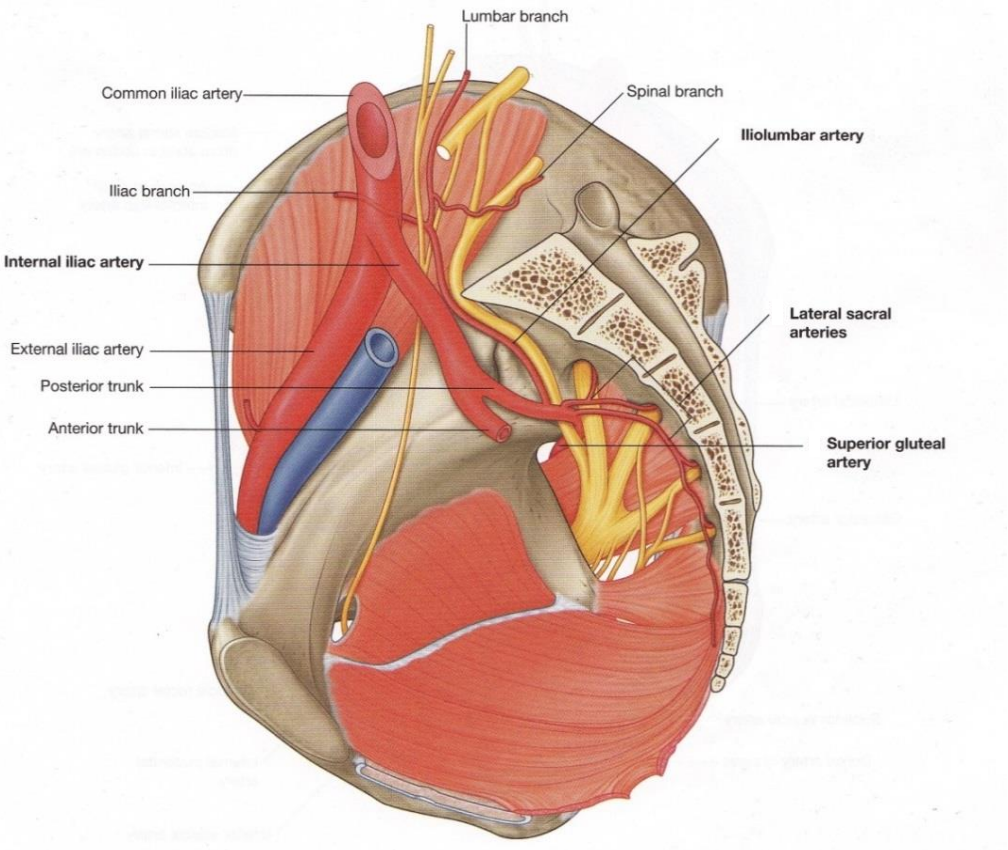

Figure 2.14: The lateral sacral artery from the posterior branch of the internal iliac artery (taken from Drake *et al*, 2005).

The lateral sacral arteries give three or four branches that descend in front of the sacral plexus, pass into the anterior sacral foramina to supply the sacrum, the anterior rami of the sacral spinal nerves, and muscles posterior to the sacrum. The lateral sacral artery anastomoses with the anterior and posterior spinal arteries that supply the spinal cord (Palastanga and Soames, 2012; Moore *et al*, 2013). In addition, the median sacral artery originates directly from the abdominal aorta, just superior to the bifurcation of the aorta at the L4 level, courses along the anterior surface of the sacrum to anastomose with the lateral sacral arteries to supply the sacrum and surrounding structures (Drake *et al*, 2005).

The sacral veins follow the course of the arteries, with the lateral sacral vein draining into the internal iliac vein which passes in front of the sacroiliac joint and joins the external iliac vein to form the common iliac vein (Snell, 2008). The median sacral veins coalesce to form a single vein joining the left common iliac vein or draining directly into the common iliac vein into the inferior vena cava.

The spinal veins form from the external and internal venous plexuses, outside and inside the vertebral canal, respectively. The veins of the external plexuses of the vertebral column and the sacrum form a complex plexus drained by posterior intercostal veins, lumbar and lateral sacral veins. The large, tortuous basivertebral veins from the sacral bodies drain into the internal vertebral plexus and finally anastomoses with the external venous plexus via the intervertebral veins (Snell, 2008; Moore *et al*, 2013). The basivertebral veins are the principal veins of the vertebral body (Bogduk, 2005).

The nerves surrounding the sacrum can be divided into two groups, the somatic plexus (sacral plexus and lumbosacral trunks) and the visceral plexus (paravertebral sympathetic chain and prevertebral plexus) (Figure 2.15).

The somatic plexus adjacent to the sacrum is mainly the sacral plexus and lies in front of the piriformis muscle and originates from the four anterior sacral foramina. The sacral plexus is formed by the anterior rami of the 4th and 5th lumbar nerves, and the anterior rami of the 1st – 4th sacral nerves. The 4th and 5th lumbar nerves unite to form the lumbosacral trunk. The sacral plexus and the lumbosacral trunk give branches to the sciatic nerve, the largest nerve in the human body to supply motor and sensory fibers to the posterior thigh, leg and foot, along with the pudendal, superior and inferior gluteal nerves, pelvic splanchnic nerves (visceral nerves) and nerves supplying the pelvic wall and pelvic floor muscles (Drake *et al*, 2005; Snell, 2008).

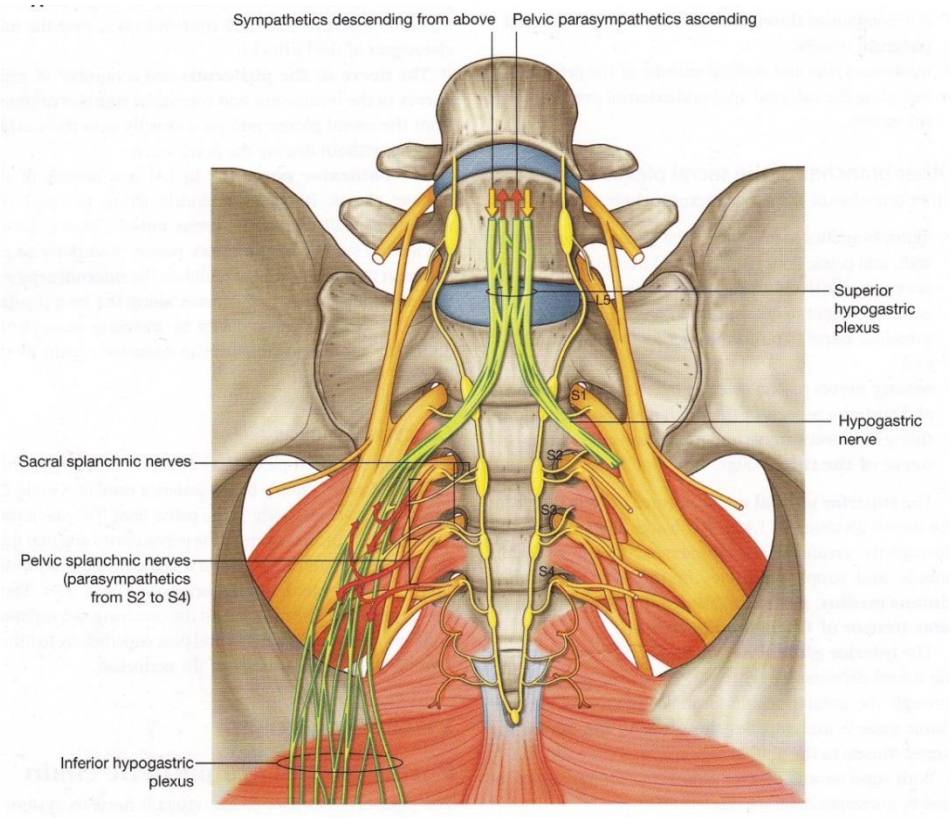

Figure 2.15: The anterior view of the somatic and visceral plexus at the posterior pelvic region (taken from Drake *et al*, 2005).

Embryology of the sacrum

The vertebrae originate from the sclerotomes (ventromedial) portion of the somites derived from paraxial mesoderm that lies on both sides of the neural tube. The first process of separating the paraxial mesoderm called 'initial segmentation' occurs in a craniocaudal direction between the 20th and 30th day of development and is coordinated with the development of segmented structures such as the peripheral spinal nerves, axial muscles and early blood vessels (Saga and Takeda, 2001; Sadler, 2010). The sclerotomes then migrate around the notochord and spinal cord to merge with the opposing somites (Sadler, 2010) to contribute to vertebral formation.

As development continues, a process called 'resegmentation' is said to occur (Figure 2.16), where the cranial half of each sclerotome fuses with the adjacent caudal half of the adjacent sclerotome forming a vertebra and bringing together the intersegmented muscles from the same somites (Huang *et al*, 2000; Saga and Takeda, 2001; Sadler, 2010). Resegmentation is a crucial process that produces movement of the vertebral column (Huang *et al*, 2000).

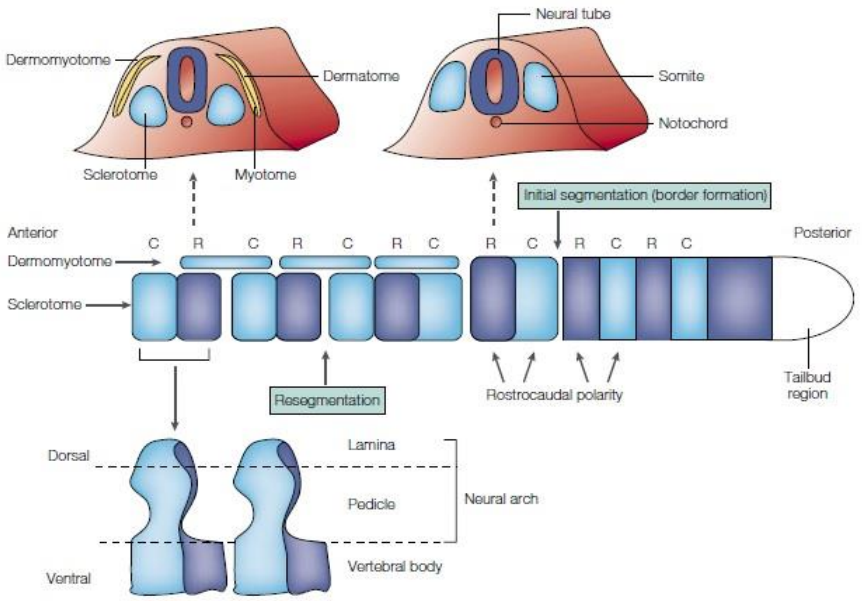

Figure 2.16: The initial segmentation of the paraxial mesoderm and resegmentation of the upper and lower halves (rostral and caudal) of two successive sclerotomes forming a vertebra (taken from Saga and Takeda, 2001).

Between 6-7 post-ovulatory weeks and the end of fetal life, the length of the vertebral column remains constant at around 2/3rd of crown-rump length. At the end of the embryonic period proper, approximately 12 weeks post-ovulatory, a typical cartilaginous vertebra is formed which consists of a centrum, two half neural arches with pedicles, articular and transverse processes (O'Rahilly *et al,* 1980). Although almost all of the vertebrae share these similar features, there are some differences in the pattern of the vertebrae in the five regions, regulated by the Homeobox (HOX) genes which play an important role in regulating the specification of regional identity of the hindbrain and the vertebral column (Wellik, 2007; Alexander *et al,* 2009).

Formation of each of the individual vertebrae depends on the successful expression of their unique HOX codes, described as HOXA, HOXB, HOXC and HOXD along the HOX clusters of the 3' end to the 5' end (Alexander *et al*, 2009; Sadler, 2010). Mutation of the HOX genes, either by failure or overexpression of this gene family can lead to axial skeletal abnormalities such as vertebral dysmorphogenesis and sacral agenesis (Hagan *et al*, 2000).

Following the establishment of the segmented axial skeleton morphology around the end of the first embryonic month (Sadler, 2010), the sacrum is first found as a definitive cartilaginous unit at the end of the embryonic period proper (12 weeks post-ovulatory) with additional alar elements that are absent in the lumbar region (O'Rahilly *et al*, 1990). O'Rahilly *et al.* (1980) found that fusion of these cartilaginous sacral elements started during Carnegie stage 18, around 44-48 days post-ovulatory, and all 5 sacral elements were involved in fusion in Carnegie stage 21 (53-54 days post-ovulatory).

Endochondral ossification of the cartilaginous sacral vertebrae begins with approximately 21 primary ossification centres at 3-6 fetal months (Francis, 1951; Fazekas and Kosa, 1978) and continues until birth (Scheuer and Black, 2000). It

commences as five primary ossification centres at the centrum, paired neural arches and paired lateral (costal) elements in the S1-S3 vertebrae, and only the centrum and the neural arches in the S4-S5 vertebrae, although this may vary between individuals (Handy, 1854; Frazer, 1965).

The shape of the centrum is concave anteriorly and wider than the posterior part. The centra for S1 and S2 have two articular facets on both of their lateral surfaces. The anterior articular facet will articulate with the lateral (costal) element and the posterior articular facet with the neural arch. There is limited evidence of lateral elements in S3-S5 vertebrae, and if they are present, they are only very small-rounded bones (Scheuer and Black, 2000).

These separated osseous components fuse within each individual vertebral level around 2 – 6 years forming 5 separate sacral vertebrae. The neural arch and lateral elements fuse together before they join with the centrum and the more distal elements fuse first (Francis, 1951; Frazer, 1965). The auricular surface of the sacrum is contained in the alar region of the bone (O'Rahilly *et al,* 1990).

At puberty, fusion of the five sacral vertebrae commences in a caudocranial direction by fusion of the laminae and the costal (alar) processes with each other. During this period, approximately 14 secondary ossification centres will appear, with 10 at the upper and lower borders of the 5 sacral bodies, 2 epiphyseal plates for the auricular surfaces and 2 epiphyseal plates for the lateral margin of the sacrum, below the auricular areas (Frazer, 1965). The final consolidation of the sacrum occurs rather late in life with S1 and S2 being last to fuse completely around 25 years (Scheuer and Black, 2000). It has been highlighted that the importance of bipedalism and weight transmission across the sacrum influences the completion of sacral fusion, which does not occur in the paraplegic patient as the region does not bear weight (Abitbol, 1987; Esses *et al,* 1991).

2.4 Sexual dimorphism in the sacrum

Sex determination from skeletal remains is of medico-legal importance in the identification of the deceased and is extremely difficult when the availability of the whole skeleton is absent. Traditionally, sex identification from the sacrum using non-metric evaluation has been customary among many anatomists, forensic anthropologists and forensic experts (Handy, 1854; Brothwell, 1981) which is supplemented by metric assessment in the determination of sexual dimorphism (Mishra *et al,* 2003; Tague, 2007; Baptist *et al*, 2008). Although the differences between a typical male and female sacrum are quite distinct, relying on one parameter alone for sex determination is deemed inadequate (Baptist *et al,* 2008; Mishra *et al*, 2003). Among the parameters used for sexing the sacrum are the maximum length and width of the bone (Figure 2.17), curved length, width of the S1 body and maximum length of the auricular surface. It was reported that the sacral index (maximum width/maximum length x 100), sacral width and width of the S1 body were found to be applicable in sex determination of the sacrum (Flander, 1978; Başaloğlu *et al*, 2005; Baptist *et al*, 2008).

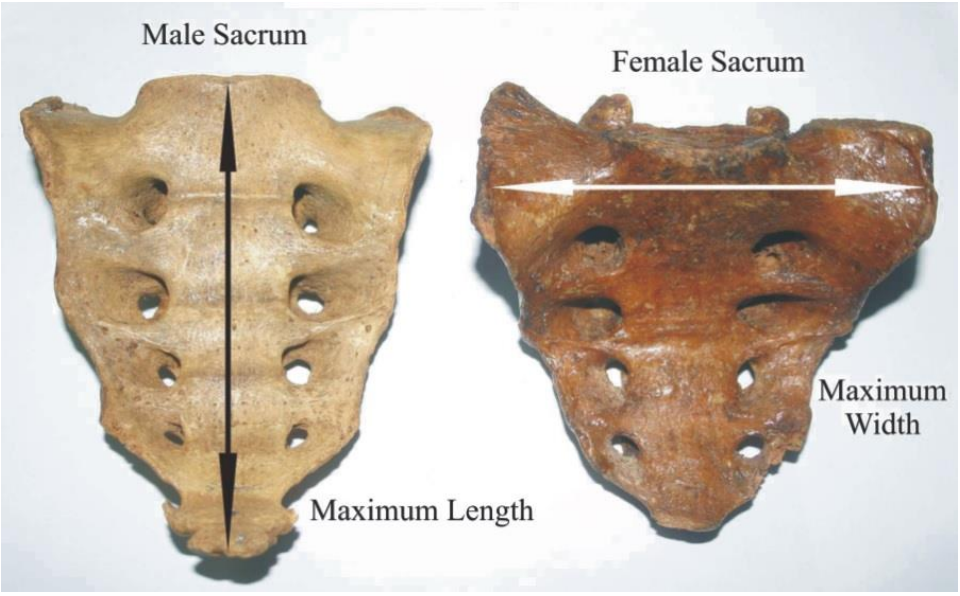

Figure 2.17: The maximum length in the male sacrum and the maximum width on the female sacrum (taken from Baptist *et al,* 2008).

Qualitatively, the male sacrum can be distinguished from the female sacrum by having a greater degree of anterior curvature (Martini *et al,* 2006) that is more pronounced and intrusive into the pelvic aperture. The female is less pronounced and less intrusive in order to reduce the risk of obstruction during childbirth as safe delivery of a baby through the pelvis is paramount. The male sacrum is generally longer and the width of the body is greater than the ala (Figure 2.18), while the width of the female sacral body is approximately equal to the width of its ala (Bass, 1987). These result in the male sacral alae appearing to be smaller with a larger body and female sacral alae appearing to be more similar in size.

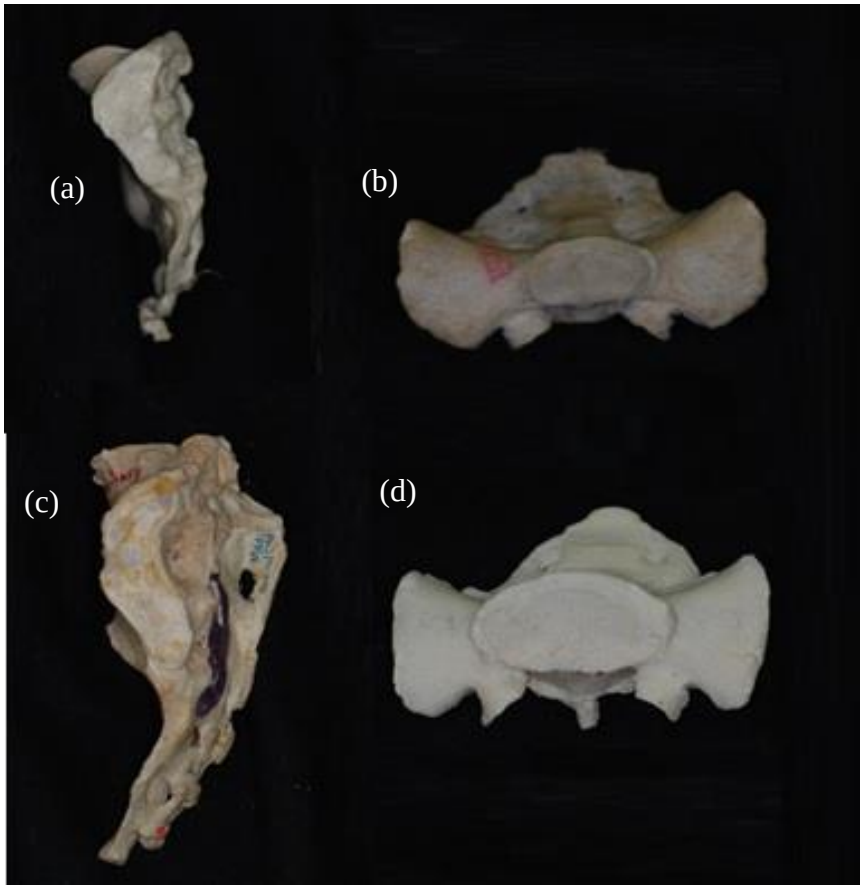

Figure 2.18: Four different sacra with two (a) & (b) females, and two (c) and (d) males. The width of S1 body of a (d) male sacrum is large compared to its corresponding alae, while the width of S1 body of a (b) female is similar or smaller than its alae.

The promontory of the male sacrum is very prominent compared to a female sacrum (Handy, 1854). The triangular shape of the sacrum in the male is narrower and more tapered than the female sacrum which is relatively broader at its base and appears shorter. In males, the auricular surface of the sacrum usually extends down to the middle of the third sacral segment, but in females, it usually involves only the first and second sacral segments (Brothwell, 1981). The pelvic angulation of the sacrum is at the 3rd sacral vertebra in the male, while in the female, it is often at the 4th sacral vertebral level (Brothwell, 1981).

The differences between the male and female sacrum are outlined in Figure 2.19.

Male	Female
• More curved	• More flat
• Bigger body, smaller alae	• Body 1/3, ala 1/3 (each)
• Longer	• Shorter
• Narrow	• Broad
• Curvature is more evenly distributed over the whole length	• Upper ½ - nearly flat, lower ½ - greatest amount of curvature
• Larger auricular surface (3rd sacral segment)	• Smaller auricular surface (2nd sacral segment)

Figure 2.19: The dimorphic features between male and female sacra.

The disparity between male and female sacra was found to be compatible with the discernible differences between male and female pelves mainly due to obstetrical imperatives (Handy, 1854; Caldwell and Moloy, 1938; Houghton, 1974; Finnegan, 1978; Brothwell, 1981; Drake *et al*, 2005; Moore *et al*, 2013).

However, despite the sexually dimorphic pattern exhibited by the sacrum (Flander, 1978; Tague, 2007), the sacral auricular area shows an insignificant degree of disparity between males and females with the sacroiliac joint lacking in sexual dimorphism (Ali and Maclaughlin, 1991; Sutter, 2003; Başaloğlu *et al*, 2005), although in some ethnic groups, there is reported to be some dimorphism (Mishra *et al*, 2003). The indistinguishability of the sexes from the auricular surface contradicts the reported sacral segments involved in sacroiliac articulation that depend on the forces transmitted through it (Bellamy *et al*, 1983; Mahato, 2011), which raises questions as to whether the axial loads may be bypassing the sacroiliac joint via the associated ligaments (DonTigny, 1985; Last, 1978; Sinnatamby, 2006; Vleeming *et al*, 2012, Moore *et al*; 2013).

2.5 Joints, ligaments and muscles associated with the sacrum

Stabilisation of the sacrum and the joints around it by efficient interactions of muscular, fascial and ligamentous interconnections are essential for effective load transmission from the axial skeleton to the pelvis and lower limbs (Vleeming *et al,* 2012). The sacrum alone is unstable since its lower end and the coccyx are prone to rotate posterosuperiorly by the superincumbent body weight exerted upon the lumbosacral and sacroiliac joints. Thus it needs integrated, interdependent and dynamic joints and soft tissue support structures to perform its function optimally (Snell, 2008).

Joints associated with sacrum

Among the joints directly associated with the sacrum are the lumbosacral joint superiorly, the sacrococcygeal joint inferiorly, the sacroiliac joints laterally and the zygapophyseal joints posteriorly (Drake *et al,* 2005; Moore *et al,* 2013). These joints are of paramount importance in balancing the function of the sacrum as a skeletal junction between the axial and appendicular skeleton.

The lumbosacral joint is formed by the articulation of the L5 and S1 vertebra with an interposed intervertebral disc between the bodies. The sacrum is tilted at around 130-160º to L5 forming the lumbosacral angle (Moore *et al*, 2013). The two zygapophyseal joints formed by the articulation between the inferior articular processes of L5 and the superior articular processes of S1 also form the posterior part of the lumbosacral joints (Drake *et al,* 2005).

One of the pivotal joints of the sacrum that bridge and unite the axial and appendicular skeleton is the sacroiliac joint. Further details on the sacroiliac joint are discussed in the next chapter (Chapter 3).

The sacrococcygeal joint is a secondary cartilaginous joint that is situated between the body of the coccyx (Co1) and the apex of the sacrum, with the cornua of Co1 joined to the sacral cornua by ligaments (Snell, 2008, Moore *et al*, 2013). The apex of the sacrum is convex and the body of the coccyx is concave, thereby forming a transversely-oriented joint (Palastanga and Soames, 2012), which usually synostoses with age (Scheuer and Black, 2000).

Ligaments associated with the sacrum

The numerous ligamentous structures (Figure 2.19) surrounding the sacrum serve to ensure that it is stabilised as the weight of the trunk thrusts downwards onto its base and consequently rotates the apex upwards. The shape of the sacrum contributes little to the stability of the vertically aligned sacroiliac joint (Snell, 2008). Superiorly, the sacrum is supported by the lumbosacral ligaments reinforcing the lumbosacral joint from the transverse process of L5 to the alae of the sacrum, and by the iliolumbar ligaments from the transverse process of L5 to the iliac crest (Drake *et al*, 2005).

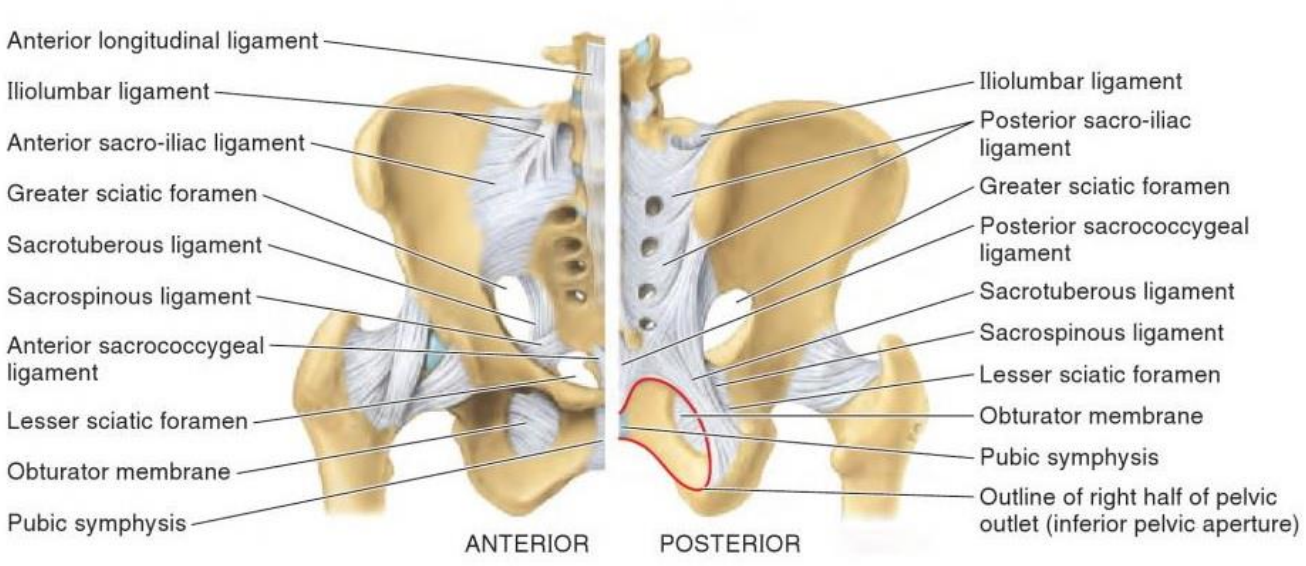

Figure 2.19: The ligamentous complex supporting the sacrum, ilium and the pelvis (taken from Moore *et al*, 2013).

The iliolumbar ligament is reported to play an important role in stabilising the sacroiliac ligament through its sacroiliac parts which blend with the interosseous sacroiliac ligaments (Pool-Goudzwaard *et al*, 2000).

Anteriorly, the sacrum and the sacroiliac joints are reinforced by the anterior longitudinal ligament and the anterior sacroiliac ligaments, respectively (Figure 2.20). The broad anterior longitudinal ligament is attached to the front and sides of the vertebral bodies and runs continuously from the base of the skull to the body of S2-S3 vertebrae (Drake *et al*, 2005).

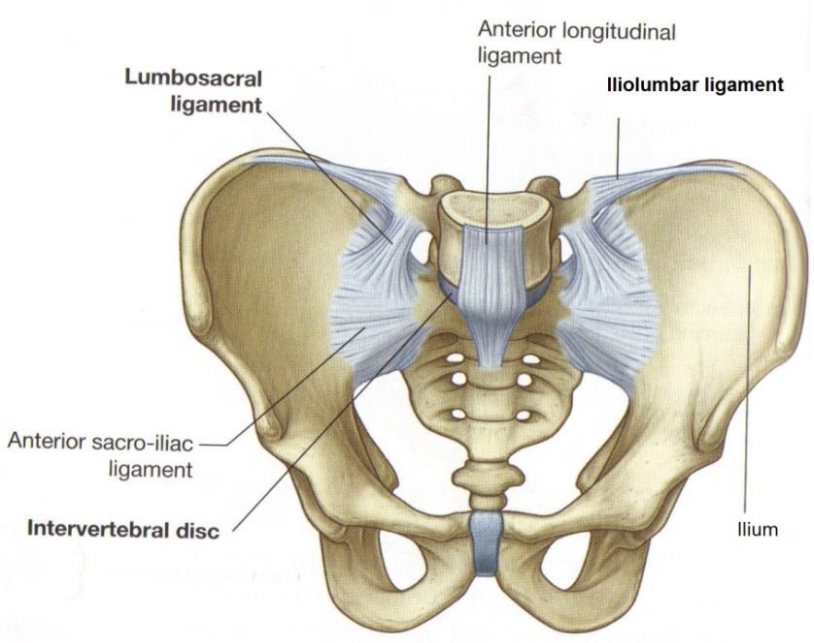

Figure 2.20: Anterior sacroiliac ligaments (taken from Drake *et al*, 2005).

The anterior sacroiliac ligament bridges the sacroiliac joint anteriorly and inferiorly, and inserts on the periosteal margins of the auricular surfaces of both the ilium and the sacrum, from S1-S3 vertebrae (Jaovisidha *et al*, 1996). The anterior sacroiliac ligaments (Figures 2.20-2.21) are thin and relatively weak, and resist the anterior movement of the sacral promontory, however they stretch easily and tear following even slight separation of the pubis (Albee, 1909; Sashin, 1930; Bowen and Cassidy, 1981, Alderink, 1991).

The thickness of the anterior sacroiliac ligament is around 2mm, covering the superior half and blending inferiorly with the joint capsule: thickening of the joint capsule is frequently seen in middle age and older individuals (Schunke, 1938; Bowen and Cassidy, 1981; Jaovisidha *et al*, 1996).

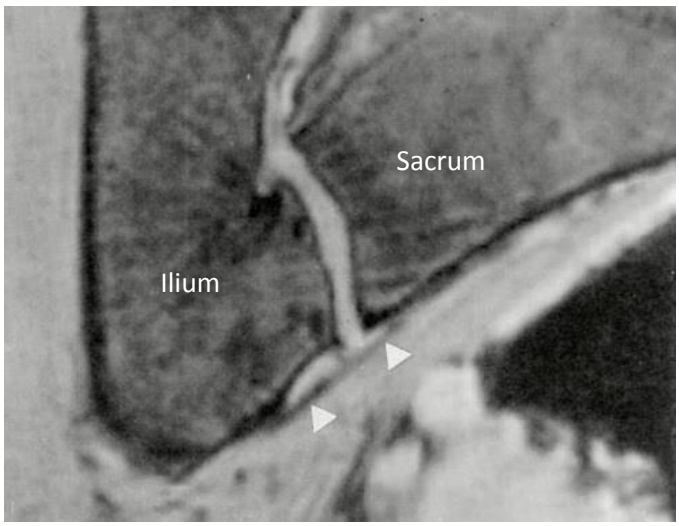

Figure 2.21: A 3D reconstructed coronal section MRI of the anterior sacroiliac ligament (arrowheads) traversing the sacroiliac joint (taken from Jaovisidha *et al*, 1996).

The weak anterior sacroiliac ligament manifests its fragility in pelvic ring fracture following external rotatory forces which leave the posterior sacroiliac complex intact: this is classified as open-book pelvic disruption (Tile, 1988).

The posterior region of the sacrum is occupied by a strong ligamentous complex (Figure 2.22) comprising the posterior longitudinal ligament on the posterior sacral bodies, interosseous ligaments, posterior sacroiliac ligaments (long and short fibers), and the small ligaments connecting L5 to S1 such as the supraspinous and interspinous ligaments as well as the ligamentum flavum (Drake *et al,* 2005, Snell, 2008; Moore *et al,* 2013). Of all of these, the interosseous and the posterior sacroiliac ligaments are the primary ligamentous structures holding and stabilizing the normal position of the sacrum and the sacroiliac joint in the pelvic ring – acting like a biomechanical bridge (Tile, 1988).

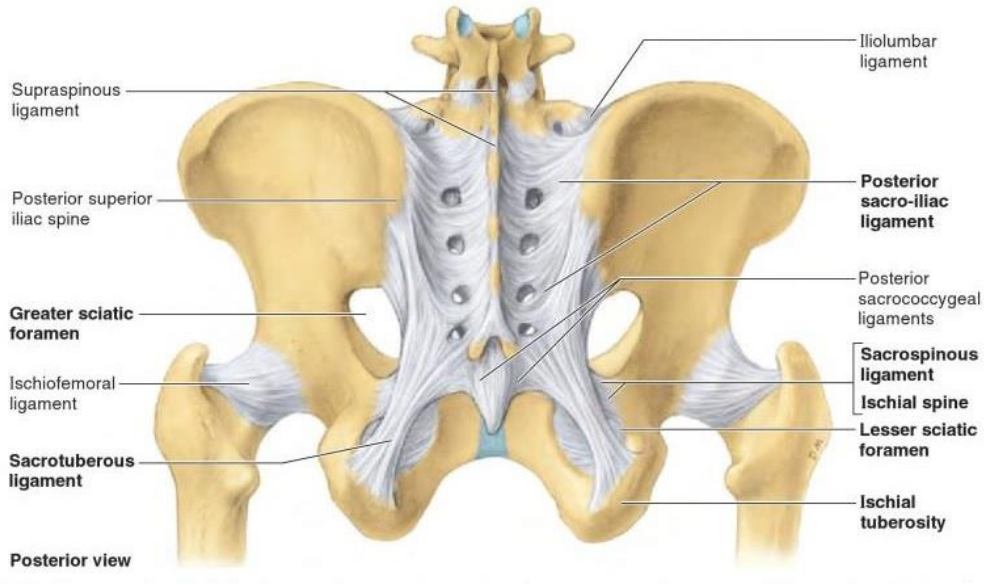

Figure 2.22: The ligamentous structure posterior to the sacrum (taken from Moore *et al*, 2013).

The posterior sacroiliac ligaments consist of long and short fibres and lie superficial to the interosseous ligaments. The short posterior sacroiliac and interosseous ligaments have common origins (lateral sacral crest, sacral and iliac tuberosities) and their fibres run obliquely upward and outward from the sacrum towards the ilium and along with body weight, compressing the sacrum downward with the ilia inward and medially, thus lock the two surfaces of the sacroiliac joint together (Moore *et al*, 2013).

The long posterior sacroiliac ligament is the longest and most superficial of the posterior ligamentous complex of the sacrum, with fibres running almost vertically downward from the posterior superior iliac spine to the 3rd and 4th transverse tubercles of the sacrum to resist backward movement of the sacral promontory in relation to the ilium (Vleeming *et al*, 1996; Palastanga and Soames, 2012) and blends with the sacrotuberous ligament at the ischial tuberosity (Figure 2.22) (Vleeming *et al*, 2002). This long ligament has a close anatomical relationship with the erector spinae muscles, posterior thoracolumbar fascia, and sacrotuberous ligament (the tuberoiliac part) (Vleeming *et al*, 1996).

The function of the long posterior sacroiliac ligament is antagonistic to that of the sacrotuberous ligament, with forward movement of the sacral promontory inducing relaxation of the long ligament while producing tension in the sacrotuberous ligament, and vice versa (Vleeming *et al*, 1996). In patients with low back pain, this long ligament should be included in the causative factors as this could indicate a spinal condition with sustained counternutation of the sacroiliac joint, as well as entrapment neuropathy as it provides pathways for the dorsal sacral rami (Vleeming *et al*, 1996; McGrath *et al*, 2009).

The strong interosseous ligament fill the roughened surface between the tuberosity of the sacrum and the ilium and lies deep within the posterior sacroiliac ligaments, like a suspension bridge connecting pillars at each end (Figure 2.23).

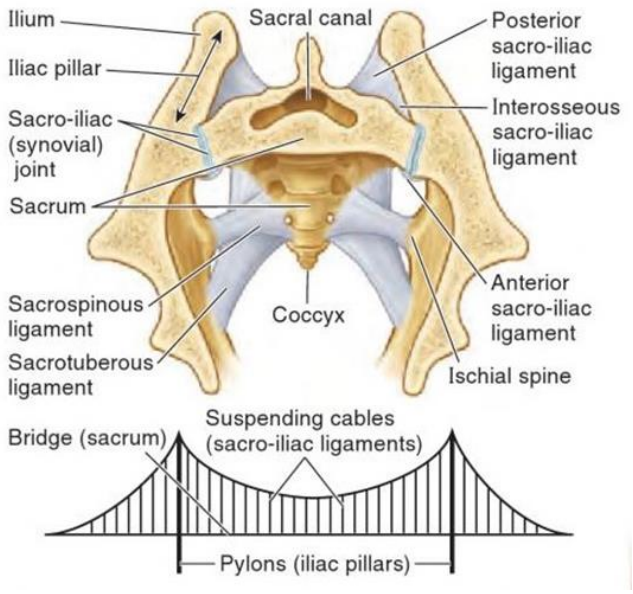

Figure 2.23: Anterosuperior view of the ligamentous structure in the region of the sacrum with comparison of a suspension bridge (taken from Moore *et al*, 2013).

It consists of superficial and deep parts: the superficial interosseous ligaments may blend with the posterior sacroiliac ligaments, and has been said to be the primary constraint to excess sacroiliac movement (Williams and Warwick, 1980; Alderink,

1991) and transferring the weight of the axial skeleton to the ilia (Moore *et al*, 2013). The interosseous ligaments never tear when the bones are forcibly separated; it detaches from one bone and remains fixed to the other, usually the sacrum (Albee, 1909; Sashin, 1930; Bowen and Cassidy, 1981).

In addition to the above ligaments, the sacrotuberous and sacrospinous ligaments contribute to the stability of the sacrum and the sacroiliac joints by preventing nutation of the sacrum (Figure 2.24) with respect to the innominate (Vleeming *et al,* 1989; Snell, 2008). The sacrotuberous ligament is a strong, flat, triangular ligament attached superiorly at the posterior superior iliac spine and blends with the long posterior sacroiliac ligaments, and to the lateral part of the sacrum below the auricular surface and to the superior coccyx. The expansive attachments pass downwards to attach on the medial surface of the ischial tuberosity (Moore *et al,* 2013).

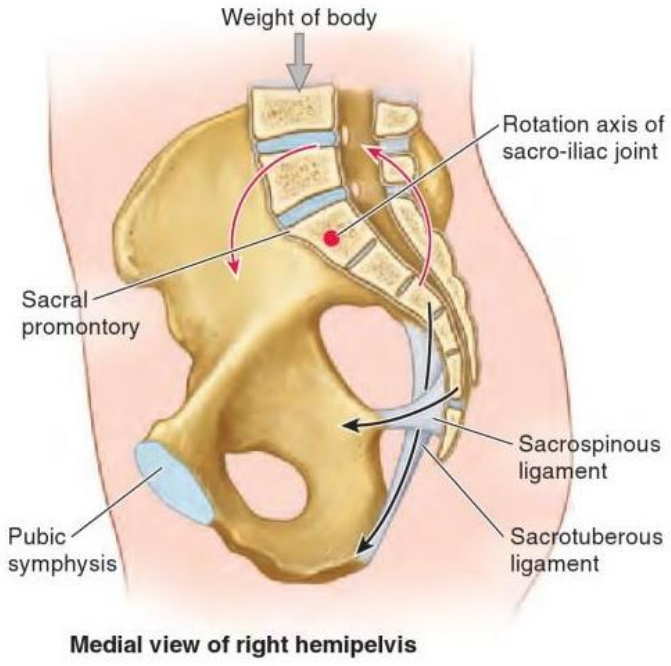

Figure 2.24: The point of forward movement of the sacral promontory which is prevented by the action of the sacrotuberous and sacrospinous ligaments (Modified from Moore *et al,* 2013).

Sinnatamby (2006) mentioned that the sacrotuberous ligament blends with the posterior sacroiliac ligament and binds the ischial tuberosity to both the sacrum and ilium. The sacrotuberous ligament resists both rotational (external and internal) and shearing forces in the vertical plane (Tile, 1988).

The sacrospinous ligament lies deep to the sacrotuberous ligament, with its broad base attached to the edge of the lower sacral and upper coccygeal segments and the narrow apex attached to the ischial spine (Snell, 2008). It resists external rotation of the hemipelvis (Tile, 1988). The sacrococcygeal ligaments are the intervening interosseous ligaments, consisting of lateral and posterior sacrococcygeal ligaments, attaching the inferior part of the sacrum to the coccyx (Figure 2.22).

The strong, self-tightening ligamentous complex surrounding the sacrum and sacroiliac joint stabilise and minimize every movement in this region for an optimal functional system (Gerlach and Lierse, 1992; Snijders *et al,* 1993; Pel *et al,* 2008; Vleeming *et al,* 2012): loosening of any of structure may produce local pain due to irritation to the lumbosacral trunk (Gerlach and Lierse, 1992). Brooke (1934) believed that there are three functions of the sacroiliac ligaments: (i) to transmit weight from the trunk to the lower limb, (ii) to act as a buffer to reduce the force transmitted from the lower limb, and (iii) to be involved in movement of the joint especially in pregnant women, children and in the higher apes. The ligaments will be altered with advancing age, becoming very thin and atrophic, and sometimes ossify to bone.

Muscles associated with the sacrum

Anterolateral to the sacrum

Piriformis: a triangular muscle that originates from the anterior surface of the sacrum between the four anterior sacral foramina, and inserts at the medial side of the superior border of the greater trochanter of the femur (Figure 2.25). It forms a large part of the posterolateral wall of the pelvic cavity and separates the greater sciatic foramen into two regions, one above and one below the muscle. Piriformis rotates the extended hip joint laterally and abducts the flexed hip joint.

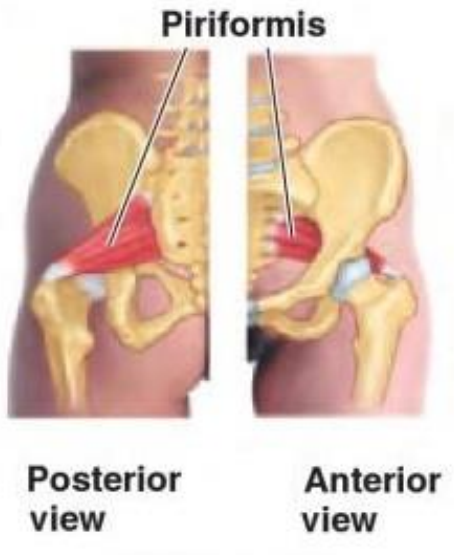

Figure 2.25: The origins and attachment of piriformis (taken from Moore *et al*, 2013).

Anteroinferior to the sacrum

Levator Ani muscles: especially pubococcygeus and iliococcygeus (Figure 2.26), and puborectalis (indirectly). The levator ani muscles form most of the pelvic diaphragm, support pelvic viscera and resist increases in intra-abdominal pressure (Moore *et al*, 2013).

1. Pubococcygeus: originates from the body of the pubis and passes posteriorly to attach along the midline as far posteriorly as the sacrum and coccyx.
2. Iliococcygeus: originates from the tendinous arch, a thickening of the fascia covering obturator internus and joins in the midline to form a raphe from the anal aperture to the coccyx.
3. Puborectalis: originates from the posterior aspect of the pubic bone and passes inferiorly on each side to form a sling around the terminal part of the rectum. It then attaches to the superior surface of the perineal membrane.

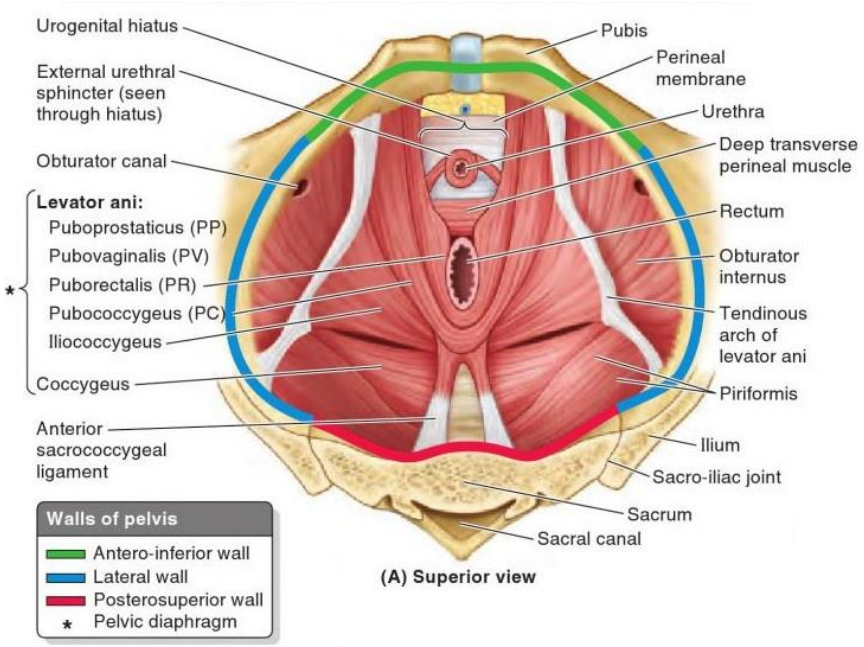

Figure 2.26: The levator ani muscles that attached to the anterior sacral curvature (taken from Moore *et al*, 2013).

Inferolateral to the sacrum

Coccygeus: Coccygeus is triangular in shape and originates from the lateral margins of the coccyx and sacrum (Figure 2.26), and attaches to the tip of the ischial spine. It flexes the coccyx and assists levator ani muscles to support the pelvic diaphragm (Snell, 2008). Posterior to the sacrum

Tendon of Intermediate layer of the Intrinsic Back Muscles (Iliocostalis, Longissimus):

The erector spinae muscles comprise the intermediate layer of intrinsic back muscles and consist of iliocostalis, longissimus and spinalis. Longissimus and iliocostalis (Figure 2.27) arise from a thick tendon attached to the sacrum, spinous processes of the lumbar and lower thoracic vertebrae and the iliac crest to the corresponding tubercles and angles of the ribs, cervical transverse processes and mastoid process of the temporal bone (Drake *et al*, 2005). The erector spinae muscles are the strong extensors of the vertebral column (Moore *et al*, 2013).

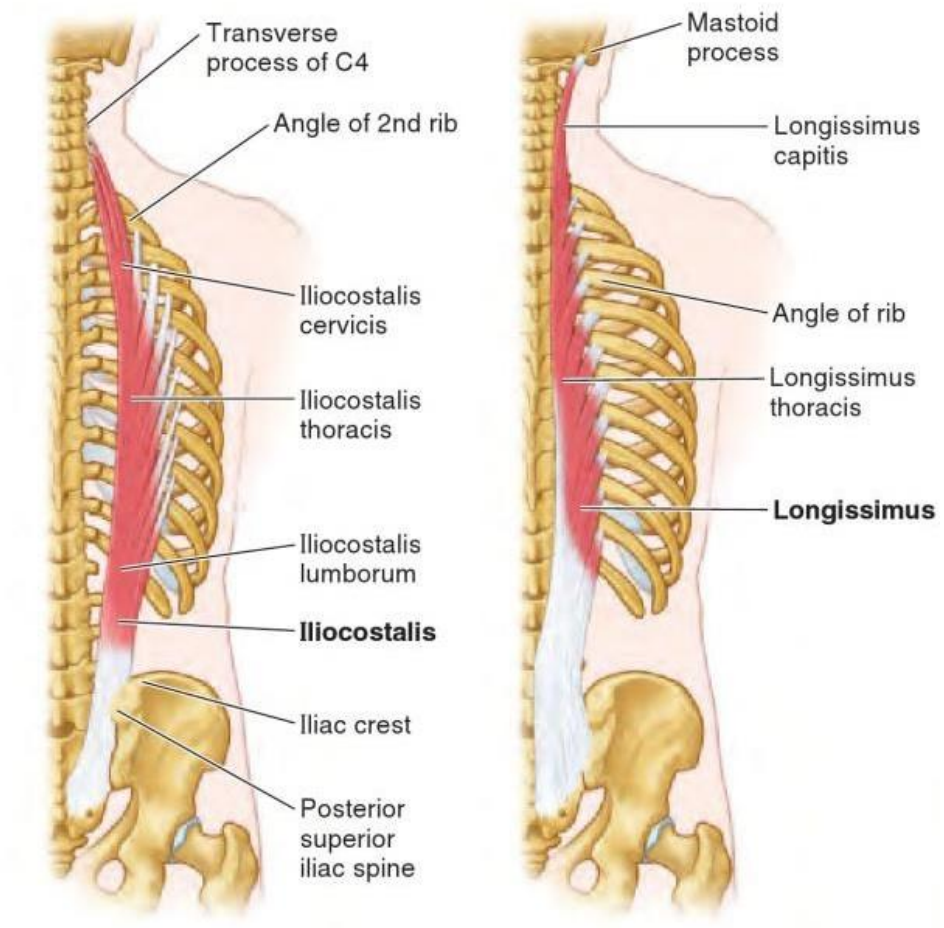

Figure 2.27: The iliocostalis and longissimus attachment to the sacrum (taken from Moore *et al*, 2013).

Deep Layer of Intrinsic Back Muscles (Multifidus): Multifidus is one of the deep layers of the intrinsic back muscles, apart from semispinalis and rotatores. It lies deep to the semispinalis and erector spinae muscles and originates from the posterior sacrum (Figure 2.28) and the erector spinae fascia, the mammillary processes of the lumbar vertebrae, transverse processes of the thoracic vertebrae and the articular processes of C4-C7 vertebrae. From this expansive origin the muscle attaches above to the spines of C1-L5. The action of multifidus is to extend and laterally flex the trunk, and rotate it to the left and right together with internal and external oblique, rotatores and semispinalis (Palastanga and Soames, 2012).

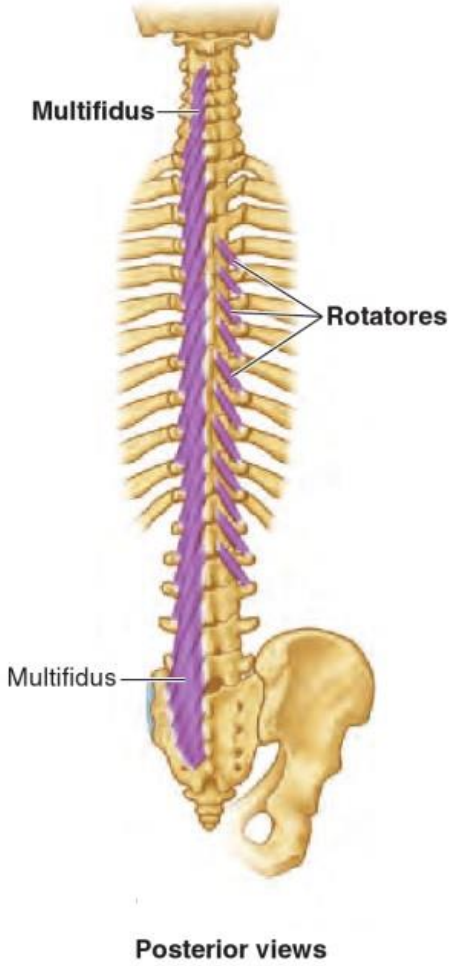

Figure 2.28: The attachment of the multifidus to the posterior sacrum (taken from Moore *et al*, 2013).

2.6 Anatomy and embryology of the ilium

Anatomy of the ilium

In humans, the ilium is the largest part of the innominate and present on both sides of the pelvis (Handy, 1854). It consists of two parts, the superior flat wing (ala) and the inferior body (Figure 2.29). The body of the ilium is fused with the ischium and the pubis at the acetabulum. A faint line that extends posteriorly from the margin of the acetabulum marks the fusion of the body of the ilium with the ischium. The iliopubic eminence, a small elevation located below the anterior inferior iliac spine, marks the fusion of the ilium with the pubis (Figure 2.29).

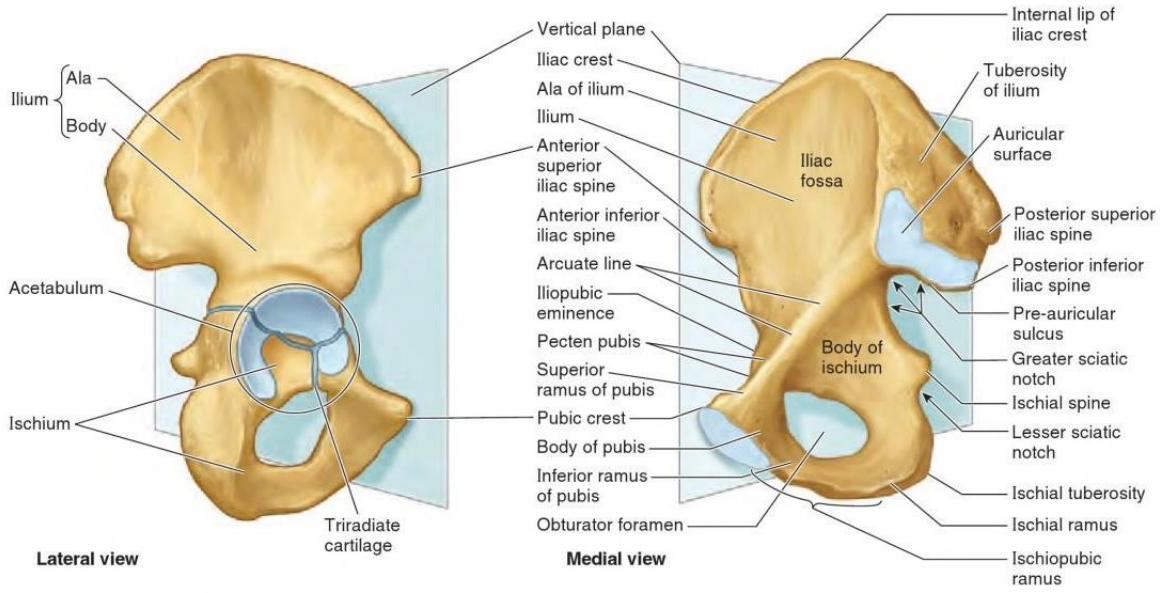

Figure 2.29: The lateral and medial view of the right innominate (taken from Moore *et al*, 2013).

The ilium has four borders, anterior, posterior, superior and inferior. The anterior border starts at the prominent anterior superior iliac spine, which can be palpated clinically, and marks the attachment of the inguinal ligament, tendon of sartorius and tensor fascia lata (Snell, 2008; Moore *et al*, 2013).

Superiorly, the ilium is bordered by the iliac crest, which is divided into outer and inner lips, the site of attachment of many abdominal muscles (White and Folkens, 2005). The iliac crest curves from anterior to posterior in the form of a sinuous band. The most posterior part of the iliac crest is thicker for the attachment of numerous posterior ligaments. The tubercle of the crest is a thickening or a prominent expansion of the outer lip approximately 5cm posterior to the anterior superior iliac spine (Drake *et al*, 2005, Moore *et al*, 2013). An imaginary line which joins the highest points of the two iliac crests is called the supracristal plane and passes through the spine of vertebra L4; a landmark used for identifying the vertebra (Moore *et al*, 2013).

The posterior border begins at the posterior superior iliac spine and extends inferiorly to the posterior inferior iliac spine. It then turns abruptly forward and joins the posterior border of the ischium leaving a notch, termed the greater sciatic notch (Figure 2.30), through which the sciatic nerve and various other structures passes.

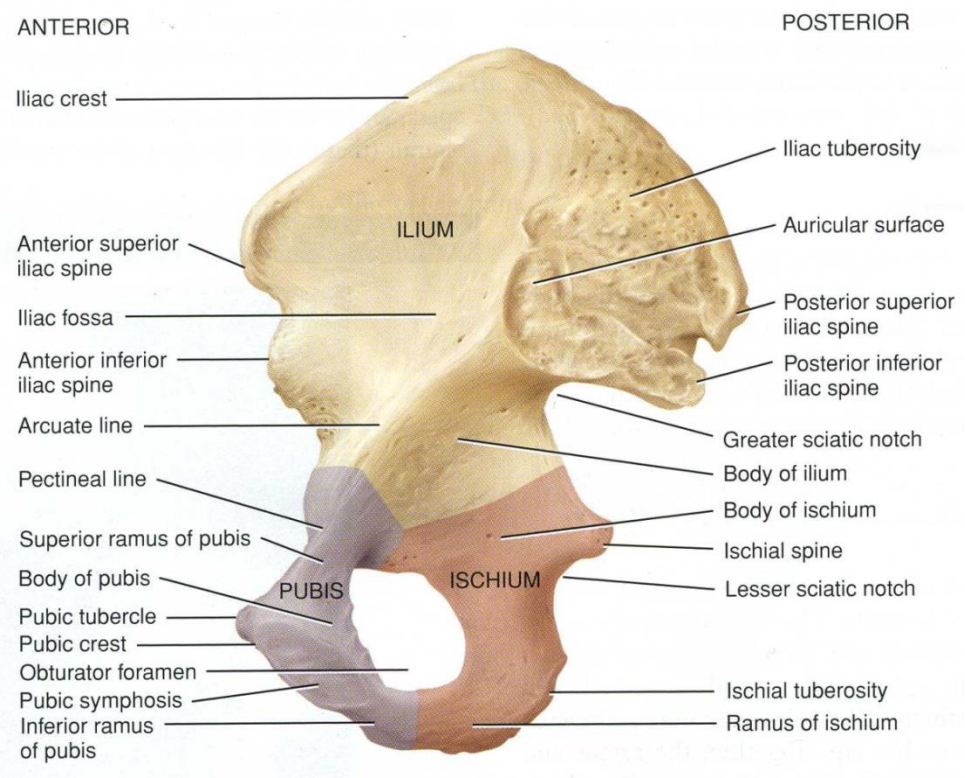

Figure 2.30: Right ilium, medial view (taken from Tortora and Nielsen, 2009).

The inferior border of a juvenile ilium forms the acetabulum and at puberty will fuse with the ischium posteroinferiorly and pubis anteroinferiorly.

The human ilium is a predominantly flat, but irregularly shaped bone with three surfaces: pelvic, gluteal and acetabular. The pelvic surface has a smooth anterior surface and a rougher posterior surface (Figure 2.31). The pelvic surface can be functionally divided into two distinct regions; a smooth anterior iliac fossa for the site of the principal nutrient foramen and the site of attachment of the iliacus muscle which are considered to be responsible for the initial ossification of the cortical shell (Delaere and Dhem, 1999). The rough and thickened posterior part contributes to the auricular and post-auricular surfaces of the ilium.

The auricular surface of the ilium is the site of articulation with the sacrum, forming the sacroiliac joint (Last, 1978). Projecting anterior and inferior to the auricular surface is the arcuate line of the ilium, which marks the border of the true pelvis with the false pelvis (Figure 2.31). The morphology of the auricular surface of the ilium has been investigated extensively to establish age at death in the adult (Lovejoy *et al*, 1985; Buckberry and Chamberlain, 2002; Igarashi *et al*, 2005; Mulhern and Jones, 2005). However, it has been shown that the auricular surface of the ilium has little to contribute to the establishment of the sex of an individual (Ali and Maclaughlin, 1991) due to minimal differences between the sexes, although some studies suggest that there may be some value in sex determination in subadult remains (Weaver, 1980; Mittler and Sheridan, 1992; Schutkowski, 1993).

The post-auricular surface of the ilium is represented by a roughened and tuberous area, functioning as a major site of ligamentous attachment for the strong interosseous sacroiliac ligament, the short posterior sacroiliac ligament (Weisl, 1954) and the sacroiliac part of the iliolumbar ligament, which is reported to be associated with

stabilisation of the sacroiliac joint (Pool-Goudzwaard *et al,* 2001). The morphology of this area is heavily dictated by anatomical interactions between these tightly bound ligaments and the adjoining bones, with accessory sacroiliac articulations occurring in this region (O'Rahilly *et al,* 1969).

The gluteal surface of the ilium projects laterally and posteriorly and lies below the iliac crest. It is marked by three lines; the inferior, anterior and posterior gluteal lines (Figure 2.31). These lines are important landmarks for the attachment of the gluteal muscles.

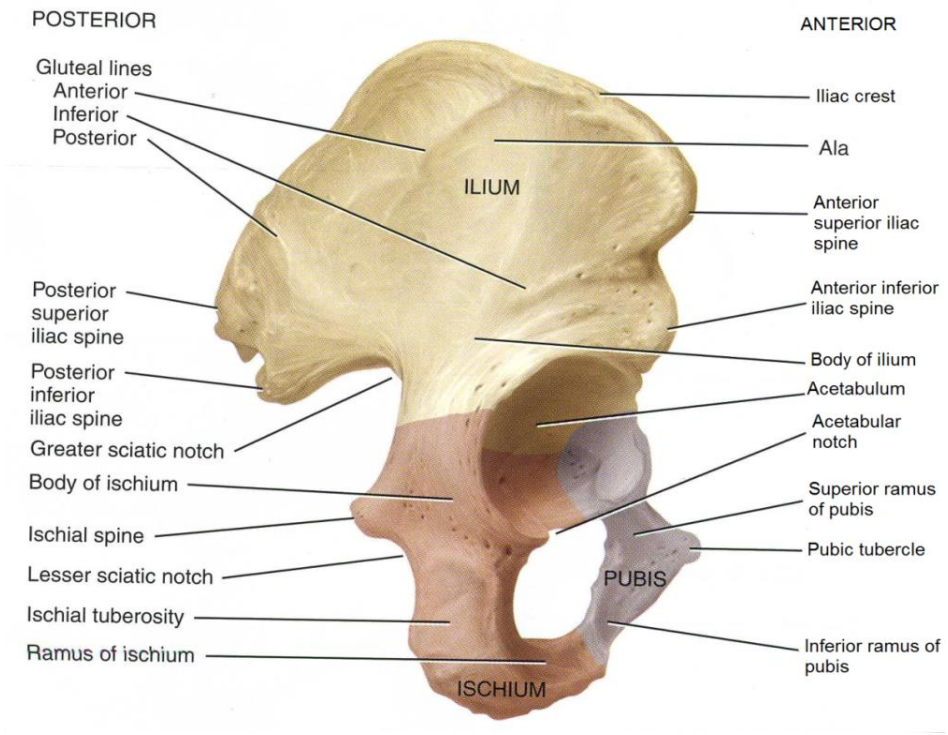

Figure 2.31: Right ilium, lateral view (taken from Tortora and Nielsen, 2009).

The inferior gluteal line, which is the most anterior, is located just above the anterior inferior iliac spine and passes posteroinferiorly 2-3 cm above the acetabulum, towards the apex of the greater sciatic notch (Figure 2.31). Rectus femoris attaches to the anterior inferior iliac spine and to a roughened area of bone between the inferior gluteal

line and the superior margin of the acetabulum (Snell, 2008). The anterior gluteal line starts at the outer lip of the iliac crest, approximately 2 cm behind the anterior superior iliac spine, curves at the tubercle of the iliac crest and arches downward across the gluteal surface towards the greater sciatic notch (Figure 2.31). Gluteus minimus originates from the area between the anterior and inferior gluteal lines.

The posterior gluteal line begins about 5cm above the posterior superior iliac spine, and descends almost vertically to the front of the posterior inferior iliac spine (Figure 2.31). Gluteus medius attaches to the bone between the anterior and posterior gluteal lines, while gluteus maximus attaches posterior to the posterior gluteal line and to the posterior surface of the lower sacrum (Drake *et al*, 2005).

The associated vessels and nerves surround the ilium

An abundance of neurovascular networks lie extraperitoneally against the ilium and the posterior pelvic wall, confirmed by the high mortality rate reported due to massive haemorrhage in pelvic trauma patients (Cook *et al*, 2002; Gillespie, 2009). The major arterial supply to the pelvis arises from the external and internal iliac arteries, which originate from the common iliac artery (Figure 2.32) at the L5/S1 level (Drake *et al*, 2005), as a result of bifurcation of the abdominal aorta at L4.

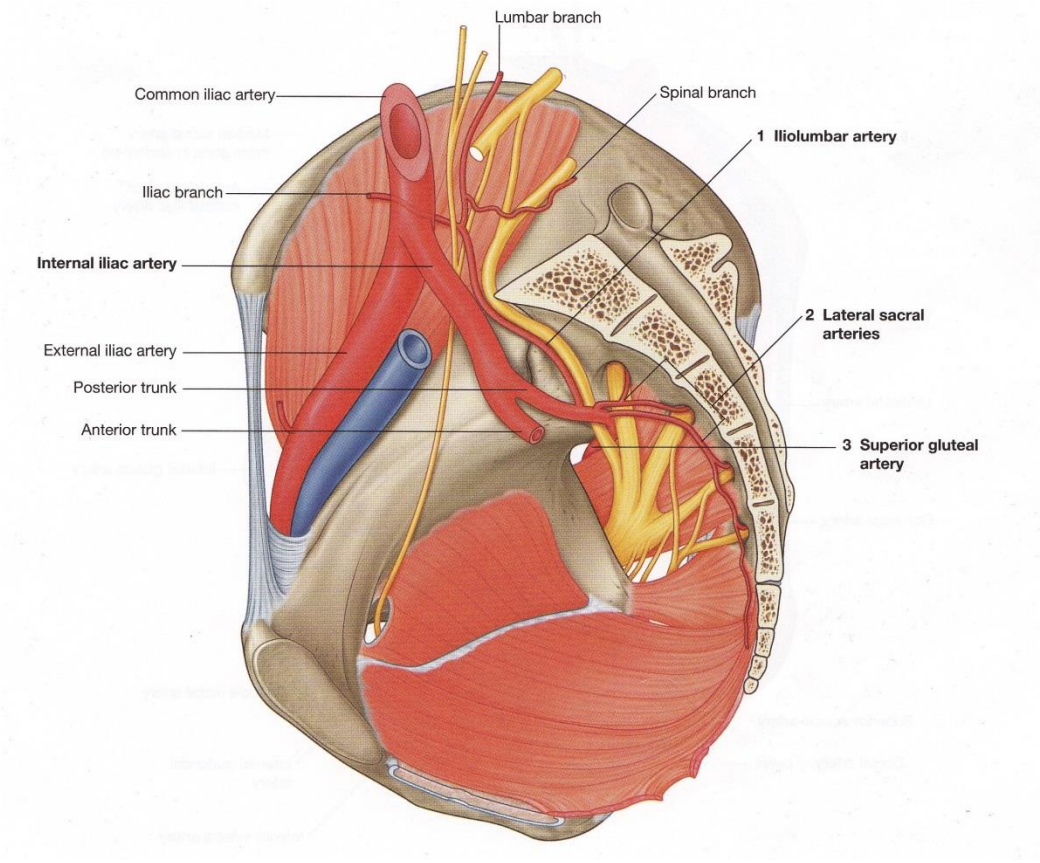

Figure 2.32: The bifurcation of the common iliac artery which is closely related to the ilium and the pelvic region (taken from Drake *et al*, 2005).

The main arterial supply for the ilium is the nutrient artery, a branch of the obturator artery from the anterior division of the internal iliac artery, and ilioumbar arthery from its posterior division (Moore *et al*, 2013). The nutrient artery enters the cortical bone at the region superior to the greater sciatic notch to invade the trabecular cartilaginous anlage: it bifurcates into superior and inferior branches, which influence the initiation of osteogenic formation of the bone (Trueta, 1963; Ortega *et al*, 2004; Cunningham and Black, 2010).

The main venous drainage of the pelvic regions is from the internal iliac vein, which drains from tributaries that correspond to branches of the internal iliac arteries and pass

upward in front of the sacroiliac joint to join the external iliac veins at the L4-L5 vertebrae to form the common iliac veins that drain into the inferior vena cava.

The nerve bundles associated with the ilium have been largely discussed in section 2.3 in this chapter in the pelvic nerves of the sacrum. However, it is important to note the pathways of the major nerves in relation to the ilium, such as the lumbosacral trunk and most of the branches of the sacral plexus pass inferiorly to the ilium, specifically at the greater sciatic foramen to form the sciatic and pudendal nerves (Snell, 2008).

Embryology of the ilium

The ilium originates from the parietal layer of the lateral plate mesoderm (Figure 2.33). It is one of the derivatives of the mesodermal layer, which also forms the paraxial and intermediate mesoderm. As the paraxial mesoderm differentiates to form the vertebral column, and the intermediate mesoderm the urogenital system, the lateral plate mesoderm divides into parietal (somatic) and visceral (splanchnic) layers (Sadler, 2010).

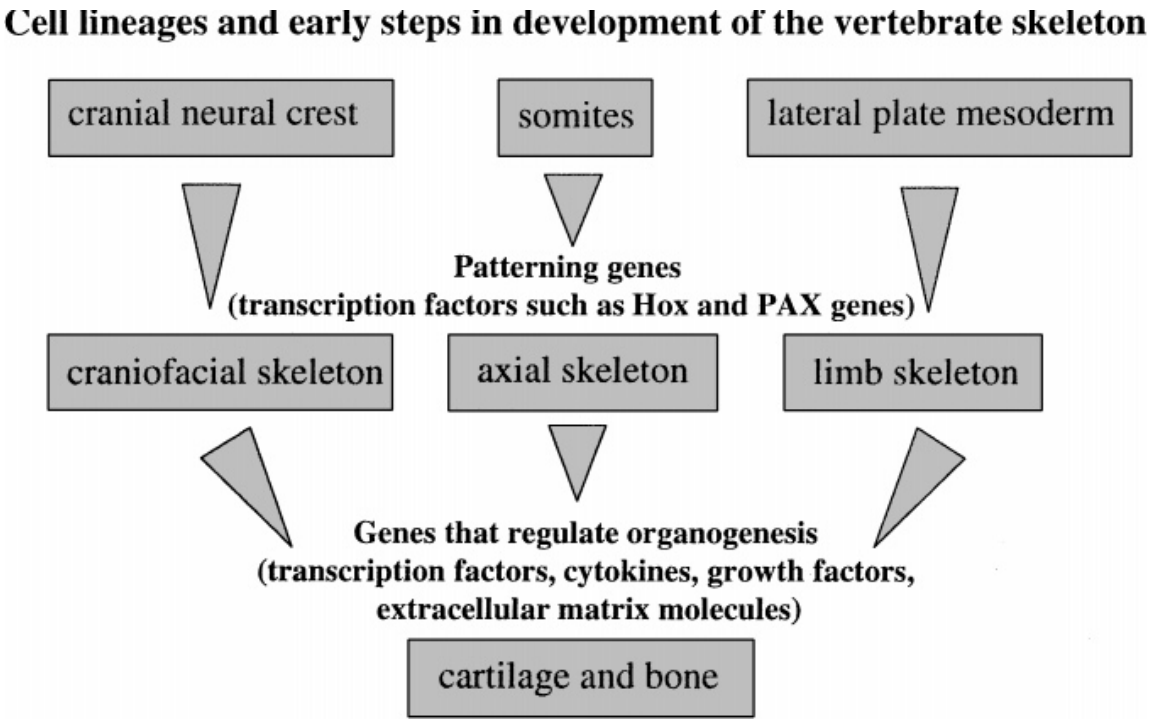

Figure 2.33: Summary of the gene pattern regulating neural crest cells, somites (paraxial mesoderm), and lateral plate mesoderm during organogenesis (cartilage and bone) (taken from Olsen *et al*, 2000).

The visceral layer of the lateral plate mesoderm forms the wall of the gastrointestinal tube. The parietal layer of the lateral plate mesoderm differentiates into the dermis of the skin in the body wall and limbs, and the bones and connective tissue of the pelvic and shoulder girdles, limbs and sternum (Sadler, 2010).

At the end of fourth week of development, growth of the hindlimb buds starts to appear 1-2 days later than the forelimb buds, in a proximodistal sequence regulated by Homeobox gene expression, Shh (Sonic hedgehog) and TBX4 and FGF10 (hindlimb) secreted by lateral plate mesoderm cells (Johnson and Tabin, 1997; Sekine *et al*, 1999; Takeuchi *et al*, 2003; Sadler, 2010). By six to eight weeks of development, the bone-forming capacity of the mesenchymal cells of the parietal layer of lateral plate mesoderm undergo condensation to ultimately form a hyaline cartilage model (chondrification) for the bones of the lower limbs and pelvis, with the ilium being the first visible skeletal element of the pelvic girdle, regulated by the ectodermal and paraxial mesodermal signals and SOX9 genes (Olsen *et al*, 2000; Malashichev *et al*, 2008).

Once chondrification is complete at around eight weeks of development, the primary centre of ossification for the ilium appears just superior to the greater sciatic notch at the end of the second and beginning of the third intrauterine months (Laurenson, 1964). This intramembranous ossification subsequently proceeds by periosteal means, depositing bone in a fan-like manner on both the gluteal and pelvic cortical surfaces of the cartilaginous anlage of the ilium (Delaere *et al*, 1992). The internal cancellous structure, which is formed by the endochondral ossification, does not occur until invasion of the cortical shell by nutrient vessels allowing the entry of osteoblastic precursors. This endochondral ossification adapts to the space occupying demands of the vascular supply of the ilium (Cunningham and Black, 2010).

At puberty, the ilium undergoes further ossification at its secondary centre. This process occurs at the iliac crest and acetabular region (Frazer, 1965). The iliac crest ossifies from two different centres: the anterior superior iliac spine and posterior superior iliac spine which expand towards the centre of the crest. The epiphysis of the anterior

inferior iliac spine commences ossification earlier than that of the posterior superior iliac spine.

The acetabulum is the meeting point for the innominate as secondary ossification centres appear here at puberty. Medially, the triradiate anlage is formed by the ossifying bones, growth cartilage and epiphyseal cartilage represented by the ilium, ischium and pubis, while the lateral part is the cup-shaped articular cartilage which is deficient inferiorly (Harrison, 1958; Scheuer and Black, 2000). The cup-shaped acetabulum is formed by the ilium that constitutes the superior two-fifths, the ischium inferoposterior two-fifths and the pubis inferoanterior one-fifth (Handy, 1854).

In the adult, the ilium is reported to play a significant role in load-transfer during bipedal movement, with the forces generated during locomotion actively contributing to the morphology of the bone (DonTigny, 1985; Aiello and Dean, 1990; Dalstra and Huiskes, 1995). In the quadrupedal ape pelvis, the iliac auricular surface and the iliac tuberosity are much smaller as a direct result of minimal body weight support through the pelvis compared to humans (Aiello and Dean, 1990). Interestingly, recent studies investigating the cortical and trabecular morphology of the neonatal ilium suggest further additional factors that may contribute to its development (Cunningham and Black, 2009a; 2009b; 2009c; 2010) including genetic, vascular and neurogenic influences, retrograde forces from limb movement and metaphyseal “drivers” for the vascularisation of the ilium.

2.7 Embryological comparison between the sacrum and the ilium

The embryological origins and development of the sacrum and ilium are distinct, even though together, they form a large and important diarthrodial joint via their auricular parts. To begin with, both the sacrum and the ilium originate from different mesodermal germinal layers: the sacrum from the paraxial mesoderm and the ilium develop from the parietal layer of the lateral plate mesoderm (Mundlos and Olsen, 1997; Olsen *et al*, 2000; Sadler, 2010). This is in contrast to all other major diarthrodial joints in the human body such as the hip, knee, shoulder and elbow joints which all share the common origin of lateral plate mesodermic germinal layer (Johnson and Tabin, 1997; Tickle, 2003). The only other place in the body where the paraxial and lateral plate mesoderm coincide is at the chondrosternal junction (Carter and Loewi, 1962; Ogden *et al*, 1979; Scheuer and Black, 2000; Sadler, 2010) with the rib cartilages being somatic in origin and the sternum originating from lateral plate mesoderm.

Salsabili and Hogg (1991) studied 13 human embryos and fetuses ranging from 50 postovulatory days (21mm crown-rump length) to 20 postovulatory weeks (185mm crown-rump length): they reported that the ilium ossified earlier than the sacrum. The formation of bone tissue in the ilium was detected in 8.5 week, 9 week and 12 week fetuses, while the sacrum remained entirely cartilaginous until 14 fetal weeks when the centres of ossification are established in the centra and arches of the sacral vertebrae. These observations support those of Brooke (1924) who reported early ossification of the ilium, with the sacrum still being cartilaginous in a five month fetus. Between the ossifying ilium and the chondrogenic sacrum, an area of undifferentiated mesenchymal tissue with high cellular activity is seen, which later becomes the sacroiliac joint (Brooke, 1924).

The early ossification of the ilium compared to its sacral counterpart may suggest a relationship with the early degenerative changes shown by the iliac auricular cartilage when compared to the sacral auricular cartilage (Macdonald and Hunt, 1952; Bowen and Cassidy, 1981, Kampen and Tillmann, 1998), with the joint as a whole starting to show degeneration early around the third decade of life, most commonly in males (Sashin, 1930; Schunke, 1938). The cranial limb is more commonly affected by synostosis and this may be related to its function in transmitting forces in an erect position (Valojerdy *et al*, 1989).

While the ilium is persistently reported to ossify earlier than the sacrum, the sacral auricular cartilage is reported to be consistently thicker than that of the ilium (Albee, 1909; Sashin, 1930; Schunke, 1938; Macdonald and Hunt, 1952; Carter and Loewi, 1962; Bowen and Cassidy, 1981; Vleeming *et al*, 1989). Additionally, dissimilarity in the appearance of both joint surfaces was of particular interest due to consistent findings in the literature with the iliac auricular cartilage reported to be bluish, dull-looking, striated and fibrocartilaginous in nature, while the sacral counterpart was seen as smooth, glistening and creamy with a hyaline origin (Brooke, 1924; Carter and Loewi, 1962; Bowen and Cassidy, 1981). The differences in the nature of the auricular cartilage of the ilium (fibrocartilaginous) and sacrum (hyaline), the thickness and appearance, along with the progressive changes in the sacroiliac joint shows that it is not a typical large synovial joint of the human body, but that it is also poorly understood. The characteristics of the sacroiliac joint will be discussed in the next chapter (Chapter 3).

2.8 Joints, ligaments and muscles associated with the ilium

Joints associated with the ilium

Joints that are directly associated with the ilium are the sacroiliac joint and the hip joint. Together with the symphysis pubis, these three joints make up the entire human pelvic articulations. As the sacroiliac joint will be discussed in detail in the next chapter (Chapter 3), the hip joint will receive a review here.

The hip joint is a synovial, multiaxial ball and socket joint between the acetabulum of the pelvic bone and head of the femur (Figure 2.34). It is designed for stability and weightbearing during stance and mobilisation, and to balance between stability and flexibility. The articular surfaces of the hip joint are formed by the spherical head of femur and the lunate surface of the acetabulum, both of which are lined by hyaline cartilage (Drake *et al*, 2005). The circumferential joint capsule is reinforced by the fibrous acetabular labrum that bridges the acetabular notch inferiorly as the transverse acetabular ligament, converting the notch into a foramen.

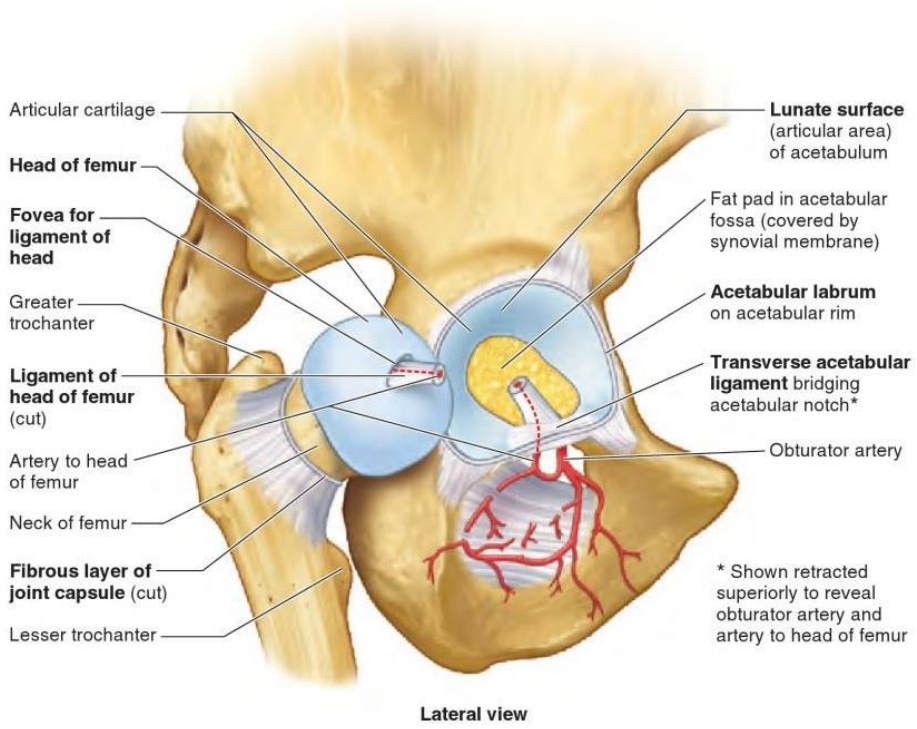

Figure 2.34: The hip joint from lateral view (taken from Moore *et al*, 2013).

Ligaments associated with ilium

The ilium gives attachment to numerous ligaments on its posteromedial aspect, including the anterior and posterior sacroiliac, interosseous, iliolumbar, sacrotuberous and sacrospinous ligaments which have been addressed in the earlier section of this chapter. However, only the inguinal ligament (Figure 2.35) is found to be directly attached to the anterolateral part the ilium, suggesting that the anterior pelvic wall may be extremely stable by virtue of the symphysis pubis, while posteriorly the unstable sacroiliac joint relies upon the abundant ligamentous complex, which are the strongest in the body (Tile, 1988; Pel *et al*, 2008, Vleeming *et al*, 2012). Additionally, it may also be due to the most of the body weight being transmitted at the posterior region of the pelvis, and not anteriorly.

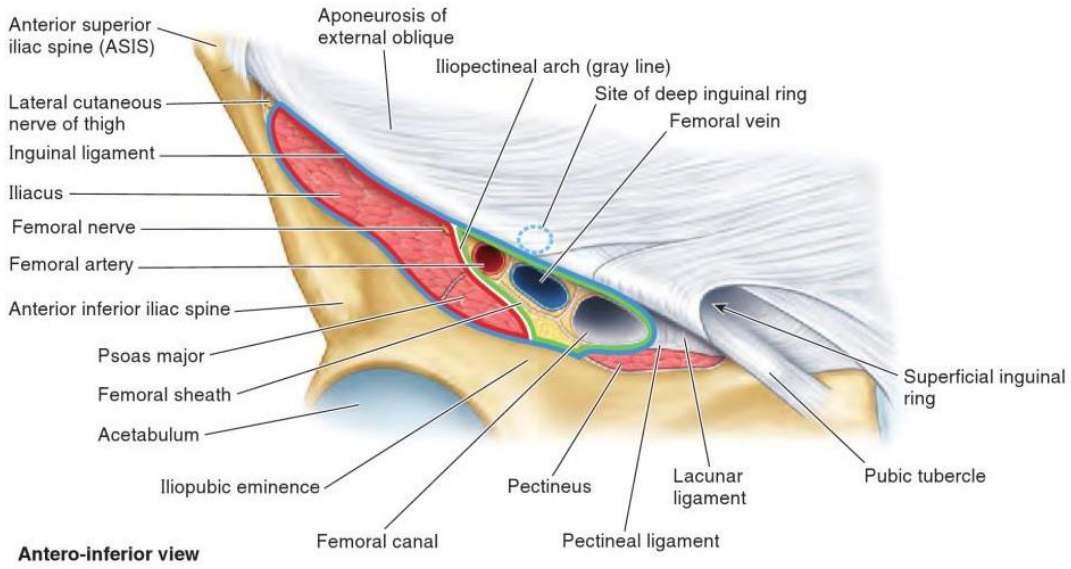

Figure 2.35: The inguinal ligament from anteroinferior view (taken from Moore *et al*, 2013).

Muscles associated with the ilium

The ilium gives attachments for several muscles on its pelvic and gluteal surfaces. Anteromedially, the iliacus muscle (Figure 2.36) attaches from the superior two thirds of the iliac fossa, ala of the sacrum and the anterior sacroiliac ligament to the lesser trochanter of the femur along with the psoas major tendon. Although psoas major does not originate from the ilium, it is attached along with the iliacus muscle on the femur, and together these two muscles flex the thigh and stabilise the hip joint. Quadratus lumborum originates from the L5 transverse process, iliolumbar ligament and iliac crest, and inserts into the tips of the lumbar transverse processes and inferior border of rib 12 (Moore *et al*, 2013).

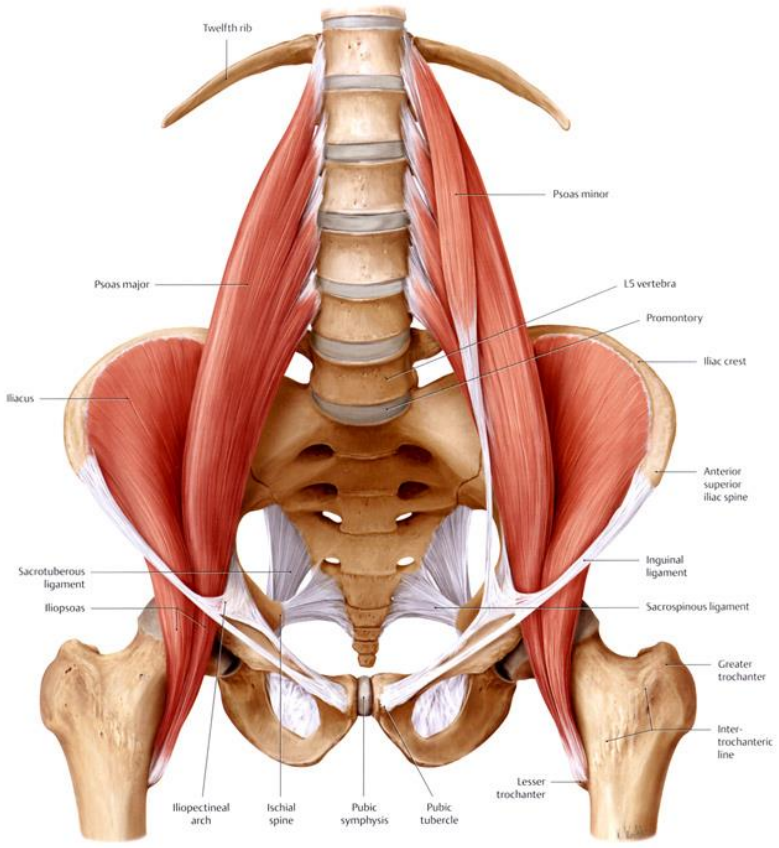

Figure 2.36: The attachment of the iliacus muscle on the superior part of the iliac fossa (http://www.painreliefvermont.com/iliacus.html).

The lateral (gluteal) region consists of two large groups of muscles divided into a superficial layer (the gluteus maximus, gluteus medius and gluteus minimus) and a deep layer (piriformis, obturator internus, superior and inferior gemelli and quadratus femoris) (Figure 2.37).

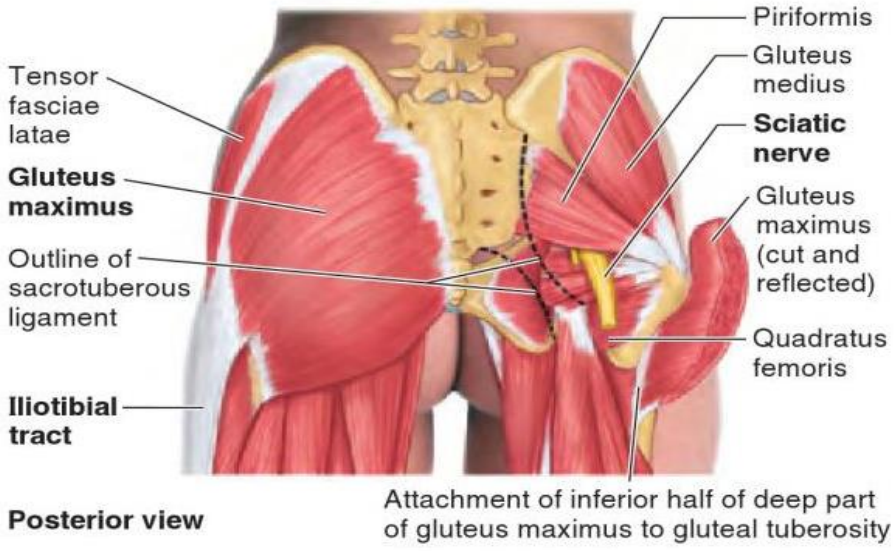

Figure 2.37: Posterior muscular attachments on the ilium (taken from Moore *et al*, 2013).

CHAPTER 3

The sacroiliac joint: anatomy, embryology and biomechanics.

3.1 Introduction

This chapter will discuss the basic concept of a joint, how a joint is formed in the developing embryo and progresses throughout ontogeny, with particular reference to the sacroiliac joint. The study of the sacrum and the ilium is deemed insufficient without addressing the sacroiliac joint since it is the articulation between the two bones. Biomechanically, the load transmitted from the axial skeleton to the lower extremities must pass through the sacrum and ilium via the sacroiliac joints, either partially or completely, or via its surrounding soft tissues.

The distinctiveness of the sacroiliac joint (SIJ) from other large synovial joints has been known since the time of Hippocrates, who noted that the female pelvis separated during labour and remained so thereafter (Walker, 1992). Although largely immobile, the SIJ is designed to accommodate different requirements with regards to sex and age. It has to possess equilibrium between stability as the region where the axial and appendicular skeleton meet, together with allowing some movement during parturition at the expense of the main function of a synovial joint: free mobility.

The vertically-oriented sacroiliac joint must possess strong support from the adjacent soft tissue structures to maintain its stability for optimum axial-appendicular skeletal function even though it was developed as a synovial joint in nature (Albee, 1909; Sashin 1930; Macdonald and Hunt, 1952). This contradicting developmental-functional capacity leaves a big question as to why this is happening as though the joint was indeterminate of its purpose and functionally unstable.

In addition, some authors report that this joint undergoes changes from an initially diarthrodial joint into an amphiarthrodial joint in mid-life and later becomes a synarthrodial articulation in old age often displaying a degree of synostosis (Brooke, 1924; Sashin, 1930; Bowen and Cassidy, 1981). This chapter discusses the sacroiliac joint, especially its morphological structure and biomechanics.

3.2 Basic concept of a joint

A joint is a site where two skeletal elements meet, either with or without a joint cavity: it is a crucial element in skeletal morphogenesis required for mobility in vertebrates (Guo *et al,* 2004). A joint can be synovial, where there is a joint cavity separating the two bony elements, or a solid joint (cartilaginous, fibrous) in which there is no cavity and the bony components are united by connective tissue (Drake *et al,* 2005). The three types of joint in Figure 3.1 (fibrous, cartilaginous and synovial) show the differences in development between and within them (O'Rahilly, 1957). The joints also can be categorised as diarthrosis, amphiarthrosis and synarthrosis (Handy, 1854; Brooke, 1924) according to the ability to permit movement.

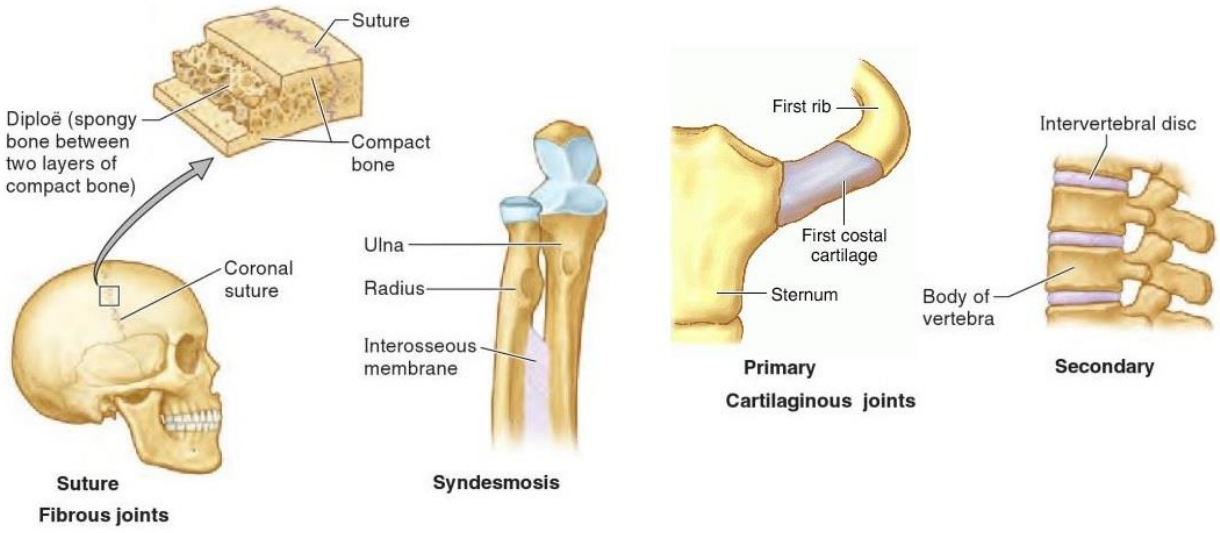

Figure 3.1: The fibrous and cartilaginous joints (modified from Moore *et al,* 2013).

A solid joint is restricted in movement compared to a synovial joint. It consists of fibrous and cartilaginous joints (Figure 3.1) with fibrous connective tissue, cartilage or fibrocartilage connecting the bony elements.

A synovial joint (Figure 3.2) is a connection between skeletal components separated by a narrow joint cavity, cartilage (usually hyaline) lines the articular surfaces with a joint capsule consisting of an inner synovium secreting synovial fluid and an outer fibrous membrane of dense connective tissue, with or without ligamentous reinforcement (Drake *et al*, 2005; Moore *et al*, 2013).

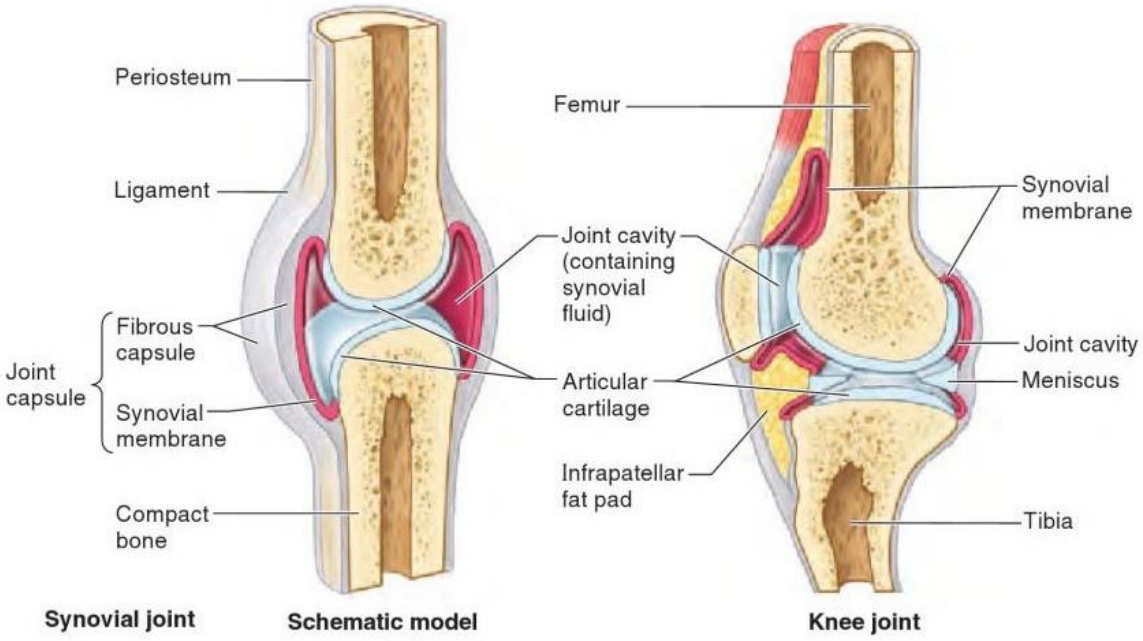

Figure 3.2: Example of a synovial joint (taken from Moore *et al*, 2013).

Many large joints in the human body are synovial articulations, for example the shoulder, elbow, hip and knee, and are classified according to the shape of the articulating surfaces or the movement permitted. The sacroiliac joint, however, has a variable description: synovial, partly synovial partly syndesmotic, amphiarthrosis or synarthrosis (Brooke, 1924; Palastanga and Soames, 2012; Moore *et al*, 2013).

Joint formation is a complex multistep process based on two main events: (i) interzone formation and (ii) cavitation during the embryonic period proper (O'Rahilly, 1957). The interzone formation is regulated by GDF-5, with Wnt-14 regulating the nonchondrogenic process, BMPs (bone morphogenetic proteins) and its antagonists, noggin (Hartmann and Tabin, 2001; Archer *et al*, 2003; Guo *et al*, 2004; Khan *et al*, 2007). The interzone consists of three layers; two chondrogenic covering the opposing surfaces of the future articular cartilages and a narrow middle layer forming the interzone "proper" (Figure 3.3), characterised by a thin mesenchymal layer forming at the future joint site (Onyekwelu *et al*, 2009).

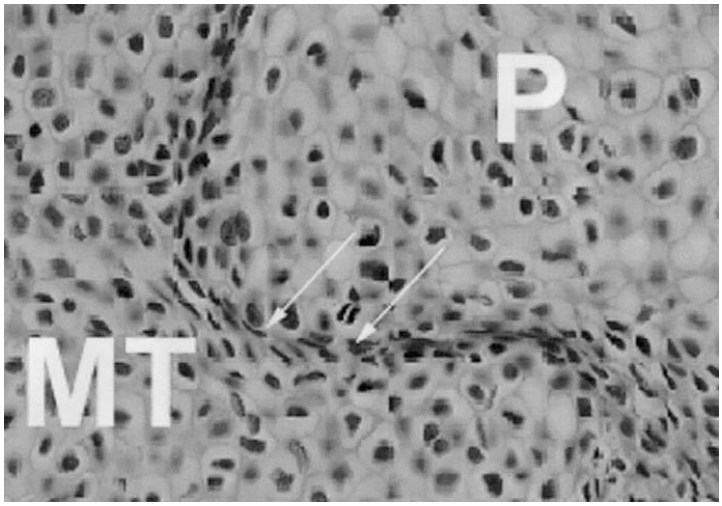

Figure 3.3: The thin, central interzone (white arrows) layer sandwiched between two chondrogenic layers of a phalanx (P) and metatarsal (MT) of an opossum before cavitation has occurred (taken from Archer *et al*, 2003).

Following formation of the central interzone, cavitation occurs within it by the action of hyaluronan synthesised by the interzone cells: later on the articular cartilage develops through appositional growth of the progenitor cells residing in the articular surface (Archer *et al*, 2003). Recently, it has been found that Indian hedgehog (Ihh) is the

critical and possible direct regulator of synovial joint development: in the absence of Ihh, GDF-5 function is impaired (Koyama *et al*, 2007; Onyekwelu *et al*, 2009).

3.3 Anatomy of the sacroiliac joint

The sacroiliac joint is a paired synovial joint reinforced by various ligaments, located at the junction between the appendicular and axial skeleton (Figure 3.4), thus making this joint distinct in some of its characteristics (not freely mobile) compared to a typical large synovial joint (Forst *et al*, 2006; Moore *et al*, 2013). The main functions of the sacroiliac complex are to stabilize and transmit loads from the trunk to the lower limb in the erect posture and to the ischial tuberosities during sitting (Kapandji, 1974; Palastanga and Soames, 2012). Nevertheless, the importance of mobility of this joint in females in the third trimester of pregnancy and during parturition is not questioned, mostly attributable to hormonal influences during pregnancy (Brooke 1924; Sashin, 1930; Walker, 1992, Vleeming *et al*, 2012).

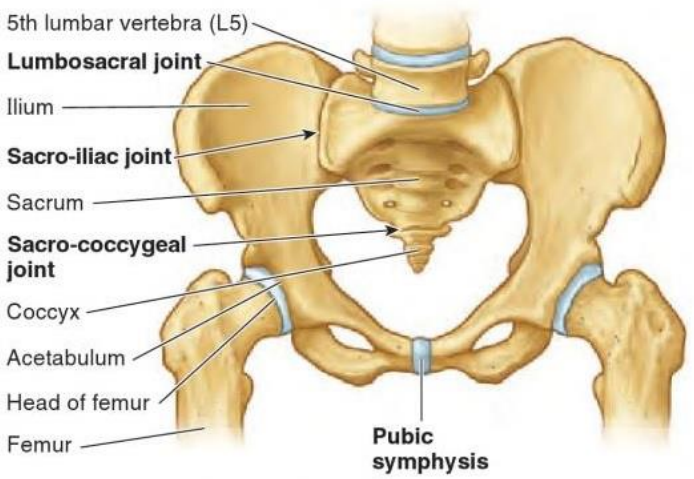

Figure 3.4: The sacroiliac joint (taken from Moore *et al*, 2013).

Albee (1909) reported that the sacroiliac joint is a true diarthrodial joint, having a synovial membrane, synovial fluid, hyaline articular cartilage, joint capsule, joint cavity, although with limited in mobility. Recently, the sacroiliac joint has been referred

to as being synovial anteriorly and a syndesmoses posteriorly (Palastanga and Soames, 2012; Moore *et al*, 2013). The ligamentous complex surrounding the sacroiliac joint plays a crucial role in stabilising the joint and has been discussed in Chapter 2.

The sacroiliac joint is a bilateral joint to the right and left of the sacrum, between the auricular surfaces of the sacrum and ilium. The joint articulates between the antero-internal aspect of the upper posterior ilium with the lateral masses of the first and second sacral vertebrae (Brooke, 1934), and sometimes the third sacral vertebra especially in males (Brothwell, 1981; Bellamy *et al*, 1983; Mahato, 2011).

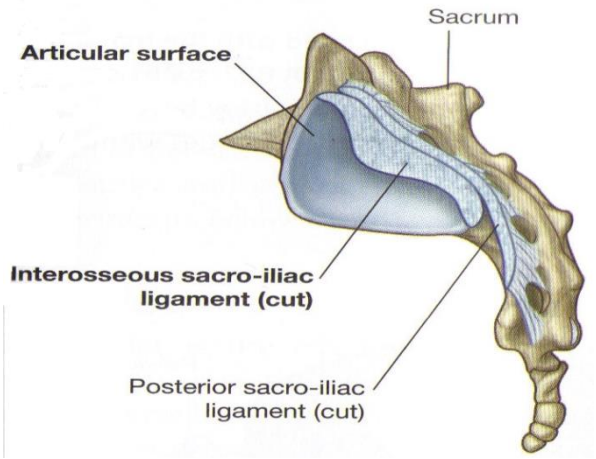

Figure 3.5: The articular surface of the sacroiliac joint (taken from Drake *et al*, 2005).

The sacroiliac joint, comprises a synovial membrane and joint cavity, with a strong joint capsule (Albee, 1909). The joint surfaces are roughly L shaped, with superior (cranial) and inferior (caudal) limbs. The junction between the two projects anteriorly and slightly inferiorly (Figure 3.5).

The surface area is reported to be approximately 1.5cm² at birth, 7cm² at puberty, and 17.5cm² in the adult joint (Brooke, 1924) and the length and width of the adult auricular surface varies from 5.3cm and 8cm to 1.8cm and 4.1cm, respectively (Schunke, 1938). This demonstrates that the surface area of the auricular surface is five times larger

during puberty than during infancy, but only less than 3 times larger in adulthood than during puberty. This suggests that rapid and major incremental growth in this area occurs during the subadult years (Rissech and Malgosa, 2005), which may be due to the fact that the pelvis is experiencing major functional changes related to advancing locomotive development.

Appearance, thickness and type of auricular cartilages

The joint surface is reported to be initially flat with an irregular interlocking contour to resist movement appearing during puberty (Schunke, 1938; Bowen and Cassidy, 1981; Vleeming *et al,* 1989). The presence of an intra-articular tubercle, especially in males, suggests that the increased interlocking between the auricular surfaces is for stability and strength of the joint (Brooke, 1924, Vleeming *et al,* 1989). However, Salsabili and Hogg (1991) state that the auricular surfaces display an iliac concavity with a corresponding sacral convexity present from intrauterine life,

The thickness of the sacral auricular cartilage is greater than the iliac (Albee, 1909; Brooke, 1934, Paquin *et al*, 1983), and has been consistently reported as such (Sashin, 1930; Schunke, 1938, Macdonald and Hunt, 1952; Carter and Loewi, 1962; Vleeming *et al*, 1989; Bowen and Cassidy, 1981; Salsabili *et al,* 1995). However, there are no reported differences in auricular cartilage thickness between males and females (Salsabili *et al*, 1995).

The dissimilarity of the two joint surfaces is of particular interest due to the constant references in the literature. The macroscopic appearance of the sacral auricular cartilage is frequently described as smooth, glistening and whitish, while the iliac auricular cartilage is bluish, striated and dull-looking in fetal life becoming more marked

throughout life (Sashin, 1930; Brooke, 1934; Carter and Loewi, 1962; Bowen and Cassidy, 1981). These findings may be attributed to the different mesodermal embryological origins of the sacrum and ilium, since the differences in thickness of the two auricular surfaces is present during intrauterine life, suggesting that this is not the result of differential stresses and strains between these two surfaces (Bowen and Cassidy, 1981).

Despite the major consensus on the disparity of the thickness of sacroiliac joint auricular cartilages, the type of cartilage on the sacral and iliac auricular area has been disputed (Schunke, 1938; Kampen and Tillmann, 1998). Many studies report that the auricular surface of the sacrum is covered by hyaline cartilage while that of the ilium is by fibrocartilaginous (Bowen and Cassidy, 1981; Paquin *et al*, 1983; Salsabili and Hogg, 1991) with frequent transition seen in the sacral auricular cartilage from fibrocartilaginous into hyaline cartilage during ontogeny (Schunke, 1938), while others report that both are hyaline in nature (Albee, 1090; Brooke, 1924). However, it is known that the sacroiliac joint possesses hyaline as well as fibrocartilage that makes it different from other typical diarthrodial joints (Forst *et al*, 2006).

Joint capsule and synovium

A fibrous capsule completely surrounds the joint: anteriorly it is thin and weak frequently rupturing during symphysiotomy (Albee, 1909). The anterior capsule is merely the thin anterior sacroiliac ligament forming the fibrous capsule of the synovial joint (Moore *et al*, 2013). Posteriorly, the capsule is thick and reinforced by the large posterior ligaments (Albee, 1909; Bowen and Cassidy, 1981).

The synovial membrane forms a continuous layer attached to the margins of the articular cartilage in a similar manner to any other joint (Brooke, 1924; Sashin, 1930; Schunke, 1938). It is reported to first appear as vascularised synovial mesenchymal tissue with synovial villi within the capsule of the sacroiliac joint at 20 weeks post-ovulation (Bowen and Cassidy, 1981; Salsabili and Hogg, 1991). This shows that formation of the synovial membrane of the sacroiliac joint is later in appearance compared to other joints in the human body, some of which occur as early as 12 fetal weeks (Bowen and Cassidy, 1981).

Degenerative changes and joint fusion

Irrespective of the nature of the articular cartilages, the sacroiliac joint exhibits precocious degenerative changes compared to other large synovial joints in humans (Kampen and Tillmann, 1998). These early degenerative changes commonly occur at the iliac auricular cartilage which shows a rough, dull-looking surface coated with fibrous plaques with eroded cartilage, especially in the third decade in males (Sashin, 1930; Schunke, 1938; Macdonald and Hunt, 1952; Bowen and Cassidy, 1981; Kampen and Tillmann, 1998), with synostosis frequently occurring in the 7^{th} decade without any evidence of arthritic processes (Macdonald and Hunt, 1952). The difference in auricular thickness may also explain the early degenerative changes of the iliac auricular cartilage, being thinner compared to that on the sacrum, and frequently used in age estimation at death (Lovejoy *et al*, 1985; Buckberry and Chamberlain, 2002; Igarashi *et al*, 2005).

One possible reason for early degenerative changes in this joint is because it is not as freely mobile as other diarthrodial joints in the human body, consequently the body is trying to adapt to this immobility by assisting the sacroiliac joint to fuse, especially in

males. In addition, the centre of gravity in males is more anterior than in females, being approximately in line with the sacroiliac joint, suggesting that more load may be transmitted across the joint requiring more stability. For this reason the adaptation in males showing more prominent ridges and depressions (Vleeming *et al,* 1989).

Furthermore, the sacroiliac joint may fuse later in life. The joint begins as a diarthrodial, eventually become amphiarthrodial in both sexes (middle age in males and old age in females) and finally transforms into a synarthrodial joint in elderly males, and progresses to complete bony ankylosis (Brooke, 1934; Valojerdy *et al,* 1989). Sashin (1930) found that bony ankylosis was present in 51% of 30-59 year olds and 82% of 60 year old males, whereas in females, the figures were 5% and 30%, respectively. The cranial limb of the joint is more commonly affected with osteophytes and synostosis. This may reflect the important role played by the cranial limb in transmitting the forces in the erect posture, with osteophytes being more common on the ilium than the sacrum (Valojerdy *et al*, 1989).

Mobility of the sacroiliac joint

Albee (1909) purported that motion is present at the sacroiliac joint; however, it is extremely limited, being slightly greater during rotation about a transverse axis owing to the presence of the interlocking and uneven articulating surfaces, as well as the many supporting ligaments (Schunke, 1938).

Mobility of the sacroiliac joint, although minimal, is reported to occur during two phases of life; first during perinatal life, and secondly in pregnancy (Brooke, 1924; Schunke, 1938; Macdonald and Hunt, 1952; Solonen, 1957; Vleeming *et al,* 1989). During fetal life, motion of the joint increases after the sixth month and achieves its

greatest mobility at birth: formation of the joint cavity occurs around three months of fetal life and is completed around the eighth fetal month (Schunke, 1938; Macdonald and Hunt, 1952).

It is almost impossible to draw any distinction between the sexes during the first 12 to 14 years of life as in both the joint is immobile, but after puberty, the female sacroiliac ligaments are more lax and the joint more mobile, especially in the third decade (Brooke, 1924). This may suggest that physiologically, the female body is being prepared for pregnancy.

The joint and its surrounding ligaments are known to be lax and have the greatest mobility during late pregnancy under hormonal influences, particularly relaxin, as the mobility of the sacroiliac joint is two and a half times greater than the maximum degree of movement in non-pregnant women (Sashin, 1930): this persists until four months post-delivery (Brooke, 1924).

Accessory Sacroiliac Joints

Accessory sacroiliac joints are not uncommon, being mainly located posterior to the joint: their presence is thought to be acquired as the incidence is correlated with age (Trotter, 1940; Bowen and Cassidy, 1981; Walker, 1992). An accessory sacroiliac joint is also thought to be one of the sources of lower back pain (Walker, 1992).

The sacral articular facet is commonly located lateral to the first or second dorsal foramen, and the iliac articular facet on the medial surface of the posterior superior iliac spine (Figure 3.6), which could be unilateral or bilateral, single or double in appearance (Schunke, 1938; Ehara *et al*, 1988). Many of these accessory joints show evidence of degeneration (Bowen and Cassidy, 1981).

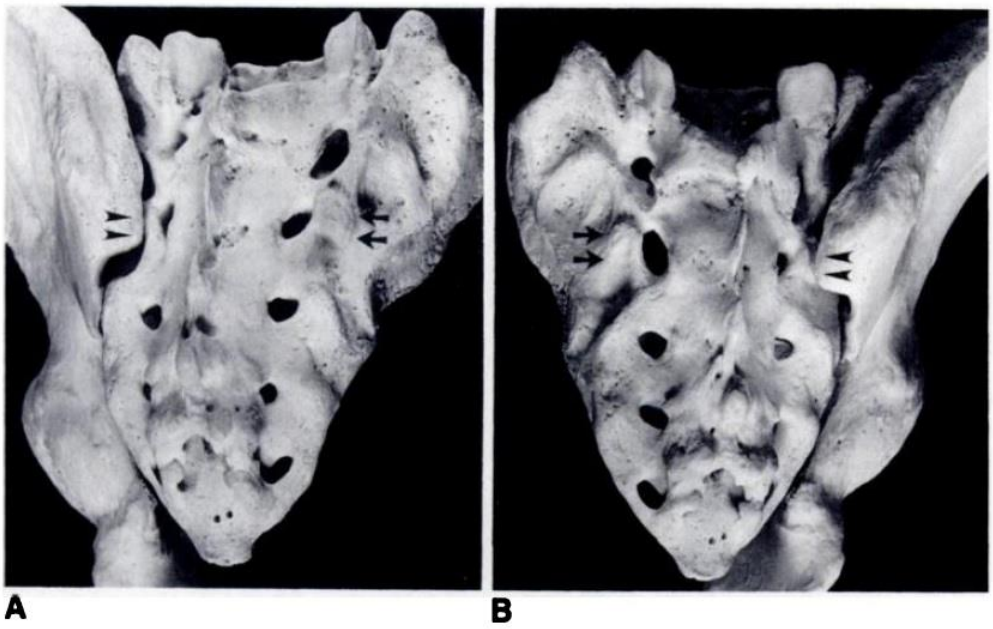

Figure 3.6: Posterior view of the facets of accessory sacroiliac joints on the sacrum at the level of second sacral foramen (arrows) and the posterior superior iliac spine of the ilium (arrowheads). The (A) right innominate and the (B) left innominate have been removed (taken from Ehara *et al,* 1988).

Trotter (1940) studied 958 pelves of white and black individuals of both sexes, ranging in age from 15 to 88 years, and found that 36% showed evidence of accessory sacroiliac articulations. There was a higher prevalence in males compared to females, with the former being up to 40% and the latter 21%, and more common in white individuals than black. It has been suggested that accessory sacroiliac articulations are more commonly found in males and are a result of functional responses to the stresses associated with an upright posture, where males are generally heavier than females (Stewart, 1938).

Auricular surface for age at death estimation

The human skeleton shows age-related changes at different rates throughout life: the auricular surface of the ilium is one of the important markers in the estimation of age at death due to its higher survival rate than the pubic symphysis (Lovejoy *et al,* 1985;

Buckberry and Chamberlain, 2002). The morphology of the auricular surface of the ilium has been investigated extensively in establishing age at death in the adult (Lovejoy *et al*, 1985; Buckberry and Chamberlain, 2002; Igarashi *et al*, 2005; Mulhern and Jones, 2005) as there are regular changes taking place at this joint with increasing age (Sashin, 1930).

The auricular surfaces can be divided into apex, superior demifacet, inferior demifacet, and the retroauricular area as described by Lovejoy *et al.* (1985). Buckberry and Chamberlain (2002) used five features on the auricular surface for the estimation of age at death, which are the transverse organization of striae on the auricular surface, surface texture, microporosity, macroporosity and apical changes. These criteria are frequently revised and the results often combined and scored to obtain an estimated age (Buckberry and Chamberlain, 2002; Igarashi *et al*, 2005). It is reported that the texture of the auricular surface plays a significant role in distinguishing between younger and older individuals, with a fine texture being typical in younger and heavily, granular and porous surfaces in older individuals (Igarashi *et al*, 2005).

The auricular surface of the ilium also exhibits strong correlations between age determined by the morphological changes on the iliac auricular surface and the pubic symphyseal surface (Lovejoy *et al*, 1985). Some studies suggest that sexual dimorphism may be seen in the sacroiliac auricular surface of subadult remains (Weaver, 1980; Mittler and Sheridan, 1992; Schutkowski, 1993), however this is controversial and largely unsubstantiated (Sutter 2003; Blake, 2011) with studies reporting limited evidence of sexual dimorphism in the adult sacroiliac joint (Ali and MacLaughlin, 1991).

The associated vessels and nerves surround the sacroiliac joint

The neurovascular bundles associated with the sacroiliac joint have been discussed in detail in Chapter 2, however it is worth noting that the vascularisation of a joint is from vessels arising from nearby arteries, which often communicate to form a network of peri-articular arterial anastomoses covering the whole joint (Moore *et al*, 2013). The articular veins, which are mostly located in the joint capsule, accompany the arteries. Innervation of the sacroiliac joint is from nerve fibres within the joint capsule and surrounding ligaments arising from the ventral rami of L4 and L5, the superior gluteal nerve, and the dorsal rami of L5 - S2, and sometimes as far as S5 (Forst *et al*, 2006).

3.4 Embryology of the sacroiliac joint

The sacroiliac joint forms around the 3rd month of fetal life (Schunke, 1938). Salsabili and Hogg (1991) found that as early as 8.5 weeks post-ovulation, small foci of cavitation start to appear in the region of the future sacroiliac joint (Figure 3.7), at the level of S1 vertebra, from the cranial part of the joint via central interzones.

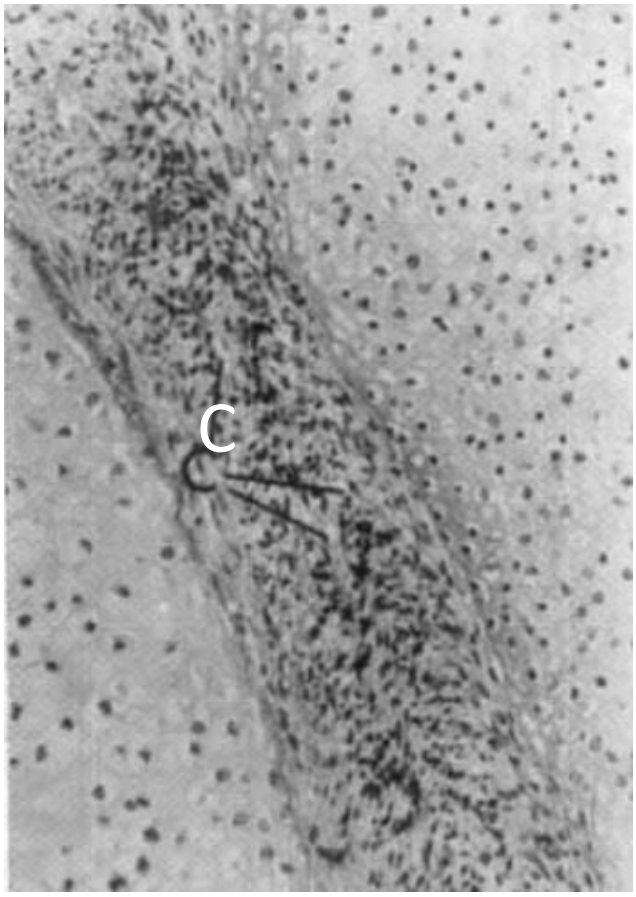

Figure 3.7: The cranial region of the future sacroiliac joint showing small foci of (C) cavitation at the central interzone region in 8.5 weeks fetus (modified from Salsabili and Hogg, 1991).

At 9 weeks post-ovulation, the anterior, posterior and interosseous sacroiliac ligaments start to develop, although cavitation is still confined to the S1 vertebra with a more prominent and well defined cavity: the joint capsule begins to appear on the inner aspect of the anterior sacroiliac ligament (Salsabili and Hogg, 1991).

At 12 weeks post-ovulation, the joint cavity starts to expand within the middle region of the joint, with fibrous interconnecting bands that later divide the auricular cartilage into cranial and caudal limbs (Vleeming *et al*, 2012). Following this more developed cranial and caudal limbs occur at 14 to 20 fetal weeks, together with many blood vessels supplying the mesenchyme synovia (McAuley and Uhthoff, 1990; Salsabili and Hogg, 1991). The development of the synovial membrane varies between studies, ranging

from 20 to 37 weeks of fetal life (Schunke, 1938; Bowen and Cassidy, 1981; Salsabili and Hogg, 1991).

It is not until the 8th fetal month that cavitation is reached fully (Schunke, 1938), with the iliac side always in advance of the sacral side (McAuley and Uhthoff, 1990). The formation of the sacroiliac joint is rather late in comparison with other large synovial joints of the limbs, which are well-developed before 12 weeks of fetal life (O'Rahilly and Gardner, 1978). This is most likely due to the central location of the joint at the junction of the axial and appendicular skeleton which permits limited movement (Murray and Drachman, 1969; Vleeming *et al*, 2012)

Cleaves (1937) reported that in the first year of life the sacroiliac joint appears as two fissures between the ilia and the lateral masses of the sacrum: being wider at the caudal than the cranial region. The fissures become narrower around 4 years of age. At the age of 15-18 years, changes can be seen where the secondary ossification centre (epiphysis) arises in the auricular cartilage of the sacrum. This centre is concentrated at the anterior margin of the sacrum, resulting in a wider anterior compared to posterior auricular margin of the sacrum. After this, at around 19 to 20 years, the epiphyses fuse (Cleaves, 1937; Scheuer and Black, 2000).

3.5 Biomechanics of the sacroiliac joint.

The sacroiliac joint, being at the junction of the axial and appendicular skeleton, transmits gravitational forces from the trunk to the ground and vice versa, and requires a synergistic action of the joint, ligaments and muscles around it to stabilised the joint (Walker, 1992; Vleeming *et al*, 2012). As the capsule is relatively weak anteriorly with the wedge shape of the sacrum contributing little to the stability of the joint, it needs strong support externally from the posterior ligamentous complex and internally from

the irregular auricular surface for interlocking to function optimally (Vleeming *et al*, 1989; Snell, 2008).

Studies on the biomechanics of the sacroiliac joint come from various approaches, either direct cadaveric dissection or non-invasive radiological studies of the trabecular architecture of the bones, muscles and ligaments associated with the joints, or biomechanical model analysis of the pelvic complex (DonTigny, 1985; Pal and Routal, 1989; Pal, 1989; Snijders *et al*, 1993; Vleeming *et al*, 1996; Peretz *et al*, 1998; Snijders *et al*, 1998; Pool-Goudzwaard *et al*, 2003; Wingerden *et al*, 2004; Pel *et al*, 2008; Cunningham and Black, 2009b; Mahato, 2010b; Mahato, 2010c; Mahato 2011).

The biomechanics of the sacroiliac joint are determined by the intricate musculoskeletal and ligamentous interactions of the trunk, pelvis and body posture, under the influence of gravity (Kapandji, 1974), to ensure stability by inhibiting sacroiliac joint movement. If movement does occur, it is only a slight gliding and rotatory movement between the sacrum and the innominate (Palastanga and Soames, 2012). The biomechanics of the sacroiliac joint can be analysed by dividing it to three different aspects: muscular forces, ligamentous tension and the bones involved.

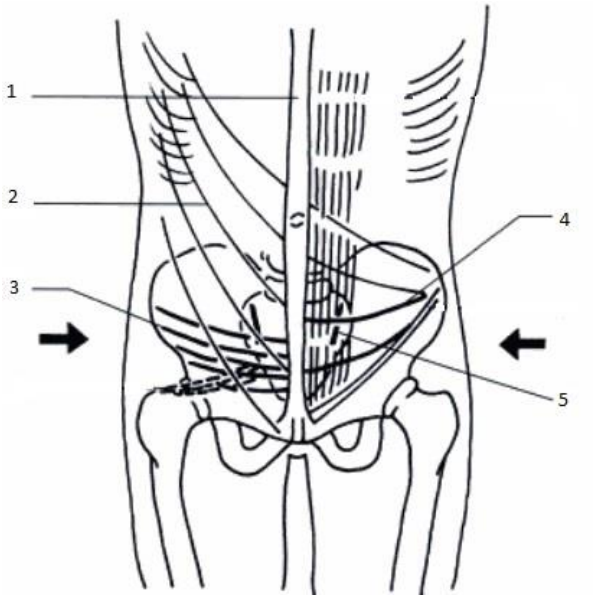

Figure 3.8: The ‘self-bracing’ mechanism provided by the transversely-oriented muscles (arrows) on the innominates to help stabilise the sacrum. (1) linea alba, (2) external oblique, (3) transversus abdominis, (4) internal oblique, and (5) sacroiliac joint (modified from Nordin and Frankel, 2001).

The position of the transversely-oriented anterolateral abdominal muscles imposes a compressive ‘self-bracing’ mechanism on the symphysis pubis and the sacroiliac joint (Snijders *et al*, 1998). This action stabilises the sacroiliac joint by ‘sandwiching’ the sacrum between the two innominates (Figure 3.8) to prevent shear loading of the sacroiliac joint caused by longitudinally-oriented muscles and gravity (Nordin and Frankel, 2001). In addition to the action of the anterolateral abdominal wall muscles, unilateral activation of biceps femoris, gluteus maximus and the erector spinae have been reported to stabilize the sacroiliac joint, even when the individual muscles contract separately (Wingerden *et al*, 2004). As a result, load transfer from the spine to the legs becomes more effective as the activation of these muscles prevent shear forces across the sacroiliac joint.

The anterolateral abdominal muscles bracing the sacroiliac joints are the external oblique, internal oblique and transversus abdominis which lie approximately transverse

to the pelvis, originate from the thoracolumbar fascia at the back, lower ribs and the iliac crest, and insert at the linea alba, a midline raphe formed by the strong aponeuroses of the muscles (Snell, 2008; Moore *et al,* 2013). Recently, it has been reported that activation of transversus abdominis and the pelvic floor muscles increases sacroiliac compression force by 400% accompanied by a reduction of 40% in the vertical sacroiliac joint shear force, hence contributing to stabilising the joint (Pel *et al,* 2008). It is suggested that training transversus abdominis to stabilise the sacroiliac joint is one option in the treatment of low back pain (Richardson *et al,* 2002; Pel *et al,* 2008).

The sacroiliac joint is unstable by nature (Snell, 2008), with the only major factor holding it in its normal position, apart from the auricular ridges and troughs, is the supporting posterior ligaments. Not only do they support the articulation, but most importantly transfer the trunk load to the lower limbs (Last, 1978; DonTigny, 1985; Palastanga and Soames, 2012).

During standing, the vertebral column, pelvis and lower limbs form a coordinated articular system by virtue of two joints: the sacroiliac joint and the hip joint (Kapandji, 1974). The centre of gravity falls posterior to the centre of the acetabulum, tilting the posterior pelvis downward and the anterior pelvis upward, hence the posterior pelvis bears most of the weight transferred from the upper trunk, as the centre of gravity lies on the tip of sacral promontory, anterior to the sacroiliac joint (Kapandji, 1974; DonTigny, 1985; Palastanga and Soames, 2012). The weight transferred stretches the posterior ligaments and draws the sacrum between the innominates (DonTigny, 1985).

Rotational movements of the sacrum in relation to the innominates although small are known as nutation (forward movement of the sacral promontory) and counter nutation (the opposite movement) (Kapandji, 1974). To ensure stability of the joint, the sacrotuberous and sacrospinous ligaments resist nutation (Figure 3.9) along with the anterior sacroiliac ligaments, while the posterior sacroiliac ligaments resist counter nutation (Kapandji, 1974; Vleeming *et al*, 1989; Vleeming *et al*, 1996). In addition to the posterior ligaments restraining sacroiliac joint movement, the iliolumbar ligament is reported to play a similar role as some of the fibres that attach to the superior sacral alae and iliac tuberosity, specifically preventing rotation of the joint in the sagittal plane (Pool-Goudzwaard *et al*, 2000; Pool-Goudzwaard *et al*, 2003).

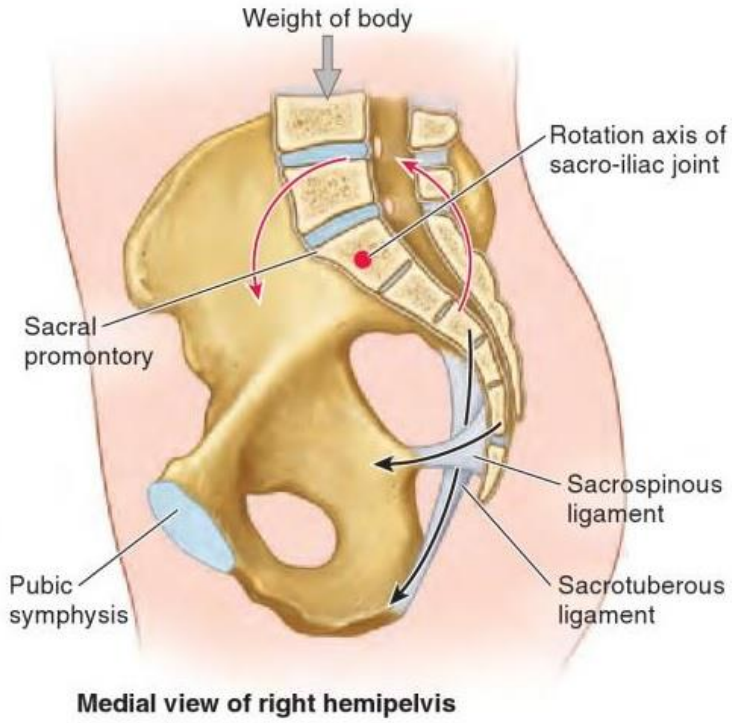

Figure 3.9: The rotational movement of the sacrum either by nutation (red arrows) or counter nutation (the opposite) (black arrows). Nutation of the sacral promontory is

prevented mainly by the sacrotuberous ligament with a small contribution from the sacrospinous ligament (taken from Moore *et al,* 2013).

Apart from the adjacent ligamentous and muscular action to ensure sacroiliac joint stability, the friction between the two articular surfaces of the sacroiliac joint is largely influenced by their surface texture. This includes the coarse texture and the ridges and troughs which are believed to be a physiological adaptation rather than a pathological reaction of the joint, where the influence of the ridges and depressions is larger than the coarse texture (Vleeming *et al,* 1989).

The biomechanics of the sacroiliac joint has also been studied in terms of the trabecular arrangement within the sacrum, either by direct bony dissection or radiographic imaging, mostly in adults (Pal and Routal, 1989; Pal, 1989; Mahato, 2010c; Mahato 2011). Weight was suggested to be transferred from the vertebral column through the vertebral bodies and its posterior facets to the sacral neural arches and bodies then towards the auricular region, with the area of attachment of the interosseous ligaments on the sacrum exhibiting distinct sets of trabeculae passing towards both sides of the auricular surface, without any bilateral differences (Pal, 1989). This was supported by Mahato (2010c, 2011) who suggested that the weight passed from the sacrum to the ilium through the auricular surface of the sacroiliac joint, although it is difficult to provide clear evidence as the suggestion is based on non-metric qualitative observation.

A recent trabecular quantitative study on the iliac part of the sacroiliac joint in the juvenile ilium (Cunningham and Black, 2009b) showed that the auricular surface had a lower bone volume fraction whilst the post-auricular area exhibited higher trabecular bone volume fraction and trabecular numbers. This suggests that the ligamentous support of the sacroiliac joint, especially posteriorly, may play a crucial role in transmitting the load of the trunk to the lower limbs (Last, 1978; DonTigny, 1985),

bypassing the auricular area of the sacroiliac joint, or perhaps, partially transmitting through it.

The biomechanical ability of the sacroiliac joint has been a subject of much debate, with some authors regarding that this joint to be weight bearing (Bellamy *et al,* 1993; Vleeming *et al,* 1996; Pel *et al,* 2008), whilst others disagree, expressing that the surrounding ligaments bear the body loads (Last, 1978; DonTigny, 1985; Palastanga and Soames, 2012). Despite the disagreement on the biomechanics in this posterior pelvic region, over the last two decades, studies on the sacrum and the sacroiliac joint have been more focused on the clinical condition of the sacroiliac joint as one of the causes of lower back pain (Cibulka, 1992; Strender *et al,* 1997; Wurff *et al,* 2000; Riddle and Freburger, 2002; Laslett *et al,* 2005) due to the high prevalence of cases in the back pain clinics (Schwarzer *et al,* 1995). Additionally, more focus has been put on the management of sacral and pelvic fracture as it has been one of the causes of debilitating impact on the quality of life and health economy (Denis *et al,* 1988; Jamieson and Steege, 1996; Mathias *et al,* 1996; Zelle *et al,* 2004), with pelvic fractures reported as the third most common cause of death in motor-vehicle accidents (Dalinka 1985; Giannoudis *et al,* 2007).

Despite extensive clinical research on the sacroiliac joint and pelvic region, little is known about the ontogenetic changes of the growing sacrum. Thus, the current study was designed to highlight the importance of biomechanical pathways in the juvenile sacrum as well as the sacroiliac joint by studying the trabecular architecture of the sacrum using recent investigative techniques aiming to increase the understanding of the nature of the joint and the bones that constitute the complex which it supports.

CHAPTER 4

Materials and Methods

4.1 Introduction

Recent investigations on bone biomechanics (Ryan and Krovitz, 2006; Genant *et al*, 2008; Burghardt *et al*, 2011) suggested that the advancement in non-invasive multidimensional and multimodalities such as computed tomography (CT), micro-computed tomography (μCT), magnetic resonance imaging (MRI) and micro-magnetic resonance (μMR), have strengthened the understanding on the assessment of trabecular bone microstructure (Drews *et al*, 2008). This is mainly due to these advanced techniques being able to extract the three-dimensional (3D) representations of the bony structures non-destructively. It was around the mid-20th century that the traditional methods, including histomorphometric techniques in evaluation of the spongy bone architecture, were highlighted (Davis, 1961; Lindahl, 1976; Goldstein *et al*, 1983) that contribute to current modern procedures. In addition, the rapid evolution of computer software producing high-quality tools, particularly during the early 21st century (Abramoff *et al*, 2004; Rosset *et al*, 2004; Parkinson *et al*, 2008; Scherf and Tilgner, 2009), augmented the study of human skeletal ontogeny.

In view of the advancement of the modalities available, this research aimed to determine the internal architecture of the developing juvenile sacrum as well as the growth pattern of the juvenile ilium, and use the results to evaluate sacral development and its interaction with the ilium. The research focused on the sacroiliac joint and the surrounding areas, and utilised specimens of the juvenile ilium and juvenile sacrum.

These two bones were studied in detail with particular attention paid to the auricular surfaces of the ilium and the sacrum and thus the sacroiliac joint.

The research was undertaken as three different studies: two on the juvenile sacrum and one on the juvenile ilium. The two studies on the sacrum were interrelated in which one is the preliminary qualitative study of the cortical and trabecular areas of juvenile sacra (Chapter 5), which was followed by a more precise and detailed quantitative study (Chapter 6) of the trabecular microarchitecture of juvenile sacra. The final study is a quantitative evaluation on the growth of the pelvic surface area of the juvenile ilium.

The materials used in this study were selected from the Scheuer Collection. The details on the collection with various techniques adopted to analyse the juvenile sacra and ilia are discussed in this chapter.

4.2 Materials: Scheuer Collection

The material used in this study was selected from the Scheuer Collection, housed within the Centre for Anatomy and Human Identification (CAHId), University of Dundee. The collection consists of more than 100 juvenile skeletal remains obtained from various archaeological, forensic and anatomical sources: they range from early fetal remains through to late adolescence (Cunningham and Black, 2009a). Many of the specimens in this collection have a documented age. However, for others, skeletal age assessment was assigned by metric evaluation from Fazekas and Kosa (1978) for fetal material and Scheuer and Black (2000) for all other specimens. The Scheuer Collection is an active repository for complete skeletons, partial skeletons or isolated skeletal elements. Each individual specimen is stored in a labelled plastic storage box at room temperature and careful attention was taken during handling of the specimens.

The juvenile sacrum

The total number of juvenile sacra in the Scheuer Collection represents 80 different individuals of various degrees of maturation. The age range is from 18 weeks *in utero* until late adolescence. As the sacrum originates from approximately 21 separate primary ossification centres at the 3rd fetal month (Francis, 1951; Scheuer and Black, 2000), the younger specimens appeared as multiple small ossified nodules, especially in the fetal and perinatal groups: sometimes these sacral elements remained associated by mummified cartilages surrounding the bones.

Meanwhile, the separate ossified sacral elements usually present as 5 sacral elements consisting of a centrum, paired neural arches and paired lateral elements for the first three sacral vertebrae (S1, S2 and S3) and 3 sacral elements consisting of a centrum and

paired neural arches for S4 and S5 (Figure 4.1). The lateral part of the lateral elements forms the auricular surface of the sacroiliac joint (Frazer, 1965; Scheuer and Black, 2000).

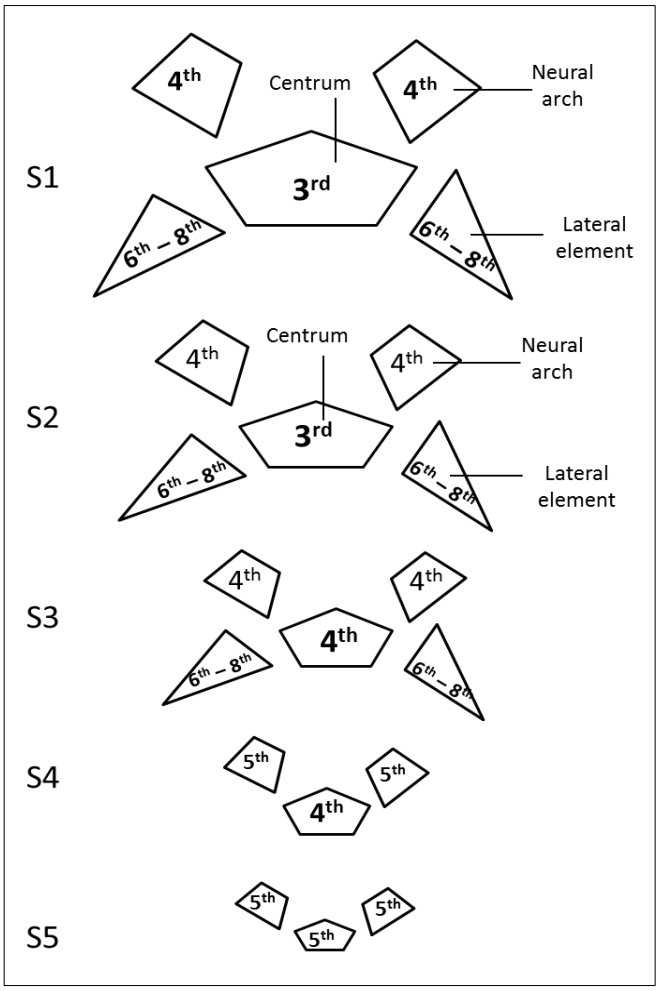

Figure 4.1: Schematic diagram illustrating the timing of occurrence of primary ossification centres of the sacrum in fetal months.

The primary ossification centre commences ossification at the 3rd fetal month in the S1 and S2 centra, followed by S3 and S4 centra with paired neural arches of S1 – S3 at the 4th fetal month (Francis, 1951). At the 5th fetal month, the S5 centrum and paired neural arches of S4 and S5 start to ossify. Finally, the lateral elements of S1 – S3 ossify around the 6th to 8th fetal months (Figure 4.1) which suggests that at birth, all the primary ossification centres are generally present (Scheuer and Black, 2000).

Appearance	Age	*n*
Fused in mummified surrounding soft tissues	Fetal – Neonatal	14
Unfused 5 (S1-S3) and 3 (S4-S5) sacral elements	Perinatal – 6 months	8
Unfused 5 sacral elements in S1, all elements in S2-S5 fused	1 year – 4 years	15
All 5 elements fused in each individual S1-S5	4 – 11 years	20
Complete intervertebral S1-S5 fusion	11 – late adolescence	23
		80

Table 4.1: The appearance and number (*n*) of sacra in the Scheuer Collection, University of Dundee

Although the younger sacra in the Scheuer Collection had already commenced ossification, all of the fetal and some neonatal specimens (n = 14) appeared as being joined together with mummified soft tissues surroundings (Table 4.1). The rest of the perinatal and neonatal specimens (n = 8) were present as 21 separate sacral elements (Figure 4.2), however as these specimens were excavated from various burial sites, some sacra had incomplete elements or were in a poor state of preservation.

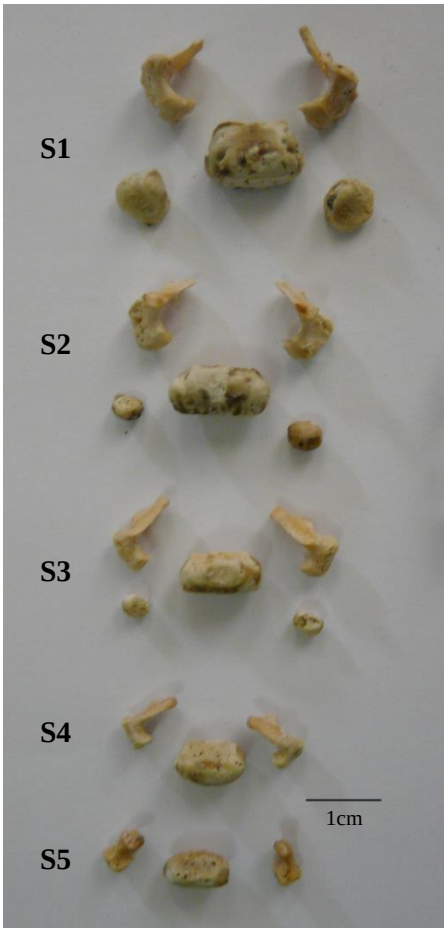

Figure 4.2: A perinatal sacrum with 21 ossified sacral elements.

In theory, the process of fusion within the elements in each of the five sacral vertebra commences around 2-6 years (Frazer, 1965; Scheuer and Black, 2000). In some of the specimens, the fusion of sacral elements occurred as early as 1 year, in a caudocranial direction, and was completed as early as 4 years, although the majority were in the 2-6 years range. By the age of 7, the sacra present as 5 separate individual vertebrae (Figure 4.3).

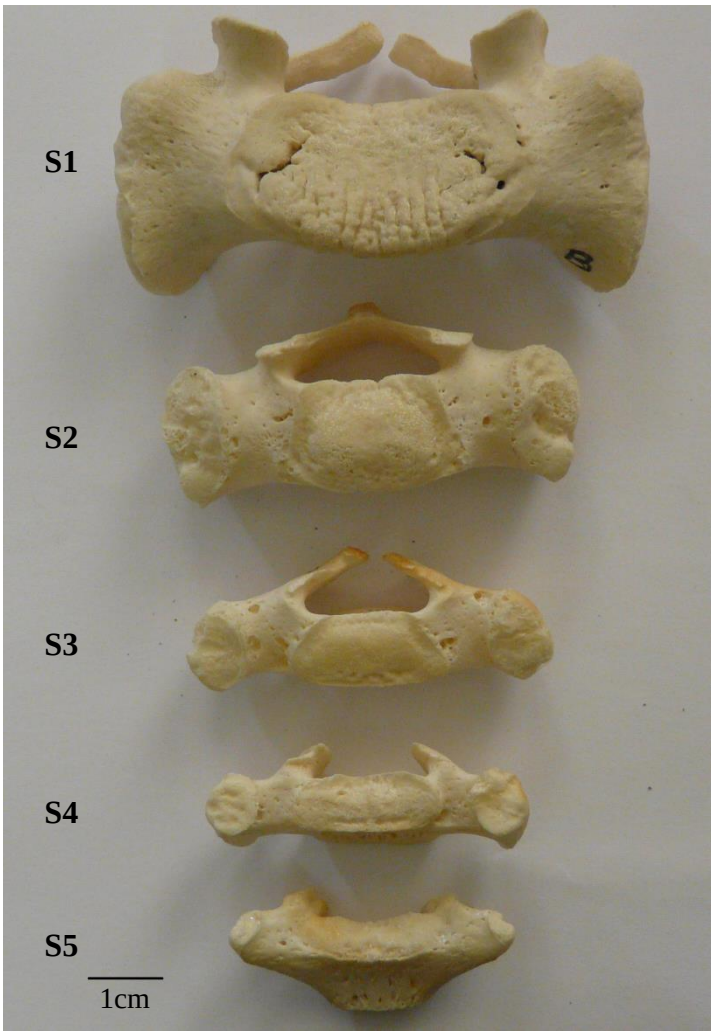

Figure 4.3: A 7 year old specimen presenting in 5 individual vertebrae that fused at each level.

The second fusion occurs at puberty, joining the 5 sacral vertebrae starting from S5 progressing towards S1 (Figure 4.4). Although this process is said to occur at puberty, progress varies among individuals and between sexes: the youngest specimen to show complete intervertebral fusion (S1-S5) was an 11-14 year old specimen. This second fusion is expected to be fully completed around 25 years (Frazer, 1965) with the last area to complete fusion occurring between the bodies of S1 and S2 (Scheuer and Black, 2000).

Figure 4.4: A late adolescent sacrum showing almost complete fusion. The fusion lines between the bodies and some of the alae are still visible.

Although there are 80 sacra in the Scheuer Collection, not all were included in this study as some showed a considerable amount of damage that warranted exclusion. Thus, only 68 sacra were selected for the preliminary study in Chapter 5, and from this pool, 26 were selected for the more detailed study in Chapter 6.

The juvenile ilium

The total number of juvenile ilia in the Scheuer Collection was 112 right and left ilia ranging from fetal to late adolescent age. The youngest fetal specimen was 18 weeks *in utero*. The human ilium develops from a primary ossification centre in the region of the greater sciatic notch around the 3rd fetal month (Laurenson, 1964). The external cortex of the ilium forms from intramembranous ossification while the internal trabecular structures arise from a cartilaginous template which transforms into bone via endochondral ossification.

The ilium originates as a single, relatively flat bone (Figure 4.5) and remains separate from the ischium and the pubis bone until puberty, when the three bones fuse to form the innominate (Figure 4.6).

Figure 4.5: A 2 year old specimen with left (a) ilium in pelvic view appeared separated with the (b) ischium and the (c) pubic bone.

Figure 4.6: A pelvic view of late adolescent ilium (left), fused with the ischium and pubis at the (*) acetabular area.

4.3 Methods

The methods used in this study are described according to the nature of the procedure conducted for this research. It is divided into two sections; (i) techniques involved with imaging modalities and (ii) techniques related to various software. These procedures were applied individually in the next three chapters (Chapters 5, 6 and 7).

4.3.1 Imaging modality adopted in this research

i) Digital macroradiograph (Chapter 5) - 2D Analysis

The study in Chapter 5 uses macroradiography (Figure 4.7) to capture an image of the juvenile sacra. Macroradiography is a technique used in radiographic imaging to enlarge an image corresponding to the size of the object, within an acceptable distance from the imaging plane (Davidson and Bowman, 2002). The advantages are direct magnification of the images with no increase in photographic blurring (Whitley *et al,* 2005).

All of the 68 juvenile sacra were macroradiographed at the Radiology Department, Ninewells Hospital and Medical School, Dundee, using a Siemen Multix Tube & Table CPH, with focus film distance (FFD) of 140 cm and an object film distance (OFD) of 30 cm, and exposure factors up to 50 kilovolt (kV) and fine focus of 1.25 – 1.6 milliampere second (mAS). The kV is the component that controls the quality of the x-ray beam and the grayscale produced on the x-ray film, in other words the penetrating power of the x-ray photons (Whitely *et al,* 2005). The specimen image was taken with the maximum value of 50 kV which is equivalent to 50,000 volts. The mAS controlled the quantity or intensity (amount of radiation used) of the x-ray photons produced on the x-ray film.

Figure 4.7: An example of a Siemen Multix CPH macroradiograph (taken from http://www.medwow.com/med/rad-room-analog/siemens/multix-cph/25384.model-spec).

Before capturing the image, the specimen was laid on the imaging plate over the tabletop and labelled accordingly. The unfused sacrum was laid with the superior part facing the x-ray tube (source of the x-ray beam) and the inferior part on the imaging plate. The x-ray beam was then directed on the superior part of the sacrum which produced an image from the superoinferior (SI) view. In the fused sacrum, the anterior part was laid on the imaging plate facing the beam, producing anteroposterior (AP) views. The imaging plate was processed by a computed scanner and transformed into an 8-bit, uncompressed digitized image. Each image was stored as a TIFF file consisting of 256 grey levels. The procedure was performed by a trained and experienced radiographer.

ii) Micro-computed Tomography (μCT) (Chapter 6) – 3D Analysis.

Research using micro-computed tomography (micro-CT) was introduced in the 1980s (Burstein *et al,* 1984; Feldkamp *et al,* 1989), 10 years after the production of clinical CT machines to provide higher quality resolutions and good image quality for scanning smaller subjects/animal models. The use of micro-CT includes investigations of bone anatomy and density, osteoporosis, bone resorption, remodelling and ontogenetic changes of the trabecular architecture (Ryan and Krovitz, 2006). This imaging modality allows the user to extract the model of the osseous material studied and explore the cortical and trabecular arrangements non-invasively.

The current quantification study on the sacral trabecular architecture in Chapter 6 was analysed in the context of the law of bone remodelling (Ruff *et al,* 2006), commonly known as Wolff's Law and Bone Functional Adaptation theory – how internal trabecular osseous material adapts to external forces and loading. The final result of the bone remodelling will lead to orientated internal cancellous bone along the principal stress trajectories to optimise mechanical adaptability thereby creating a robust structure.

The sacral specimens in Chapter 6 were scanned using micro-CT apparatus at the Centre for Medical Engineering and Technology, University of Hull by a trained technician. The micro-CT used was an X-Tek HMX 160 (X-Tek Systems Ltd, Tring UK). The voltage was set between 80-90 kV and 20-30 microampere (μA) current with an aperture setting of 50%. The filter used was a 0.1mm copper filter for the bone filtration and a beryllium gun as the radiation source. The source-detector distance (SDD) was adjusted to approximately 50cm and the object-detector distance (ODD) was 25 cm. Each sacrum was scanned at an average of 3 hours per single bone. This slow scan mode is used for optimization of the scanned data resolution. In this study, the

micro-CT image resolution of the specimens was kept between 25-92µm as the reported resolution of 14 – 100µm provides strong resolution dependency from micro-CT (Müller *et al*, 1996).

Figure 4.8: An example of a micro-CT scanner (taken from Natural History Museum, London).

The construction principle behind a micro-CT machine (Figure 4.8) relies on three main features, which are (i) the radiation source (generating gun), (ii) examined object and (iii) X-ray detector. The radiation source produces an x-ray beam or light path which is directed onto the examined object located in between the source and the X-ray detector.

In general, there are two types of construction principles in micro-CT scanning. The first involves a scanner with the source and the X-ray detector mounted on a gantry which rotates around the object. In the second constructed principle, the object itself rotates in the course of beams between the source and the detectors.

The micro-CT scanner used this second principle in this study. For the unfused specimen, each of the sacral specimens was positioned vertically with the lateral border (auricular surface) of the vertebra facing upwards and the anterior surface facing the radiation source (Figure 4.9), and the gantry holding the specimen rotates 360º. For the fully fused specimens, the bone was held on the gantry turntable vertically with the superior articular facets facing upwards and the anterior concavity of the sacrum facing the radiation source. The specimen was rotated 360º during scanning and the scanning process required around 3 hours per sample. The images produced were reconstructed using CT-Pro reconstruction software supplied by the manufacturer and stored as 2D micro-CT slices 16-bit in TIFF format.

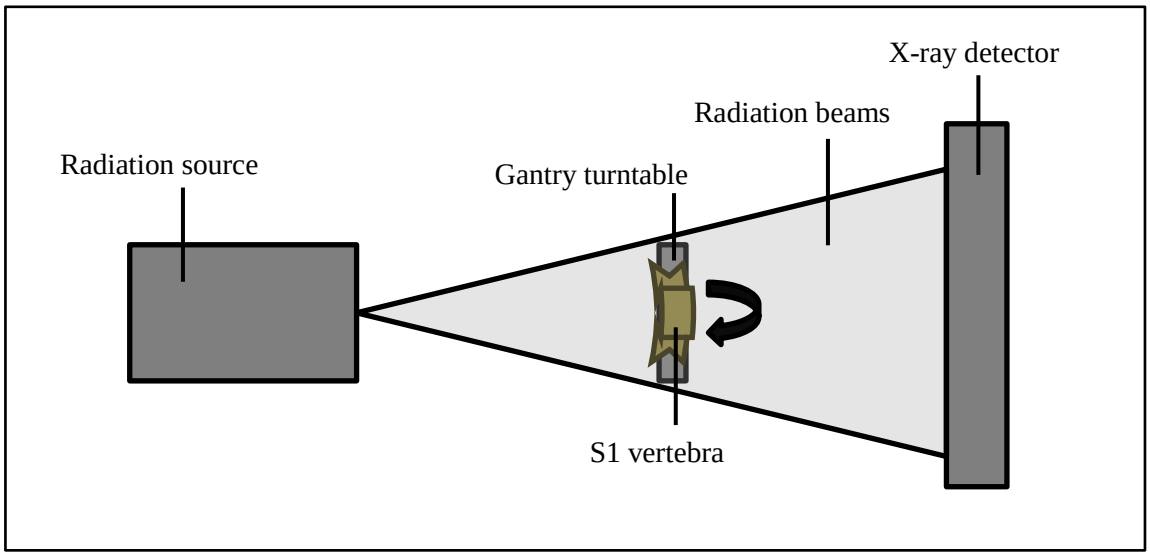

Figure 4.9: Schematic diagram of principles in the micro-CT scanner during scanning an S1 vertebra.

Advantages and disadvantages of micro-CT scanning

The advantages of micro-CT scanning are direct non-destructive measurement of 3D structure in a highly automated and shorter period of time compared to 2D histomorphometry (Jiang *et al,* 2000). Although stereology applied to the histological section is still considered to be the gold standard in obtaining the quantitative nature of the trabecular bone structure, the use of micro-CT in recent quantitative studies (Banse *et al,* 2002, Chappard *et al,* 2005; Thomsen *et al,* 2005) suggests that there are significant linear correlations between the conventional 2D histomorphometry studies of trabecular bone stereology with the micro-CT analysis (Thomsen *et al,* 2005) (Figure 4.10).

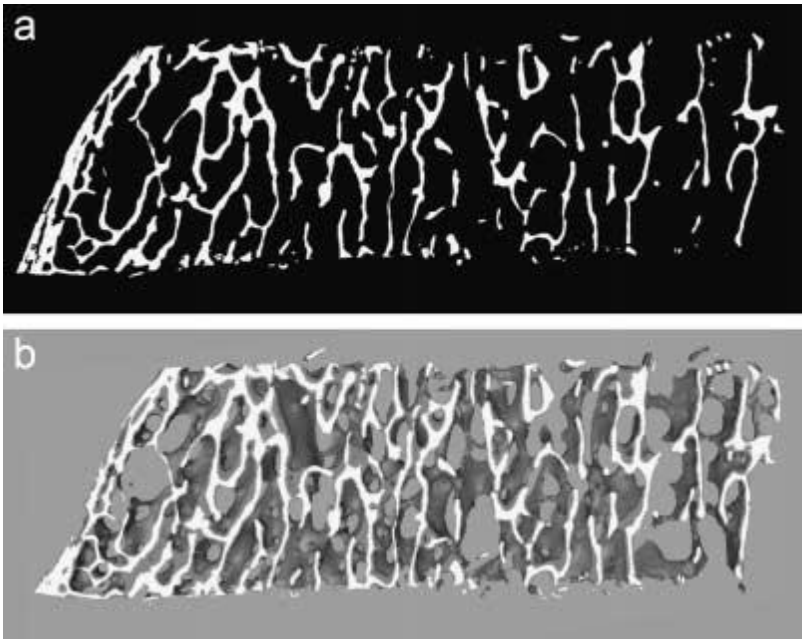

Figure 4.10: A comparison of (a) 2D histological sections of proximal tibial biopsy with (b) a 3D reconstructive image of the same specimen scanned by micro-CT (taken from Thomsen *et al,* 2005).

Non-invasive and non-destructive micro-CT scanning allows repeated testing of the subject matter, as well as better prediction on the functionality and quality of a 3D structure (Hildrebrand and Rüegsegger, 1997). The micro-CT method is an advance over conventional radiography and clinical CT due to its ability to precisely evaluate bone stereology at high resolution due to high X-ray density of osseous materials (Fajardo and Muller, 2001). Despite the advancement of micro-CT compared to clinical CT, this apparatus does have some limitations when compared to other imaging modality. This includes reduced soft tissue contrast and high radiation dose compared to micro-MRI (µMRI) and should be considered as a complementary and adjunct technique to µMRI (Schambach *et al,* 2010) and bone histomorphometry rather than a replacement.

iii) Digital photography (Chapter 7)

For the third study involving the juvenile ilium, a Nikon D80 Digital single-lens reflex (SLR) 10.2 megapixel camera was used to capture a two-dimensional (2D) image.

Figure 4.11: An example of a Nikon D80 DSLR camera.

The DSLR camera (Figure 4.11) was used because of the superior image quality due to enhanced resolution of an isolated targeted image from the background due to full

control over depth of field. As the ilium is a relatively flat bone, it was laid on a horizontal surface with the pelvic surface positioned superiorly. A photographic scale was placed next to each specimen. The camera was stabilised on a tripod, with the lens positioned directly above and parallel to the specimen. The image taken was stored on an SD memory card in JPEG format.

4.3.2 Software used in this study

i) Adobe Photoshop CS3 (Chapter 5)

Adobe Photoshop is the main programme used for processing the 256 gray levels of a digitized macroradiograph sacral image. This software allows grayscale radiographic images to be transformed into a more comprehensive processed image for ease of interpretation. The grayscale colour, which is a set range of 256 shades of gray without any colour, was compared with the four colour mapping (yellow, violet, orange and blue) with the values being as follows:

(i) Yellow colour 0-30% opacity = gray values of 1-75 

(ii) Violet colour 31-50% opacity  = gray values of 76-127 

(iii) Orange colour 51-70% opacity  = gray values of 128-178 

(iv) Blue colour 71-100% opacity  = gray values of 179-256

The selections on percentage of opacity (%) in each of the four colours were based on a previous study on the neonatal ilium (Cunningham and Black, 2009a), so that this result will be standardized for comparative purpose. The higher the gray level (towards 256 levels), the higher the opacity of the image, which appeared as white, and directly presents as blue in the processed gradient mapped image. The blue colour, which represents the 71-100% opacity, indicates the highest density areas present in the juvenile sacrum.

The Conversion of the grayscale image into a processed gradient mapped Adobe Photoshop is as follows:

1. The desired sacral image was opened using the Adobe Photoshop CS3 (File → Open → sacra image)
2. The black and white sacral image appeared in the middle window of the Adobe Photoshop programme.
3. Then the image was set into an RGB (red, green, blue) mode (Image → Mode → RGB)
4. The image was then desaturated to produce a greater scope of the image colour (Image → Adjustment → Desaturate)
5. Finally, the desaturated image was transformed into a four-coloured gradient image (Figure 4.12) for better interpretation compared to the black and white image (Image → Adjustment → Gradient Map) with the percentage of the four different colours as described above.

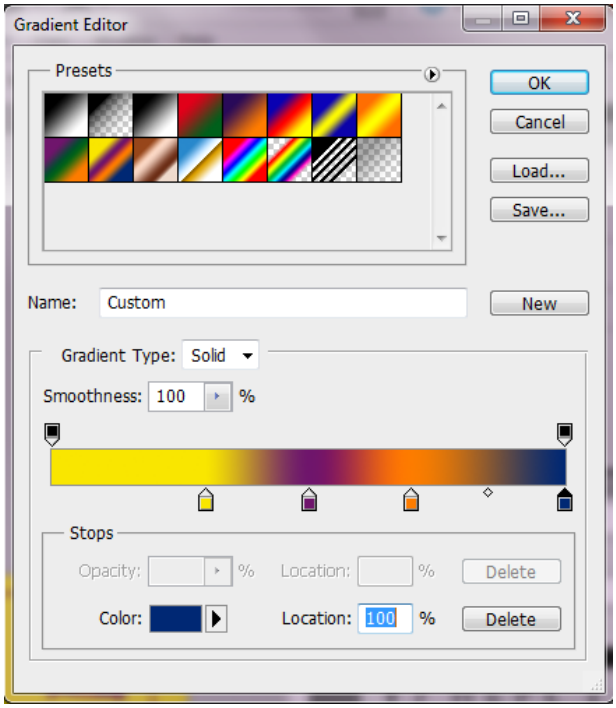

Figure 4.12: Adobe Photoshop CS3 screenshot during one of the image transformation procedure in processing the greyscale radiographic image.

The final result of this method was to transform a plain, black and white radiographic image into a four gradient colour map according to density regions of the sacrum (Figure 4.13).

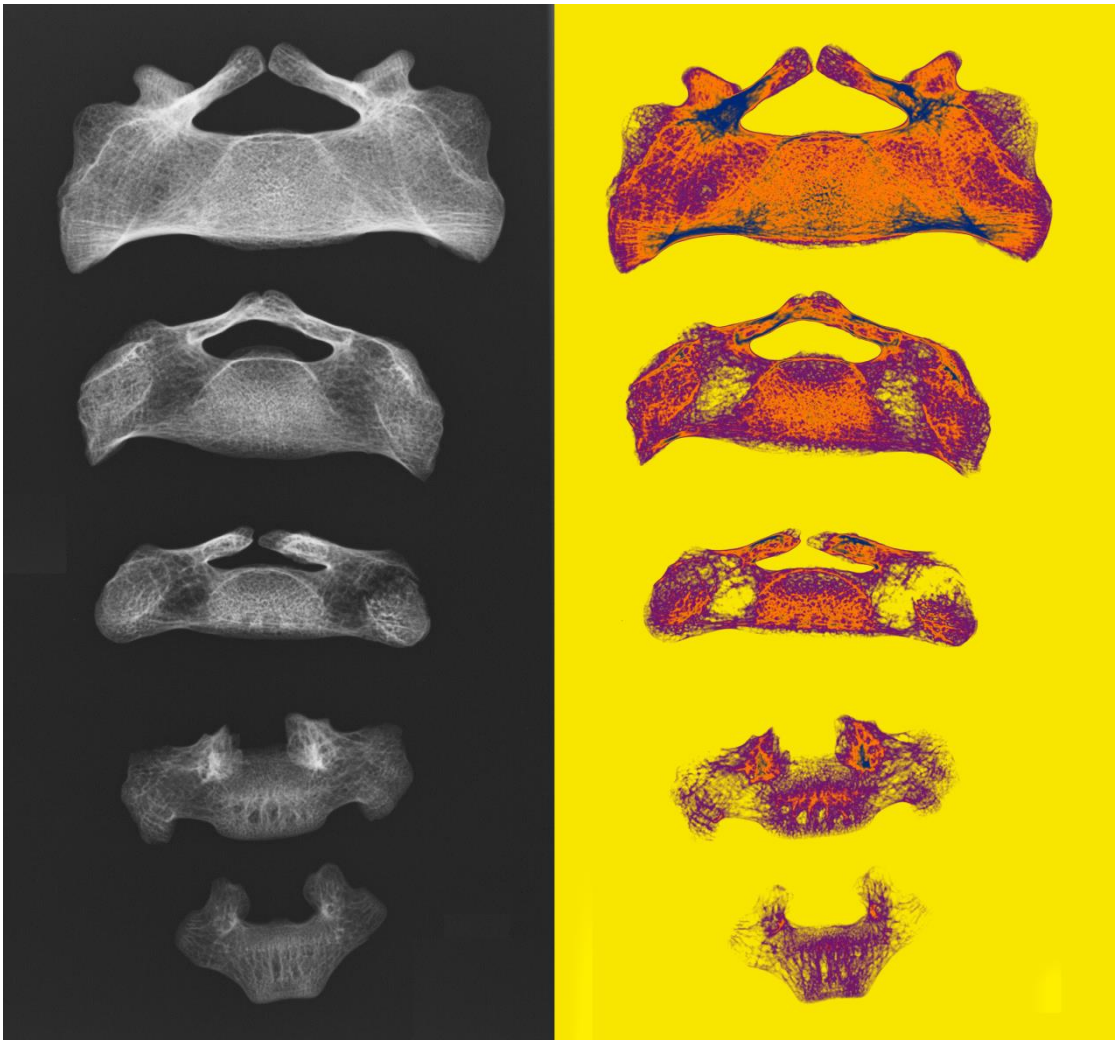

Figure 4.13: A 5-8 years sacrum in (a) plain radiographic image and (b) Adobe Photoshop's transformed image into four gradient colour mapping.

This conversion method was published by Cunningham and Black (2009a). Subsequently, this method served as a preliminary study that expanded into the quantitative and definitive research of the trabecular architecture (Cunningham and Black, 2009b, 2009c and 2010).

iii) OsiriX 3.9.4 (Chapter 6)

OsiriX is an open source software (OSS) released in 2004 (Rosset *et al,* 2004) for navigation and visualisation of 2D, 3D and 4D images to produce high-quality analysis tools that meet user needs. The software offers all modern rendering modes; surface rendering (Figure 4.14), volume rendering, multiplanar reconstruction (MPR) and maximum intensity projection (Ratib and Rosset, 2006). It only runs on Apple Macintosh and the 32-bit is distributed free under GNU General Public Licence and its source code is available widely. However, due to the large file size associated with each specimen's data (Chapter 6), the 64-bit OsiriX was purchased for this study to facilitate the analysis.

Figure 4.14: A 3-dimensional surface rendering of S1 vertebra in a 4-6 year old specimen using OsiriX.

In this study, OsiriX was selected to overcome a problem with the sacral images scanned by micro-CT. The sacral images were scanned from the lateral view, while the study of the sacra was designed from a superoinferior view. Thus, OsiriX is used for multiplanar reconstructions of the images to produce the desired view. It can visualise the scanned sacral images from 3 different views; the superoinferior (SI), anteroposterior (AP) and lateral. As the reconstructed image of the sacrum scanned by micro-CT was from the lateral view, the image was resliced using OsiriX to obtain the SI view. This SI view would enable the next software (Skyscan CTAnalyser) to analyse the selected VOIs (volume of interests) placed on the sacrum.

The steps for MPR (multiplanar reconstruction) with some screenshot images of the S1 vertebral using OsiriX 3.9.4 are explained below:

1. The sacral files were open using OsiriX 3.9.4 (Local Default Database).
2. The image file was clicked.
3. The image was opened in a 2-dimensional view (Figure 4.15).

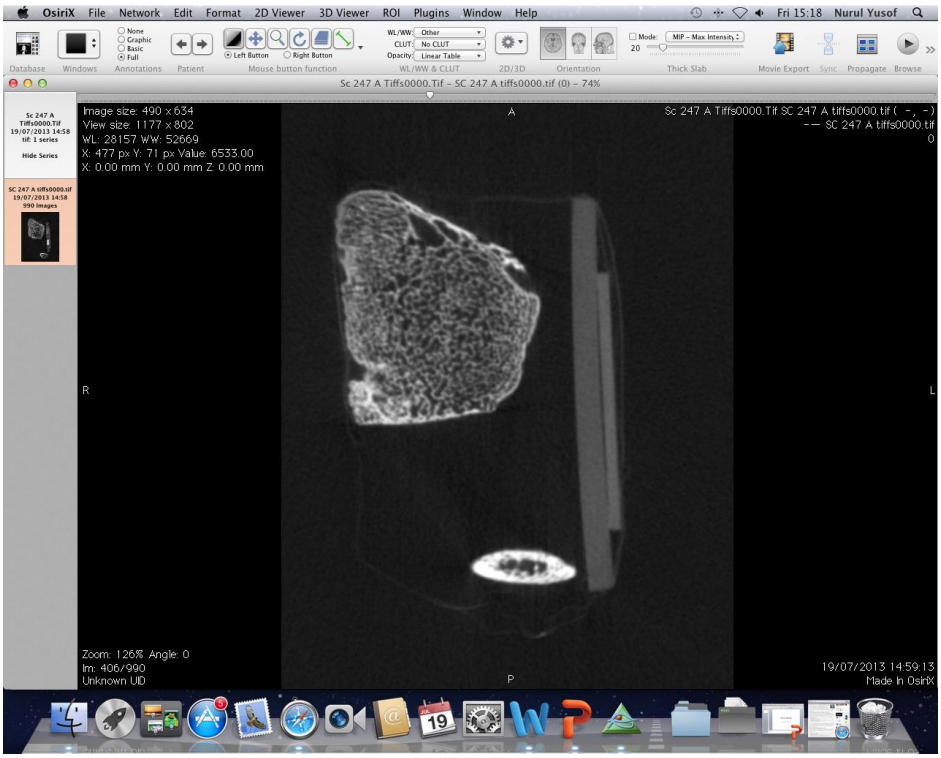

Figure 4.15: An initial lateral view of the sliced S1 vertebra in 2D image.

4. 2D Viewer icon was selected and the ‘Reset Image View’ button was clicked.
5. Then 3D viewer was selected, and 3D MPR option was clicked with the resolution for x, y and z planes set according to the specimen’s data.
6. Three windows appeared and the sacrum was viewed from three different angles; superoinferior (SI), anteroposterior (AP) and lateral (Figure 4.16).

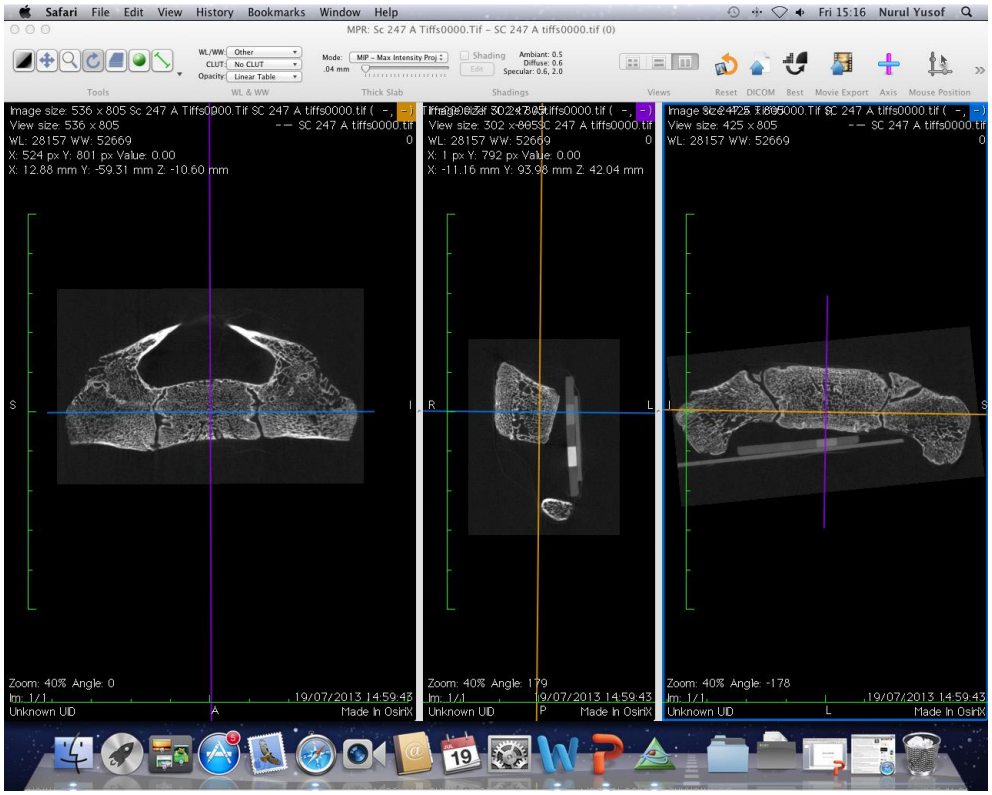

Figure 4.16: A multiplanar reconstructive image of S1 vertebra in three different angles.

7. The SI view was selected and in the screenshot below, the S1 vertebra showed an inferior-half of the vertebra (Figure 4.17).
8. The image was then adjusted to achieve the best possible symmetry of the right and left sides of the vertebra and the files were exported by clicking the ‘export (DICOM)’ button.

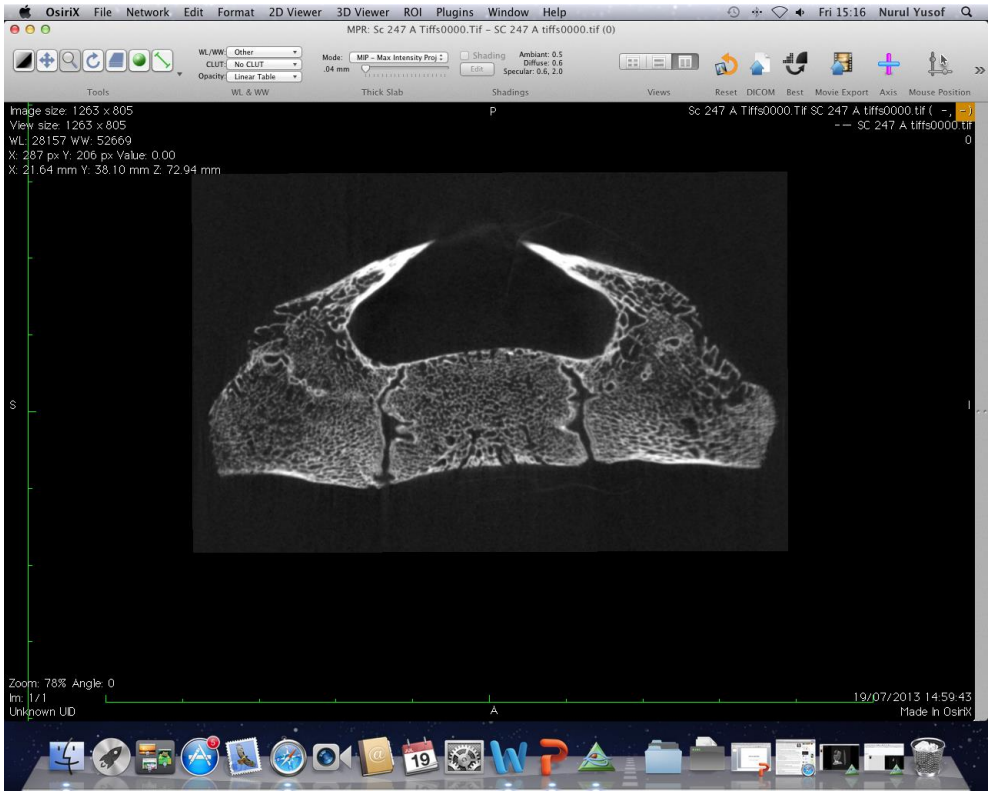

Figure 4.17: The desired (SI) view of the S1 vertebra.

9. The box for ‘same as thickness’ was ticked and the quality was set as ‘Current Quality’ and ‘Full 16-bit BW’ (Figure 4.18).
10. The files were saved as TIFF files.

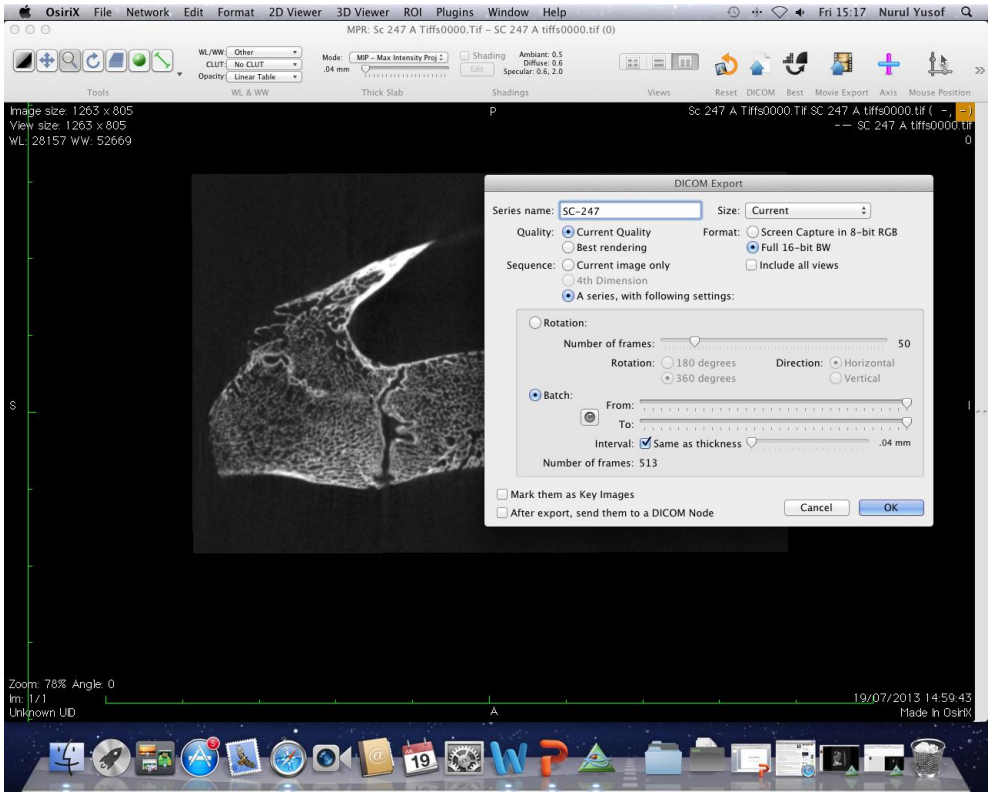

Figure 4.18: The SI view of the S1 vertebra was saved in full 16-bit TIFF format as post-MPR (multiplanar reconstruction) files.

11. The saved post-MPR sacral files were then converted using Adobe Photoshop CS5 to a readable format for Skyscan analysis.

iii) Skyscan CTAnalyser 1.11 (Chapter 6)

Skyscan CTAnalyser (CTAn) is a programme that has been used for image processing in a number of recent trabecular and cortical studies (Chappard *et al*, 2005, Beaupied *et al*, 2006; Cunningham and Black 2009b; Cunningham and Black 2009c). The studies used typical morphological parameters obtained in 3D binarised volumes using Skyscan CTAnalyser to measure quantitative parameters and construct visual models obtained from Skyscan micro-CT scanner or other imaging modalities. CTAn allows real time volume rendering model viewing. The tools provided for highly flexible volume of interest (VOI) delineation, which were organised in five main stages; (1) raw images → (2) region of interest → (3) binary selection → (4) morphometry → (5) custom processing. An example of stage 4 (morphometry) in obtaining trabecular thickness (Tb.Th) and trabecular separation (Tb.Sp) in a specific VOI is illustrated in Figure 4.19.

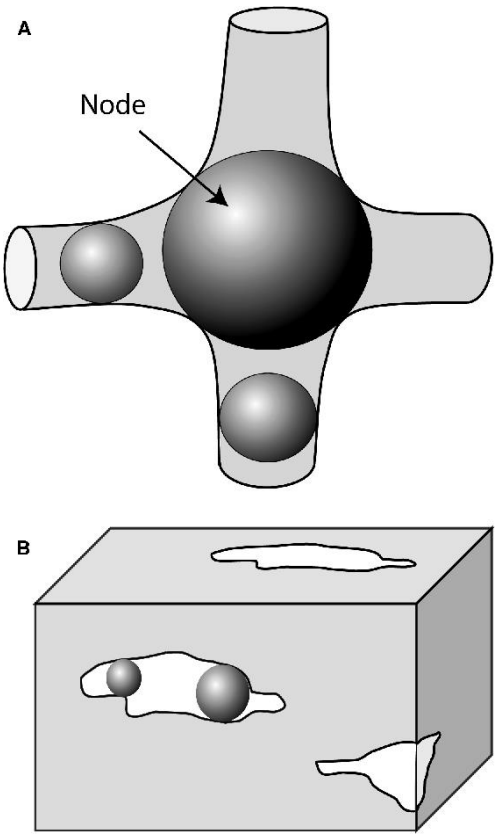

Figure 4.19: The sphere algorithm used to measure (A) Tb.Th using trabecular nodes and (B) Tb.Sp in the marrow cavity (taken from Chappard *et al*, 2005).

As the Skyscan CTAn is the essential programme used in quantifying the sacrum in the study of Chapter 6, the step by step guides are laid out for better understanding of analysing these post-MPR images by OsiriX earlier.

1. Initially, the Skyscan CTAn version 1.11 was opened (Figure 4.20).

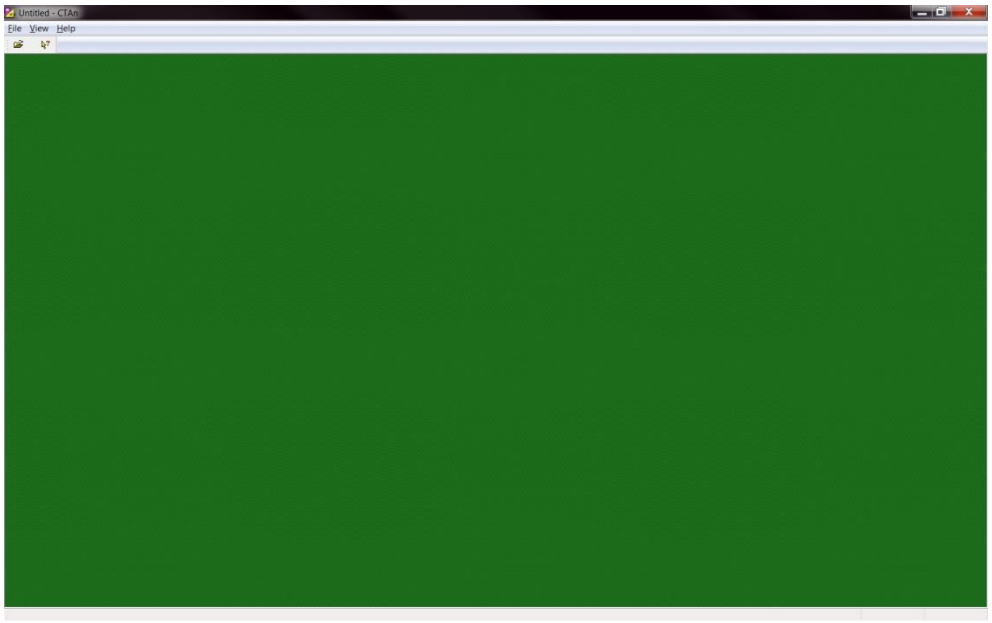

Figure 4.20: The initial window of the Skyscan CTAn version 1.11.

2. The TIFF files (from the converted Adobe Photoshop CS5) were opened.
3. The ‘Image’ icon was clicked and then ‘Properties’ clicked. This serves to calibrate the pixel size in accordance with the resolution of the selected sacral images. The parameter was set in micrometre (µm).
4. The unit of the analysis was set to ‘mm’ and nomenclature was set as ‘Bone ASBMR’ in the ‘File’ → ‘Preferences’ →‘General’. Bone ASBMR (American Society of Bone and Mineral Research) nomenclature used the recommendations of the ASBMR committee on histomorphometric terminology that is applicable for trabecular bone study (Parfitt *et al*, 1987), while the ‘General Scientific’ nomenclature is more appropriate for other studies.

5. Next, one sliced image from the stacked files of a specimen is selected and then clicked at the ‘Palette’ at the right-hand side of the window. The ‘Grayscale’ of the image was selected and adjusted. The image in Figure 4.21 is an example of the superior-half of an S1 vertebra seen from superoinferior (SI) view.

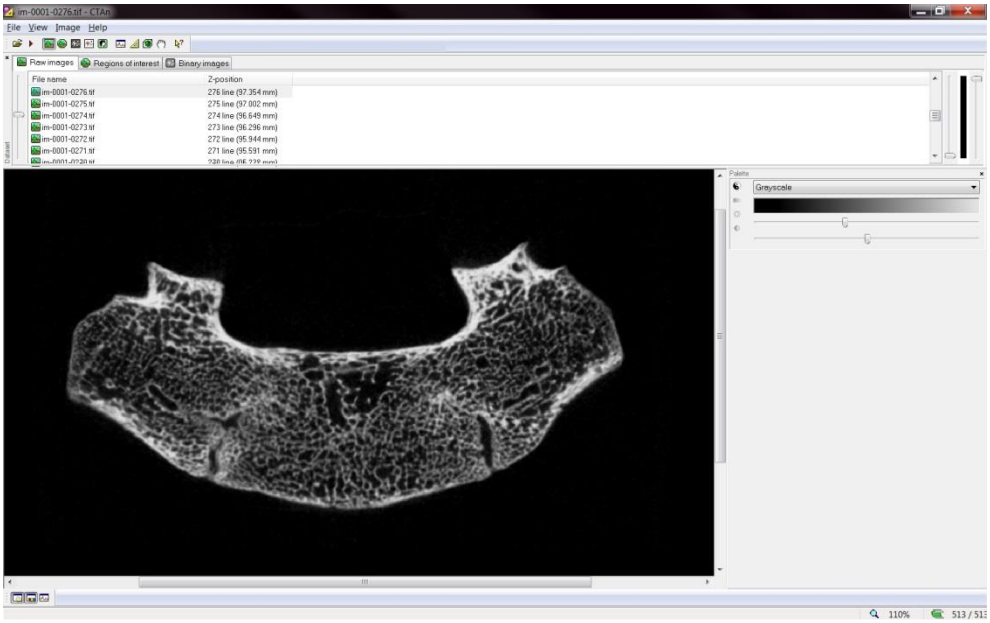

Figure 4.21: A 2D view at the level approximately superior half of an S1 vertebra.

6. The orientation of the images was from inferior to superior, so that the smaller image numbers of TIFF files was the lower part of the S1 vertebra and the larger image numbers of TIFF files was the upper part of the S1 vertebra.
7. After confirming the orientation of the S1 vertebra, a transparent copier sheet was laid on the desktop, directly over the S1 image. The outer lining of the S1 was delineated using a marker pen and the 14 volume of interests (VOIs) of the superior-half and inferior-half of the S1 were drawn. A comprehensive explanation on the production and justification of the 28 VOIs is described in Chapter 6.

8. The volume of interest (VOI) was defined by setting up the ‘top selection’ (right-hand click) in the uppermost targeted VOI which still has trabecular regions, and the ‘bottom selection’ (right-hand click) for the lowermost VOI that still showed trabecular bone (Figure 4.18). This has to be done with caution so as to not include the cortex in the selected VOI. The thickness of the sacrum was calculated from the top and bottom selection and divided in half, so that the upper half would be the superior (s) VOIs and the lower half would be the inferior (i) VOIs.
9. The ROI icon (represents the region of the VOI) on the toolbar was clicked and ‘Interpolated’ was selected for easier delineation.
10. A Wacom tablet was used to delineate the targeted regions in the selected VOIs which consisted of 28 VOIs (14 superior and 14 inferior) in each sample. The selected VOI appeared as a red region in the sacra image (Figure 4.22).

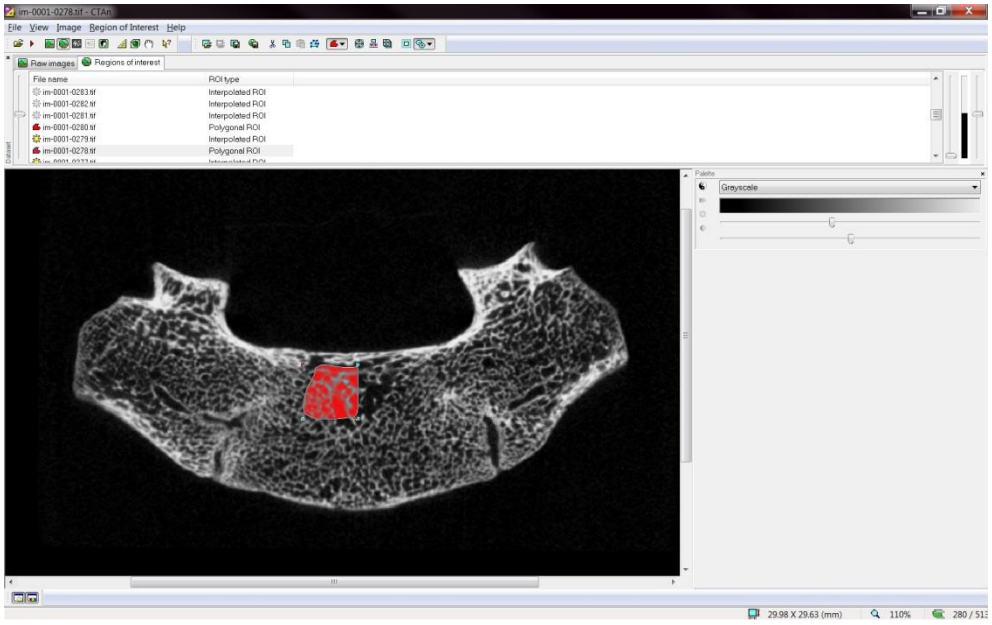

Figure 4.22: The selected area of interest (red-coloured region) was aligned between the uppermost and lowermost part of the specific VOI (volume of interest).

11. The ‘Binary images’ button was selected for binary conversion to detect which part is bone (white) and non-bone (black).
12. Then the ‘Toggle halftone view’ and ‘Toggle VOI view’ were selected and the Histogram was set to make sure that bone appeared in pink (selected trabecular bone), and the remaining areas were green (soft tissues and the air) (Figure 4.23). It was then checked for every layer of the selected VOI (Figure 4.24).

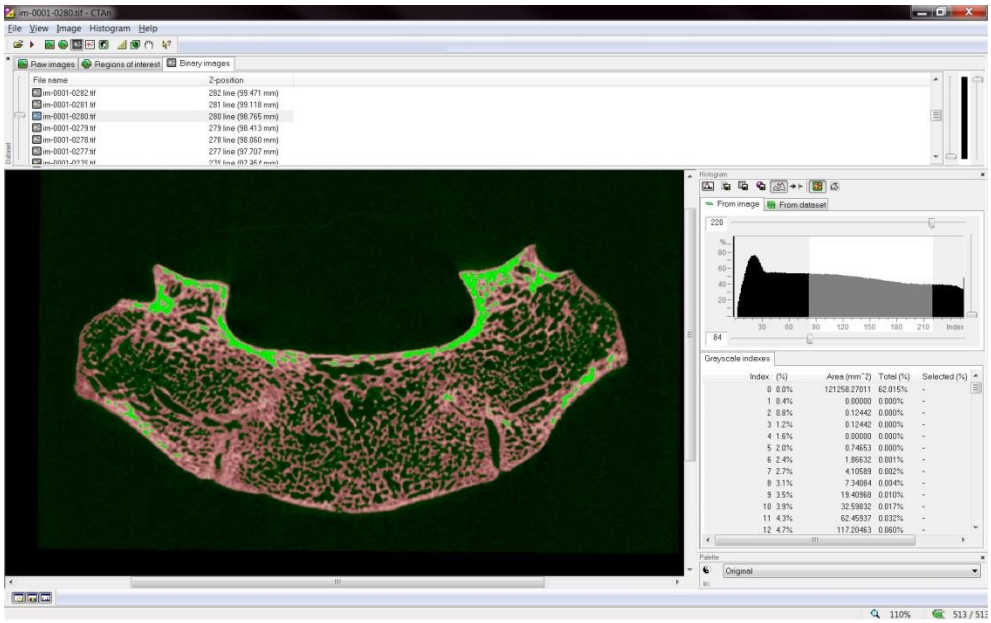

Figure 4.23: The trabecular area appeared in pink and the remaining (soft tissues and air) appeared in green.

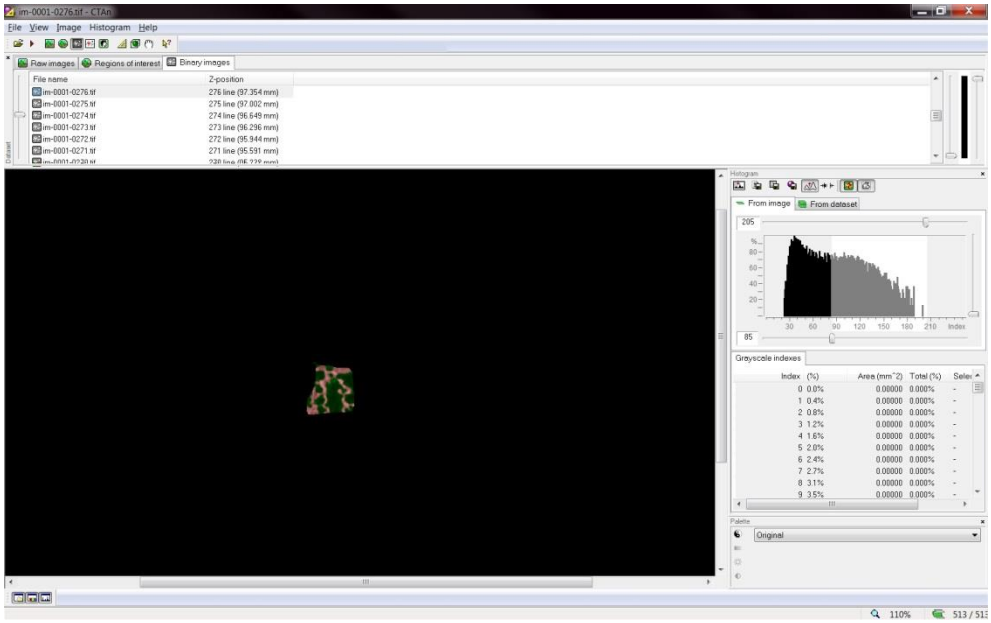

Figure 4.24: The desired VOI was selected and processed.

13. The ‘Processed Images’ button was clicked and then ‘3D analysis’ on the right hand side was selected.
14. The box of ‘Basic values’ and the ‘Additional values’ were ticked. Then the ‘continue’ button was clicked.
15. The results of the bone parameters appeared after a few minutes. Only six parameters were selected for this study:
    i) BV/TV% (percentage of bone volume fraction)
    ii) Tb.Th (trabecular thickness)
    iii) Tb.Sp (trabecular separation)
    iv) Tb.N (trabecular number)
    v) SMI (structural model index)
    vi) DA (degree of anisotropy).

These processes were repeated for each of the 28 VOIs. The details on the six bone histomorphometry nomenclature (Parfitt *et al,* 1987; Hildebrand and Rüegsegger, 1997; Odgaard, 1997; Hildebrand *et al,* 1999; Jiang *et al*, 2000) and the results obtained are discussed in Chapter 6.

iv) Image J (Chapter 7)

"ImageJ", a java-based program for image processing and analysis, was used to measure the defined surface areas of the photographed ilia. This program is used to calculate surface areas, pixel value statistics, distances and angles and supports standard image processing functions in their standard data format type (Abramoff *et al*, 2004). In the study of Chapter 7, ImageJ was used to measure the surface area of four regions in the juvenile ilium (Figure 4.25).

Before the measurements were taken, the images were calibrated using the software calibration feature in ImageJ to address some aspects of image distortion. It is recognised that the reduction of a three dimensional (albeit relatively flat) object to a two dimensional image, will result in some error: this might be overcome in future research through a three dimensional scanning approach.

Figure 4.25: An example of a 2 year old ilium (pelvic surface).

Each area of interest on the photographed ilium was outlined (Figure 4.25) using a Wacom tablet system - a cordless, pressure-sensitive digital pen that allows the user to achieve more precise and repeatable digital drawings. This tablet was connected to the computer and replaced the mouse function directly. After the targeted region was delineated, the surface area was calculated and the result expressed in millimetres squared (mm^2). The results of the four targeted surface areas on the juvenile ilium are presented in Chapter 7.

CHAPTER 5

Qualitative Radiographic Analysis of the Architectural Pattern of the Juvenile Sacrum – The Gradient Mapped Sacra

5.1 Introduction

This chapter presents the results of a qualitative radiographic study undertaken on 68 human sacra from the Scheuer Collection of juvenile skeletal remains housed within the Centre for Anatomy and Human Identification, University of Dundee. Specimens ranged in age from the fetal period to late adolescence.

The sacrum was chosen in this study because it is located at the intersection between the axial and appendicular skeleton where the body weight is transferred to the innominates. Although extensive research has been undertaken on the lower lumbar regions, little is known about the internal osseous architectural pattern at this crucial junction (Pal, 1989; Peretz *et al,* 1998; Ebraheim *et al,* 2000), particularly in the developing sacrum.

The sacrum is thought to play a vital role in body weight transmission through its auricular surfaces which articulate with the iliac auricular surfaces to form the paired sacroiliac joints (Williams and Warwick, 1980; Bellamy *et al*, 1983). However some authors argue that the vertically-oriented joint does not bear load (Last, 1978; DonTigny, 1985) and instead the load is proposed to be suspended by the sacroiliac ligaments (Palastanga and Soames, 2012). Thus, the sacroiliac joint is regarded as an atypical joint in relation to weight transfer (Brooke, 1934; Last 1978; Bellamy *et al,* 1983; DonTigny, 1985). Furthermore, detailed qualitative and quantitative study of the ilium, which forms the opposing side of the sacroiliac joint, has previously been undertaken and showed interesting results for the sacroiliac region where the auricular

region exhibits medium to low bone density areas (Cunningham and Black, 2009a; 2009b).

Studies on the sacrum largely focus on its clinical relevance (Young *et al*, 1986; Denis *et al*, 1988, Ayoub, 2009, Gribnau *et al*, 2009) and the biomechanical influences on the sacroiliac joint (DonTigny, 1993; Dalstra and Huiskes, 1995; Zheng *et al*, 1997; Wingerden, 2004; Pel *et al*, 2008). However, limited literature concerning the development of the sacrum is available (Broome *et al*, 1998), especially in relation to its cortical and trabecular architecture (Pal, 1989; Mahato, 2010). Further, the majority of studies focus on the adult sacrum (Pal, 1989; Peretz *et al*, 1998; Ebraheim *et al*, 2000; Wu *et al*, 2009; Mahato 2013) with extremely little known about the relevance of the bone in relation to its biomechanics in the child.

The current study aims to address this paucity of information in the developmental literature by documenting the qualitative developmental patterning of the cortical and trabecular architecture in the juvenile sacrum. This analysis will serve as a preliminary study investigating the changes in the developing sacrum, which will provide a foundation for a more specific quantitative study in Chapter 6.

5.2 Materials and Methods

Materials

Sixty-eight juvenile sacra were selected for this study ranging in age from the early fetal periods to late adolescence (Figure 5.1). The youngest fetal specimen was 18 weeks *in utero* and the oldest specimen was 20 years of age. The specimens selected were in good condition with minimal damage to the cortex: all severely damaged and

pathological specimens were excluded. The demographic details of the specimens are presented in the result section of this chapter.

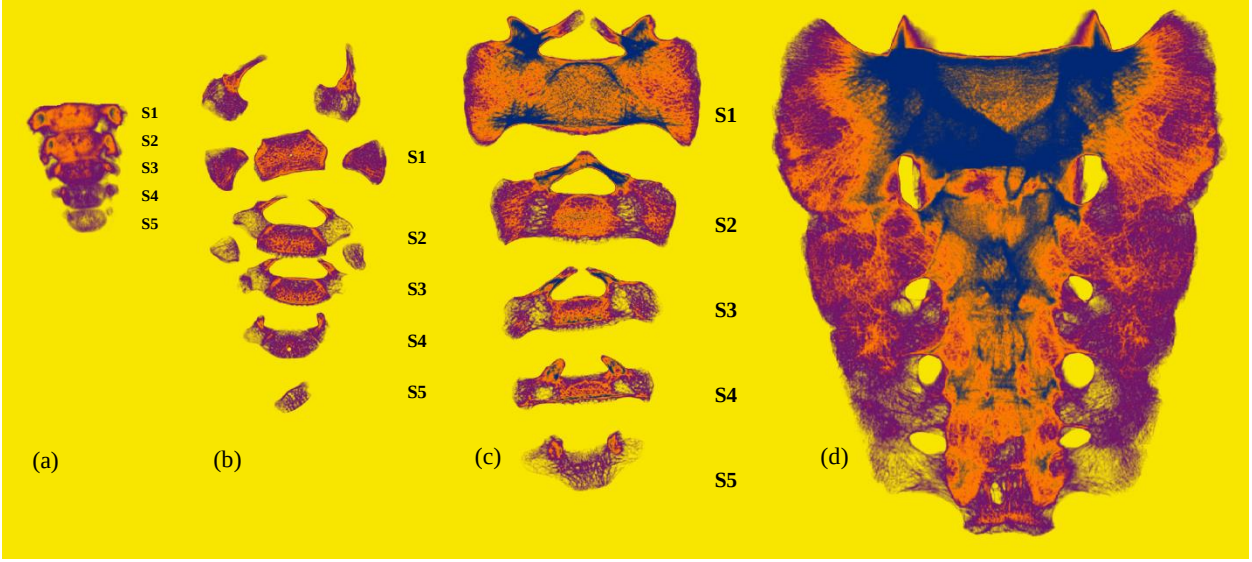

Figure 5.1: Four radiographs of sacra at various developmental stages viewed from different angles: (a) fetal sacrum (joined by mummified surrounding tissues) in anteroposterior (AP) view, (b) 1 year old sacrum in superoinferior (SI) view, (c) 7 year old sacrum in SI view and (s) 17 year old sacrum in AP view.

Methods

The 68 specimens selected were each macroradiographed using the procedure outlined in Chapter 4. For the fused sacra, the macroradiographs were taken from an anteroposterior (AP) view, while the unfused sacra were macroradiographed in a superoinferior view. Following macroradiography, each image was colour-mapped using Adobe Photoshop CS3 (Figure 5.2). Further details on the Adobe Photoshop procedure are discussed in Chapter 4 (Materials and Methods).

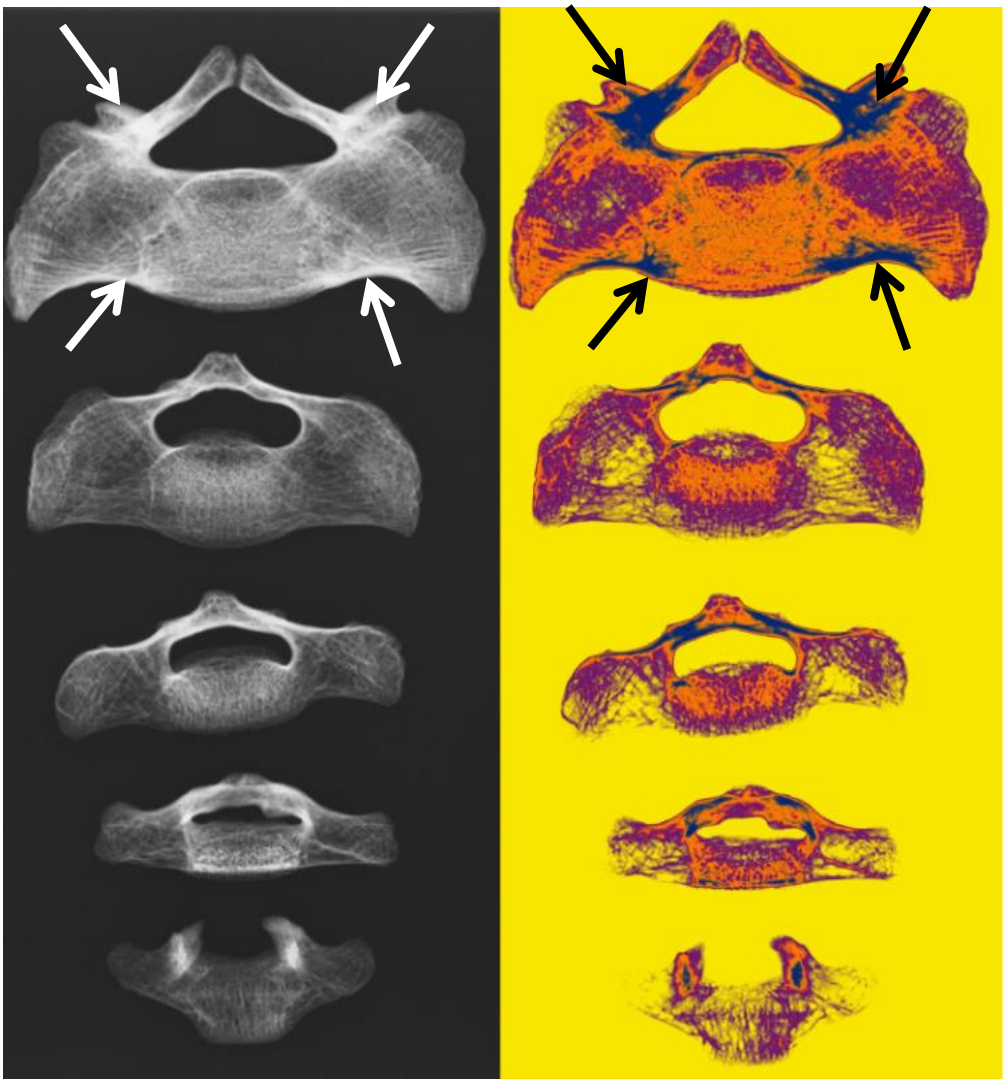

Figure 5.2: The transformation of a plain plate radiograph of an eight year old specimen (left), into a colour-mapped image using Adobe Photoshop (right). The white arrows demonstrate the radiopaque areas in S1 of the plain plate radiograph (left) and are represented by the blue colour (black arrows) in the processed image (right).

The colour mapping uses four colours applied across a gray value spectrum:

(i) Background radiographic intensity: Yellow- colour 0-30% opacity.

(ii) Low-intensity regions: Violet-colour 31-50% opacity.

(iii) Medium-intensity regions: Orange-colour 51-70% opacity.

(iv) High-intensity regions: Blue-colour 71-100% opacity.

This intensity is representative of the ‘density’ regions across the sacrum. At one extreme, yellow represents the least intense area of opacity and was set as the

background of the image, whilst blue represents a high intense area of opacity (Figure 5.3). A standard grayscale radiograph contains 256 levels of gray. These levels were then mapped to one of four colours to facilitate interpretation (Figure 5.3).

This colour mapping enables simple interpretation of the different intensity areas (represented by 4 colours) in the sacrum compared to 256 levels of gray in a plain radiographic image. Details on the conversion of the grayscale image to four different colour-mapping are discussed in Chapter 4 (Materials and Methods).

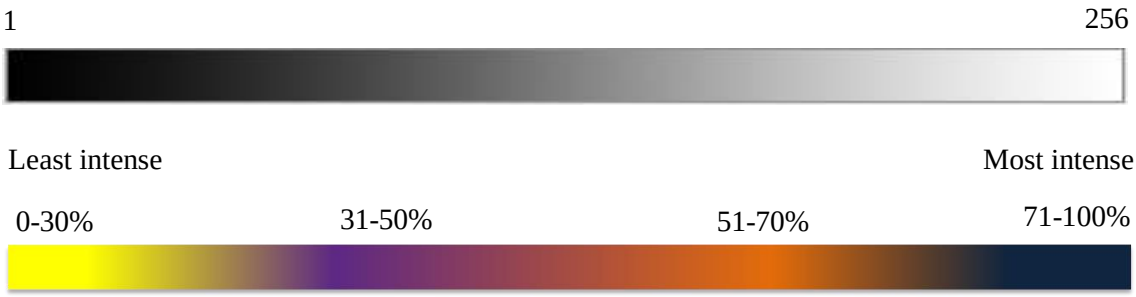

Figure 5.3: The grayscale (above) consists of 256 shades of grey, compared to the four different colour gradient using Adobe Photoshop CS3.

5.3 Results

The 68 specimens were categorised into 4 different groups according to morphological appearance and stage of fusion (Table 5.1). Specimens of a similar age may have been grouped separately due to their physical characteristics and the state of union, as there is substantial variation in the rate and timing of skeletal maturation between individuals (Tanner *et al*, 1983; White and Folkens, 2005). Thus, there was some overlapping of age between the groups. This method of grouping facilitated the interpretation of the findings within each group and aided the interpretation of changes between groups based therefore on maturity and not age directly.

Group	Appearance	Age Range	n
1	Sacrum in various stages of primary ossification	Fetal – 5 months	18
2	Unfused 5 elements in S1 with S2-S5 fused within each vertebra	1 - 4 years	14
3	Fused 5 elements in S1 with S2-S5 fused within each vertebra	4 - 11 years	16
4	Complete intervertebral S1-S5 fusion	11 - 20 years	20
		Total	68

Table 5.1: The four groups of juvenile sacra based on the appearance of ossification centres and the stages of fusion.

GROUP 1

Group 1 consists of 18 specimens from the fetal, perinatal and neonatal periods and one individual aged 5 months post-partum (Table 5.2). The fetal specimens represent individuals from 18 weeks through to term. Specimens in this group either presented as a unified structure (Figure 5.4 (a)) or as separate bony components (Figure 5.4 (b)). All the primary centres of ossification of the specimens are generally present at birth and identifiable in isolation (Scheuer and Black, 2000).

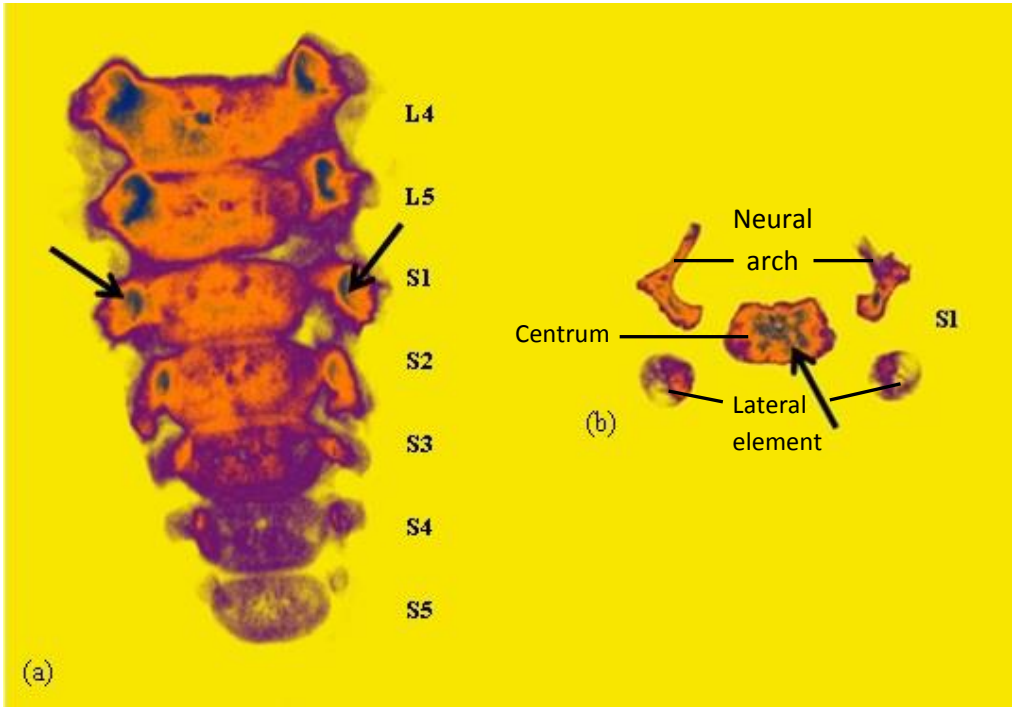

Figure 5.4: An example of (a) fetal sacrum of 36-38 weeks *in utero* with L4/L5 in anteroposterior (AP) view and (b) perinatal sacrum (S1) in superoinferior (SI) view. The

large black arrows point to the highest density areas on S1 vertebra in both AP and SI views.

No.	Specimen	Age
1	SC-274	18-20 weeks *in utero*
2	SC-272	20-22 weeks *in utero*
3	SC-273	22-24 weeks *in utero*
4	SC-270	22-26 weeks *in utero*
5	SC-271	22-26 weeks *in utero*
6	SC-269	26-30 weeks *in utero*
7	SC-266	30-32 weeks *in utero*
8	SC-267	32 weeks *in utero*
9	SC-268	32-36 weeks *in utero*
10	SC-265	36-38 weeks *in utero*
11	SC-092	Perinate
12	SC-097	Perinate
13	SC-151	Perinate
14	SC-161	Perinate
15	SC-262	Neonate
16	SC-263	Neonate
17	SC-264	Neonate
18	SC-021	5 months

Table 5.2: The 18 sacral specimens in group 1

General Appearance and Stage of Ossification

Fetal specimens

The fetal sacra in Figure 5.4 (a) represent the appearance of 10 fetal specimens in this group and are at a very early stage of ossification. Therefore limited information can be deduced due to the fact that all ossified components are connected by the mummified cartilage template of the sacrum. It was therefore difficult to make a comparison between those specimens that could only be viewed in AP orientation compared with those that could be viewed in the SI orientation. The SI orientation was considered a

preferable orientation to examine differences that may be attributed to biomechanical/locomotor influences.

Perinatal-neonatal-5 months specimens

The remaining 8 specimens consist of perinatal, neonatal and 5 months post-natal specimens are the older age specimens in this group, with each sacral element being separate and identifiable in isolation (Figure 5.4 (b)). There is no fusion between any of the sacral elements at this stage. By this age, the 21 separate ossification centres were generally present in most specimens, while a few had incomplete sacral elements. It is likely that the small size of the ossified nodules led to them simply not having been recovered or perhaps having been lost over time in the curatorial process.

Appearance and Intensity Pattern of sacral elements in the perinatal – 5 months specimens (n = 8)

The descriptive findings of the four colour-coded gradient mapped sacra in this group were divided according to the centrum (Figure 5.5), neural arch (Figure 5.6) and lateral element (Figure 5.7). Each colour (violet – orange – blue) represents different regions of intensity. The background radiographic intensity was represented by a yellow colour map and represented 0-30% opacity which confirmed the absence of any bony structure. For the descriptive findings on the specimens in this group, the S1 vertebra (centrum, neural arch and lateral element) illustrated here represent the 5 sacral vertebrae of 21 ossified osseous materials.

Centrum

The centrum presents in each of the 5 sacral segments in all of the specimens of this group. It appeared as a rounded nodule in the younger specimens while in the older specimens it had more well-defined margins, with a longer convex anterior border and shorter concave posterior border with sloping lateral borders (Figure 5.5). The angle between each lateral and the posterior border is well defined. The anterior and posterior borders show a crenulated appearance.

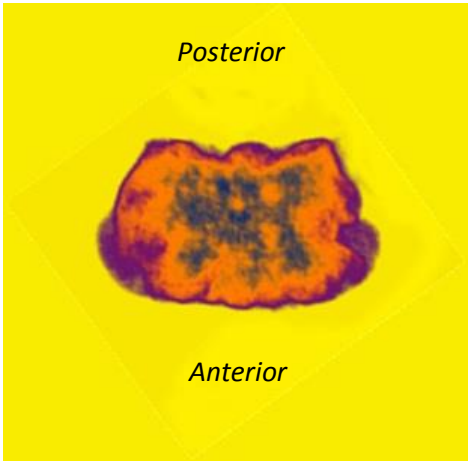

Figure 5.5: A perinatal S1 centrum.

The centrum is easily identified from the neural arches and the lateral elements due to its shape and size. Nevertheless, sometimes it was difficult to identify the anatomical segmental position of the centrum in this age group, especially for the more distal sacral vertebrae.

S1-S2: The centra are characterized by a dense, central concentric colour of high intensity (blue) surrounded by regions of diminishing intensity (orange and violet). The violet regions tend therefore to be restricted to the outer margins of the centra.

S3: The centrum shows a central core of medium intensity (orange) surrounded by a margin of reduced intensity (violet).

S4-S5: Although areas of medium intensity (orange) are visible, these centra tend to be almost exclusively of low intensity (violet) coloration.

Neural arch

The neural arches present as paired elements on each of the 5 sacral segments in all specimens of this group. They have a characteristic L-shape appearance, with gracile elongated laminae and more robust pedicles (Figure 5.6). The position of the superior articular facets was often difficult to identify in this age group. As with the centrum, the distal neural arches are smaller in size compared to those more proximal.

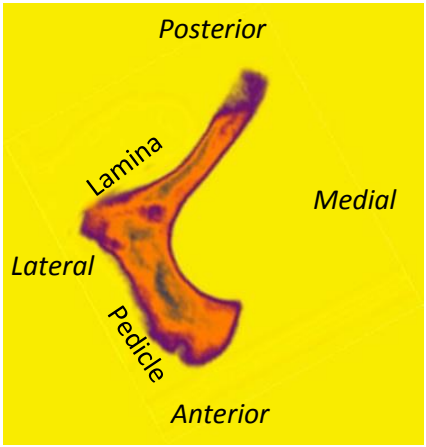

Figure 5.6: A right perinatal S1 neural arch.

S1-S2: In general, the neural arch exhibits dense areas within the core of the pedicle and along the axis of the lamina towards the base of the transverse process. Nevertheless, medium intensity (orange) dominates almost the entire neural arch except the tip of the lamina and around the margins which are lower intensity violet colour.

S3: The neural arches were difficult to recognize in this age group as they are small and showed an area of medium intensity (orange), with low intensity (violet) on the laminae.

S4-S5: The neural arches showed low intensity regions (violet) throughout the elements, although some areas of medium intensity (orange) were occasionally observed.

Lateral element (Sacral alae)

The lateral elements are only present in the first two sacral vertebrae, albeit sometimes appearing in S3. These elements were easily identified in the first two sacral vertebrae, while in the remaining lower sacral vertebrae, the lateral elements often appeared as very small nodules. In the upper vertebrae, the lateral elements usually present as a triangular-shape bone, with the apex facing medially for articulation with the centrum and the base facing laterally for articulation with the ilium, forming the sacroiliac joint (Figure 5.7).

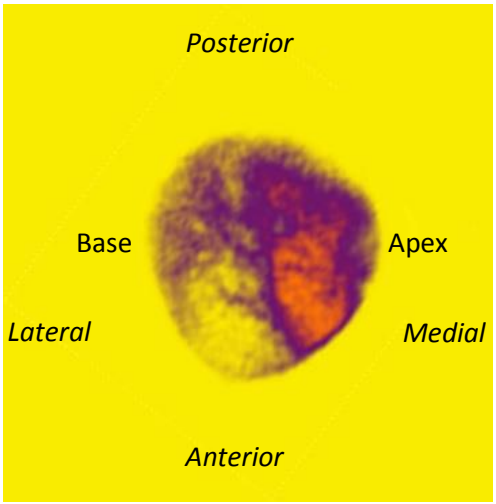

Figure 5.7: A right perinatal S1 lateral element.

S1-S2: These upper two sacral vertebrae showed recognizable lateral elements which exhibited medium intensity areas on the medial side (Figure 5.7). The lateral half of the lateral element represents the auricular surface of the sacroiliac joint and exhibited low intensity areas (violet colour of 31-50% opacity).

S3: The lateral element of S3 only exhibits low intensity (violet) and was hardly recognizable in this group. Some of the specimens did not have lateral elements associated with the S3 vertebra.

GROUP 2

Group 2 consists of specimens from 1 year until 4 years of age (Table 5.3). The 14 sacra shared a common appearance in that S1 appeared as 5 unfused elements (Figure 5.8). This group also showed varying degrees of fusion of S2, where the younger specimen (1 year) showed neurocentral fusion but unfused lateral elements, while in the older specimen (4 years), all the 5 elements of S2 has fused. All of the S3 – S5 were already fused at their respective vertebral level.

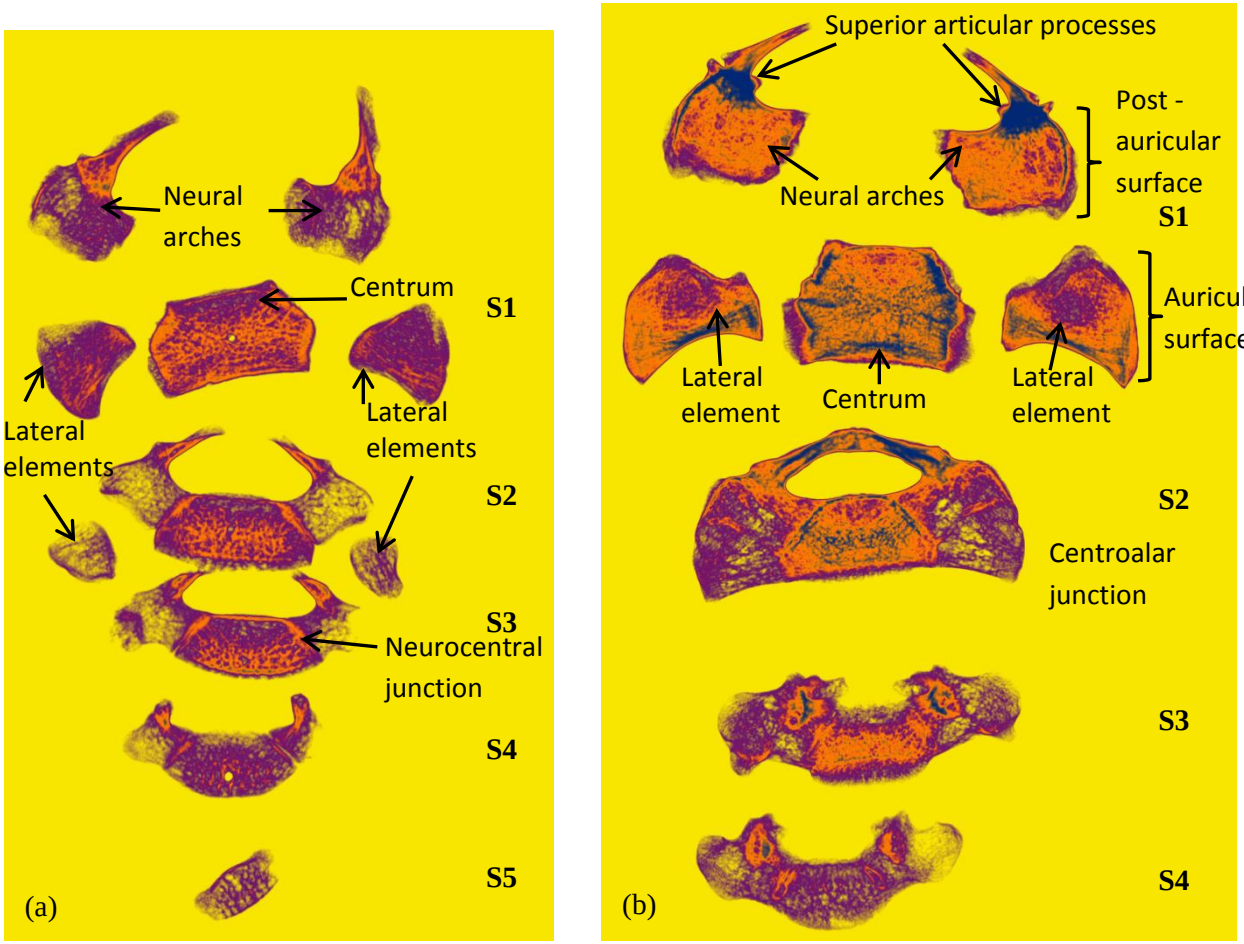

Figure 5.8: The appearance of the unfused S1 elements (paired neural arches, paired alae and a centrum) in (a) 1 year 2 months and (b) 4 years sacra. Note that the lateral elements (sacral alae) of S2 vertebra (a) are still not fused.

No.	Specimen	Age
1	SC-023	1 year
2	SC-067	1 year 2 months
3	SC-068	1 year 3 months
4	SC-069	1 year 3 months
5	SC-070	1 year 6 months
6	SC-137	1.5-2 years
7	SC-071	1 year 11 months
8	SC-024	2 years
9	SC-025	3 years
10	SC-072	3 years
11	SC-073	3 years
12	SC-074	3 years 6 months
13	SC-075	3 years 11 months
14	SC-010	4 years

Table 5.3: The 14 sacral specimens in group 2

General Appearance and Stage of Fusion

In this age group, despite various degrees of fusion in the distal vertebra, the S1 vertebra remains in its unfused 5 element state throughout this group. These 5 sacral elements in S1 also appear in a more identifiable and definite shape as maturity increases from 1 year to 4 years of age. The youngest specimen in Figure 5.8 (a) will be compared with the oldest specimen (b) in the description of this group, which represents the changes occurring within this age group.

Appearance and Intensity Pattern in 1 – 4 year old specimen

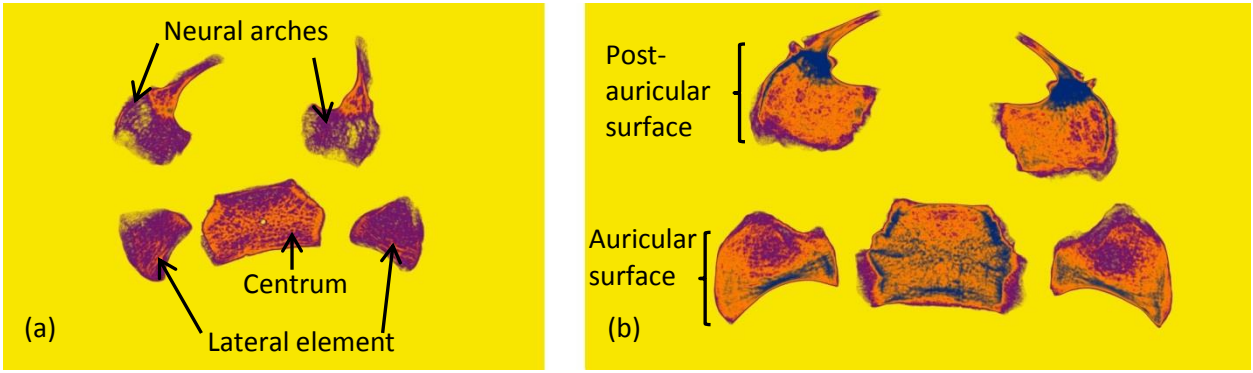

Figure 5.9: The S1 centrum, neural arches and lateral elements (sacral alae) of (a) 1 year and (b) 4 year old specimens.

S1 Centrum

1 year specimen

The S1 centrum in Figure 5.9 (a) appeared as a more identifiable shape than the previous age group, with well-defined sharp, parallel and angled margins on each of its lateral surfaces for articulation with the neural arch posteriorly and the lateral element anteriorly. The central margins are more well defined than the previous age group. The intensity pattern in the centrum in Figure 5.9 (a) is dominated by a medium region (orange) with a posterior triangular area of low intensity (violet). Violet is also present at the periphery of the centrum. The 2 and 3 year old specimens also showed similar appearances.

4 year specimen

In the 4 year old specimen in Figure 5.9 (b), the centrum displays paired billowed articular surfaces on its lateral border. The anterior half of the lateral margin articulates with the lateral element while the posterior half articulates with the neural arch. The demarcation between the two surfaces is very clear. The anterior margin of the centrum

is wider and more concave than the posterior margin which is narrower and straight. By this age, the centrum started to exhibit high intensity areas (blue) at the anterior part of the centrum, and the lateral part that lines the articular margins, as well as blue areas that cross into the middle centrum (Figure 5.9 (b)). The posterior region of the centrum was represented by a medium intensity area (orange) and also a small area of violet in the centre along the posterior border. The anterior half of the lateral-most margin of the centrum appeared with low intensity (violet).

S1 Neural arch

1 year specimen

The S1 neural arch in Figure 5.9 (a) appears small with relatively thick laminae and the remainder is rectangular in shape. The superior articular processes are difficult to identify in this 1 year specimen. In the 2 to 3 year old specimens, the laminae are thinner while the superior articular processes become more prominent. The intensity pattern of the neural arch in Figure 5.9 (a) is dominated by low intensity (violet), with medium intensity (orange) at the proximal part of the laminae. There is also yellow intensity suggesting very little bone is present. There are minimal high intensity (blue) patches at the superior articular processes in Figure 5.9 (a). The older specimens in this group showed similar findings with increased high intensity (blue) areas at the region of superior articular processes.

4 year specimen

In an older 4 year specimen (Figure 5.9 (b)), the neural arches appear bigger, with longer, thin laminae and a more square-shaped billowed articular surface for articulation with the centrum medially and the alae anteriorly. The superior articular process can be seen at the junction between the laminae and the remainder of the neural arch. The

spinous processes of S1 remain separate from 1 year to 4 years at the S1 vertebra. By this age, the intensity pattern of the S1 neural arch showed prominent high intensity areas (blue) (Figure 5.9 (b)) on the superior articular processes which extended on to the post-auricular area by a thin blue line, while the laminae and the remainder of the neural arches are represented by a medium intensity area (orange). Low intensity (violet) areas appeared at the anterior and medial peripheral margins of the neural arches where it approximates to the alae and centrum respectively.

S1 Lateral element (Sacral alae)

1 year specimen

The lateral (costal) element appears as a distinct shape in the 1 year specimen (Figure 5.9 (a)). It has a triangular shape compared to the rounded nodules seen in the previous age group. The apex of this triangular bone faces medially for articulation with the centrum, and the base faces laterally for articulation with the ilium, forming the sacroiliac joint. The anterior border is concave while the lateral border is convex. The older specimens displayed more well-defined borders than the 1 year specimen. The intensity pattern of the lateral elements in Figure 5.9 (a) are dominated by low intensity areas (violet) largely at the centre and along the posterior border, with medium intensity (orange) at its anterior concavity region. There are no high intensity areas detected at this age.

4 year specimen

In the 4 year old specimen (Figure 5.9 (b)), the shape of the lateral elements was more definite: it exhibited four well-defined borders. The lateral element demonstrated a more prominent anterior concavity, with the posterior billowed area for articulation with the

neural arches and medial border for articulation with the centrum. The lateral border appears wider and more convex forming the auricular surface of the sacroiliac joint. By this age, the intensity pattern of the S1 lateral element showed prominent high intensity areas (blue) (Figure 5.9 (b)) focused on the anteromedial concavity region and extending to the medial articulation with the centrum. The lateral region that forms the auricular surface is mainly represented by a medium intensity area (orange), with very minimal high intensity (blue) at the tip of the sacral alae. The low intensity (violet) areas appeared at the middle posterior region of the lateral elements and along the posterior border.

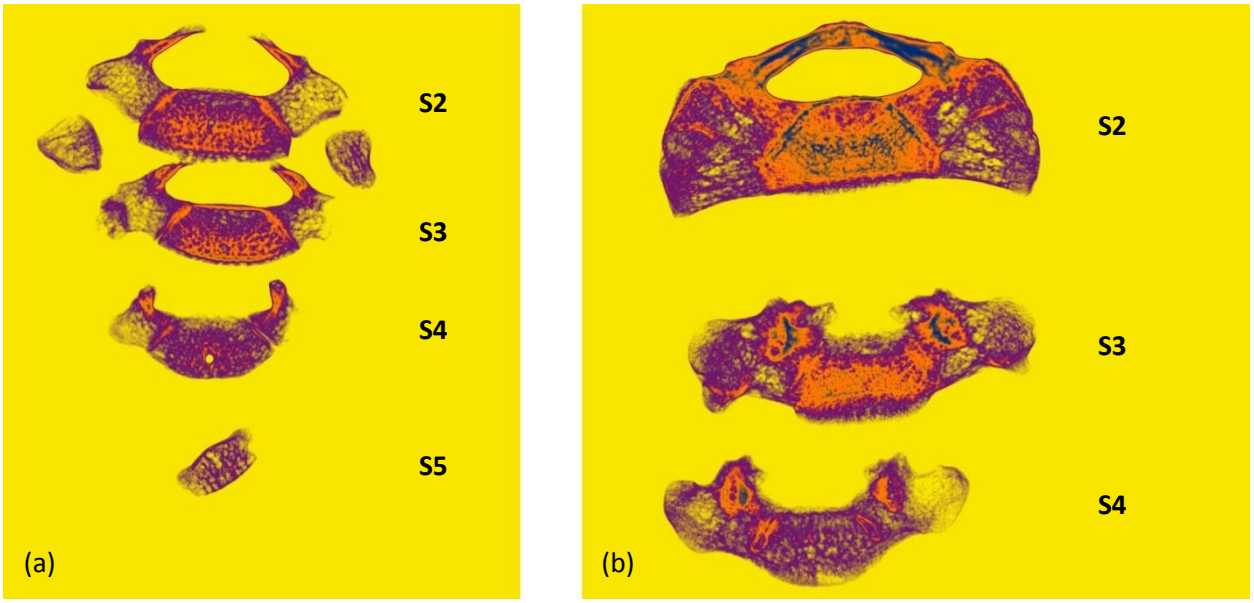

Figure 5.10: The S2 – S5 of 1 year sacrum (a) and S2 – S4 of 4 year old sacrum (b).

Appearance of the S2 – S5 vertebrae in the 1 year specimen

In the 1 year sacrum (Figure 5.10 (a)), the elements in S3 – S5 have started to fuse within each vertebral level, from distal to proximal. The neural arches of S2 – S5 have fused with their centra, with the neural arches of S5 being rudimentary. The spinous process of S2 – S5 still remain unfused. The small lateral elements of S3 have fused

with the neural arches, while the S2 lateral elements remain separate. When the actual specimen is inspected, fusion of the neurocentral junction occurred from posterior to anterior of the junction at each vertebral level. The sacral specimens showed that the lateral elements are present in S3 but appear very small, and attach to the neural arch component if indeed they were ever separate. The older specimens show a more unified fusion of S2-S5 within their vertebral level with the 5 elements in S1 remaining unfused.

Intensity patterns of the three sacral elements in the 1 year specimen:

S2 – S5 Centrum

The S2 and S3 body in Figure 5.10 (a) are dominated by medium intensity (orange) with a posterior triangular area of low intensity (violet). A violet area is also present at the periphery of the centrum. The fusion lines (orange) in Figure 5.10 (a) are visible at both the neurocentral junction of S2 – S3. S4-S5 are mainly represented by a low intensity region (violet) with minimal medium intensity (orange) at the central part of S4 body. In the older specimens, the medium intensity (orange) region on the S2-S3 bodies becomes more prominent, but no high intensity (blue) area is detected before 4 years.

S2 – S5 Neural arch

The neural arches in Figure 5.10 (a) are visible at the S2 – S4, all mainly dominated by low intensity (violet) with medium intensity (orange) laminae. There is no high intensity (blue) area observed. The older specimens show minimal changes with increased medium intensity (orange) at the laminae only.

S2 – S3 Lateral elements (Sacral alae)

The S2 – S3 lateral element/sacral alae in Figure 5.10 (a) are dominated by low intensity (violet) only. The S2 lateral element/alae are part of the caudal auricular surface of the sacroiliac joint. There are no medium or high intensity areas detected at this age. The 2 to 3 year old specimens show similar findings with no medium intensity regions detected.

Appearance of the S2 – S5 vertebrae in the 4 yearold specimen

S2 – S5 vertebrae

The 4 year old sacrum showed complete fusion of the sacral alae in S2 – S4, while all the neural arches are already fused with their centra (Figure 5.10 (b)). The fusion lines can still be seen at the neuroalar junction of S2, and the neurocentral junction of S4, lined by the orange colour. At this age, the posterior synchondrosis has fused in S2, but the rest of the sacral laminae remain bifid.

Intensity patterns of the three sacral elements in the 4 year old specimen:

S2 – S5 Centrum

By this age, the S2 body started showing high intensity areas (blue) at the mid to anterior region (Figure 5.10 (b)) with a faint blue line extending towards the posterior margin. A low intensity area (violet) is seen lining the anterior margin of the S2 body. The S3 body is mainly represented by medium intensity (orange), while the S4 body remains mostly a low intensity (violet) area.

S2 – S5 Neural arch

By this age, the S2 neural arch shows high intensity areas (blue) (Figure 5.10 (b)) at the laminae, while the remainder of the S2 neural arches showed anterior-half low intensity (violet) with posterior-half medium intensity (orange) regions. The S3 – S4 neural arches have a common appearance in which both show small areas of high intensity (blue) at the angle of the small laminae, surrounded by medium intensity (orange) areas around it, while the rest of the S3 and S4 neural arches are seen as low intensity (violet) areas.

S2 – S3 Lateral elements (Sacral alae)

By this age, only the S2 alae were easily recognized, S3 alae were very rudimentary. Both S2 and S3 alae were represented by low intensity (violet) areas, and the fusion lines of the S2 and S3 centroalar junction were marked by medium intensity (orange) lines (Figure 5.10 (b)).

GROUP 3

The third group (*n* = 16) includes specimens from 4 years up until 11 years of age (Table 5.4) where S1 has completed fusion, and the sacrum is represented by 5 complete and separate sacral vertebrae (S1 – S5) (Figure 5.11).

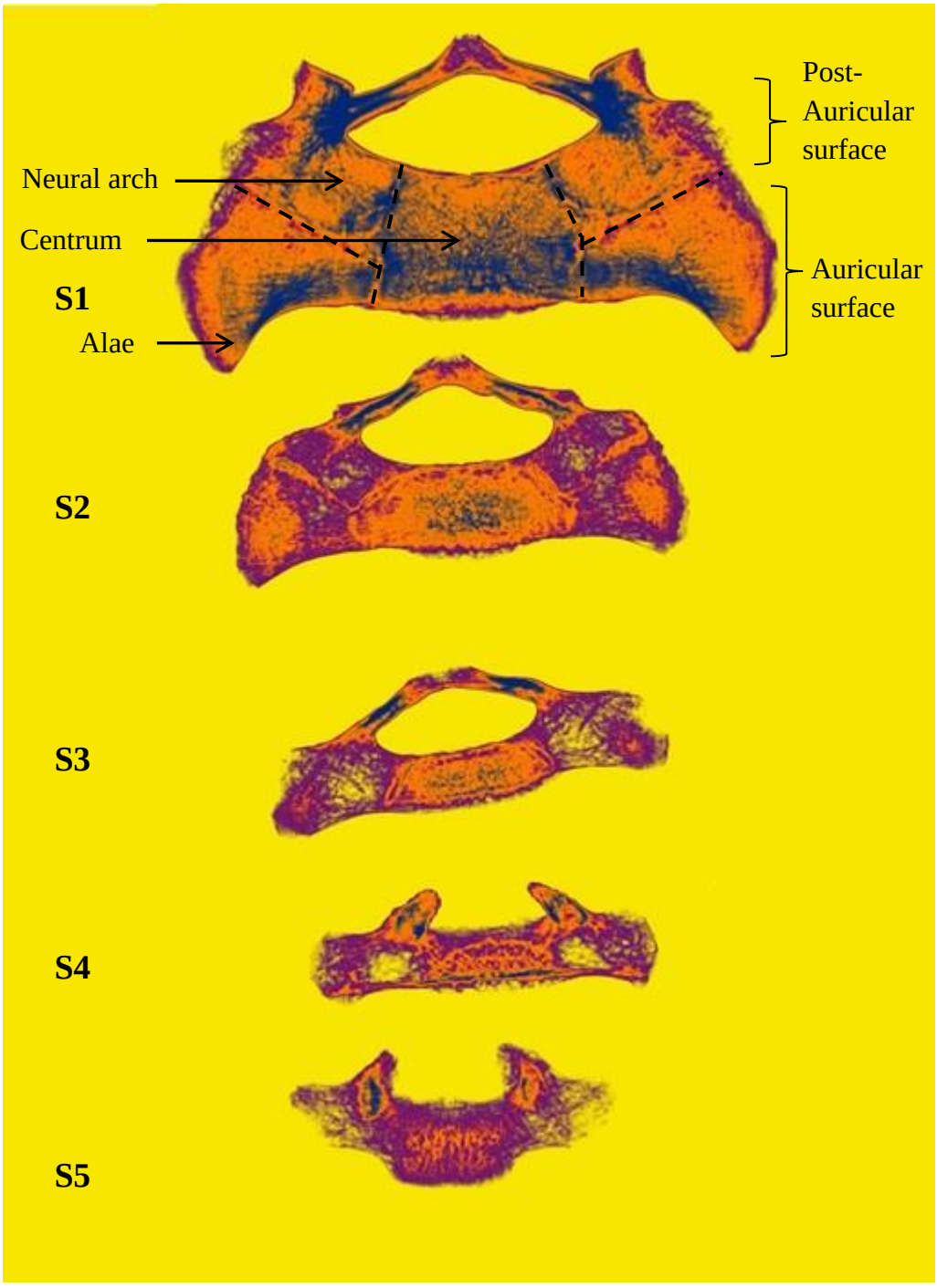

Figure 5.11: Five fused sacral elements (neural arches, alae and centrum – separated by the dotted lines delineate the fusion lines) of S1 in a 4-6 year old specimen.

No.	Specimen	Age
1	SC-026	4 years
2	SC-027	4-5 years
3	SC-247	4-6 years
4	SC-140	4-6 years
5	SC-019	5-6 years
6	SC-076	5 years
7	SC-001	5-8 years
8	SC-077	6 years
9	SC-078	6 years
10	SC-081	6-8 years
11	SC-248	6-10 years
12	SC-095	7 years
13	SC-132	8 years
14	SC-029	8 years
15	SC-171	9-12 years
16	SC-030	11 years

Table 5.4: The 16 specimens in group 3 have a common appearance in which all 5 elements are fully fused within each vertebral level.

General Appearance and Stage of Fusion

In this group, all five sacral elements (paired neural arches, paired alae and a centrum) in the S1 vertebra have fused. Theoretically, by the age of 6 years, all primary centres may unite within each sacral vertebral level except at the posterior synchondrosis of S1-S5, which begins to fuse around 7-15 years (Scheuer and Black, 2000). Many specimens after the age of 6 years showed varying degrees of posterior synchondrosis, however, the majority of specimens in this group are still separated from each other as the fusion between the adjacent sacral vertebrae starts at puberty and progresses in a caudocranial direction (Frazer, 1965, Scheuer and Black, 2000).

Appearance and Intensity Pattern of 4 year old up until 11 year old specimens

The S1 vertebra in this group is labeled accordingly to aid in the interpretation of the various regions that exhibit different intensity pattern.

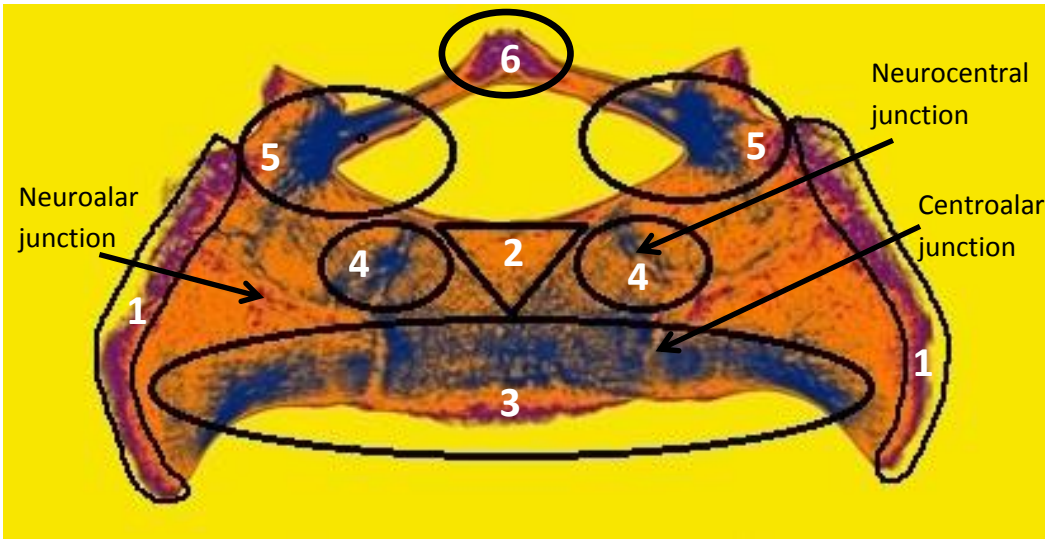

Figure 5.12: S1 vertebra of a 4-6 year old specimen divided into six regions, 1 = lateral S1, 2 = posterior centrum, 3 = pelvic brim, 4 = neurocentral junction, 5 = superior articular facets, 6 = spinous process.

S1 vertebra

The S1 vertebra (Figure 5.12) is represented by high intensity areas (blue) at 3 regions representing the posterior pelvic brim (region 3) formed by the anterior half of the centrum and the anterior alae. The high intensity area (blue) also found in the neurocentral junction (marked by region 4 on both sides), and at the superior articular processes and proximal laminae of region 5.

Region 2 is the only area in the centrum that is represented by medium intensity (orange). The lateral-most areas of S1 are represented by low intensity areas (violet) marked by region 1. The anterior half of region 1 represents the lateral-most part of the auricular surface area, and posterior half of region 1 represents the lateral-most part of

the post-auricular area (Figure 5.12). Region 6 exhibits low intensity (violet) at the posterior synchondrosis. Apart from the marked regions, a medium intensity area (orange) covers the posterior half of the alae with a patchy distribution on the neural arches. Throughout this age group, the entire S1 vertebra showed similar high intensity (blue) areas in regions 3, 4 and 5.

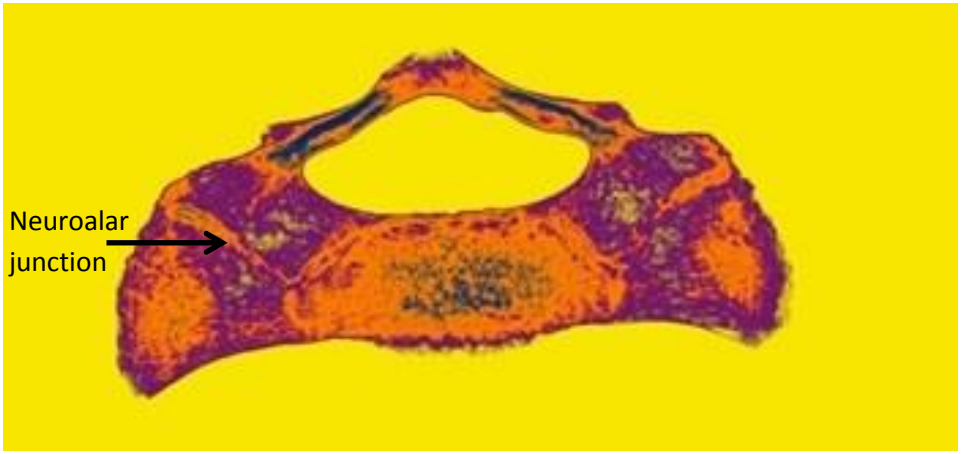

Figure 5.13: S2 vertebra of a 4-6 year old specimen.

S2 vertebra

The S2 specimen in this group exhibits marked reduced areas of high intensity (blue) (Figure 5.13) compared to the S1 vertebra (Figure 5.12). It only appeared on the central part of the centrum and the laminae. A medium intensity (orange) region covers the peripheral part of the S2 centrum and lateral part of the sacral alae. An area of medium intensity (orange) outlines the fusion line of the neuroalar junction. The posterior synchondrosis also shows medium intensity (orange) areas. Apart from the regions described above, the rest of S2 was represented by low intensity areas (violet). The anterior sacral alae which showed a high intensity area (region 3) in S1 (Figure 5.12) exhibits low intensity (violet) area in S2.

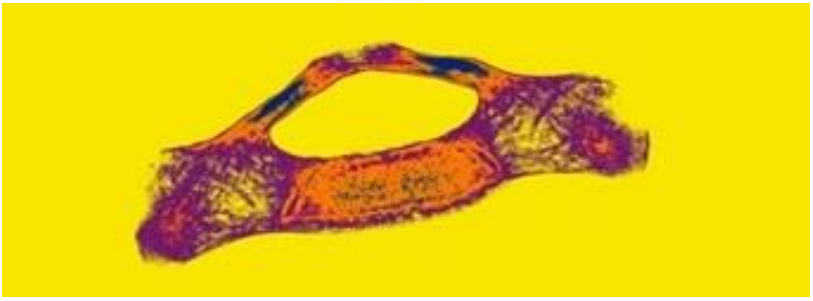

Figure 5.14: S3 vertebra of a 4-6 year old specimen.

S3 vertebra

S3 vertebra in this group showed similar findings to S2, where high intensity (blue) areas were observed, although quite faint, at the central part of the centrum and the laminae (Figure 5.14). The medium intensity represents the area of the peripheral S3 body and lateral alae and both proximal and distal ends of the laminae. Apart from the regions described above, the rest of the S3 vertebra was represented by low intensity (violet) areas which were consistently found throughout S3 specimens in this group.

Figure 5.15: S4 vertebra of a 4-6 year old specimen.

S4 vertebra

S4 vertebra in this group is represented by minimal high intensity (blue) areas only at the anterior centrum and mid laminae (Figure 5.15). The centrum is mainly represented by a medium intensity (orange) area and the anterolateral alae, as well as both proximal

and distal ends of the laminae. The rest of the S4 vertebra exhibit low intensity (violet) areas.

Figure 5.16: S5 vertebra of a 4-6 year old specimen.

S5 vertebra

The last vertebra (Figure 5.16) showed high intensity (blue) areas only at the laminae. The centrum was represented by a central medium intensity (orange). The peripheral S5 centrum and the rest of the neural arch are represented by low intensity (violet) areas.

GROUP 4

The fourth group consists of sacra from 11 years to late adolescence (Table 5.5). Sacra in this group (n = 20) present in a fully fused adult form (Figure 5.17). As adolescence is a variable range rather than specific time, the criteria for selection in this group was based on total fusion of the sacrum.

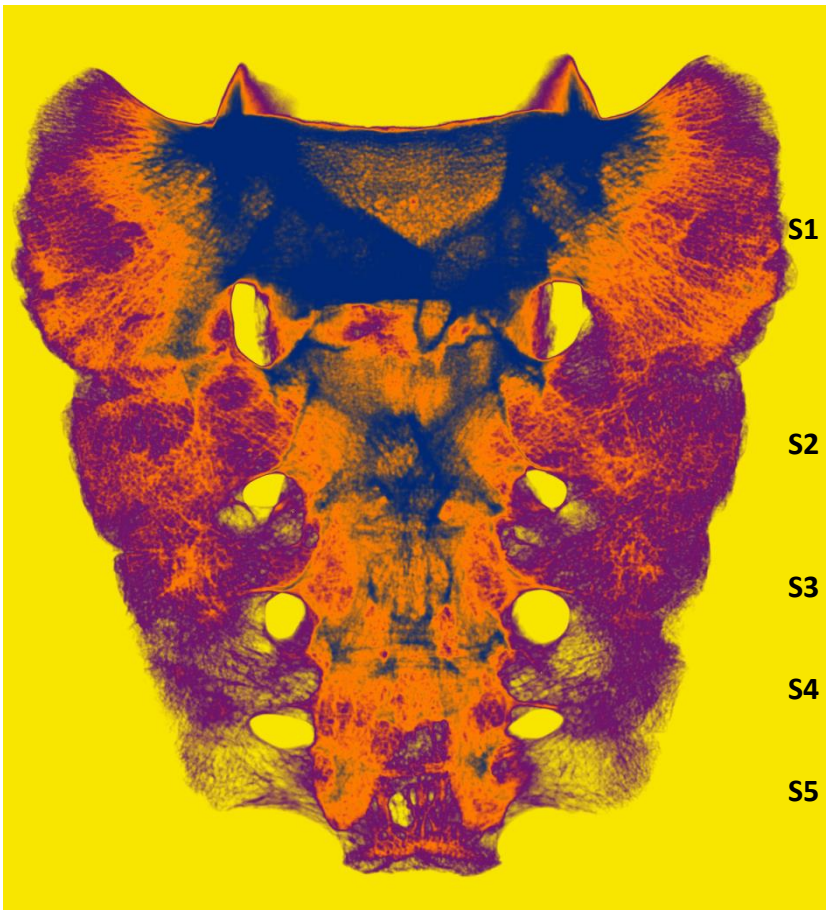

Figure 5.17: A 17 year old sacrum fused into adult features.

No.	Specimen	Age
1	SC-290	11-14 years
2	SC-031	12 years
3	SC-032	12 years
4	SC-249	12-14 years
5	SC-018	13-14 years
6	SC-033	14 years
7	SC-034	17 years
8	SC-035	19 years
9	SC-036	19 years
10	SC-037	19 years
11	SC-038	19 years
12	SC-094	Late Adolescent
13	SC-099	Late Adolescent
14	SC-100	Late Adolescent
15	SC-101	Late Adolescent
16	SC-102	Late Adolescent
17	SC-103	Late Adolescent
18	SC-104	Late Adolescent
19	SC-105	Late Adolescent
20	SC-138	Late Adolescent

Table 5.5: The 20 specimens in group 4 have achieved complete fusion.

General Appearance and Stage of Fusion

After puberty, the whole sacrum usually presents in a fused form. S1 – S5 exhibit fusion as early as puberty although complete consolidation is attained after the age of 25 (Frazer, 1965). Hence, the radiographic images of the sacra in this group are restricted to an anteroposterior (AP) view, compared to the previous groups which were imaged from a superoinferior view. Although there are some limitations extracting information from this view, the sacra observed exhibit specific characteristics which can be interpreted and so a summary of this stage is offered here with the acceptance that there can be no direct comparison with the younger age groups.

Intensity Pattern in 11 year old to late adolescence

The intensity pattern is described from the perspective of an AP view. Any intensity pattern observed is interpreted with caution due to superimposition of the bony parts in this view.

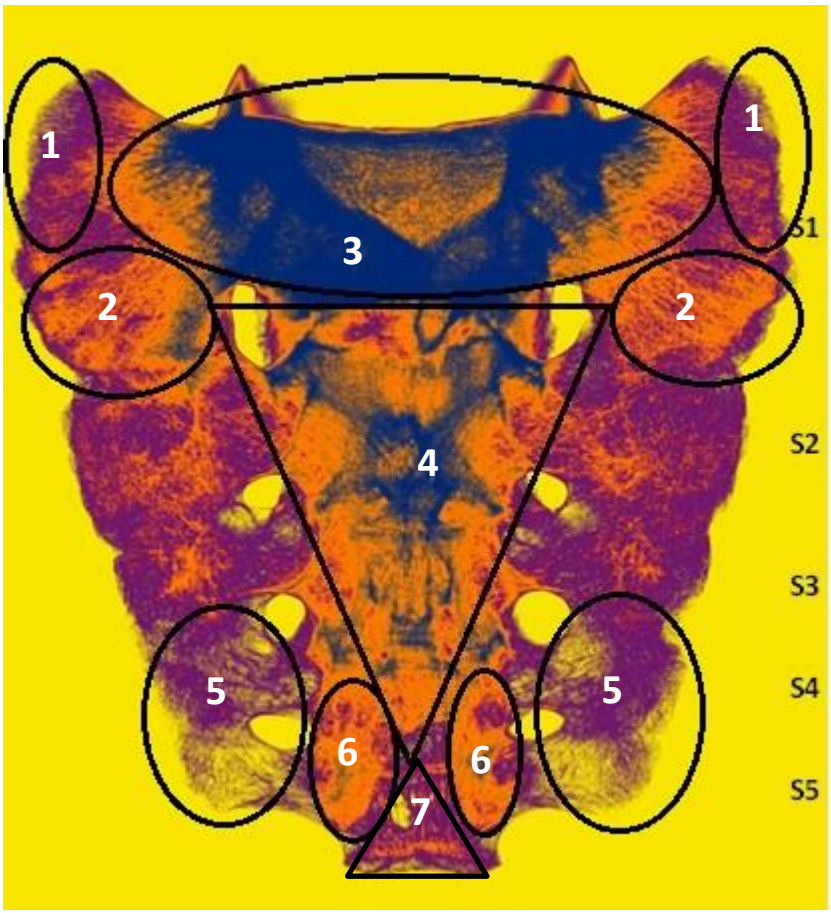

Figure 5.18: A 17 year old sacrum fused into adult features marked with different intensity areas.

The most prominent high intensity areas are observed in the central part of the S1 vertebra (region 3) with patchy distribution downwards to the S3-S4 bodies (region 4) (Figure 5.18). The medium intensity region (orange) represents the lower-half of the S1 alae (regions 2) and the sacral cornua (regions 6). There are patchy areas of medium intensity (orange) at the level of S2 alae. The low intensity (violet) areas were observed

at the superior half of the S1 alae (regions 1), most neural arch areas of the S4 and S5 (regions 5) and at the lower part of the sacrum (region 7) at the sacrococcygeal articulation. These findings were consistent throughout the specimens of this age group.

Despite the restricted information gathered from the fused sacrum in an AP view, the relative differences should be highlighted. One is the absence of high intensity (blue) areas on the lateral aspect of S1 alae which form the auricular part of the sacroiliac joint (regions 1 and 2). The sacrum demonstrates that the more distal the vertebra, the less intense the areas of density represented. This finding corresponds to the findings in the younger, unfused groups which reveal similar observations. Although the overlapping areas exhibit high intensity regions, especially at the uppermost and central part of the sacrum, these high intensity regions are confined to these upper areas.

5.4 Discussion

The qualitative radiographic study on the intensity pattern of the juvenile sacrum exhibits a particular pattern in each age cohort with the trabecular bone pattern expected to be closely related to the magnitude and direction of stresses put on it (Lanyon, 1974; Pal, 1989). Although it was appropriate to place specimens into different categories according to the sacral fusion state, there are some individuals of a similar age grouped into different cohorts based on maturity status. This is because the rate and timing of sacral fusion is not precise and overall growth and skeletal maturation varies between individuals, mainly influenced by genetic, hormonal, nutritional and health status (Tanner *et al,* 1966; Broome *et al,* 1998; Rogol *et al,* 2000; Weise *et al,* 2001).

From the intrauterine period until shortly after birth, the juvenile sacra display a central core of medium to high intensity bone especially in the upper two sacral vertebrae, and the neural arches of S1-S2 particularly at the junction between the laminae and the articular facets. There is no evidence of high intensity bone in the alar elements where the lateral part represents the auricular region of the sacroiliac joint. This could easily be attributed to the absence of direct stance-related weight transfer during this age group (Pal, 1989; Vleeming *et al,* 1996; Pel *et al,* 2008). However, the central core of medium to high intensity areas observed in the centrum of this non-weight bearing sacral vertebra may suggest some form of load or action-based transmission during intrauterine life perhaps as a result of muscular-related biomechanical fetal kicking movements (McColl *et al,* 2006). An alternative to consider is that there may be a genetic template for the future weight-bearing region of the sacrum, something that has been suggested for the neonatal ilium (Cunningham and Black, 2009a, 2009b, 2009c).

As the child grows particularly between 1 and 4 years, they undergo critical gross motor development particularly changing from sitting and transient quadrupedal movement to

independent bipedal walking and gait maturation (Sutherland *et al*, 1980; Keen, 1993). This results in this age cohort exhibiting enhanced high intensity areas in the region described in the younger group (centrum and laminae of the neural arch at the superior articular facets), with additional involvement of the sacral alae. In this age group, the neural arches displayed specific areas of high intensity in the superior articular facets of S1 and both laminae of S1-S2, and sometimes S3. These areas were thought to be one of the regions involved in lumbosacral weight transmission (Davis, 1961; Pal, 1989; Mahato, 2010b).The upper centrum especially in S1 exhibit high intensity regions on its anterior and lateral parts, with low to medium intensity regions on its posterior aspect where bone is most likely replaced by the basivertebral veins (Sinnatamby, 2006; Moore *et al*, 2013). The S1 sacral alae displayed medium to high intensity areas specifically at the anterior region that forms the posterior pelvic brim. However, there are minimal high intensity areas observed on the auricular areas of S1 and S2 in this fully independent walking age group, reflecting minimal load passing through this area. The post-auricular areas also exhibit medium to low intensity regions. Additionally, the results also show that the intensity areas reduce towards the more distal sacral vertebrae, most probably due to diminished involvement in weight transmission of the lower sacral vertebrae (Bellamy *et al*, 1983; Ebraheim *et al*, 2000).

However, in the third age cohort of 4 to 11 years, the intensity pattern observed in the previous group becomes more enhanced. During this period, the pelvic complex witnesses functional changes of visceral descent into the pelvis and fusion of the ischiopubic ramus before the age of 6 years and gait maturation around 8 years (Inman *et al*, 1981; Keen, 1993; Li *et al*, 1996; Scheuer and Black, 2000; Verhulst, 2003; Kubo and Ulrich, 2006). The sacrum fuses within its own vertebral level and appears as 5 separate sacral vertebrae. S1 exhibits the most prominent intensity areas involving the laminae, superior articular facets, medial-half of the pedicles, anterior and lateral

centrum as well as the anterior sacral alae, except at the areas forming the auricular surface. The lateral-half of the neural arch which forms part of the post-auricular area also exhibits medium to low intensity regions. This reflects that the body weight transmission across the sacrum towards the innominates may not entirely pass through the sacroiliac joint, but perhaps, divides into several routes. The functional capacity of the surrounding ligaments may play an important role in dissipating the remaining weight for optimum load transmission (Last, 1978; DonTigny, 1993; Palastanga and Soames, 2012). The auricular area of S3 vertebra in this group displays ambiguous results as there was no intention of sex segregation and this region was thought to transmit body weight in males owing to greater body loads (Brothwell, 1981). S4 and S5 exhibit medium intensity regions confined to the central body and the proximal laminae only as minimal weight is distributed through this distal area. The distal part of the sacrum that exhibits minimal dense areas supports the theory of weight transmission that essentially passes through the upper sacrum, especially S1 and S2 (Bellamy *et al*, 1983; Ebraheim *et al*, 2000). It was noted that in all specimens in this age group, S1 exhibit the most pronounced high intensity areas which necessitate further analysis to quantify the current qualitative radiographic study.

The final age cohort that includes the 11 year to late adolescence specimens displayed a single and nearly complete fused sacrum which resembles adult features. Although highly superimposed as the view is from an anteroposterior (AP) compared to the previous groups of superoinferior (SI) views, there is some consistency and relevant findings. The highest intensity areas were noted specifically focused on the uppermost (especially at the S1 vertebra) and central part of the sacrum, where the body, medial-half of the neural arches, superior articular facets, laminae and part of the sacral tuberosity are located. The lateral sacral areas exhibit medium to low intensity. The S1 auricular areas showed lower-half of medium intensity while the upper-half lacked any

dense areas. The S2 and some of the S3 auricular areas display variable medium to low intensity areas. Nevertheless, the auricular and post-auricular areas were overlapped in this view and could not be interpreted separately. The absence of high intense areas on the auricular region may suggest that the weight transmission from the upper lumbar vertebrae may not fully pass through the sacroiliac joint.

Clinically, several studies report that screw fixation at the sacrum in adults has a high failure rate which may result from several factors, such as inappropriate direction or depth of screw insertion or low bone density areas within the region of the sacrum (Smith *et al*, 1993; Leong *et al*, 1998; Zheng *et al*, 2000). In cases of sacral fracture in the paediatric age group, although uncommon (Hart *et al*, 2004), it needs to be emphasized which areas on the sacrum where it is appropriate for screw insertion should be directed (Zheng *et al*, 2000). This study suggested that the anterior and lateral centrum, anterior sacral alae and the medial neural arch especially in the S1 vertebra which exhibit high bone density areas, may be the best location of entry, direction and depth for sacral screw insertion.

As expected, understanding the internal architecture of S1 vertebra in this study is unlikely to unlock the mechanism by which weight transfer is effected from the axial to the lower appendicular skeleton. Further quantification study of bone histomorphometric analysis is needed on the S1 vertebra in order to provide better understanding of this particular region.

CHAPTER 6

Quantitative Analysis of the Trabecular Bone Architecture of the Juvenile S1 vertebra

6.1 Introduction

This study utilised 26 juvenile sacra selected from the preliminary study in Chapter 5, by considering the period of critical physical developmental changes involving the transition from supine and sitting position to transient quadrupedal stance, bipedal movement and gait maturation (Sutherland *et al,* 1980; Keen, 1993; Taanila *et al,* 2005).

This developmental period involves the presentation of separate sacral elements within a vertebra and most specimens appear as separate unfused vertebrae. It is only after puberty that complete sacral fusion commences in a caudocranial direction (Cleaves, 1937; Frazer, 1965; Scheuer and Black, 2000). It is pertinent in this study to utilise these early sacral vertebrae to identify the trabecular arrangement and any changes that may occur throughout maturity especially during these critical developmental years. It is postulated that the trabecular pattern in the juvenile sacrum will undergo changes in direction and density according to postural-related changes, as was found in the developing human femur and tibia (Ryan and Krovitz, 2006; Gosman and Ketcham, 2009).

Studies on the relationships between trabecular bone organisation associated with weight transmission have been widely conducted over the past three decades (Goldstein, 1987), and evolved from conventional, manually-operated (Davis, 1961; Lindahl, 1976; Goldstein *et al*, 1983) to non-invasive, sophisticated, software-dependant studies

(Fajardo and Muller, 2001; Genant and Jiang, 2006; Cunningham and Black, 2009a; Abel and Macho, 2011; Shaw and Ryan, 2012).

Much research has been undertaken to understand the pattern of weight transmission in the vertebral column, especially in the lumbar region, however limited studies have been undertaken on the trabecular pattern in the sacrum, which may not follow a similar pattern as the upper vertebrae due to the angulation at the lumbosacral angle (Twomey *et al*, 1983; Pal and Routal, 1987; Twomey and Taylor, 1987; Pal, 1989). As the sacrum is a dynamic region in which the internal architecture may reflect specific biomechanical demands, more research is needed on the trabecular structure of the sacrum (Mahato, 2010). However, recent literature on studies of the trabecular and cortical pattern of the sacrum focus on the adult population (Ebraheim *et al*, 2000; Mahato, 2010c; Mahato, 2013) with limited information on the quantification of the microstructural arrangement of the sub-adult group. Thus this study aimed to quantify different regions in the S1 vertebra of the juvenile sacrum, and to study the possible evidence for transfer of forces from the axial to the lower appendicular skeleton and *vice versa* (Vleeming *et al*, 2012).

6.2 Materials and Methods

Materials

Twenty-six sacra were selected from the juvenile skeletal remains of the Scheuer Collection, housed within the Centre for Anatomy and Human Identification, University of Dundee. The selection of the specimens was based on three criteria:

(i) Within the specimens selected the significant developmental milestones of locomotion occurred, between birth until 8 years.

(ii) Only the sacral elements which have an identifiable shape and could be reliably identified.

(iii) Before their complete fusion (S1-S5) as in a mature sacrum.

The samples selected were in good condition, without any visible damage on the cortex or the trabecular area. The details of the sacral specimens were described in Chapters 4 and 5.

Methods

The methods used in this study were described in detail in Chapter 4, however in this chapter, the methods are summarised for easier reference. First, the specimens were scanned with micro-CT and the image produced was stored in TIFF format and processed using OsiriX 3.9.4 to reconstruct the image into the desired view (superoinferior view). Following this, the post-multiplanar reconstruction (MPR) images were converted into a readable Skyscan format using Adobe Photoshop CS3. An error study was performed on 5 specimens (SC-001, SC-071, SC-074, SC-077 and SC-078) for the pre and post-MPR image to exclude any disparity in the image resolution.

The results showed that there was no statistically significant difference between the pre and post-MPR images (Table 6.1).

Parameters	*p* value
BV/TV (%)	0.690
Tb.Th (mm)	0.620
Tb.Sp (mm)	0.995
Tb.N (mm^{-1})	0.678
SMI	0.572
DA	0.646

Table 6.1. An error study using one-way Analysis of Variance (ANOVA) on 5 specimens for pre and post-MPR of the six parameters.

Finally, the post-MPR images were processed using Skyscan CT Analyser (CTAn) software. This software was chosen for this study as it has been succesfully used in recent cortical and trabecular studies (Chappard *et al*, 2005, Beaupied *et al*, 2006; Cunningham and Black 2009b; Cunningham and Black 2009c). Skyscan CTAn provides detailed 3-D quantification of trabecular architecture in a targeted region for various bone parameters, including the percentage of bone volume fraction (BV/TV %), trabecular thickness (Tb.Th), trabecular separation (Tb.Sp), trabecular number (Tb.N), structural model index (SMI) and degree of anisotropy (DA). Studies have shown that areas with high-density, plate-like trabecular structure are commonly found in high stress regions of the bone compared to a low-density, rod-like trabecular structure, suggesting that trabecular pattern highly correlates with mechanical properties (Ding *et al*, 2002). Six parameters were selected for this study which include:

1. **BV/TV (%):** Percentage of Bone Volume per Tissue Volume.

The trabecular bone morphometric analysis quantified the bone volume fraction (BV/TV) from voxel based 3-dimensional reconstructions of micro-CT images (Rüegsegger *et al*, 1996; Odgaard, 1997). The fraction is based on dividing the bone volume (BV), which is the total volume of a binarised solid object in the selected VOI

(volume of interest), by the tissue volume (TV), which is the total volume in the selected region. This parameter is relevant in the study of trabecular bone in which solids and spaces present in a selected volume. However, it is not applicable for the study of cortical bone as it does not contain the biphasic region (bone and non-bone state).

2. Tb.Th: Trabecular Thickness.

This parameter represents the thickness of the trabecular bone in millimetres. It measures the diameter of the largest non-overlapping sphere (Figure 6.1) which is entirely bounded within the solid spaces (Hildebrand and Rüegsegger, 1997a). The average thickness of all trabeculae is calculated within a specified volume of interest (VOI). In the adult lumbar vertebral body, the average trabecular thickness was reported to be 122-139 ± 18-28µm (Hildebrand *et al,* 1999).

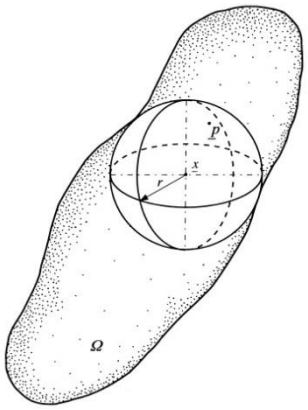

Figure 6.1: The local thickness of a trabecular strut measured by fitting the maximal sized sphere to the structure (taken from Hildebrand and Rüegsegger, 1997a).

3. Tb.Sp: Trabecular Separation.

Trabecular separation measures the width of the spaces within the VOI (Figure 6.2 (b)) (Jiang *et al*, 2000). It is a similar approach to that used to measure trabecular thickness but this time it is applied to the space rather than the solid voxels (Hildebrand *et al*, 1999). The value is given as the average value of all spaces in the VOI.

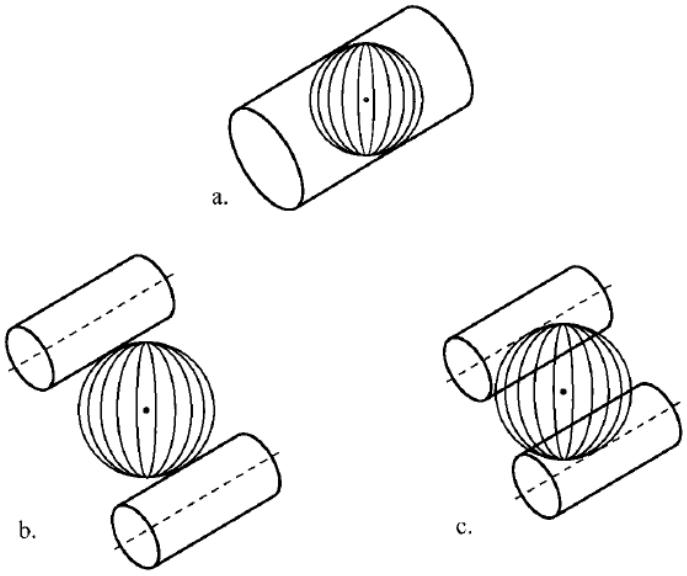

Figure 6.2: Three examples of the automated calculation by Skyscan CTAn 1.11 based on fitting the maximal diameter of the sphere placed within (a) trabecular for the average thickness (Tb.Th), or (b) the marrow space (Tb.Sp), and (c) the inverse of the average diameter placed between the mid-axis of the trabecular (Tb.N) (taken from Fajardo and Muller, 2001).

4. Tb.N: Trabecular Number.

Trabecular number is the number of trabecular traversals per millimetre (Figure 6.2 (c)) in a specific VOI (Fajardo and Muller, 2001). The number of traversals gives the total trabecular number in a selected VOI. The higher the value, then the higher the number of trabecular struts. Trabecular number is equal to the inverse sum of Tb.Sp and Tb.Th (Hildebrand *et al*, 1999).

5. SMI: Structural Model Index.

SMI quantifies the relative proportion of plates and rods by addressing the surface convexity of trabecular branching in the selected VOI. It measures the appearance of these branches (Figure 6.3) according to a spectrum ranging from 0 for a purely plate-like structure, to 3 for a purely rod-like structure, and 4 for an ideal sphere structure (Nicholson *et al*, 2001). Thus in a specific VOI, Skyscan automatically calculates the relative number of the plates, rods and spheres and gives the average of the result between 0 and 4. For example, 0.245 represents a plate-like structure whereas 3.123 reflect a rod-like framework. SMI was reported to show highly negative correlation with BV/TV in adult lumbar vertebral bodies (Hildebrand *et al*, 1999).

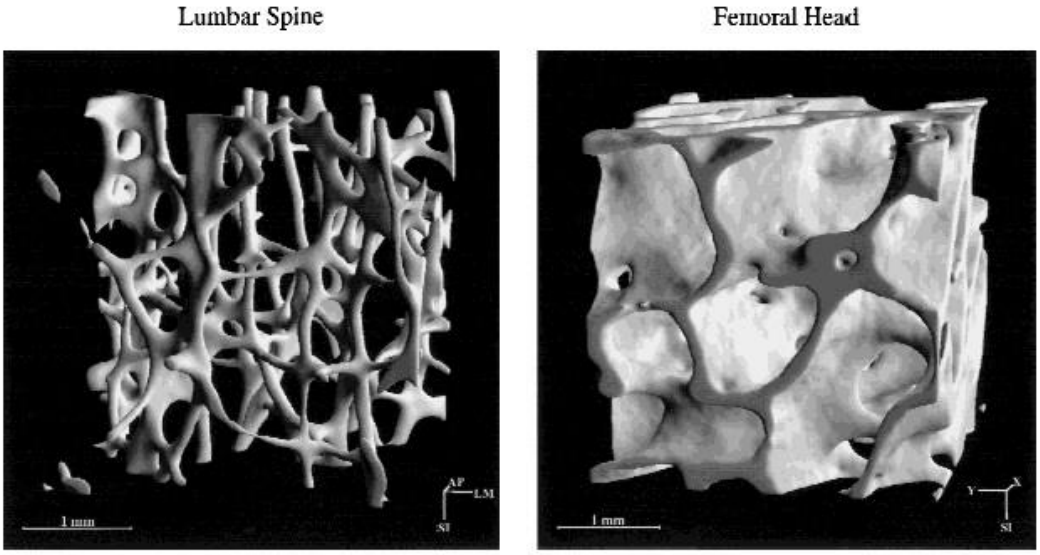

Figure 6.3: Micro-CT scan of (left) adult human lumbar vertebral body showing rod-like architecture (SMI = 2.5) compared to a (right) plate-like trabecular structure of the femoral head (SMI = 0.16) (taken from Hildebrand *et al*, 1999).

6. DA: Degree of Anisotropy.

Isotropy indicates an organised trabecular pattern and anisotropy indicates an unorganised or more random pattern. The results for the organised trabecular pattern are represents by 0 for isotropy, and unorganised are represented by 1 for anisotropy. For example, a value of 0.133 is more isotropic than 0.987. The DA is calculated based on the ratio between the maximal and minimal radius of the mean intercept length (MIL) ellipsoid, distributed by superimposing parallel test lines in different directions on a 3D image (Hildebrand *et al,* 1999). Recent findings suggest that the degree of anisotropy of trabecular bone correlates with loading regimes, where more load is transmitted to a particular region the more anisotropic the area (Fajardo and Muller, 2001). It is the second important parameter after bone volume fraction in determining bone strength (Odgaard, 1997).

6.3 Volume of Interest (VOI)

Only the right half of the S1 vertebra was analysed in this study and each was divided into 14 VOIs (volumes of interest), with each then divided into a superior half and an inferior half, thus giving 14 VOIs for the superior half of the right S1 vertebra and 14 VOIs for the inferior half. The 14 VOIs were divided according to the three sacral elements: the neural arch, the sacral ala and the centrum (Figure 6.4).

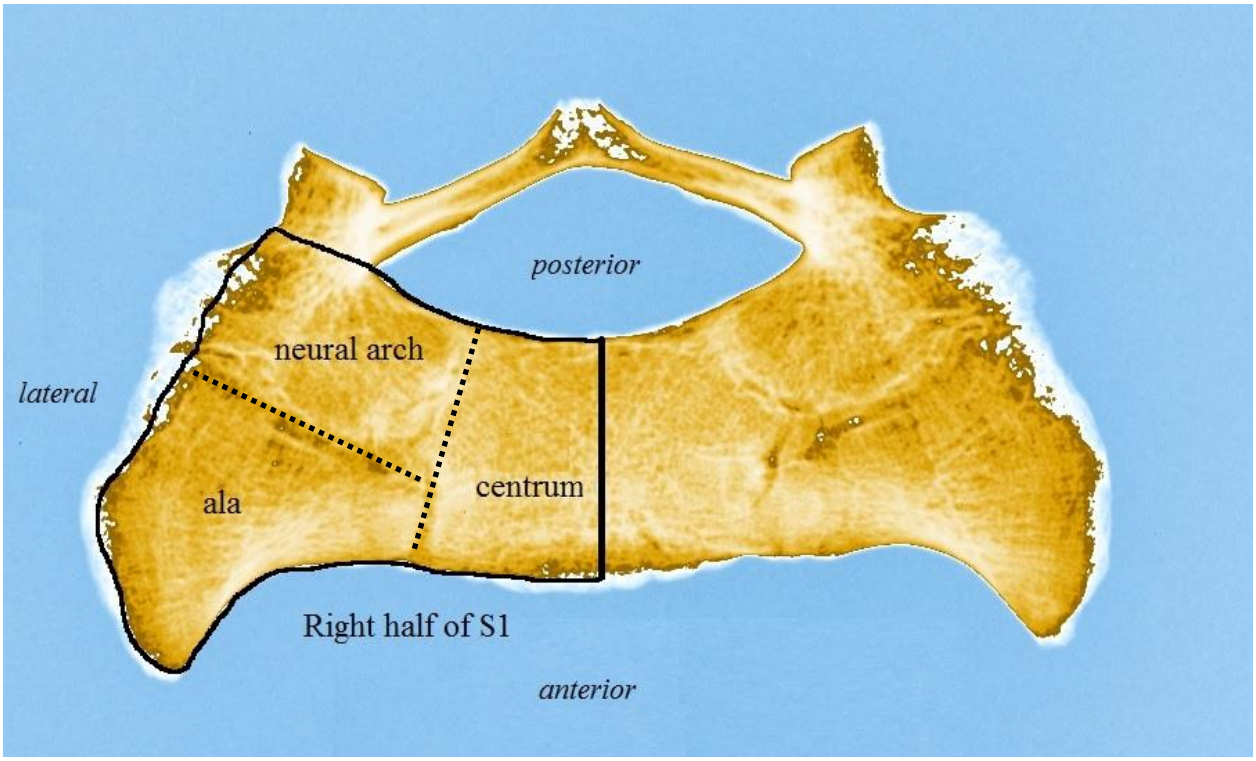

Figure 6.4: Superoinferior view of 4 year old S1 vertebra showing right half of three regions studied: the neural arch, sacral ala and the centrum, with fusion lines (dotted line).

The criteria for VOI placement were based on anatomical reference points (bony angles and fusion lines) and measurement proportions on the neural arch, sacral ala and the centrum. The placement was also established with reference to the preliminary

qualitative results of the sacra in Chapter 5, particularly in relation to the most dense areas on the anteromedial sacral alae and anterior centrum of S1 vertebra.

The examples shown below are the VOI placement on the unfused specimen, where these reference points and measurements proportions were reproducible in every specimen, either fused or unfused from infancy to 8 years.

1. VOI placement for centrum (Figure 6.5)

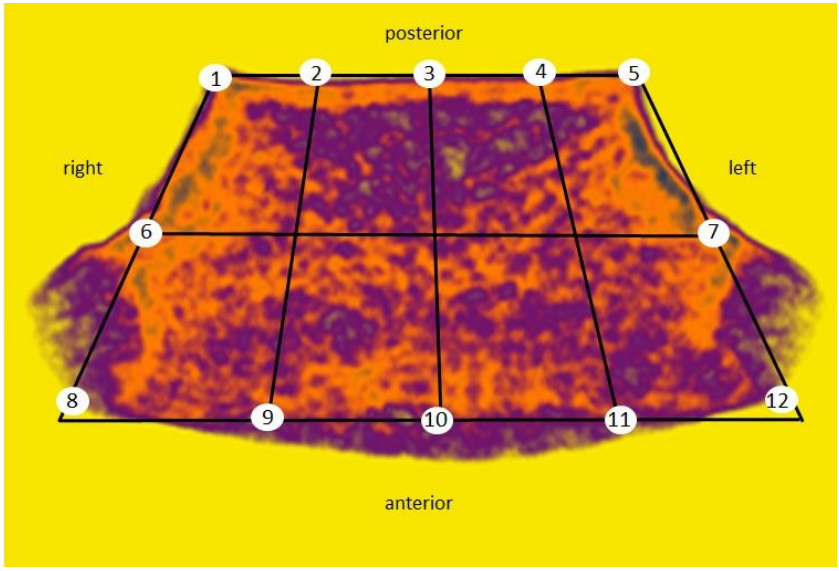

Figure 6.5: The anatomical reference points and measurement proportions for 1 year old centrum.

1. Posterior right
2. Midpoint between no. 1 and 3
3. Midpoint between no. 1 and 5
4. Midpoint between no. 3 and 5
5. Posterior left
6. Midpoint between no. 1 and 8
7. Midpoint between no. 5 and 12
8. Anterior right
9. Midpoint between no. 8 and 10
10. Midpoint between no. 8 and 12

11. Midpoint between no. 10 and 12
12. Anterior left

2. VOI placement for sacral ala (Figure 6.6)

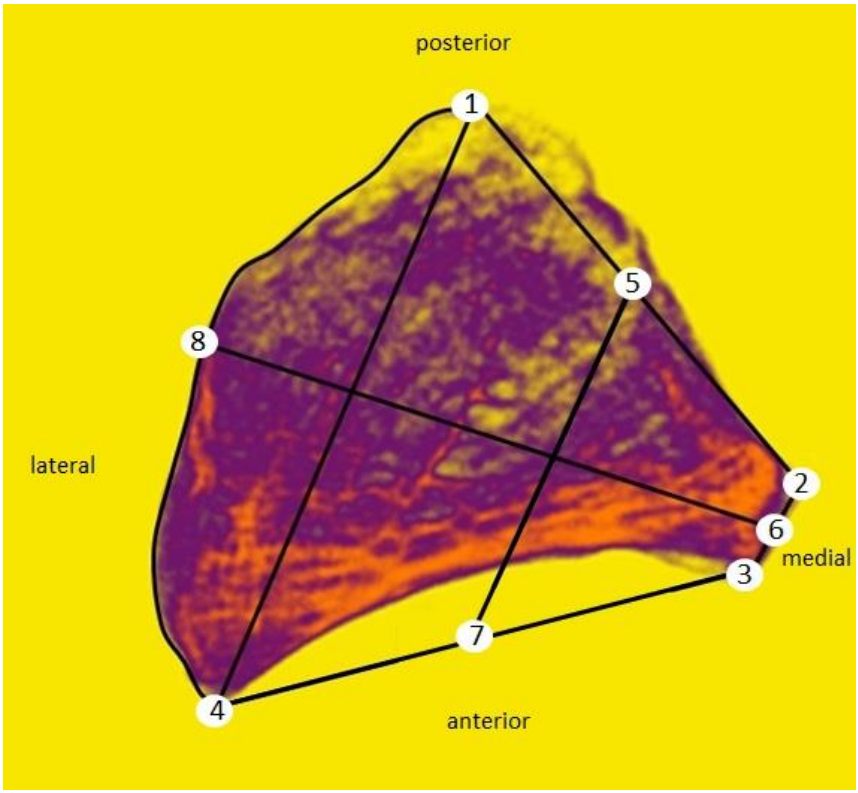

Figure 6.6: The anatomical reference points and measurement proportions for 3 year old right sacral ala.

1. Posterolateral tip of ala
2. Posteromedial tip of ala
3. Anteromedial tip of ala
4. Anterolateral tip of ala
5. Midpoint between no. 1 and 2
6. Midpoint between no. 2 and 3
7. Midpoint of line between no. 3 and 4
8. Midpoint of line between no. 1 and 4, and extended out to lateral border of the ala

3. VOI placement for neural arch (Figure 6.7)

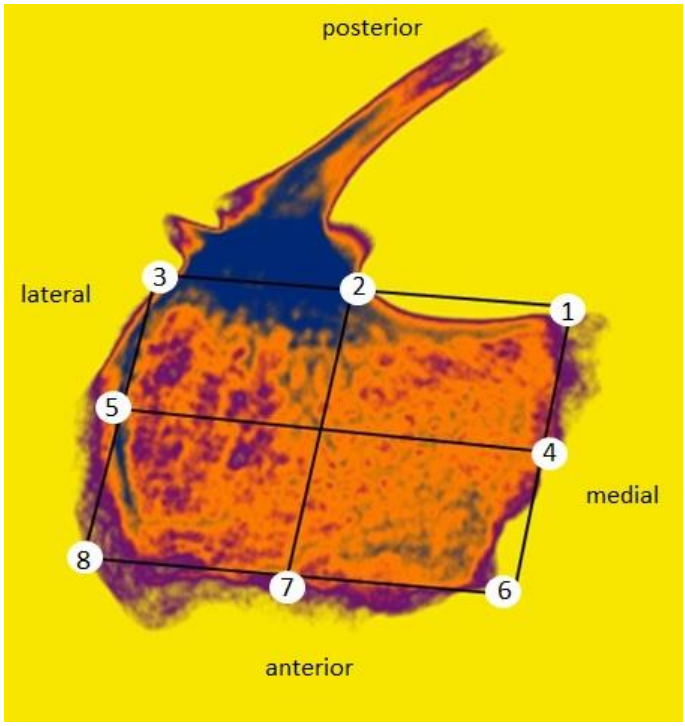

Figure 6.7: The anatomical reference points and measurement proportions for 4 year old right neural arch.

1. Tip of posteromedial angle
2. Midpoint between no. 1 and 3
3. Angle immediately below the Superior Articular Facet
4. Midpoint between no. 1 and 6
5. Midpoint between no. 3 and 8
6. Tip of anteromedial angle
7. Midpoint between no. 6 and 8
8. Tip of anterolateral angle

The 28 VOIs which consist of superior (14) and inferior (14) halves were distributed through the S1 vertebra (Figures 6.8, 6.9).

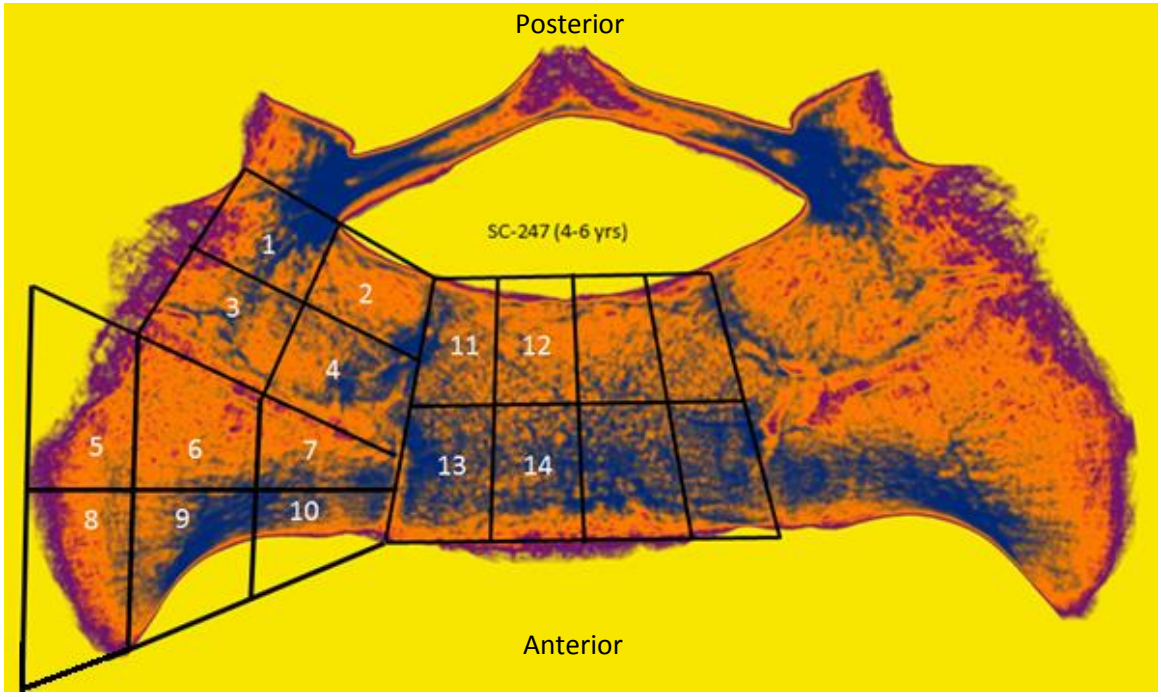

Figure 6.8: The superior view of VOIs for S1 vertebra. Each VOI has a superior (s) and inferior (i) component. The total number of VOIs on the right half of S1 = 28.

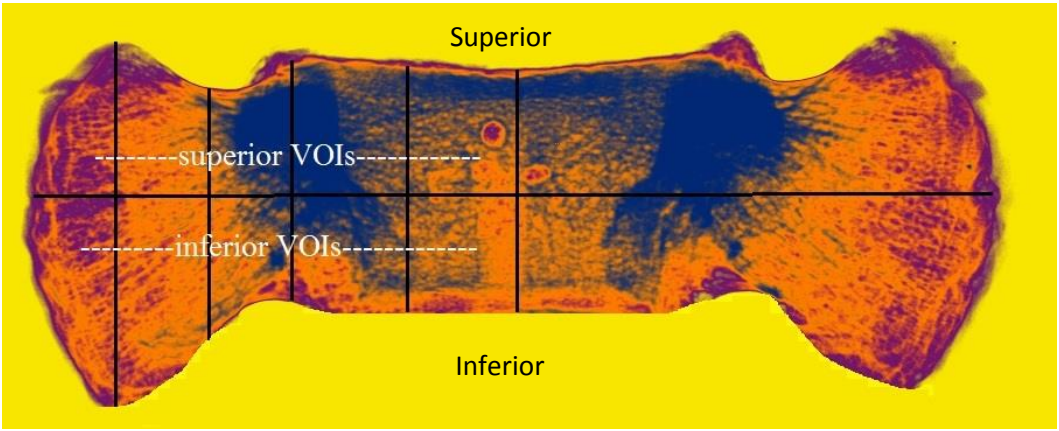

Figure 6.9: The anterior view of a different specimen (8 year old) showing the division into the superior (s) and inferior (i) VOIs.

1. **Neural arch: VOIs 1 – 4, both superior (s) and inferior (i) (Figure 6.10)**

   VOI1s and 1i = posterolateral region of the neural arch (post-auricular area)
   VOI2s and 2i = posteromedial region of the neural arch (lateral sacral crest)
   VOI3s and 3i = anterolateral region of the neural arch (post-auricular area)
   VOI4s and 4i = anteromedial region of the neural arch

2. **Sacral ala: VOIs 5 – 10, both superior (s) and inferior (i) (Figure 6.10)**

   VOI5s and 5i = posterolateral region of the ala (posterior-half auricular area)
   VOI6s and 6i = mid posterior region of the ala
   VOI7s and 7i = posteromedial region of the ala
   VOI8s and 8i = anterolateral region of the ala (anterior-half auricular area)
   VOI9s and 9i = mid anterior region of the ala
   VOI10s and 10i = anteromedial region of the ala

3. **Centrum: VOIs 11 – 14, both superior (s) and inferior (i) (Figure 6.10)**

   VOI11s and 11i = posterolateral region of the centrum
   VOI12s and 12i = posteromedial region of the centrum
   VOI13s and 13i = anterolateral region of the centrum
   VOI14s and 14i = anteromedial region of the centrum

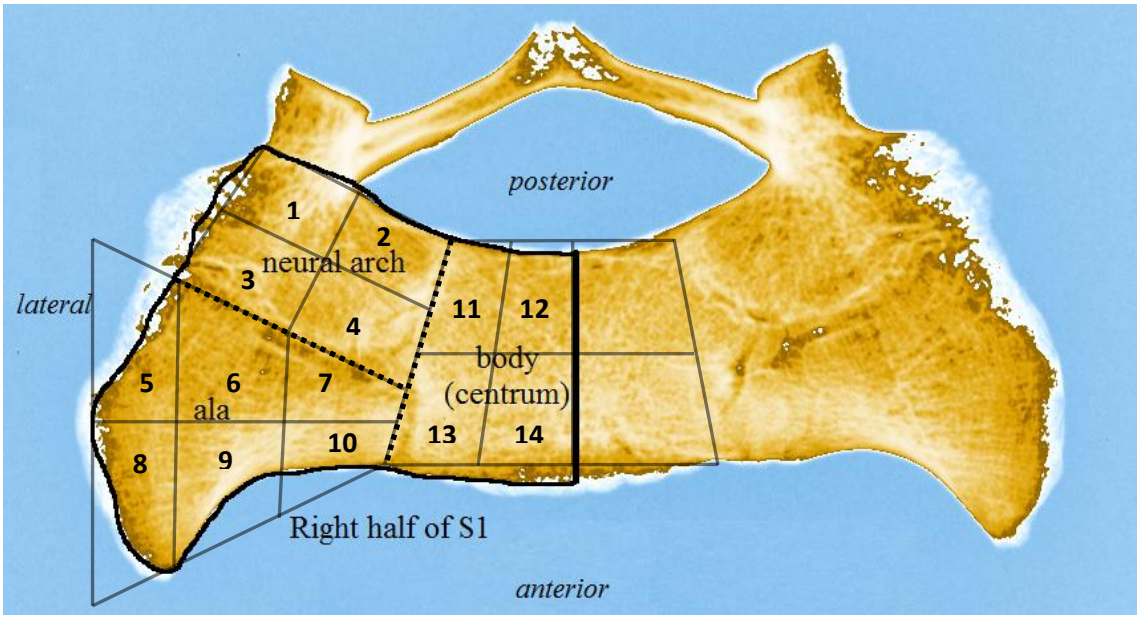

Figure 6.10: A 4 year old S1 vertebra illustrating position of 14 VOIs at the three areas: neural arch, ala and centrum.

From the preliminary study of the gradient mapping of juvenile sacra (Chapter 5), it was observed that S1 exhibits the most intense areas of high density bone compared to S2 and the remaining sacral vertebrae, across all age groups. The qualitative study on the intensity patterns of S1 were shown to be evenly distributed on its right-half and left-half, in all age groups. Subsequently, statistical analysis of five specimens (SC-068, SC-071, SC-078, SC-073, SC-247) comparing the right and left halves of S1 vertebra was performed and the results showed that there was no significant difference between the right and left halves of the S1 vertebra (Table 6.2). Consequently, given the limited time available, only the right half of S1 is considered in this study. The evenly distributed microarchitectural arrangement of the right-half and left-half of the adult sacrum has also been reported in a few studies with no bilateral differences (Pal, 1989; Ebraheim *et al,* 2000).

Bone Parameter	*p* value
BV/TV	0.690
Tb.Th	0.888
Tb.Sp	0.927
Tb.N	0.879
SMI	0.841
DA	0.327

Table 6.2: One-way analysis of variance (ANOVA) using Sigmaplot 12.0 comparing the right and left halves of the S1 vertebra from 5 different specimens.

6.4 Results

The 26 specimens ranging from infancy to 8 years were grouped into 4 age cohorts to aid in the interpretation of results and for comparison between different age groups (Table 6.3). This grouping was based on the timing of gross motor developmental milestones (Forssberg, 1985; Keen, 1993) and functional changes in the pelvis with

descent of the abdominal viscera into the pelvis, as well as ischiopubic ramus fusion prior to full maturation of gait around 8 years (Sutherland *et al,* 1980; Scheuer and Black, 2000; Kubo and Ulrich, 2006). This resulted in a relatively even distribution of the sample across the 4 age groups.

Group	Age range	*n*
G1	Infancy - 18 months	7
G2	18 months – 3 ½ years	7
G3	3 ½ years - 6 years	7
G4	6 years - 8 years	5

Table 6.3: The age cohorts of 26 sacra in this study

The results for each of the 28 VOIs of the four age groups are described according to the 6 bone parameters:

1. Bone volume fraction (BV/TV) (%)
2. Trabecular thickness (Tb.Th) (mm)
3. Trabecular separation (Tb.Sp) (mm)
4. Trabecular number (Tb.N) (mm^{-1})
5. Structural model index (SMI)
6. Degree of anisotropy (DA)

The descriptive statistics (mean, standard deviation, minimum value, maximum value, coefficient of variation) are presented in the Tables 6.4 – 6.9. The raw data for the results on these six parameters are presented in Appendix. The coefficient of variation (CV) was calculated to determine the inter-specimen variation, considering the substantial age range within a group (around 18 – 30 months). It was anticipated that the CV would increase and vary within each group with advancing age.

VOI	Infancy – 18 months	18 months - 3 ½ years	3 ½ years – 6 years	6 – 8 years

Table 6.4: Descriptive statistics of bone volume fraction (BV/TV) for each VOI in the four age groups

VOI	Infancy – 18 months	18 months - 3 ½ years	3 ½ years – 6 years	6 – 8 years

Table 6.5: Descriptive statistics of trabecular thickness (Tb.Th) in mm for each VOI in the four age groups

VOI	Infancy – 18 months	18 months - 3 ½ years	3 ½ years – 6 years	6 – 8 years

Table 6.6: Descriptive statistics of trabecular separation (Tb.Sp) in mm for each VOI in the four age groups

VOI	Infancy – 18 months	18 months - 3 ½ years	3 ½ years – 6 years	6 – 8 years

Table 6.7: Descriptive statistics of trabecular number (Tb.N) in mm^{-1} for each VOI in the four age groups

VOI	Infancy – 18 months	18 months - 3 ½ years	3 ½ years – 6 years	6 – 8 years

Table 6.8: Descriptive statistics of trabecular structural model index (SMI) for each VOI in the four age groups

VOI	Infancy – 18 months	18 months - 3 ½ years	3 ½ years – 6 years	6 – 8 years

Table 6.9: Descriptive statistics of trabecular degree of anisotropy (DA) for each VOI in the four age groups

Comparison between the superior half and inferior half of the S1 vertebra

All of the superior half and inferior half of the 14 VOIs, across the four age groups, were compared using ANOVA and pairwise multiple comparison method (Sigmaplot 12.0) and the results revealed that there is no significant difference ($p > 0.05$) between the superior and inferior regions. Thus, only the superior half is used for the analysis of the S1 vertebra.

Three Analyses across the 6 bone parameters

Subsequently, the data obtained were compared in three different analyses using ANOVA and pairwise multiple comparison method (Sigmaplot 12.0). The 3 analyses are divided into a group comparison (first analysis) and two VOI comparisons (second and third analyses).

The group comparison consists of:

1. First analysis: combined all VOIs in one age group, comparisons were made between group 1 and group 2 and so on (Purple arrows in Figure 6.11). This is a general analysis to determine any changing pattern between the four age groups.

The VOI comparison consists of:

2. Second analysis: combined all four age groups, comparison was made between VOI 1 and VOI 2 and so on (Blue arrow in Figure 6.11).

3. Third analysis: within each age group, the comparison was made between VOI 1 and VOI 2 and so on (Orange arrow in Figure 6.11). This is a more specific analysis than the second analysis.

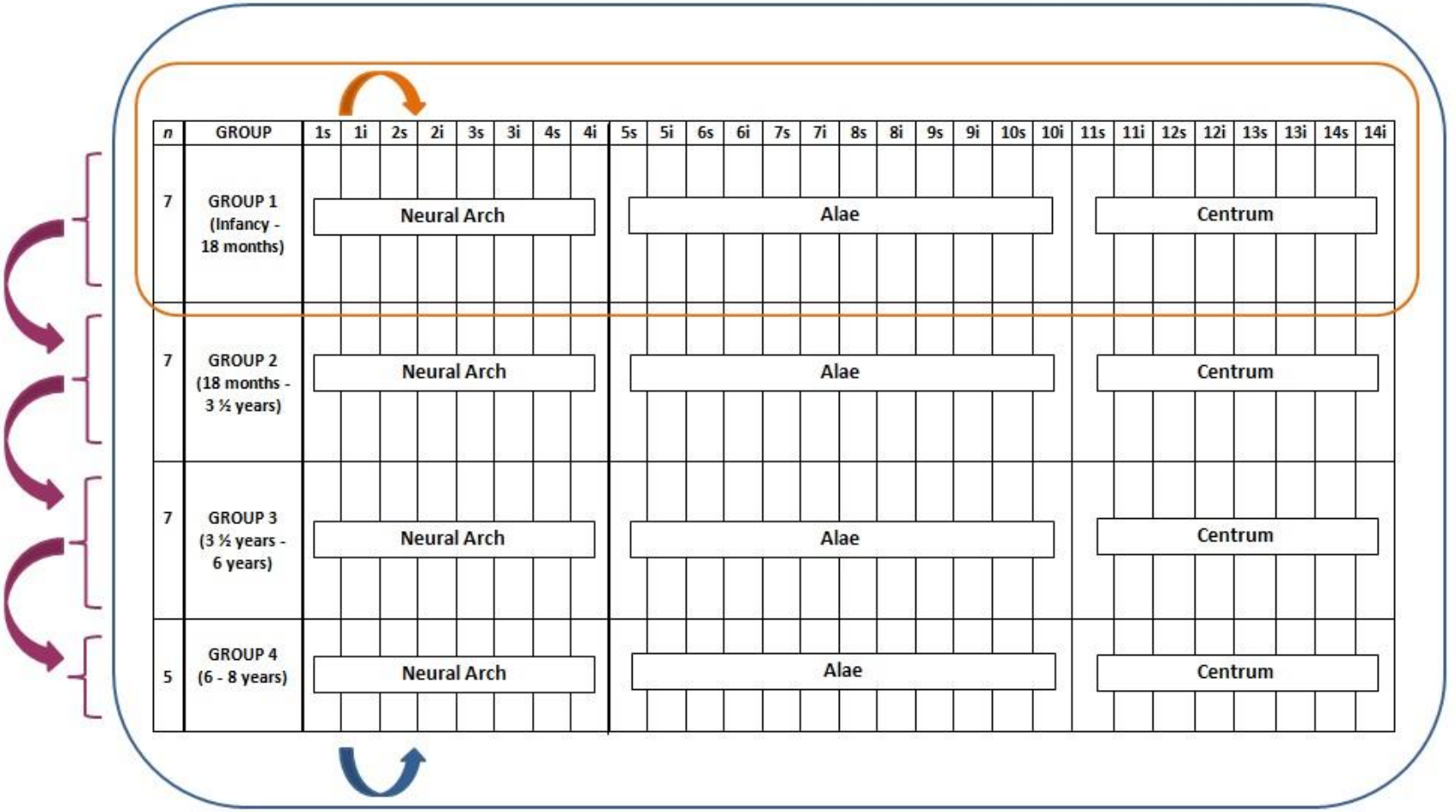

Figure 6.11: A simplified diagram of three different ways to interpret the data using ANOVA or pairwise multiple comparison method (Sigmaplot 12.0). The three analyses were repeated for all 6 bone parameters. The purple arrows represent the analysis comparing the four age groups. The blue and orange arrows represent the analysis comparing the VOIs, where the orange arrow specifically focusing on one age group at a time.

First Analysis

The first analysis (Purple arrow in Figure 6.11) was performed using one way analysis of variance (ANOVA) and pairwise multiple comparison method between the age groups within each of the 6 bone parameters (Table 6.10). For reference, the mean and standard deviation (SD) of each age group are also presented below (Table 6.11).

	BV/TV	Tb.Th	Tb.Sp	Tb.N	SMI	DA
G1 with G2	<0.001*	<0.001*	<0.001*	<0.001*	<0.001*	0.251
G1 with G3	0.759	< 0.001*	< 0.001*	< 0.001*	0.533	0.279
G1 with G4	0.006*	< 0.001*	< 0.001*	< 0.001*	0.225	0.180
G2 with G3	<0.001*	0.164	0.376	<0.001*	<0.001*	0.919
G2 with G4	0.346	< 0.001*	< 0.001*	0.109	0.001*	0.326
G3 with G4	<0.001*	<0.001*	<0.001*	<0.001*	0.044*	0.589

Table 6.10: Pairwise multiple comparison method (Sigmaplot 12.0) exhibits statistically significant changes (*purple shades) ($p < 0.05$) between the age groups for all VOIs (Purple arrows in Figure 6.11). The results are in *p* values.

	BV/TV (%) mean (SD)	Tb.Th (mm) mean (SD)	Tb.Sp (mm) mean (SD)	Tb.N (mm^{-1}) mean (SD)	SMI mean (SD)	DA mean (SD)
G1	34.42 (7.77)	0.274 (0.024)	0.456 (0.070)	1.362 (0.23)	1.622 (0.438)	0.511 (0.120)
G2	27.35 (6.34)	0.351 (0.028)	0.636 (0.093)	0.793 (0.154)	2.052 (0.298)	0.478 (0.125)
G3	33.81 (6.98)	0.363 (0.033)	0.615 (0.092)	0.932 (0.14)	1.539 (0.377)	0.482 (0.164)
G4	28.96 (6.33)	0.402 (0.027)	0.763 (0.141)	0.729 (0.138)	1.746 (0.372)	0.453 (0.1697)

Table 6.11: The mean and standard deviation (SD) of all age groups across the 14 VOIs for each bone parameters.

The first analysis of the 6 bone parameters between the four age groups was conducted to obtain a general overview on the 'ontogenetic' changes that occur within this bone as age increases. The results of this first analysis showed that in general, there are significant changes in the mean values in five bone parameters (BV/TV, Tb.Th, Tb.Sp, Tb.N and SMI) across the four age groups (Table 6.10). However, DA showed no significant changes across the age range.

Bone Volume Fraction (BV/TV) %

The BV/TV results in Tables 6.10 - 6.11 displayed a sinusoidal pattern of the average bone density in the right half of S1 vertebra. It started in group 1 (infancy - 18 months) with a mean value of 34.42% (SD 7.77%), significantly decreasing in group 2 (18 months – 3 ½ years) to a mean value of 27.35% (SD 6.34%). The average bone density then significantly rose in group 3 (3 ½ - 6 years) (mean 33.81%, SD 6.98%), but significantly decreased again in group 4 (6 – 8 years) (mean 28.96%, SD 6.33%). The final average BV/TV values (group 4) were significantly lower than group 1 (Table 6.10). There were no significant differences in the mean values between groups 1 and 3 and between groups 2 and 4 as the average bone density values are very close. (Tables 6.10 – 6.11).

Trabecular Thickness (Tb.Th) mm

The Tb.Th mean values in Table 6.11 exhibit a progressive increase in the thickness of the trabecular bone across the right half of S1 vertebra, where it significantly increased among all of the age groups except between group 2 and 3 (Table 6.10). The average thickness (mean 0.274mm, SD 0.024mm) in group 1 increased significantly in group 2 (mean 0.351mm, SD 0.028mm). However, there was minimal increase in the average

thickness in the trabecular struts in S1 vertebra in the subsequent group (group 3) with a mean value of 0.363mm (SD 0.033mm). Finally, as the child reaches 6 – 8 years, the average trabecular thickness significantly increased to 0.402mm (SD 0.027mm). The final average value for group 4 was significantly higher than that found in the youngest age group (Tables 6.10 – 6. 11).

Trabecular Separation (Tb.Sp) mm

Similar to the Tb.Th pattern, the Tb.Sp exhibits a significantly progressive increase of the average trabecular spaces within the right half of S1 vertebra (Table 6.10) except between groups 2 and 3. Group 1 exhibits an average value of 0.456mm (SD 0.070mm) which significantly increased to an average value of 0.636mm (SD 0.093mm) in group 2. However, there is minimal change in the average spaces in group 3 (mean 0.616mm, SD 0.092mm) and it is not statistically significant. Finally, as the child reaches 6 – 8 years (group 4), the average spaces in the right half of S1 vertebra increased significantly (mean 0.763mm, SD 0.141mm) from the previous age group (group 3), and was the highest value compared to first group (Tables 6.10 – 6.11).

Trabecular Number (Tb.N) mm^{-1}

In contrast to Tb.Th, Tb.N exhibits a general significant reduction in the number of trabecular struts (Tables 6.10 – 6.11) from group 1 (mean 1.362mm^{-1}, SD 0.23 mm^{-1}) to group 4 (mean 0.729 mm^{-1}, SD 0.138 mm^{-1}). Group 2 exhibited further reduction from the early age group (group 1) with a mean value of 0.793 mm^{-1} (SD 0.154 mm^{-1}). However, between these two extreme age groups, there is a period of significant increase in the average number of trabeculae in group 3 (mean 0.932 mm^{-1}, SD 0.14 mm^{-1}), before it significantly reduced in the final age group (group 4) (mean 0.729

mm^{-1}, SD 0.138 mm^{-1}). This sinusoidal pattern average value is reflected in the similar pattern observed in the BV/TV parameter (Table 6.11).

Structural model index (SMI)

The SMI values across the four age groups revealed a general pattern of plate-like (0) towards rod-like (3) structures between the first (mean 1.622, SD 0.438) and second age group (mean 2.052, SD 0.298) (Table 6.11). Subsequently, in group 3 the average value of the SMI significantly decreased (mean 1.539, SD 0.377) where the morphology of the trabecular struts appeared more plate-like (Tables 6.10 – 6.11). Finally, in the oldest age group, there was a significant increase ($p < 0.044$) in the average SMI values (mean 1.746, SD 0.372) (Table 6.10).

Degree of Anisotropy (DA)

The DA value throughout the right half of S1 vertebra revealed a general pattern of slow reduction in the overall values, albeit there is minimal increase in the third group (mean 0.482, SD 0.164) (Table 6.11). However, there are no significant changes observed between any combination of the age groups, even between the first and the fourth group (Table 6.10).

Second Analysis

The second analysis (Blue arrow in Figure 6.11) of the trabecular pattern of the right half of S1 vertebra was performed by ANOVA and pairwise multiple comparison method (Sigmaplot 12.0). This analysis was undertaken to compare between the VOIs when the age groups were combined together. The results were presented in the Table 6.12.

	High value VOI	Low value VOI									
BV/TV	**2**	1	3	5	6	12					
	4	1	3	5	6						
	7	1	3	5	6						
	8	3	5	6							
	9	3	5	6							
	10	1	2	3	4	5	6	7	8	9	11	12
	11	1	3	5	6	9	12					
	12	3	5	6								
	13	1	3	5	6	9	11					
	14	1	3	5	6	12						

	High value VOI	Low value VOI												
Tb.N	**10**	1	3	6										
	13	1	6											

	High value VOI	Low value VOI												
SMI	**1**	2	4	10	11	12	13	14						
	3	2	4	7	10	11	12	13	14					
	5	2	4	7	9	10	11	12	13	14				
	6	2	4	10	11	12	13	14						
	8	2	4	10	11	12	13	14						
	9	2	10	11	12	13	14							

	High value VOI	Low value VOI
Tb.Th	**10**	5

	High value VOI	Low value VOI								
Tb.Sp	**1**	2	4	5	7	8	10	11	13	14
	3	10								
	6	8	10	11	13	14				
	9	8	10	13						
	12	4	8	10	13					

	High value VOI	Low value VOI												
DA	**1**	11	12	13	14									
	2	11	12	13	14									
	3	11	12	13	14									
	4	11	12	14										
	5	11	12	13	14									
	6	11	12	13	14									
	7	11	12	13	14									
	8	11	12	13	14									
	9	1	2	3	4	5	6	7	8	11	12	13	14	
	10	1	2	3	4	5	6	7	8	9	11	12	13	14

Table 6.12: The second analysis (Blue arrow in Figure 6.11) by pairwise multiple comparison procedures (Holm-Sidak method) exhibit significant difference ($p < 0.05$) between the VOIs when all four age groups are combined. The blue shades showed the repetitive occurrence of the significantly low value VOIs compared to the high value VOIs within the respective 6 bone parameters.

The results in Table 6.12 revealed that across the combined four age groups from infancy to 8 years, the six bone parameters exhibit statistically significant differences in an almost consistent pattern of VOIs. The blue shade represents the repeated occurrence of the same VOI within one bone parameter.

Bone Volume Fraction (BV/TV)

The BV/TV revealed that VOIs 2, 4, 7 – 14 are significantly higher ($p < 0.05$) than the rest of the VOI especially VOIs 3, 5 and 6 (Table 6.12). This indicates that VOIs 3, 5 and 6 persistently displayed low bone density irrespective of age. In addition, VOI 10 exhibits significantly high bone density across all other VOIs (VOIs 1 – 9, 11, 12) (Table 6.12). These findings suggest that the centrum (VOIs 11 – 14), medial neural arch (VOIs 2, 4), and anterior and medial part the sacral ala (VOIs 7 – 10) are significantly denser trabecular regions compared to the lateral neural arch (VOIs 1, 3) and posterolateral sacral ala (VOIs 5, 6).

Trabecular Thickness (Tb.Th)

The Tb.Th in Table 6.12 shows that only VOI 10 is significantly higher than VOI 5 ($p < 0.05$) where VOI 5 has very thin of trabecular struts. The remainder of the VOIs exhibit trabecular thickness values between these two extremes. VOI 10 represents the anteromedial part of the sacral ala, while VOI 5 represents the posterior half of the auricular part of the sacroiliac joint.

Trabecular Separation (Tb.Sp)

The results for trabecular separation (Tb.Sp) exhibit significantly higher values ($p < 0.05$) in VOIs 1, 3, 6, 9, 12 compared to the other VOIs (Table 6.12). Again, VOI 10

persistently exhibits significant low spacing in comparison with all of the high trabecular separation values (VOIs 1, 3, 6, 9, 12). These results show that the lateral neural arch (VOIs 1, 3), middle sacral ala (VOIs 6, 9) and the posteromedial centrum (VOI 12) exhibit high spacing compared to the rest of the region in S1 vertebra.

Trabecular Number (Tb.N)

The Tb.N in Table 6.12 showed that during the first 8 years of life, VOIs 10 and 13 exhibit a significantly higher number of trabecular struts ($p < 0.05$), compared to VOIs 1, 3, 6.

Structural model index (SMI)

SMI values in Table 6.12 exhibit significantly high SMI values ($p < 0.05$) in VOIs 1, 3, 5, 6, 8, 9. It also exhibits a large number of VOIs that have significantly lower SMI values (VOIs 2, 4, 7, 10, 11 – 14), with VOIs 2, 10 – 14 persistently exhibiting low values (Table 6.12). The high SMI values indicate a more rod-like trabecular morphology and were found along the lateral part of the S1 vertebra specifically at the lateral neural arch (VOIs 1, 3) and the lateral sacral ala (VOIs 5, 6, 8, 9). While the medial part of the neural arch (VOIs 2, 4), medial sacral ala (VOIs 7, 10) and the entire centrum (VOIs 11 – 14) exhibit a more plate-like trabecular structure.

Degree of Anisotropy (DA)

The DA exhibits interesting findings in this analysis where it showed a large number of VOIs that differ significantly from the rest ($p < 0.05$) (Table 6.12). Although the first analysis (Table 6.10 – 6.11) revealed that there was no difference between the four age groups in the overall trabecular strut arrangements, this second analysis showed that

between the VOIs, there are a large number of significant differences. Table 6.12 exhibits a pattern where the centrum (VOIs 11 – 14) exhibit significant persistently low DA compared to the rest of the S1 vertebra. In addition, VOIs 9 and 10 exhibit the most anisotropic arrangement compared to the rest of the VOIs (1 – 8, 11 – 14). Furthermore, VOI 10 exhibits a significantly higher anisotropic value than VOI 9.

Third Analysis

The third analysis (Orange arrow in Figure 6.11) is the most specific investigation among the three analyses undertaken. The test was performed using ANOVA and pairwise multiple comparison method (Sigmaplot 12.0) to compare specifically, within the same age group, any significant differences among the VOIs for each trabecular bone variable. The results are presented in the Tables 6.13 – 6.14, and the interpretations of the results are described according to the four age groups.

	High value VOI	Low value VOI
BV/TV Group 1	**2**	3 5 6
	4	6
	10	1 3 5 6 8 9 12
	13	3 6

	High value VOI	Low value VOI
BV/TV Group 2	**2**	6
	4	6
	10	1 3 5 6 9 12
	13	5 6
	14	6

	High value VOI	Low value VOI
BV/TV Group 3	**10**	1 3 4 5 6 9 12
	13	1 3 5 6

	High value VOI	Low value VOI
BV/TV Group 4	**10**	1 3 5 6

	High value VOI	Low value VOI
Tb.Th Group 3	**10**	5

	High value VOI	Low value VOI
Tb.Sp Group 3	**1**	4 8 10 13
	3	10
	6	8 10 13
	9	10
	11	10
	12	2 4 5 7 8 10 13
	14	10

	High value VOI	Low value VOI
Tb.Sp Group 4	**1**	2 4 5 7 8 9 10 11 12 13 14
	3	8 10

	High value VOI	Low value VOI
Tb.N Group 2	**10**	6
	13	6

	High value VOI	Low value VOI
Tb.N Group 3	**8**	1 3 6
	10	1 3 6
	13	1 3 6

Table 6.13: The third analysis (Orange arrow in Figure 6.11) by pairwise multiple comparison procedures (Holm-Sidak method) exhibit significant difference ($p < 0.05$) between the VOIs within the four age groups for BV/TV, one age group for Tb.Th, and two age groups for Tb.Sp and Tb.N. The orange shades showed the persistent occurrence of the significantly low value VOIs compared to the high values VOIs.

	High value VOI	Low value VOI					
SMI Group 1	1	2	13				
	3	2	11	12	13	14	
	5	2	10	11	12	13	14
	6	2	11	12	13	14	
	8	2	11	12	13	14	

	High value VOI	Low value VOI					
SMI Group 2	3	14					
	5	14					
	6	10	13	14			

	High value VOI	Low value VOI											
SMI Group 3	1	11	13	14									
	2	14											
	3	2	10	11	12	13	14						
	5	2	10	11	12	13	14						
	6	11	13	14									
	8	13	14										
	9	13	14										

	High value VOI	Low value VOI											
SMI Group 4	3	10	11	14									
	5	10	11	14									
	8	11	14										

	High value VOI	Low value VOI					
DA Group 1	3	14					
	9	11	12	13	14		
	10	11	12	14			

	High value VOI	Low value VOI			
DA Group 2	2	11			
	3	11	12	13	14
	5	12			
	9	11	12	13	14
	10	11	12		

	High value VOI	Low value VOI											
DA Group 3	1	11	12	13	14								
	3	11	14										
	5	11	14										
	7	11	14										
	9	1	2	4	6	11	12	13	14				
	10	1	2	3	4	5	6	7	8	11	12	13	14

	High value VOI	Low value VOI											
DA Group 4	5	2	11	12	13	14							
	7	2	11	14									
	9	2	4	11	12	13	14						
	10	1	2	3	4	5	6	7	8	9	11	12	13	14

Table 6.14: The third analysis (Orange arrow in Figure 6.11) by pairwise multiple comparison procedures (Holm-Sidak method) exhibit significant difference ($p < 0.05$) between the VOIs within each four age groups for SMI and DA. The orange shades showed the repetitive occurrence of the significantly low values VOIs compared to the high value VOIs.

Bone Volume Fraction (BV/TV)

Group 1 (Infancy – 18 months) (*n* = 7)

In this age group, the medial neural arch (VOIs 2, 4), the anteromedial sacral ala (VOI 10) and the anterolateral centrum (VOI 13) exhibit significantly higher bone density ($p < 0.05$) than VOIs 1, 3, 5, 6, 8, 9, 12 (Table 6.13). Furthermore, VOI 10 exhibits the highest density region compared to all of the significantly low VOIs values. The low bone density values were found to be located at the lateral S1 vertebra, specifically at the auricular area (VOIs 5, 8), post-auricular area (VOI 1, 3) and middle sacral ala (VOI 6, 9) as well as the posteromedial centrum (VOI 12). VOI 6 is shown to have persistently low bone density in this age group (Table 6.13).

Group 2 (18 months – 3 ½ years) (*n* = 7)

This group exhibited similar findings to group 1, with the addition of VOI 14 which displayed significantly high bone density ($p < 0.05$) (Table 6.13). While all of the low BV/TV VOIs (1, 3, 5, 6, 9, 12) are again seen in this age group, only VOI 8 which represents the anterior-half of the auricular surface does not exhibit a significant difference. It suggests that VOI 8 may have increased its bone density from the previous group.

Group 3 (3 ½ – 6 years) (*n* = 7)

In this group, only VOIs 10 and 13 continue to show a significantly high bone density region ($p < 0.05$), while VOIs 1, 3, 5, 6 persistently exhibit low density areas compared to the two former VOIs (Table 6.13). These low density areas are found at the posterior-half of the auricular (VOI 5) and post-auricular region (VOIs 1, 3). VOI 4 shows low bone density however, this only occurred once in this age group. VOI 9 and 12

represent the mid-anterior ala and posteromedial centrum respectively and also exhibit significantly low density areas.

Group 4 (6 – 8 years) (*n* = 5)

In this age group, only VOI 10 displayed significantly high bone density areas, with VOIs 1, 3, 5, 6 exhibiting low bone density (Table 6.13). This suggests that, throughout infancy until 8 years, VOI 10 persistently displayed high bone density. VOI 13 retained high values until age group 3 where the value declined in the oldest age group.

Trabecular Thickness (Tb.Th)

The trabecular thickness calculated throughout the four age groups revealed that only in group 3 was there a significant difference ($p < 0.05$) (Table 6.13).

Group 3 (3½ - 6 years) (*n* = 7)

This group revealed that the trabeculae in VOI 10 (anteromedial sacral ala) are significantly thicker than those in VOI 5 (posterior half of auricular area) (Table 6.13). The remainder of the VOIs exhibited no significant difference between these two VOIs.

Trabecular Separation (Tb.Sp)

Pairwise multiple comparison methods were performed throughout the four age groups for trabecular separation analysis and the results show that there are significant differences apparent only in a number of VOIs in groups 3 and group 4 (Table 6.13).

Group 3 (3 ½ – 6 years) (*n* = 7)

This group revealed that VOIs 1, 3 (post-auricular region), 6, 9 (middle sacral ala) and 11, 12, 14 (anteromedial and posterior half of centrum) exhibit a significantly high number of spaces (Table 6.13). At the other extreme, VOI 10 repeatedly exhibits the lowest trabecular spacing in this group. Additionally, VOI 8 which represents the anterior half of the auricular area displayed significantly low trabecular spacing.

Group 4 (6 – 8 years) (*n* = 5)

In this oldest age group, only VOIs 1 and 3 (post-auricular area) exhibited significantly high trabecular spaces compared to almost all other VOIs (2, 4, 5, 7 – 14) (Table 6.13).

Trabecular Number (Tb.N)

The number of trabeculae (Tb.N) for each volume of interest (VOI) was calculated in the four different age groups the results revealed a number of significant differences in groups 2 and group 3 (Table 6.13).

Group 2 (18 months – 3 ½ years) (*n* = 7)

This group exhibited significantly high numbers of trabecular struts in VOIs 10 (anteromedial sacral ala) and 13 (anterolateral centrum), while VOI 6 (mid-posterior sacral alae) displayed significantly low trabecular number (Table 6.13).

3 ½ years – 6 years (*n* = 7)

In this group, in addition to the high Tb.N values in VOIs 10 and 13 as for the previous group (group 2), VOI 8 (anterior-half of auricular area) exhibited a significantly high

number of trabecular struts, while VOIs 1, 3 (post-auricular) and 6 (mid-posterior sacral ala) exhibited significantly lower Tb.N values (Table 6.13).

Structural model index (SMI)

Group 1 (Infancy – 18 months) (*n* = 7)

In this age group, VOIs 1, 3 (post-auricular), 5, 8 (auricular) and 6 (mid-posterior ala) exhibited significantly high SMI values suggesting a rod-like structure, while VOIs 2 (posteromedial neural arch), 10 (anteromedial sacral ala) and 11 – 14 (centrum) exhibited significantly low SMI values suggesting a plate-like morphology (Table 6.14). VOIs 2, 13 showed persistently low SMI values.

Group 2 (18 months – 3 ½ years) (*n* = 7)

This group exhibited high values in the anterior half of the post-auricular area (VOI 3), posterior half of the auricular area (VOI 5) and mid-posterior sacral alae (VOI 6), similar to the previous group (group 1) (Table 6.14). During this period, only VOIs 10, 13 and 14 exhibits significantly low SMI values indicating a more plate-like morphology, with VOI 14 constantly showing low values.

Group 3 (3½ years – 6 years) (*n* = 7)

This age group exhibited the largest number of VOIs that displayed significantly high SMI values (VOIs 1 – 3, 5, 6, 8, 9) (Table 6.14). Again, VOIs 3, 5, 6 persistently exhibited high SMI values across all three age groups (group 1 – 3). The significantly low SMI values ($p < 0.05$) suggesting a plate-like trabecular morphology in this group were displayed by VOIs 2 (posteromedial neural arch), 10 (anteromedial sacral alae) and 11 – 14 (centrum).

6 – 8 years (*n* = 5)

In this oldest age group, the significantly higher SMI values are displayed in VOIs 3 (anterior half of post-auricular), 5, 8 (auricular areas), while the significantly low SMI values again were found in VOIs 10, 11, 14. SMI persistently exhibited high significant values (rod-like structure) at the lateral neural arch, and lateral ala, while the centrum, medial neural arch and anteromedial ala exhibited almost constantly low values (plate-like structure) throughout the 8 years (Table 6.14).

Degree of Anisotropy (DA)

Group 1 (Infancy – 18 months) (*n* = 7)

Significantly high DA values were observed in VOIs 3 (anterior half of post-auricular area), 9 (mid-anterior sacral ala) and 10 (anteromedial sacral ala) in this age group (Table 6.14). The significantly low degree of anisotropy, suggesting a more isotropic arrangement of the trabecular struts, is exhibited by VOIs 11, 12, 13, 14 (centrum).

Group 2 (18 months – 3 ½ years) (*n* = 7)

In addition to VOIs 3, 9, 10 that exhibited significantly high DA in the previous group (group 1), VOIs 2 and 5 also displayed high DA in this group. Again, the centrum (VOIs 11 – 14) exhibited a significantly more isotropic trabecular arrangement (Table 6.14).

Group 3 (3 ½ – 6 years) (*n* = 7)

This group showed the most number of VOIs with significantly high DA across the four age groups. It showed that VOIs 1, 3 (post-auricular), 5 (posterior half of auricular), 7, 9, 10 (medial and anterior part of the sacral alae) exhibited a more anisotropic trabecular arrangement. In addition to the centrum (VOIs 11, 12, 13, 14) that persistently exhibited a more isotropic network, VOIs 1 – 8 displayed a significantly lower than VOI 10, suggesting that VOI 10 exhibited the most anisotropic region in S1 vertebra, followed by VOI 9 (Table 6.14).

Group 4 (6 – 8 years) (*n* = 5)

In this oldest age group, only VOIs 5, 7, 9, 10 showed a significantly high degree of anisotropy (Table 6.14). It showed that VOI 10 has the highest and was the most anisotropic across the right half of S1 vertebra, while the rest of the VOIs (1 – 9, 11 – 14) were significantly lower than this anteromedial sacral alae region. VOI 2 in this age group started to show a persistently isotropic region.

6.5 Discussion

The sacrum is the region where progressive and dynamic changes in its internal microarchitecture may be considered indicative of changing biomechanical demands responding to weight transmission at the pelvic region (Ebraheim *et al*, 2000). The shape, density and orientation of the trabecular bone will be influenced by the loads that it has to support. If there is a high load in a certain region of the bone, it is reasonable to expect the trabeculae to be arranged appropriately in relation to the direction and magnitude of the loads which will best support the structure (Marcus *et al*, 2009).

Recent studies on histomorphometric evaluation of juvenile bones has highlighted the complex nature of trabecular bone development (Ryan and Krovitz, 2006; Cunningham and Black, 2009b; Gosman and Ketcham, 2009; Reissis and Abel, 2012). In the growing bone, the basis of these changes lies in the principal process of modelling and remodelling where bone formation and resorption occurs, mainly to accommodate increasing bone size, remodelling, and rearrangement of the internal microarchitecture as a response to mechanical loads (Parfitt *et al*, 2000; Frost, 2004). This mechanism is modulated by genetic control, and other physiological factors such as diet and hormonal status and one of the most important factors, is age effect (Ruff *et al*, 2006).

The early stage of vertebral bone development is represented by mineralisation of the tissue where a cartilage template is converted into bone. The complexity of this process and the subsequent microarchitectural trabecular arrangement (Parfitt *et al*, 1987), specifically at the growing sacrum, has not yet been investigated, thus initiating the current study. The quantified results on the trabecular pattern of the juvenile sacrum are discussed and compared with other studies on the juvenile trabecular network of the femur, tibia, ilium and lumbar vertebrae in various sub-adult groups (Nuzzo *et al*, 2003; Ryan and Krovitz, 2006; Cunningham and Black, 2009b; Gosman and Ketcham, 2009;

Reissis and Abel, 2012). The results from this study analysed the pattern of trabecular structural arrangement as it adapts with the ontogenicity associated with gross motor milestones and mature bipedal locomotion.

Study of the development of the juvenile sacrum in relation to specific volumes of interest on the S1 vertebra from infancy up until 8 years was considered a reasonable research project because although the sacrum increases in size over time, the shape remains virtually constant, suggesting relative phylogenetic stability and therefore a strong genetic blueprint for its development. In contrast to the uneven growth of the juvenile ilium where the crest grows approximately seven times faster than the acetabulum, studies on animal sacra exhibit constant and equal growth of the sacral breadth relative to the sacral length, and constant proportion of sacral length in relation to the developing vertebral column (Harrison, 1958; Cunningham and Black, 2010). The margins of three sacral elements; the centrum, neural arches and sacral alae in this study were identifiable throughout infancy to 8 years, even though they are fused together in the older age group, but the fusion lines (represented by neurocentral, neuroalar and centroalar junctions) are still visible, albeit faint at 8 years of age. Thus the reference points and the anatomical landmarks to outline the volume of interest (VOI) were detectable and consistently reproducible throughout these 26 specimens.

The discussion on the quantification results of this chapter is divided according to the 6 bone parameters and then summarized at the end of this chapter.

Bone volume fraction (BV/TV)

The trabecular bone volume fraction represents the percentage of bone in the selected volume of interest (VOI). Trabecular bone volume is reported to be the single most important parameter describing the trabecular microstructure and in determining the risk of fracture compared to the trabecular thickness (Parfitt *et al*, 1983; Ding *et al*, 1999). Additionally, the BV/TV value of weight-bearing bone was reported to be significantly greater than for non-weight-bearing, as a structural response to functional adaptation to locomotor behaviour, particularly in the juvenile age group (Ruff *et al*, 2006; Shaw and Ryan, 2012).

In the first group from infancy until 18 months, the bone volume fraction (BV/TV) revealed the highest percentage of bone density with a mean of 34.42% (SD of 7.77%) ($p < 0.05$) across the four age groups. Previous studies also reported that fetal lumbar vertebrae exhibit the highest BV/TV values (30-54%) compared to older individuals, with approximately 2.5 to 3 times the volume of bone compared to the young adult (Nuzzo *et al*, 2003). This high bone volume in the youngest individuals was reportedly due to the rapid rate of bone deposition, and as the individual grows, whilst the bone-forming rate decreases, the remodelling process continues (Mulder *et al*, 2007; Gosman and Ketcham, 2009). In the second group (18 months – 3 ½ years) the BV/TV values decreased significantly ($p < 0.05$) to a mean of 27.35% (SD of 6.34%) and then increased in the 3 ½ years to 6 years group (group 3) to a mean of 33.81% (SD of 6.98%). The final group (6 – 8 years) experienced a significant reduction ($p < 0.05$) in the overall bone density values with a mean of 28.96% (SD of 6.33%).

This sinusoidal pattern of BV/TV of the juvenile S1 vertebra is consistent with the percentage of BV/TV found in the infant human femur where it exhibits the highest BV/TV (range 45 – 51%) compared to the lower BV/TV percentage in older individuals

(range from infancy to 9 years) (Ryan and Krovitz, 2006). The study by Ryan and Krovitz (2006) also showed that there is a period of decreasing BV/TV with the lowest value found at 18 months (14.2%) and picked up again at the age of 5 years. The pattern of decrease and then increase throughout post-natal development is thought to be an adaptive mechanism in weight-bearing bones in a response to the early and rapid increase in total body mass (Tanck *et al*, 2001). This sinusoidal pattern of BV/TV does not occur in the fetal specimens throughout intrauterine life, as the bone volume fraction of human fetal lumbar vertebrae, femora and humeri remain constant from 4 months to 9 months of gestation (Nuzzo *et al*, 2003; Reisses and Abel, 2012).

In this current study, apart from the very high bone volume found in some of the youngest age group, the overall values for the BV/TV especially in the oldest age group (6 – 8 years) fall within the range of reported variation for adults (4 – 48%) and juveniles (20 – 46%) from other studies (Hildebrand *et al*, 1999; Ulrich *et al*, 1999; Gosman and Ketcham, 2009).

Of the VOIs, the highest BV/TV value across the four age groups is persistently found at VOI 10, representing the anteromedial part of the sacral ala. This same region is referred to as the 'condensation zone' where dense trabecular bone is also found in the adult sacrum (Ebraheim *et al*, 2000). Additionally, VOIs 2, 4, and 13 also repeatedly exhibit significantly high bone volume values with these VOIs located at the medial neural arch (VOIs 2, 4) and the anterolateral centrum (VOI 13). These high value VOIs (2, 4, 10, 13) are observed in the period during infancy until around 3 ½ years. However, around 3 ½ - 6 years where a child has fully achieved full body balance during walking and maturing gait (Sutherland *et al*, 1980; Keen, 1993), the high BV/TV in the S1 vertebra is found to be concentrated only at the anteromedial sacral ala (VOI 10) and the anterolateral (VOI 13) centrum region adjacent to it. Finally, as the child

reaches 6 – 8 years with the period of attainment of mature adult gait, only VOI 10 exhibits the significantly high trabecular bone density. The percentage of BV/TV in this age group has settled into the range of adult values (Gosman and Ketcham, 2009). This specific site of high BV/TV areas may reflect the general adaptation process of bone modeling and remodeling influenced by initial transient quadrupedal maturing into bipedal locomotor behaviour in humans (Lovejoy, 1988; Gosman and Ketcham, 2009), where in the juvenile S1 vertebra, forces/stresses are focused in the area of the pelvic brim (VOI 10).

On the other hand, significantly low BV/TV values are persistently found in VOIs 3, 5, 6, representing the anterior half of the post-auricular, posterior half of the auricular and mid-posterior sacral ala. These regions were referred to as the 'alar void' or the 'alar emptiness' as the area exhibits low bone volume in the S1 vertebral adult age groups (Peretz *et al*, 1998; Ebraheim *et al*, 2000; Mahato 2010c).

It was noted that the BV/TV value for VOI 5 representing the posterior-half of the auricular surface, was always consistently lower than the anterior-half of the auricular surface represented by VOI 8. VOI 8 mostly appeared as a 'medium' BV/TV value lying between the both extremes of BV/TV values. This pattern of higher bone density on the ventral part of the auricular area was also noted in a non-parametric study in adult bones (Mahato 2010c).

Trabecular thickness (Tb.Th)

The trabecular struts in the juvenile S1 vertebra revealed a significantly increasing pattern from infancy towards 8 years. This is expected as a child grows, the body weight and bone size is increasing especially during the first 2 years of life when the most rapid

growth occurs (Cole, 2003). This increasing pattern of thickness of the trabecular struts was also reported in the developing human femur and tibia, with an age-related linear increase from birth to 9 years (Ryan and Krovitz, 2006; Gosman and Ketcham, 2009), but no significant variation has been reported in the growing fetal lumbar vertebrae (Nuzzo *et al,* 2003). This may suggest that the external loading factor and bone mass play a crucial role in initiating and enhancing trabecular thickness (Tanck *et al,* 2001). The gradual increase in the thickness of the cancellous structure of the S1 vertebra corresponds well with the progressive developmental milestones of a child, from predominantly sitting, crawling and cruising in the first group, where the upper limbs would play as important a role as the lower limbs (Gosman and Ketcham, 2009), into to a more stable bipedal locomotion and mature gait as the age reached 8 years, where the vertebrae and the lower limbs are the essential components of weight-bearing (Kapandji, 1974).

The range of values for Tb.Th in this study (mean ranged: 0.274 – 0.402mm) was found to be slightly higher than those reported in juvenile studies of the human trabecular pattern of the proximal femur and subepiphyseal tibia (Ryan and Krovitz, 2006; Gosman and Ketcham, 2009), ranging from 0.085 – 0.219mm (femur) and 0.076 – 0.332mm (tibia). However, these two studies were based on a few specific sites of the two long bones, and did not represent the whole bone trabecular pattern analysis, as the proximal femur was reported to display a different bone density to that of the femoral neck (Hildebrand *et al,* 1999; Lai *et al,* 2005).

Although in the developing juvenile sacrum, there are generalised increases in thickness of the trabecular struts ($p < 0.001$), it was reported that in the adult vertebra, Tb.Th was negatively correlated with age, explained by the higher occurrence of osteoporotic bone in the elderly (Dempster *et al,* 1993; Ding and Hvid, 2000). The mean trabecular

thickness of the adult lumbar vertebra ranged from 0.122 to 0.139mm (Hildebrand *et al,* 1999) and exhibited much lower values than the final value of S1 vertebra in this study in the fourth group (mean = 0.402mm), indicating that the thickness of the trabecular bone increases with age and body mass until adolescence (Gosman and Ketcham, 2009), after which it decreases progressively during adulthood into old age. Thus it is impractical to compare the juvenile trabecular bone values with adult trabecular thickness.

Despite the general increase in thickness of the cancellous bone of the S1 vertebra throughout the first 8 years of life, the results showed that the regions displaying the highest trabecular thickness in S1 vertebra is at VOI 10 (anteromedial sacral ala), especially during the 3 ½ - 6 years period. The increasing robustness of this anteromedial sacral ala region showed that the ontogenetic patterning occurred at the time of locomotive maturation in humans (Sutherland *et al,* 1980; Keen, 1993), most probably influenced by the increasing body mass and greater loading on this specific area of S1 (Doube *et al,* 2011; Shaw and Ryan, 2012).

On the other hand, the lowest trabecular thickness was persistently noted at the posterior-half of the auricular surface (VOIs 5) of S1. The low trabecular thickness and density of the posterior-half of the auricular surface may reflect the minimal amount of body weight passing through this region, as confirmed in the adult sacra (Ebraheim *et al,* 2000; Mahato 2010c).

Trabecular Separation (Tb.Sp)

Trabecular separation (Tb.Sp) is the space between the trabecular struts that represents the thickness of the marrow cavities, where maximal spheres occupying the non-bone

part of the selected VOI were calculated (Parfitt *et al,* 1987; Hildebrand *et al,* 1999). It is reported that as body mass increases, bone is actively remodeled where the understrained trabecular bone is reabsorbed thus creating more spaces (Doube *et al*, 2011).

It was noted that in S1 juvenile vertebra, as age increases, the spacing between the trabecular struts significantly increases, albeit between group 2 (18 months – 3 ½ years) and group 3 (3 ½ - 6 years), there is a slight decrease (from mean values of 0.635 to 0.615mm). However, as the child reaches 6 – 8 years, the mean trabecular spaces significantly increased to 0.763mm. This final value was compared with the adult lumbar vertebral Tb.Sp (0.792mm – 0.854mm) and adult distal radius Tb.Sp (0.75mm – 1.34mm) which suggests that by the age of 8 years, the S1 vertebral trabecular separation has already settled into the range of the adult values (Majumdar *et al,* 1997; Hildebrand *et al,* 1999). The settlement of Tb.Sp in this study into adult values at the age of 8 years also coincides with the timing of full gait maturation around 8 years (Sutherland *et al*, 1980; Keen, 1993), which was also observed in BV/TV values in this study and other ontogenetic trabecular studies (Ryan and Krovitz, 2006; Gosman and Ketcham, 2009).

The significantly low Tb.Sp value (VOI 10) was found in the areas where highest BV/TV and Tb.Th values exist, representing the anteromedial sacral ala region. This is expected as the high bone volume with thickest trabecular struts must have occupied the majority of the spaces available in VOI 10. Additionally, VOIs 1, 3, 6, 9, and 12 exhibit significantly high trabecular spaces corresponding to the post-auricular area (VOIs 1, 3), middle sacral ala (VOIs 6, 9) and posteromedial centrum (VOI 12). As VOIs 3, 6 were shown to persistently exhibit significant low bone volume, these areas would be expected to have a high amount of space. VOI 12 is most likely occupied by the

basivertebral vessels that drain into the internal vertebral venous plexus, thus creating the high Tb.Sp values in this area (Sinnatamby, 2006; Snell, 2008).

Trabecular Number (Tb.N)

The number of trabeculae in the S1 vertebra showed a significantly decreasing trend as the child grows from infancy to 8 years, albeit there is an increase in Tb.N in the third age group (3 ½ - 5 years) but as the child reaches 6 – 8 years, the number of struts in the S1 vertebra significantly reached the lowest value (0.729mm) throughout the four age groups. The final trabecular number values in the 6 – 8 years group were found to be slightly lower than the adult lumbar vertebral values (1.161 – 1.278mm^{-1}) (Hildebrand *et al*, 1999). Nevertheless, the decreasing pattern of Tb.N in this study was also observed in the juvenile femur and tibia where the Tb.N decreased abruptly especially in the first year of life, and continued to decrease gradually until late adolescence (Ryan and Krovitz, 2006; Gosman and Ketcham, 2009).

The ontogenetic pattern of Tb.N is opposite to that of Tb.Th as the remodelling process selectively removes the underutilised trabeculae while increasing the thickness of the overstrained trabeculae (Gosman and Ketcham, 2009; Doube *et al*, 2011).

Despite the declining pattern of the Tb.N in relation to age, again, the anteromedial sacral ala (VOI 10) persistently exhibited a significantly high trabecular number. This is followed by the anterolateral centrum area (VOI 13). The post-auricular area (VOI 1, 3) and mid-posterior sacral ala (VOI 6) exhibited the lowest Tb.N values across the S1 vertebra.

The approximately constant bone volume fraction in the growing S1 vertebra suggests that it was balanced by the increase in the trabecular thickness with a concomitant decrease in the trabecular number (Ryan and Krovitz, 2006; Reissis and Abel, 2012).

Structural Model Index (SMI)

The structural model index was quantified by 3D analysis of the triangulated bone surface ranging from 0 (plate) to 3 (rod), or a mixture of plates or rods, independent of the dimension (Hildebrand and Rüegsegger, 1997b; Shaw and Ryan, 2012). If the structure exhibited both plates and rods equally, the values would lie within 0 to 3, corresponding to the ratio of rods and plates. It is reported that lightly loaded bone has low density, rod-like trabecular network while in the higher load areas, the trabeculae are thicker and have a more plate-like structure (Marcus *et al*, 2009).

Although the overall SMI values between the four age groups exhibit a somewhat sinusoidal pattern similar to that seen in the BV/TV parameter, it displayed a repeatedly high value (rod-like structure) at VOIs representing the lateral part of the S1 vertebra (VOIs 3, 5, 6), while significantly low values (plate-like morphology) were observed in the medial neural arch (VOIs 2), anteromedial sacral ala (VOI 10) and centrum (VOIs 11 – 14). It was reported that a plate-like trabecular structure is found in regions of high stress, suggesting a close relationship between trabecular structure with mechanical loading (Ding *et al*, 2002). Inversely, the lateral part of the S1 vertebra exhibits high SMI values representing more rod-like trabecular struts, suggesting this region experiences low mechanical stresses.

The SMI values in the juvenile sacra in the 6 – 8 years group (means SMI 1.746) fall near to the adult values for lumbar vertebra (1.94 – 2.66) suggesting that as the child

reaches 8 years when gait matures (Inman *et al*, 1981), the structural model type has achieved the adult range (Hildebrand and Rüegsegger, 1997b; Hildebrand *et al*, 1999).

Degree of Anisotropy (DA)

The degree of anisotropy is determined using the ratio of maximum and minimum radius of the mean intercept length of an ellipsoid, by superimposing parallel test lines in various directions on the 3D image of the trabecular bone (Harrigan and Mann, 1984; Hildebrand *et al*, 1999; Ulrich *et al*, 1999a). In simpler words, DA is the preferential orientation of the trabecular bone (Ding, 2000). A fully isotropic structure has a DA of 0 while 1 represents fully anisotropic trabecular arrangements. The location of the bone plays a major role in determining the degree of anisotropy where the adult femoral head DA was reported to be significantly more anisotropic than the humeral head (Shaw and Ryan, 2012).

Although there is no significant difference in DA among the four age groups, when comparing between the VOIs, the juvenile S1 vertebra exhibits an interesting pattern in which the centrum (VOIs 11 – 14) persistently exhibits significantly low DA, indicating persistent isotropic trabecular arrangement throughout ontogeny. In contrast, VOI 10 persistently presents as a high anisotropic area, where in groups 3 and 4 it displayed its highest degree compared to the rest of S1 vertebra, most probably as a result of remodelling of the trabeculae for better adaptation to functional loading as the trabecular bone is laid down where it is most required (Keaveny *et al*, 2001; Gosman and Ketcham, 2009). It also suggests that while the centrum (VOIs 11 – 14) exhibits an isotropic trabecular arrangement, most probably as a result of direct compressive weight from L5 vertebra, VOI 10 may experience weight transmission from various directions, thus showing anisotropic trabecular arrangement.

Summary

Throughout the first 8 years of life, VOI 10 significantly exhibits the highest bone volume, thickest and highest number of trabeculae with low spaces, plate-like morphology and the most anisotropic pattern. This indicates that in the juvenile S1 vertebra, VOI 10 is the most robust trabecular area. The medial half of the neural arch (VOIs 2, 4) and the lateral centrum (VOIs 11, 13) exhibit medium to high density bone suggesting these areas are the areas behaving most similar to VOI 10. On the contrary, the auricular surface (VOIs 5, 8) does not appeared to be a robust structure, especially in the posterior half (VOI 5) of this joint, when compared to the adjacent areas of the mid-posterior sacral ala (VOI 6) and the anterior half of post-auricular (VOI 3). These three areas appeared sparse and frail with a rod-like framework. The summary of the different bone parameters is suggested to create three zones (Figure 6.12).

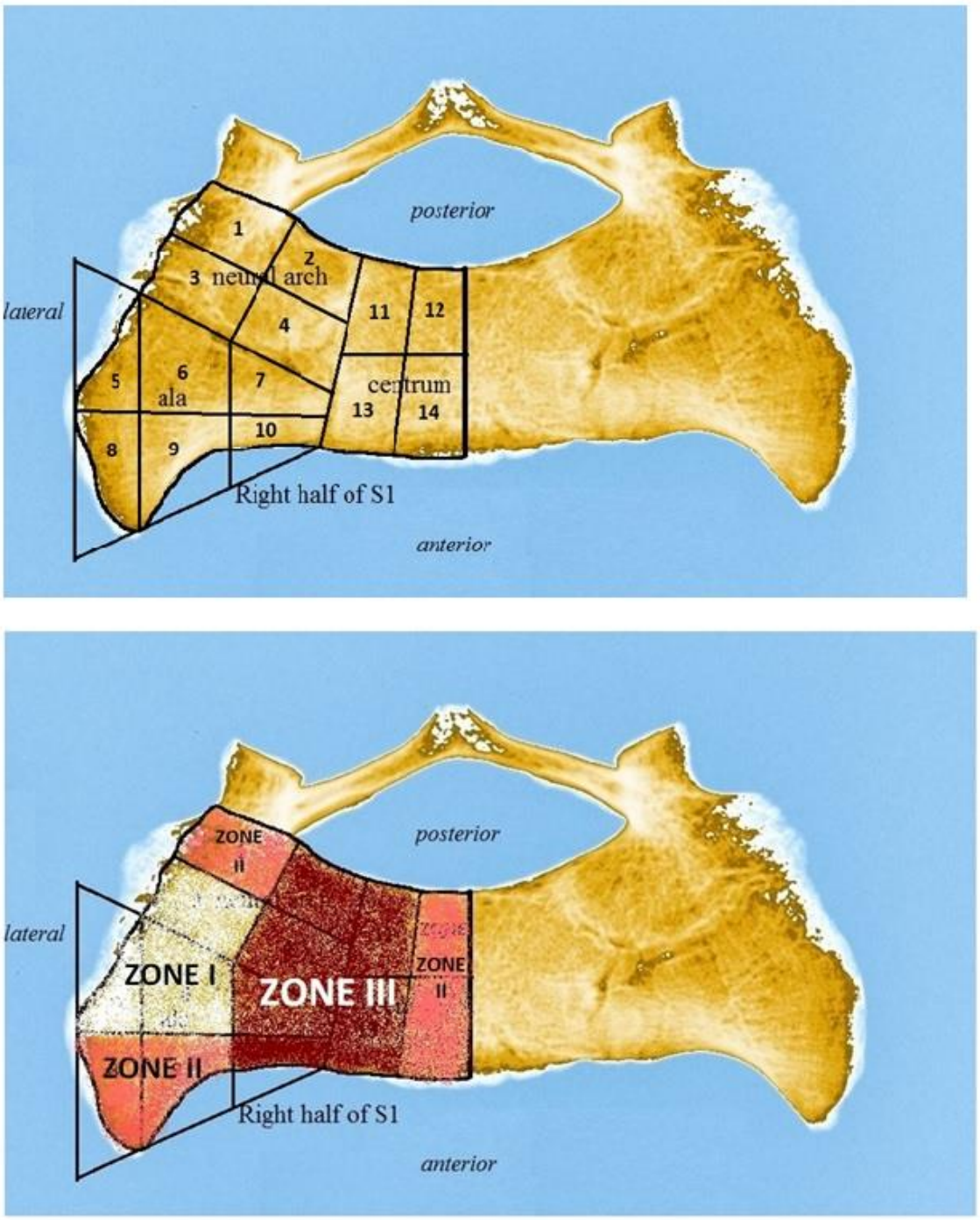

Figure 6.12: The suggested 3 Zones in the S1 vertebra, Zone I (VOIs 3, 5, 6), Zone II (VOIs 1, 8, 9, 12, 14) and Zone III (VOIs 2, 4, 7, 10, 11, 13).

Three different Zones in the S1 vertebra

From these three analyses, it is suggested the S1 vertebra can be represented by three different zones as follows (Figure 6. 12):

1. Zone I (VOIs 3, 5, 6): low bone density, low trabecular number, low trabecular thickness, high trabecular spacing, rod-like structure, more anisotropic arrangement. It represents the anterior half of the post-auricular area (VOI 3), posterior half of the auricular area (VOI 5) and the mid-posterior region of the sacral ala (VOI 6).

2. Zone II (VOIs 1, 8, 9, 12, 14): moderate bone density, moderate trabecular number, medium trabecular thickness, medium trabecular spacing, with rod-like morphology and anisotropic arrangement (VOIs 1, 8, 9) and plate-like, isotropic structure (VOIs 12, 14). It represents the posterior half of the post-auricular area (VOI 1), anterior half of the auricular area (VOI 8), anterior middle sacral ala (VOI 9) and middle centrum (VOIs 12, 14).

3. Zone III (VOIs 2, 4, 7, 10, 11, 13): high bone density, high trabecular number, thickest trabeculae, with low trabecular spaces, plate-like trabecular morphology, anisotropic arrangement (2, 4, 7, 10) and isotropic trabecular arrangement (11, 13). VOI 10 exhibits the highest bone density, persistently thickest trabeculae with a high number of struts, and very limited spaces, with plate-like morphology and is the most anisotropic region across the entire S1 vertebra. It represents the medial neural arch (VOIs 2, 4), posteromedial and anteromedial sacral ala (VOIs 7, 10), and lateral centrum (VOIs 11, 13).

CHAPTER 7

Growth of the Human Ilium – The Anomalous Sacroiliac Junction

7.1 Introduction

Despite the major anatomical interactions associated with the pelvic surface of the human ilium, little is understood about its pattern of growth (Hoppa, 1992; Rissech and Malgosa, 2005). A recent study suggests that growth in the width of the human ilium is accelerated during the period of infancy to 4 years and then again at puberty (Rissech and Malgosa, 2005), suggesting that two defined periods of increased growth might occur, concomitant perhaps with defined developmental milestones of maturing gait and secondary sexual changes. This study was conducted to investigate growth in four regions of the pelvic surface of the developing ilium, from birth through to adulthood.

7.2 Materials and Methods

Eighty (80) human ilia were available for study from the Scheuer Collection of juvenile skeletal remains housed within the Centre for Anatomy and Human Identification, College of Life Sciences, University of Dundee (Table 7.1).

Age	Number of specimens (*n*)
Neonate	5
4-6 months	3
1 year	2
2 years	2
3 years	4
4 years	4
5 years	2
6 years	2
7 years	2
8 years	3
9 years	2
10 years	1
11 years	2
12 years	12
13 years	2
14 years	1
15 years	2
16 years	2
17 years	2
18 years	16
19 years	9
Total	80

Table 7.1: Age and number (*n*) of juvenile ilia.

Not all individuals within the collection are of documented age: some have therefore previously been assigned an age using established forensic standards based on both skeletal and dental development (Fazekas and Kosa, 1978; Scheuer and Black, 2000). This study does not consider age prediction; therefore an estimated age was sufficiently appropriate to examine broad patterns of change in relation to maturation. Documented sex was also not available for all specimens: hence no sex segregation was employed as, unlike age estimation, the determination of sex from juvenile remains is not reliable. This was not deemed to be important in this study as there was no intention of

examining sexual dimorphism and the same specimens were used for each of the four measurements so that a comparative analysis between measurements was viable.

All specimens included in this study were in an excellent state of preservation with minimal damage to the cortical shell and underlying trabecular structure. Any pathological specimens or bones which were badly damaged were excluded. Information regarding the provenance and demography of this collection has been documented elsewhere (Scheuer and Black, 2000; Cunningham and Black, 2009a).

The study focused on the measurement of four surface areas of the pelvic aspect of the ilium (Figure 7.1):

(1) auricular (A)

(2) post-auricular (PA)

(3) iliac fossa (F)

(4) the whole ilium (I)

The measurements excluded the metaphyseal acetabular surface located at the inferior portion of the ilium (marked in Figure 7.1 with an asterisk (*)). Measurements of the iliac fossa and the whole ilium could not be collected for the oldest age group as fusion at the acetabulum obliterates the junction between the iliac component and the pubis and ischium. Therefore, in the oldest age group, only the relationship between the auricular and the post-auricular regions was examined.

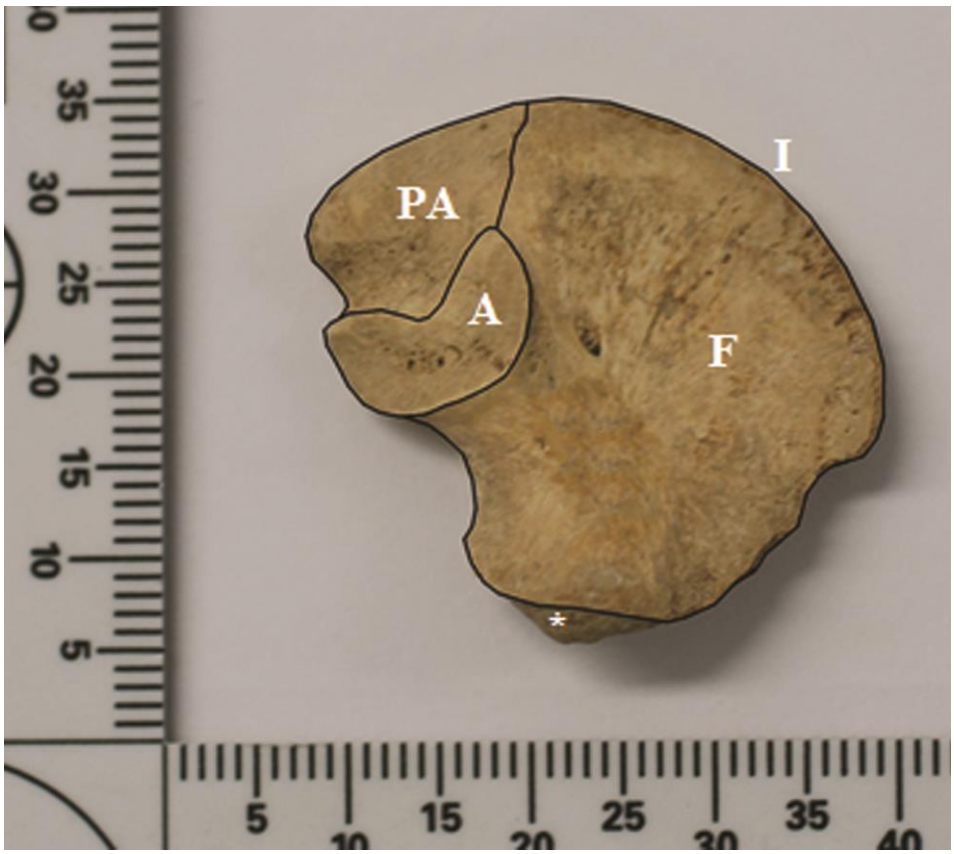

Figure 7.1: Measurements taken on the pelvic surface of a perinatal ilium; auricular (A), post-auricular (PA), pelvic fossa (F) and the whole pelvic surface of the ilium (I). *Acetabular metaphyseal surface not included in measurement of I or F.

Methods

The details on how the study was conducted has been described in Chapter 4, however the summary of the methods are discussed here for easier reference.

Digital Imaging and Image J software

All of the specimens were laid on a flat surface and photographic images of each were taken using Nikon D80 Digital single-lens reflex (SLR) 10.2 megapixel camera. The

image was stored in TIFF format. The saved image was then opened using Image J and the four surface areas were measured by delineating the desired areas (Figure 7.1) using a Wacom tablet. After the targeted region was delineated, the surface area was calculated and the result expressed in millimetres squared (mm^2).

The post-auricular region (PA) was defined by the transition between surface textures at the junction between the most posterior attachments of the iliacus muscle and the most anterior attachments of the ventral sacroiliac ligament at the spina limitans. The outline of the auricular surface (A) was defined by the auricular elevation of the joint rim. The surface area of the whole ilium (I) was measured by identifying the perimeter of the bone on the image while excluding the acetabular metaphyseal area. The surface area of the iliac fossa (F) was calculated by subtraction of the auricular and post-auricular areas from the surface area of the ilium as a whole (Figure 7.1).

7.3 Results

The specimens (Table 7.1) were divided into five age cohorts (Table 7.2) based on the results of a recent study of growth of the ilium (Rissech and Malgosa, 2005), which suggested that the period between five years of age and puberty may be a phase of restrained bone growth. In contrast, the time from infancy to four years represents a period of accelerated growth which occurs again after puberty. The pubertal/adolescent group in this study was further subdivided based on the presence or absence of fusion at the acetabulum: the youngest individual showing fusion was 14 years of age.

Therefore, the cohorts for subsequent analysis were: neonate (group 1), 4 months to 4 years (group 2), 5 to 10 years (group 3), 11 to 14 years (group 4) and 15 to 19 years (group 5). The results of the surface area measurements for these five cohorts are shown in Table 7.2. The surface area for each of the four regions was measured on three separate occasions and tested using 1-way ANOVA (Sigmaplot 12.0). There was no significant difference ($p=0.986$) between measurements; therefore, a mean of the three repeat measurements was taken as the value for each measurement.

	Group	Group 1	Group 2	Group 3	Group 4	Group 5
	Age	**Neonatal**	**4 months – 4 years**	**5 – 10 years**	**11 – 14 years**	**15 – 19 years**
	n	5	15	12	17	31
Auricular (A)	Mean	74.86	246.26	418.75	589	1040.92
	SD	3.13	91.32	66.14	99.01	248.39
	Range	69.80 - 77.72	85.23 – 351.60	290.60 – 491.90	404.54 – 819.69	683.53 – 1517.65
Post-Auricular (PA)	Mean	95.87	409.04	671.37	1038.52	1812.58
	SD	8.59	179.47	129.94	188.31	462.81
	Range	85.42 – 103.42	120.66 – 689.03	517.53 – 916.77	712.28 – 1326.84	1035.86 – 2771.34
Iliac Fossa (F)	Mean	568.74	1985.42	3461.38	4983.38	-
	SD	24.45	749.35	383.3	838.4	-
	Range	542.52 – 597.08	677.00 – 2926.44	2876.06 – 3993.51	3221.87 – 6180.48	-
Whole Ilium (I)	Mean	739.47	2640.73	4551.5	6610.9	-
	SD	27.84	1010.81	531.44	1029.48	-
	Range	701.96 – 769.74	887.73 – 3957.29	3710.75 – 5201.98	4338.69 – 8074.69	-

Table 7.2: The mean, standard deviation (SD) and the range of the auricular (A), post-auricular (PA), iliac fossa (F) and the whole ilium (I) surface areas in mm^2. The data for F and I in Group 5 were not calculated because of iliac fusion.

Surface area measurements

The mean, standard deviation and range of the surface areas for each region of the pelvic surface of the ilium are shown in Table 7.2. The raw data were log-transformed to permit direct comparison between the variables, with log-transformed surface area (mm^2) plotted against age (years) (Figure 7.2).

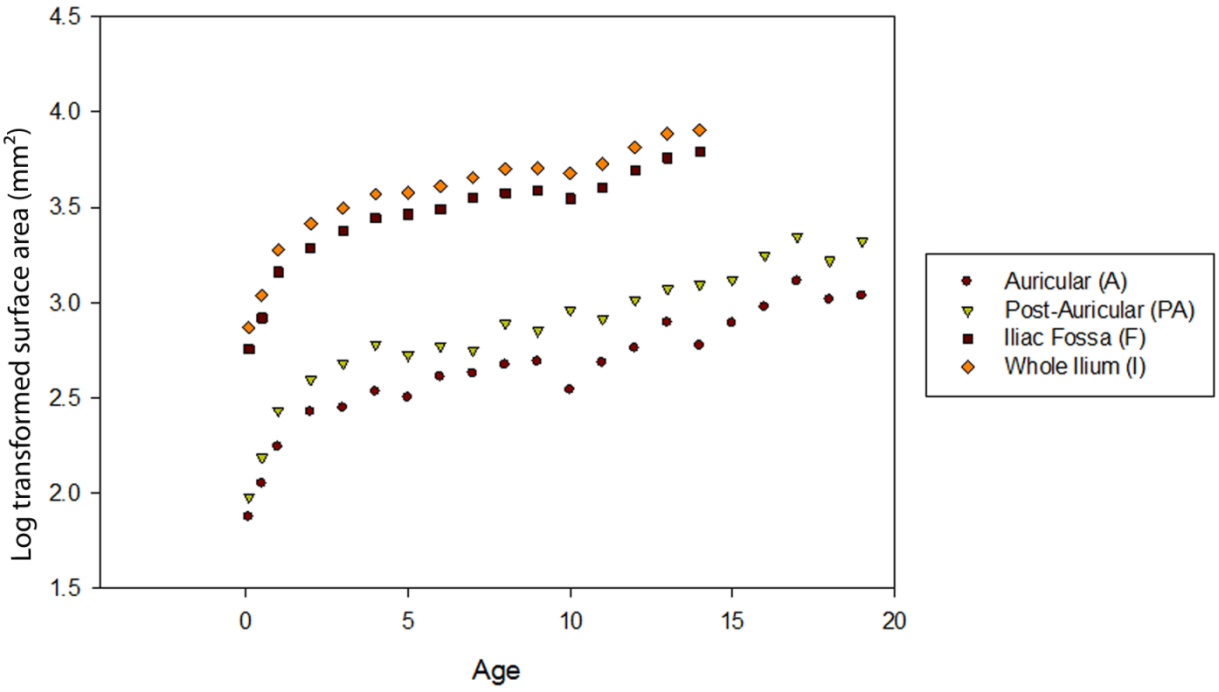

Figure 7.2: The log-transformed surface area (mm^2) of the auricular (A), post-auricular (PA), iliac fossa (F) and the whole ilium (I) throughout development.

	A				PA				F			I		
	G1	G2	G3	G4	G1	G2	G3	G4	G1	G2	G3	G1	G2	G3
Group 1														
Group 2	3.29				4.27				3.49			3.57		
Group 3	5.60	1.70			7.00	1.64			6.09	1.74		6.16	1.72	
Group 4	7.86	2.39	1.41		10.83	2.54	1.55		8.76	2.51	1.44	8.94	2.50	1.45
Group 5	13.90	4.23	2.49	1.73	18.91	4.43	2.70	1.75						

Table 7.3: Ratios of the mean surface area (mm²) among age groups for each region; A (auricular), PA (post-auricular), F (iliac fossa) and I (whole ilium), ratios are calculated as (older group area) / (younger group area).

	A					PA					F				
	G1	G2	G3	G4	G5	G1	G2	G3	G4	G5	G1	G2	G3	G4	G5
PA	1.28	1.66	1.61	1.76	1.74										
F	7.59	8.06	8.21	8.46		5.93	4.85	5.15	4.8						
I	9.87	10.7	10.9	11.2		7.71	6.46	6.78	6.37		1.3	1.33	1.31	1.32	

Table 7.4: Ratios of each of the mean surface areas (mm²) among regions of A (auricular), PA (post-auricular), F (iliac fossa) and I (whole ilium), ratios are calculated as PA/A, F/A, I/A, F/PA, I/PA and I/F for all groups (G).

Changes in each region with age

In group 2, the mean auricular surface area is more than 3 times its size in the neonate; it is almost 6 times the size by the time it reaches group 3, and nearly 8 times the size in group 4. While in group 5, it is almost 14 times the size of the neonate (Table 7.3).

The mean post-auricular surface area in group 2 is more than 4 times the size in the neonate, it is 7 times in group 3 and nearly 11 times the neonatal size in group 4. However, by the time it reaches group 5, the post-auricular surface is nearly 19 times the size it was during the neonatal period suggesting that this surface shows a greater level of growth compared to that seen in the auricular surface.

There is more than a 3-fold increase in surface area of the iliac fossa and of the bone as a whole between group 1 and group 2, in group 3 the area is 6 times, and in group 4, nearly 9 times the neonatal size (Table 7.3).

Changes between regions

When the surface areas are considered as ratios across the different age groups (Table 7.4) it can be seen that the ratio post-auricular/auricular area ranges between 1.28 and 1.74, with the ratios being greater with increasing age. The remaining ratios of areas are more consistent throughout ontogeny, albeit with some differences especially between the youngest age groups. Thus, iliac fossa/auricular area, is approximately 8; whole ilium/auricular area, 10; iliac fossa/post-auricular area, 5; whole ilium/post-auricular area, 7. It is therefore suggested that the auricular and post-auricular areas are not behaving the same in terms of growth, with the post-auricular area keeping up with the iliac fossa and whole ilium to a greater extent than the auricular area.

The period between five years to puberty (groups 3 and 4) has been shown in this study to be a relatively quiescent period of growth for the ilium. Although initially the post-auricular region shows a minimal increase (ratio of 1.64) in group 3 compared to the auricular (ratio of 1.70), it then accelerates more (ratio of 1.55) than the auricular (ratio of 1.41) in group 4. In addition, the auricular surface continues to exhibit the slowest rate of growth in group 4 (ratio of 7.86) compared to the post-auricular, iliac fossa and the whole ilium.

Age group 5 represents the mid to late pubertal age in which the auricular and post-auricular regions both started to show some degree of accelerated growth (ratios of 1.73 and 1.75, respectively) compared to group 4 (ratios of 1.41 - 1.55).

By the end of puberty, the auricular surface is 14 times the size it was in the neonate, but by comparison, the post-auricular region is 19 times its neonatal size. In the age groups up to and including 14 years of age, the rate of growth is consistently greater in the post-auricular area (ratio of 10.83) than the rest of the regions measured (ratios of 7.86, 8.76 and 8.94 for the auricular, iliac fossa and whole ilium, respectively).

7.4 Discussion

As the ilium grows, it must be able to respond to alterations imposed by factors that impact on its development. The earliest of these is reflected in the changes that occur as the child progresses through the different phases of early transitive locomotion. During the first two years the child progresses from a supine and static state to, albeit inefficient, bipedal stance and locomotion (Keen, 1993). Adaptations to the changing forces through the previously unstrained junction between the axial and the lower appendicular skeleton would be expected to be seen in the pelvis within the first two years of life. As it continues to grow, the pelvis finally achieves a capacity where the viscera can descend from the abdomen into the pelvic cavity: this occurs around 3-4 years of age, significantly altering the location of the centre of gravity associated with continued bipedality (Scheuer and Black, 2000). The stability of growth in the pelvis at this time is evidenced by its fusion at the ischiopubic ramus (around 5 years of age) and no further appositional growth can now occur in this region after this period. However, the child continues to grow with a mature gait not being achieved until around 8 years of age (Inman *et al*, 1981; Keen, 1993).

Consequently, areas of the ilium associated with locomotive maturation would be expected to continue to respond appropriately during this period, whereas features associated with increasing body size might be more quiescent. The sex related steroids released at puberty bring about a remodelling of the pelvic complex (Greulich and Thoms, 1944) which facilitates the changes required for final adult pelvic morphology. These require preferential alteration to the pelvic brim, which passes across the margins of the sacroiliac joint and so it is reasonable to suggest that the region of the joint may respond to these biomechanical stimuli.

All regions of the pelvic surface of the ilium in this study appear to follow an initially similar pattern with regard to the relationship between growth and age in that a rapid increase in size is seen (Figure 7.2) in the first 1-2 years after birth, continuing, albeit at a slower rate, until approximately 4 years of age when the rate of growth is further reduced, and picks up again after 10 years but to a lesser extent. From the ratios of the mean surface areas between the groups, the post-auricular surface continues to shows accelerated growth compared to the other regions. It is not unreasonable to hypothesise that this represents a response mechanism to the requirement for enhanced and enlarged ligamentous development to provide stability to the child during standing and walking. In contrast, the auricular region exhibits the slowest growth compared to the other three regions during the earlier age range, and surprisingly this persists throughout the remaining age groups.

The period between five years to puberty (groups 3 and 4) has been shown in this study to be a relatively quiescent period of growth for the ilium. Although initially the post-auricular region shows a minimal increase (ratio of 1.64) in group 3 compared to the auricular (ratio of 1.70), it then accelerates more (ratio of 1.55) than the auricular (ratio of 1.41) in group 4. In addition, the auricular surface continues to exhibit the slowest rate of growth in group 4 (ratio of 7.86) compared to the post-auricular, iliac fossa and the whole ilium. This minimal response to pubertal influences may explain the limited evidence for sexual dimorphism at the auricular surface of the sacroiliac joint (Ali and MacLaughlin, 1991; Sutter 2003; Blake, 2011). Age group 5 represents the mid to late pubertal age in which the auricular and post-auricular regions both started to show some degree of accelerated growth (ratios of 1.73 and 1.75, respectively) compared to group 4 (ratios of 1.41 - 1.55). The results in this section must be interpreted with the awareness that males and females have been combined and therefore sexual dimorphism has not been taken into account (Iuliano-Burns *et al,*

2009). While males continue to grow, females experience cessation of growth up until the end of the late adolescent years.

The findings in the present study are largely in line with research undertaken on the growth in width of the human ilium (Rissech and Malgosa, 2005), which also found that the period between 5 to 10 years is a non-growth stage prior to the growth spurt. However, further work requires to be undertaken particularly in the 1-3 months age category where the sample size was restricted. The results suggest that there is a progressive and enhanced growth of the post-auricular surface compared to the auricular which can reasonably be attributed as a response to the load placed on it by the post-auricular ligaments as they respond to the stresses and strains associated with the onset of bipedal locomotion and an upright posture largely prevalent by the end of the first year (Sutherland *et al,* 1980; Forssberg, 1985; Keen, 1993). This might suggest that the post-auricular region more than the auricular region demonstrates advanced growth to meet the demands of bipedality, bringing into question the role that the auricular surface may play in direct weight transfer.

By the end of puberty, the auricular surface is 14 times the size it was in the neonate, but by comparison, the post-auricular region is 19 times its neonatal size. In the age groups up to and including 14 years of age, the rate of growth is consistently greater in the post-auricular area (ratio of 10.83) than the rest of the regions measured (ratios of 7.86, 8.76 and 8.94 for the auricular, iliac fossa and whole ilium, respectively).

The increased growth throughout the development of the ilium for the post-auricular area, suggests that it responds to the alteration of ontogenetic bipedality with a resultant shift in the centre of gravity (Aiello and Dean, 1990). This suggests that bipedal locomotion impacts on the post-auricular area rather than the auricular surface.

In addition, the increased growth noted after puberty in this study is presumably due to the changing morphology of the pelvis associated with secondary sexual changes (Greulich and Thoms, 1944). In the past, sexual dimorphism has been found to be very low in the auricular surface (Ali and MacLaughlin, 1991) and the post-auricular region might be more productive for investigation into sexual dimorphism as it appears to reflect growth and alteration in response to bipedal locomotion and perhaps weight transfer.

It is therefore possible that the auricular surface of the sacroiliac joint *per se* simply reflects an embryological junction, in that it marks the boundary between paraxial (sacrum) and lateral plate mesoderm (ilium) derived skeletal elements (Scheuer and Black, 2000). This boundary is a largely vertically oriented joint that is not optimally equipped to respond to the demands of the specifics of weight transfer during stance and locomotion. These demands may, in fact, be met by the post-auricular region where the ligamentous attachments are increased and strengthened to maintain the integrity of the joint as it responds to shifting functional requirements particularly in relation to locomotion and later puberty, which both alter the biomechanics of the pelvic complex. The lower growth rate seen in the auricular area compared to the post-auricular region during puberty also suggests that this joint may not be primarily influenced by the elevated sex hormones and secondary sexual changes. Furthermore, its behaviour differs from the other weight-bearing joints of the skeleton, for example it does not cavitate in the same manner as the hip joint in response to increased loading (LeVeau and Bernhardt, 1984), may further suggest that this joint is actually behaving as a non-weight-bearing junction. The commonly held view that the sacroiliac is a route of transfer of load from the axial to the appendicular skeleton may be overly simplistic and it is likely that the role of the post-auricular region has been perhaps inappropriately marginalised.

CHAPTER 8

General Discussion

Studies considering ontogenetic trabecular bone patterning in human juvenile bones are limited (Ivarsson *et al,* 2013). In particular, there is no specific study which considers the developing trabecular bone architecture in the juvenile sacrum. However, despite the paucity of research in the sacrum, extensive work on understanding trabecular bone stereology has been undertaken in the juvenile femur, tibia, and calcaneus with results demonstrating that the trabecular architecture is influenced by its loading environment throughout ontogeny (Ryan and Krovitz, 2006; Skedros *et al,* 2007; Gosman and Ketcham, 2009). Additionally, several studies have been conducted on the developing juvenile ilium perhaps by virtue of its precocious maturation during the fetal-neonatal period (Cunningham and Black 2009b, 2009c). Much of this previous research has considered bones which arise from a single primary ossification centre, however the current study differs in that it considers a bone which forms from multiple primary ossification centres that ultimately fuse with one another (Scheuer and Black, 2000; Cunningham and Black, 2009a, 2009b, 2009c; Abel and Macho, 2011; Wilson *et al*, 2011).

The location of a bone within the skeleton plays an important role in determining its trabecular architecture (Hildebrand *et al,* 1999; Lai *et al*, 2005). For example, it is reported that the weight-bearing femoral head exhibits substantially higher bone volume fraction and thicker trabeculae compared to the non-weight bearing humeral head (Shaw and Ryan, 2012). Additionally, in the human tibia, the persistent compressive forces experienced by the load-bearing metaphyseal areas result in strengthening of these sites demonstrated via remodelled trabecular bone architecture (Goldstein *et al* 1983). These areas of remodelled bone architecture are an essential part of bones 'self-regulating

mechanism' where mechanical loading stimulates bone remodelling (Frost, 2004), enabling bone to achieve its optimal structural morphology for accommodating forces (Lanyon, 1974; Lee and Taylor, 1999; Doube *et al*, 2011). In particular it has been demonstrated that a high bone volume fraction, plate-like structure and high degree of anisotropy corresponds with a trabecular bone area that experiences increased mechanical stresses (Ding *et al*, 2002).

This thesis comprised three different studies; two studies pertaining to the juvenile sacrum and one study considering growth of the juvenile ilium. The two sacral studies are inter-related, with the first (sacral study) pertaining to the qualitative assessment of intensity patterns from radiographic images of the developing sacrum. This study investigated the gross representation of increased density areas throughout the bone. The second study involved the quantification of the trabecular architecture of the S1 vertebra from histomorphometric analysis of micro-CT slice data. These two sacral studies enabled an investigation of the trabecular bone response to the physical developmental milestones the sacrum undergoes from birth to 8 years of age. These milestones that include the adoption of a sitting posture, transient quadrupedal to bipedal locomotion and finally gait maturation. Each of these milestones were investigated in relation to their potential influence on the microarchitectural properties of S1 trabecular bone (Sutherland *et al*, 1980; Keen, 1993; Keaveny *et al*, 2001) in line with the theory of bone functional adaptation in response to mechanical loading (Lanyon, 1982; Beauprê *et al*, 1990; Lee and Taylor, 1999; Ruff *et al*, 2006). It is important to note that in addition to the mechanical stresses that influence the remodelling potential of bone, other factors such as genetic, hormonal, environmental and nutritional factors also play an important role for cortical and trabecular bone growth and development (Keaveny *et al*, 2001; Ruff *et al*, 2006; Doube *et al*, 2011).

The iliac part of the study focused on the growth of the developing ilium via analysis of the pelvic surface area. The pelvic surface area was of interest due to the presence of the auricular and post-auricular regions and the relationship of these surfaces with the sacrum via the sacroiliac joint. The function of the sacroiliac joint is disputed, particularly with regard to the ability of the joint to transfer weight from the vertebral column to the innominate due to the vertical alignment of the joint surfaces and the fact that the bones on either side of the joint have different embryological origins (Last, 1978; DonTigny, 1985; Pel *et al*, 2008; Palastanga and Soames, 2012; Vleeming *et al*, 2012). This study aimed to resolve this controversial issue especially in the subadult group where limited literature is available pertaining to the sacrum as well as the sacroiliac joint. In addition, it aimed to infer the areas of body weight distribution through the developing sacrum.

Statistical analysis in the juvenile sacral study has shown that there are no significant differences between the right half and the left half of the juvenile S1 vertebra, which was also seen in the trabecular pattern of the adult group, with the reported no bilateral difference (Pal, 1989; Ebraheim *et al*, 2000). This suggests that the body weight from the vertebral column is equally distributed to both the right and left sides of S1 vertebra where each half of the vertebra bears an equal amount of weight compared to the total amount experienced by the vertebral column. In addition, the analysis also shows that the superior half of the S1 vertebra is analogous with its inferior half, with no statistically significant difference being observed. Although embryologically the superior half and the inferior half of the vertebra underwent the process of resegmentation, where the caudal half of a sclerotome fuses with the cranial half of the adjacent sclerotome (Huang *et al*, 2000; Saga and Takeda, 2001; Sadler, 2010), functionally these two regions were shown to behave similarly.

The result of the radiographic sacral study revealed an interesting trabecular arrangement which was maintained throughout early development where the juvenile sacrum persistently exhibited high density areas at the most superior part of the sacrum (S1, to a lesser extent S2) specifically at the centrum and its immediate surrounding area. The quantification of S1 revealed that these high density areas marked as Zone III (VOIs 2, 4, 7, 10, 11, 13) represented the lateral centrum, medial neural arch and the anteromedial aspect of the sacral ala. Of these large zones, VOI 10 consistently exhibited the highest bone volume fraction and highest trabecular number with the least spaces within the S1 vertebra. This specific region also displayed increasing values for trabecular thickness throughout development, with a more plate-like morphology and the most anisotropic trabecular organisation as the child grows. These features suggest that the anteromedial aspect of the centrum (VOI 10) experiences the highest amount of stresses resulting in the optimisation of this volume for functional loading in response to body weight transmission (Keaveny *et al*, 2001; Ding *et al*, 2002). It has been reported that areas with high-density and a plate-like trabecular structure are commonly found in high stress regions of the bone suggesting that trabecular morphology and density correlates with mechanical properties (Ding *et al*, 2002; Marcus *et al*, 2009). Studies on juvenile femora and tibiae also revealed that the initial dense, numerous small isotropic trabecular long bones at birth, underwent reorganisation by functional adaptation processes following initiation and maturing bipedal walking resulting in fewer, thicker trabeculae with a high degree of anisotropy (Ryan and Krovitz, 2006; Gosman and Ketcham, 2009).

The alar region, in particular most of the auricular area of the juvenile sacrum revealed sparse, low intensity areas. Trabecular quantification revealed that this area referred to as Zone I (VOIs 3, 5, 6), persistently exhibited low bone volume fraction, thin and fewer trabeculae, rod-like trabecular morphology and were less anisotropic than VOI

10. This suggest that this region experiences minimal weight transmission as described by Wolff's law of bone functional adaptation where the developing trabecular bone will remodel in accordance with the functional need of the area, in response to the external loading environment (Lanyon, 1974; Skedros and Baucom, 2007; Doube *et al*, 2011).

It is pertinent to note that the alar part of the sacrum is embryologically analogous to the costal elements of the thoracic region which go on to become the ribs. The ribs are not designed to be load bearing, therefore by making this embryological comparison it is not surprising that the sacral alae do not possess a trabecular bone signature which is indicative of weight transfer (O'Rahilly *et al,* 1990; Palastanga and Soames, 2012). This theory of minimal weight transfer associated with the alar part of the sacrum is further supported by the ilium growth study. In this study, the auricular surface demonstrated restricted growth throughout development compared to the persistently larger surface area and advanced growth of the post-auricular (PA) areas. This suggests that the soft tissue structures surrounding the sacroiliac joints may have a greater role to play in load transfer than previously thought. These soft tissues include the strong and abundant interosseous and posterior sacroiliac ligaments which predominantly arise from the deepest depression at the post-auricular area of S1, that blend with the strong sacrotuberous ligaments (Vleeming *et al,* 1996; Vleeming *et al,* 2002; Snell, 2008; Moore *et al*, 2013). The constant advancement and higher surface areas of the PA compared to the auricular surface area may be an indication that more load is being transferred via the soft tissues associated with the PA than through the sacroiliac joint itself.

The findings in this study are comparable to the pattern described for the adult sacrum, where Zone III has been described as the 'condensation area' where the lateral centrum and centroalar junction meet. This area has been shown to demonstrate high bone

density with thicker trabecular, arranged in a cruciate pattern (Peretz *et al,* 1998). Zone I has been referred to as the 'alar void' in the adult S1 vertebra as the area was seen to be sparsely occupied by trabecular bone on the lateral part of the sacral alar (Pal, 1989; Peretz *et al,* 1998; Ebraheim *et al,* 2000). The findings of the juvenile S1 vertebral trabecular pattern that is maintained into adulthood is most probably due to the child adopting an upright sitting position at around 6 months, whereby S1 is bearing the body weight being transmitted from L5. This pattern of weight transfer is maintained until the child starts to walk (Robson, 1984; Aiello and Dean, 1990; Keen, 1993; Carruth and Skinner, 2002). There is no major change in habitual bipedal locomotion or posture in the human from the attainment of walking around 18 months of age until adulthood, thus explaining the comparatively almost similar trabecular pattern in S1 especially in Zones I and III observed in this study compared with the adult pattern reported in the literature (Pal, 1989; Peretz *et al,* 1998; Ebraheim *et al,* 2000).

Additionally, the radiographic findings on the juvenile sacrum revealed that the more distal sacral vertebrae (S3 – S5) displayed much reduced density, most probably due to very minimal weight passing through this region (Bellamy *et al,* 1983; Peretz *et al,* 1998). These features were also persistently observed throughout the sacral ontogeny.

This study postulates that the body weight is transmitted from the body and facets of L5 vertebra to the facets and centrum of S1 (Pal, 1989; Mahato 2013), where it is reflected in the trabecular bone architecture of zone III that represents the lateral centrum, medial neural arch and anteromedial alae especially VOI 10 that exhibit the highest robusticity. However, the posteromedial part of the centrum (VOI 12) exhibits a much reduced density region which may be explained by the presence of the invading nutrient arteries and exiting basivertebral veins (Snell, 2008; Moore *et al,* 2013). These space occupying blood vessels are essential to support active growth of the sacrum. As the juvenile bone

continues to develop, this space-occupying vascularity also increases where bone is remodelled resulting in higher spaces, fewer trabeculae with a compensatory increase in trabecular thickness (Cunningham and Black, 2010).

Posteriorly, body weight is postulated to be transferred from the sacrum through the surrounding soft tissue structures attached at the post-auricular area as well as the posterior neural arch. These soft tissues constitute the abundant and strong posterior sacroiliac and interosseous ligaments that attach the sacrum to the post-auricular aspect of the ilium and its adjacent areas (Figure 8.1). It is suggested that they may be responsible for transferring a large amount of the body weight by virtue of tensile forces as these ligaments brace the sacrum from downward displacement by the vertebral column, with the ilia 'sandwiching' the unstable sacrum (Snell, 2008). Through this bracing load is transferred to the ilium and thus to the acetabulum and lower limbs by tension in the posterior sacroiliac ligaments and their attachment to the ilium. This bracing action by the posterior ligaments is further reinforced by the strong sacrotuberous and sacrospinous ligaments which act to stabilise the sacrum and the sacroiliac joint (Williams and Warwick, 1980; Tile, 1988; Alderink, 1991; Moore *et al*, 2013). This posterior passage of load transfer is further supported by the increased growth and proportional surface area observed at the post-auricular area of the ilium.

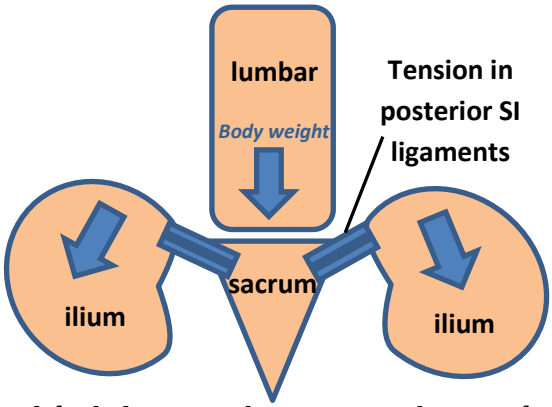

Figure 8.1: A simplified diagram showing weight transfer pathway from the lumbar vertebrae to the ilium via the posterior sacroiliac ligaments.

Anteriorly, at the anterior boundary of the juvenile S1 vertebra (VOI 10), body weight is proposed to be distributed via three pathways:

Firstly, the body weight is transferred via compressive load downward to S2 vertebra (Ebraheim *et al*, 2000). Secondly, via lateral transmission of load via the anterior aspect of sacral alae where moderate bone volume fraction was observed: load will ultimately passes across the sacroiliac joint. Thirdly, via the anterior sacroiliac ligament that attaches at the anterior border of the sacral ala in the region of VOI 10 to the junction between the cranial and caudal limbs of the iliac auricular surface near to the greater sciatic notch (Drake *et al*, 2005; Moore et al, 2013). This region has been reported to exhibit the highest bone volume fraction with the thickest trabecular struts (Cunningham and Black, 2009b). Although reportedly thin, the anterior sacroiliac ligament traverses the joint (Schunke, 1938; Bowen and Cassidy, 1981; Jaovisidha *et al*, 1996; Drake *et al*, 2005) and withstands some of the downward forces associated with the suspended sacrum. The anterior sacroiliac ligament, together with the sacrotuberous and sacrospinous ligaments prevent nutation of the sacral promontory (Vleeming *et al*, 1989; Snell, 2008), thus creating a constant tension at the anterior region of the pelvic brim area where VOI 10 is located.

As this complex mechanism of weight transmission around the posterior pelvic area has revealed, there is no evidence of a direct weight transfer pathway across the entire sacroiliac joint in the studies reported in this thesis, which is at odds with the previously held view that the sacroiliac joint was a weight bearing structure (Bellamy *et al*, 1983; Vleeming *et al*, 1996; Pel *et al*, 2008). Furthermore, the two opposing bones forming the joint originate from different embryological origins with the ilium developing from lateral plate mesoderm and the sacrum from paraxial mesoderm (Mundlos and Olsen, 1997; Olsen *et al*, 2000; Sadler, 2010). The differences in the embryological origin

between the two auricular spaces is in contrast with other weight-bearing synovial joints including the hip and knee joints which all share the common origin of lateral plate mesodermic germinal layer (Johnson and Tabin, 1997; Tickel, 2003). Additionally, the constant disparity of the two sacroiliac auricular cartilaginous surfaces are consistently reported where the ilium persistently appeared thinner, bluish, dull-looking, fibrocartilaginous in nature with signs of early degenerative changes, while the sacrum appeared thicker, smooth, glistening and hyaline in origin (Brooke, 1924; Carter and Loewi; Macdonald and Hunt, 1952; Bowen and Cassidy, 1981, Kampen and Tillmann, 1998). These explicit contrasts of the joint surfaces may suggest that the joint is actually not behaving as a 'normal' synovial joint in order to allow weight transfer.

The S1 vertebral biomechanics are somewhat comparable to the pectoral region where the upper limbs are suspended in the natural posture bearing gravitational weight. These loads are transformed into tensile forces at the shoulder joint stabilised by strong muscular attachment of the rotator cuff muscles, deltoid and the glenohumeral ligaments (Bassett *et al,* 1990; Bigliani *et al,* 1992). In this region, the weight and forces are transferred from the appendicular skeleton to the axial region, while in the pelvic region, the body weight from L5 to S1 vertebra are transformed into tensile forces via its surrounding ligaments, mainly bypassing the vertical sacroiliac joint.

The strength of this study lies in the immediate availability of the juvenile sacra and iliac specimens of the Scheuer Collection. The collaboration with the Centre for Medical Engineering and Technology, University of Hull provided the micro-CT apparatus for this analysis. The importance of scanning the juvenile specimens with this equipment was to achieve micrometre voxel size for high resolution images compared to the clinical CT. The new multiplanar reconstruction (MPR) technique developed in this study via OsiriX software in providing the correct orientation for the analysis of the

S1 vertebra has minimised the burden of quantifying the sacra in the undesirable lateral view. The desired superoinferior (SI) view in quantification analysis of the S1 vertebra provides more precise data collection compared to anteroposterior (AP) or lateral view. Additionally, several studies have been published using the same quantification Skyscan CTAn method with regards to the current study (Cunningham and Black, 2009b, 2009c).

The limitation of this study partially lies in the complex and different stages of appearance and fusion times of the sacrum, in addition to the complex morphological shape of the bone which resulted in a number of difficulties in analysing the bone. Additionally, it is difficult to achieve qualitative radiographic interpretation for the fused sacrum in the older age group as the orientation of the specimen can only be achieve in the anteroposterior (AP) view. However, this problem has partially been resolved in the quantification study of the S1 vertebra where the preferred orientation can be manipulated via the multiplanar reconstruction (MPR). Thus, it is hoped that the remaining sacral vertebra could be studied with the similar quantification method to accomplish the whole result in the juvenile sacral study.

The early fetal and perinatal specimens could not be included in this study as the shapes of the unfused elements were unidentifiable in relation to the anatomical position of the sacrum. A number of neonatal specimens were in a poor state of preservation, thus were excluded in this study. However, this developmental stage would have been useful for comparing the changes in trabecular bone architecture from the non-weight bearing to the weight-bearing sacrum.

Furthermore, for the quantification study, some of the specimens were so small that the most lateral VOIs of the sacrum (VOIs 5 and 8) were unable to be assessed due to the rudimentary region, although this occurred in 2 – 3 specimens only. The analysis of the

superior articular facets of the S1 vertebra was deemed impossible in the younger age group (before 4 years) as the facets appeared rudimentary in more than half of the samples, although in adult sacra several studies have been undertaken (Davis, 1961; Pal, 1989; Mahato, 2010b). In hindsight, the one neonatal sample in the infancy – 18 months age group (group 1) would be excluded, as the remaining specimens in this group had already started to experience weight-bearing, either by sitting position, or started to have bipedal stance and cruising. Nevertheless, the exclusion of this one specimen may have little impact on the overall average data that were collected in this age group which comprise of a total of 7 specimens.

The manual thresholding process adopted in the quantification study was considered to be a potential limitation, due to the fact that trabecular bone was selected using visual interpretation. However, the results of the trabecular bone parameter values are comparable with other studies (Hildebrand *et al*, 1999; Ryan and Krovitz, 2006; Gosman and Ketcham, 2009) and repeatable within this study. It is hoped that in the future, trabecular bone binarisation may be conducted in an automated or semi-automated manner for increased accuracy of quantification.

Clinical correlation

Clinically, VOI 10 within Zone III is the strongest candidate for screw insertion in surgical treatment particularly pertaining to paediatric unstable sacral fractures, as bone density plays a significant role in the stability of bone-screw fixation (Carlson *et al*, 1992; Ebraheim *et al,* 2000) and Zone I is the area where screw fixation would not be indicated due to the sparse trabecular bone architecture. Similar findings were noted in the adult S1 vertebrae in relation to screw fixation, where the denser bone in the centrum suggests the highest stability compared to the lateral ala region (Smith *et al,*

1993). Fracture of the sacrum often contributes to chronic neurological problems involving the lower extremities, urinary, rectal and sexual dysfunctions with the severity of the injury depending on the type and location of the sacral fractures (Zelle *et al*, 2004). It is suggested that very early surgical management of the sacral fracture could facilitate better functional outcomes for the patient (Ayoub, 2009). Studies on the trabecular structure in the sacrum are deemed important in the management of fixation procedures applied in surgical applications in the region (Mahato, 2010c), as the complex anatomy of the sacrum with variability of its bony quality often ruining the screw placement during clinical management (Xu *et al*, 1995; Ebraheim *et al*, 2000). Of course, the selection of the best method and route for screw insertion and plate fixation still depends on the type and degree of the fractures based on Denis's classification of sacral fractures (Denis *et al*, 1988), and the approach of the internal fixation, either anterior or posterior.

Conclusion

The results of this research demonstrate that the sacrum exhibits an early pattern of trabecular bone morphology which is maintained into childhood, demonstrating that the sacrum is both phylogenetically and ontogenetically stable. The qualitative and quantitative analyses demonstrated that the sacral ala has a trabecular signature that is characterised by a low bone volume fraction which is a reflection of trabecular that are thin, sparsely distributed and low in number. This suggests that this region of the sacrum is not designed for the purposes of weight transfer which is contrary to previous belief. Instead, the data suggests that the loads which are being transmitted from the lumbar vertebral column are distributed through the sacrum via a number of pathways, with minimal involvement of the sacroiliac joint, before reaching the innominate. This

is demonstrated by signatures of advanced trabecular bone patterning in areas surrounding the sacral ala, indicating that load is being distributed predominantly through the post-auricular region towards the pelvis. This is also supported by analysis of the regional iliac surface areas which showed advanced growth of the post-auricular region compared to the auricular region. It is hoped that this study will act as a catalyst for future work to explore and discover the complex nature of weight-bearing force distribution at the posterior pelvic region, where the important sacroiliac joint complex is located.

Suggestion of future work

Although the growth of the juvenile sacrum was studied in this thesis, much more should be explored in terms of trabecular arrangement in the non-weight bearing fetal and perinatal sacra. However, the unfused individual sacral elements in the perinatal age group that appeared as ossified nodules (Scheuer and Black, 2000) were almost impossible to identify according to their anatomical position, impeding the assignment of similar and repetitive VOI throughout the specimens.

Apart from this 3D reconstructive analysis of the juvenile S1 vertebra, other methods such as finite element analysis (FEA) of studying the trabecular pattern should also be utilised to support or provide a new theory for one of the less frequently researched parts of the human body. Musculoskeletal modelling studies would ascertain the lines of action and magnitude of joint, muscle and ligament forces acting on the sacrum. This would support meaningful FEA studies linking gait development to trabecular bone structure via strain distribution.

Additionally, further work should be undertaken on the analysis of the cortical bone of the S1 vertebra to obtain a complete picture of the cortical-trabecular network

organisation in this region. It is also suggested that biomechanical testing directly on the bone to study the route of the weight transfer directly is undertaken. The study on the S1 vertebra of quadrupedal animal would provide a comparison and supplement to this study.

REFERENCE

Abel, R. & Macho, G. A. 2011. Ontogenetic changes in the internal and external morphology of the ilium in modern humans. *Journal of Anatomy,* 218**,** 324-335.

Abitbol, M. M. 1987. Evolution of the sacrum in hominoids. *American Journal of Physical Anthropology,* 74**,** 65-81.

Abramoff, M. D., Magelhaes, P. J. & Ram, S. J. 2004. Image Processing with ImageJ. *Biophotonics International,* 11**,** 36-42.

Adolph, K. E., Vereijken, B. & Denny, M. A. 1998. Learning to crawl. *Child Development,* 69**,** 1299-1312.
Abel, R. & Macho, G. A. 2011. Ontogenetic changes in the internal and external morphology of the ilium in modern humans. *Journal of Anatomy,* 218**,** 324-335.

Abitbol, M. M. 1987. Evolution of the sacrum in hominoids. *American Journal of Physical Anthropology,* 74**,** 65-81.

Abramoff, M. D., Magelhaes, P. J. & Ram, S. J. 2004. Image Processing with ImageJ. *Biophotonics International,* 11**,** 36-42.

Adolph, K. E., Vereijken, B. & Denny, M. A. 1998. Learning to crawl. *Child Development,* 69**,** 1299-1312.

Aiello, L., Dean, C. & Cameron, J. 1990. *An Introduction to Human Evolutionary Anatomy,* Elsevier Science.

Albee, F. H. 1909. A study of the anatomy and the clinical importance of the sacroiliac joint. *Journal of the American Medical Association,* LIII**,** 1273-1276.

Albert, H., Godskesen, M., Westergaard, J. G., Chard, T. & Gunn, L. 1997. Circulating levels of relaxin are normal in pregnant women with pelvic pain. *European Journal of Obstetrics & Gynecology and Reproductive Biology,* 74**,** 19-22.

Albright, J. A. & Skinner, H. C. W. 1987. Bone: structural organization and remodeling dynamics. *The Scientific basis of Orthopaedics,* 2**,** 161-198.

Alderink, G. J. 1991. The sacroiliac joint: review of anatomy, mechanics, and function. *The Journal of Orthopaedic and Sports Physical Therapy,* 13**,** 71-84.

Alexander, T., Nolte, C. & Krumlauf, R. 2009. Hox genes and segmentation of the hindbrain and axial skeleton. *Annual Review of Cell and Developmental Biology,* 25**,** 431-56.

Ali, R. S. & Maclaughlin, S. M. 1991. Sex identification from the auricular surface of the adult human ilium. *International Journal of Osteoarchaeology,* 1**,** 57-61.

Anderson, A. E., Peters, C. L., Tuttle, B. D. & Weiss, J. A. 2005. Subject-specific finite element model of the pelvis: development, validation and sensitivity studies.

Transactions of the ASME-K-Journal of Biomechanical Engineering, 127**,** 364-373.

Archer, C. W., Dowthwaite, G. P. & Francis-West, P. 2003. Development of synovial joints. *Birth Defects Research Part C: Embryo Today: Reviews,* 69**,** 144-155.

Aubin, J. E. & Bonnelye, E. 2000. Osteoprotegerin and its ligand: a new paradigm for regulation of osteoclastogenesis and bone resorption. *Osteoporosis International,* 11**,** 905-913.

Ayoub, M.A. 2009. Vertically unstable sacral fractures with neurological insult: outcomes of surgical decompression and reconstruction plate internal fixation. *International Orthopaedics,* 33, 261-269.

Baker, B. J., Dupras, T. L. & Tocheri, M. W. 2005. *The Osteology of Infants and Children*, Texas A&M University Press.

Baker, P. & Kenny, L. C. 2011. *Obstetrics by Ten Teachers*, Hodder Arnold Publishers.

Banse, X., Devogelaer, J. P. & Grynpas, M. 2002. Patient-specific microarchitecture of vertebral cancellous bone: a peripheral quantitative computed tomographic and histological study. *Bone,* 30**,** 829-835.

Baptist, M., Sultana, F. & Farzana, F. 2008. Sex differences in sacra in the Punjab region. *Biomedica,* 24.

Başaloğlu, H., Turgut, M., Taşer, F. A., Ceylan, T., Başaloğlu, H. K. & Ceylan, A. A. 2005. Morphometry of the sacrum for clinical use. *Surgical and Radiologic Anatomy,* 27**,** 467-471.

Bass, W. M. 1987. *Human Osteology: A Laboratory and Field Manual*, Missouri Archaeological Society.

Bassett, J. H. D. & Williams, G. R. 2008. Critical role of the hypothalamic–pituitary–thyroid axis in bone. *Bone,* 43**,** 418-426.

Bassett, R. W., Browne, A. O., Morrey, B. F. & An, K. N. 1990. Glenohumeral muscle force and moment mechanics in a position of shoulder instability. *Journal of Biomechanics,* 23**,** 405-415.

Beaupied, H., Chappard, C., Basillais, A., Lespessailles, E. & Benhamou, C. L. 2006. Effect of specimen conditioning on the microarchitectural parameters of trabecular bone assessed by micro-computed tomography. *Physics in Medicine and Biology,* 51**,** 4621-34.

Beaupré, G. S., Orr, T. E. & Carter, D. R. 1990. An approach for time-dependent bone modeling and remodeling—theoretical development. *Journal of Orthopaedic Research,* 8**,** 651-661.

Bellamy, N., Park, W. & Rooney, P. J. 1983. What do we know about the sacroiliac joint? *Seminars in Arthritis and Rheumatism,* 12**,** 282-313.

Bigliani, L. U., Pollock, R. G., Soslowsky, L. J., Flatow, E. L., Pawluk, R. J. & Mow, V. C. 1992. Tensile properties of the inferior glenohumeral ligament. *Journal of Orthopaedic Research,* 10**,** 187-197.

Bilezikian, J. P. 1996. *Principles of Bone Biology,* California, Academic Press.

Birrer, R. B., Griesemer, B. & Cataletto, M. B. 2002. *Pediatric Sports Medicine for Primary Care,* Lippincott Williams & Wilkins.

Blake, K. A. S. 2011. *An investigation of sex determination from the subadult pelvis: A morphometric analysis.* PhD Dissertation, , University of Pittsburgh.

Blickman, J. G., Parker, B. R. & Barnes, P. D. 2009. *Pediatric Radiology: The Requisites*, Mosby/Elsevier.

Bogduk, N. 2005. *Clinical Anatomy of the Lumbar Spine and Sacrum,* Elsevier/Churchill Livingstone.

Bowen, V. & Cassidy, J. D. 1981. Macroscopic and microscopic anatomy of the sacroiliac joint from embryonic life until the eighth decade. *Spine,* 6**,** 620-628.

Brooke, R. 1924. The sacro-iliac joint. *Journal of Anatomy,* 58**,** 299.

Broome, D. R., Hayman, L. A., Herrick, R. C., Braverman, R. M., Glass, R. B. & Fahr, L. M. 1998. Postnatal maturation of the sacrum and coccyx: MR imaging, helical CT, and conventional radiography. *American Journal of Roentgenology,* 170**,** 1061-6.

Brothwell, D. R. 1981. *Digging Up Bones: The Excavation, Treatment, and Study of Human Skeletal Remains,* New York, Cornell University Press.

Buckberry, J. L. & Chamberlain, A. T. 2002. Age estimation from the auricular surface of the ilium: A revised method. *American Journal of Physical Anthropology,* 119**,** 231-239.

Burghardt, A. J., Link, T. M. & Majumdar, S. 2011. High-resolution computed tomography for clinical imaging of bone microarchitecture. *Clinical Orthopaedic and Related Research,* 469**,** 2179-93.

Caldwell, W. E. & Moloy, H. C. 1938. Anatomical variations in the female pelvis: their classification and obstetrical significance: (Section of Obstetrics and Gynaecology). *Proceeding of the Royal Society of Medicine,* 32**,** 1-30.

Calguneri, M., Bird, H. A. & Wright, V. 1982. Changes in joint laxity occurring during pregnancy. *Annals of the Rheumatic Diseases,* 41**,** 126-128.

Carlson, G., Abitbol, J., Anderson, D., Krag, M., Kostuik, J., Woo, S.-Y. & Garfin, S. 1992. Screw fixation in the human sacrum: an in vitro study of the biomechanics of fixation. *Spine,* 17**,** S196-S203.

Carruth, B. R. & Skinner, J. D. 2002. Feeding behaviors and other motor development in healthy children (2-24 months). *Journal of American College of Nutrition,* 21**,** 88-96.

Carter, M. E. & Loewi, G. 1962. Anatomical changes in normal sacro-iliac joints during childhood and comparison with the changes in Still's disease. *Annals of the Rheumatic Diseases,* 21**,** 121-34.

Chappard, D., Retailleau-Gaborit, N., Legrand, E., Baslé, M. F. & AudraN, M. 2005. Comparison Insight Bone Measurements by Histomorphometry and μCT. *Journal of Bone and Mineral Research,* 20**,** 1177-1184.

Cibulka, M. T. 1992. The treatment of the sacroiliac joint component to low back pain: a case report. *Physical Therapy,* 72**,** 917-922.

Cleaves, E. N. 1937. Adolescent sacro-iliac joints: their normal development and their appearance in epiphysitis. *The American Journal of Roentgenology.,* 38**,** 450-456.

Cohen, S. P. 2005. Sacroiliac joint pain: a comprehensive review of anatomy, diagnosis and treatment. *Anesthesia & Analgesia,* 101**,** 1440-1453.

Cole, T. J. 2003. The secular trend in human physical growth: a biological view. *Economics & Human Biology,* 1**,** 161-168.

Cook, R. E., Keating, J. F. & Gillespie, I. 2002. The role of angiography in the management of haemorrhage from major fractures of the pelvis. *Journal of Bone & Joint Surgery, British Volume,* 84-B**,** 178-182.

Cramer, G. D. & Darby, S. A. 2013. *Clinical Anatomy of the Spine, Spinal Cord, and ANS,* Elsevier Health Sciences.

Cunningham, C. A. & Black, S. M. 2009a. Anticipating bipedalism: trabecular organization in the newborn ilium. *Journal of Anatomy,* 214**,** 817-829.

Cunningham, C. A. & Black, S. M. 2009b. Development of the fetal ilium – challenging concepts of bipedality. *Journal of Anatomy,* 214**,** 91-99.

Cunningham, C. A. & Black, S. M. 2009c. Iliac cortical thickness in the neonate – the gradient effect. *Journal of Anatomy,* 215**,** 364-370.

Cunningham, C. A. & Black, S. M. 2010. The neonatal ilium—metaphyseal drivers and vascular passengers. *The Anatomical Record: Advances in Integrative Anatomy and Evolutionary Biology,* 293**,** 1297-1309.

Cunningham, C. A. & Black, S. M. 2013. The vascular collar of the ilium— three-dimensional evaluation of the dominant nutrient foramen. *Clinical Anatomy,* 26**,** 502-508.

Currey, J. 2003. Role of collagen and other organics in the mechanical properties of bone. *Osteoporosis International,* 14**,** 29.

Currey, J. D. 2002. *Bones: Structure and Mechanics,* Princeton University Press.

Dai, L. Y. 2001. Orientation and tropism of lumbar facet joints in degenerative spondylolisthesis. *International Orthopaedics,* 25**,** 40-42.

Dalinka, M. K., Arger, P. & Coleman, B. 1985. CT in pelvic trauma. *The Orthopedic Clinics of North America,* 16**,** 471-480.

Dalstra, M. & Huiskes, R. 1995. Load transfer across the pelvic bone. *Journal of Biomechanics,* 28**,** 715-724.

Dalstra, M., Huiskes, R., Odgaard, A. & Van Erning, L. 1993. Mechanical and textural properties of pelvic trabecular bone. *Journal of Biomechanics,* 26**,** 523-535.

Davidson, R. A. & Bowman, S. 2002. Macroradiography using conventional radiographic X-ray equipment. *British Journal of Radiology,* 75**,** 831-836.

Davis, P. R. 1961. Human lower lumbar vertebrae: some mechanical and osteological considerations. *Journal of Anatomy,* 95**,** 337-44.

Delaere, O. & Dhem, A. 1999. Prenatal development of the human pelvis and acetabulum. *Acta Orthopaedica Belgica,* 65**,** 255-60.

Delaere, O., Kok, V., Nyssen-Behets, C. & Dhem, A. 1992. Ossification of the human fetal ilium. *Cells Tissues Organs,* 143**,** 330-334.

Dempster, D. W., Ferguson-Pell, M. W., Mellish, R. W. E., Cochran, G. V. B., Xie, F., Fey, C., Horbert, W., Parisien, M. & Lindsay, R. 1993. Relationships between bone structure in the iliac crest and bone structure and strength in the lumbar spine. *Osteoporosis International,* 3**,** 90-96.

Denis, F., Davis, S. & Comfort, T. 1988. Sacral fractures: an important problem retrospective analysis of 236 cases. *Clinical Orthopaedics and Related Research,* 227**,** 67-81.

Ding, M. 2000. Age variations in the properties of human tibial trabecular bone and cartilage. *Acta Orthopaedica Scandinavica Supplement,* 292**,** 1-45.

Ding, M. & Hvid, I. 2000. Quantification of age-related changes in the structure model type and trabecular thickness of human tibial cancellous bone. *Bone,* 26**,** 291-295.

Ding, M., Odgaard, A., Danielsen, C. C. & Hvid, I. 2002. Mutual associations among microstructural, physical and mechanical properties of human cancellous bone. *Journal of Bone & Joint Surgery, British Volume,* 84-B**,** 900-907.

Ding, M., Odgaard, A. & HviD, I. 1999. Accuracy of cancellous bone volume fraction measured by micro-CT scanning. *Journal of Biomechanics,* 32**,** 323-326.

Dontigny, R. L. 1985. Function and pathomechanics of the sacroiliac joint. A review. *Physical Therapy,* 65**,** 35-44.

Dontigny, R. L. 1993. Mechanics and treatment of the sacroiliac joint. *Journal of Manual & Manipulative Therapy,* 1**,** 3-12.

Doube, M., Klosowski, M. M., Wiktorowicz-Conroy, A. M., Hutchinson, J. R. & Shefelbine, S. J. 2011. Trabecular bone scales allometrically in mammals and birds. *Proceeding of Biological Science,* 278**,** 3067-73.

Drake, R., Vogl, W. & Mitchell, A. 2005. *Gray's Anatomy for Students: Deluxe,* Elsevier Science Health Science Division.

Drews, S., Matsuura, M. & Putz, R. 2008. The trabecular architecture of the superior articular process of the lumbar spine (L2–S1). *Surgical and Radiologic Anatomy,* 30**,** 209-213.

Ebraheim, N., Sabry, F. F., Nadim, Y., Xu, R. & Yeasting, R. A. 2000. Internal architecture of the sacrum in the elderly: an anatomic and radiographic study. *Spine,* 25**,** 292-297.

Ehara, S., El-Khoury, G. Y. & Bergman, R. A. 1988. The accessory sacroiliac joint: a common anatomic variant. *AJR American Journal of Roentgenology,* 150**,** 857-9.

Einhorn, T. 1996. Biomechanics of bone. *Principles of Bone Biology. Academic Press,* San Diego**,** 25-37.

Esses, S. I., Bostford, D. J., Huler, R. J. & Rauschning, W. 1991. Surgical anatomy of the sacrum: a guide for rational screw fixation. *Spine,* 16**,** S283-S288.

Fajardo, R. J. & Müller, R. 2001. Three-dimensional analysis of nonhuman primate trabecular architecture using micro-computed tomography. *American Journal of Physical Anthropology,* 115**,** 327-336.

Fajardo, R. J., Müller, R., Ketcham, R. A. & Colbert, M. 2007. Nonhuman anthropoid primate femoral neck trabecular architecture and its relationship to locomotor mode. *The Anatomical Record: Advances in Integrative Anatomy and Evolutionary Biology,* 290**,** 422-436.

Fazekas, I. & Kosa, F. 1978. Forensic fetal osteology. *Akadémiai Kaidó, Budapest*.

Finnegan, M. 1978. Non-metric variation of the infracranial skeleton. *Journal of Anatomy,* 125**,** 23-37.

Flander, L. B. 1978. Univariate and multivariate methods for sexing the sacrum. *American Journal of Physical Anthropology,* 49**,** 103-110.

Forssberg, H. 1985. Ontogeny of human locomotor control I. Infant stepping, supported locomotion and transition to independent locomotion. *Experimental Brain Research,* 57**,** 480-493.

Forst, S. L., Wheeler, M. T., Fortin, J. D. & Vilensky, J. A. 2006. The sacroiliac joint: anatomy, physiology and clinical significance. *Pain Physician,* 9**,** 61-7.

Forwood, M. R. 2008. Physical activity and bone development during childhood: insights from animal models. *Journal of Applied Physiology,* 105**,** 334-341.

Forwood, M. R. & Burr, D. B. 1993. Physical activity and bone mass: exercises in futility? *Bone and Mineral,* 21**,** 89-112.

Francis, C. C. 1951. Appearance of centers of ossification in the human pelvis before birth. *The American Journal of Roentgenology, Radium Therapy, and Nuclear Medicine,* 65**,** 778-783.

Frazer, J. E. S. 1965. *Frazer's Anatomy of the Human Skeleton,* London, Churchill.

Frost, H. M. 1987. Bone "mass" and the "mechanostat": A proposal. *The Anatomical Record,* 219**,** 1-9.

Frost, H. M. 1990. Skeletal structural adaptations to mechanical usage (SATMU): 1. Redefining Wolff's Law: The bone modeling problem. *The Anatomical Record,* 226**,** 403-413.

Frost, H. M. 1996. Perspectives: A proposed general model of the "mechanostat" (suggestions from a new skeletal-biologic paradigm). *The Anatomical Record,* 244**,** 139-147.

Frost, H. M. 2004. A 2003 Update of bone physiology and Wolff's law for clinicians. *The Angle Orthodontist,* 74**,** 3-15.

Genant, H. K., Engelke, K. & Prevrhal, S. 2008. Advanced CT bone imaging in osteoporosis. *Rheumatology,* 47**,** iv9-iv16.

Genant, H. K. & Jiang, Y. 2006. Advanced imaging assessment of bone quality. *Annals of the New York Academy of Sciences,* 1068**,** 410-428.

Gerlach, U. J. & Lierse, W. 1992. Functional construction of the sacroiliac ligamentous apparatus. *Acta Anatomica,* 144**,** 97-102.

Giannoudis, P. V., Grotz, M. R. W., Tzioupis, C., Dinopoulos, H., Wells, G. E., Bouamra, O. & Lecky, F. 2007. Prevalence of Pelvic Fractures, Associated Injuries, and Mortality: The United Kingdom Perspective. *Journal of Trauma-Injury, Infection, and Critical Care,* 63**,** 875-883 10.1097/01.ta.0000242259.67486.15.

Gillespie, P. 2009. Pelvic fracture. *Surgery (Oxford),* 27**,** 292-296.

Goldstein, S., Goulet, R. & Mccubbrey, D. 1993. Measurement and significance of three-dimensional architecture to the mechanical integrity of trabecular bone. *Calcified Tissue International,* 53**,** S127-S133.

Goldstein, S. A. 1987. The mechanical properties of trabecular bone: dependence on anatomic location and function. *Journal of Biomechanics,* 20**,** 1055-1061.

Goldstein, S. A., Wilson, D. L., Sonstegard, D. A. & Matthews, L. S. 1983. The mechanical properties of human tibial trabecular bone as a function of metaphyseal location. *Journal of Biomechanics,* 16**,** 965-969.

Gosman, J. H. & Ketcham, R. A. 2009. Patterns in ontogeny of human trabecular bone from SunWatch Village in the Prehistoric Ohio Valley: General features of microarchitectural change. *American Journal of Physical Anthropology,* 138**,** 318-332.

Greulich, W. W. & Thoms, H. 1944. The growth and development of the pelvis of individual girls before, during, and after puberty. *The Yale Journal of Biology and Medicine,* 17**,** 91.

Gribnau, A. J., Van Hensbroek, P. B., Haverlag, R., Ponsen, K. J., Been, H. D. & Goslings, J. C. 2009. U-shaped sacral fractures: surgical treatment and quality of life. *Injury,* 40**,** 1040-8.

Guo, X., Day, T. F., Jiang, X., Garrett-Beal, L., Topol, L. & Yang, Y. 2004. Wnt/beta-catenin signaling is sufficient and necessary for synovial joint formation. *Genes and Development,* 18**,** 2404-17.

Hagan, D. M., Ross, A. J., Strachan, T., Lynch, S. A., Ruiz-Perez, V., Wang, Y. M., Scambler, P., Custard, E., Reardon, W., Hassan, S., Nixon, P., Papapetrou, C., Winter, R. M., Edwards, Y., Morrison, K., Barrow, M., Cordier-Alex, M. P., Correia, P., Galvin-Parton, P. A., Gaskill, S., Gaskin, K. J., Garcia-Minaur, S., Gereige, R., Hayward, R. & Homfray, T. 2000. Mutation analysis and embryonic expression of the HLXB9 Currarino syndrome gene. *American Journal of Human Genetics,* 66**,** 1504-15.

Handy, W. R. 1854. *A Text Book of Anatomy, and Guide in Dissections: For the Use of Students of Medicine and Dental Surgery,* Lindsay & Blakiston.

Harrigan, T. & Mann, R. 1984. Characterization of microstructural anisotropy in orthotropic materials using a second rank tensor. *Journal of Materials Science,* 19**,** 761-767.

Harrison, T. J. 1958. The growth of the pelvis in the rat; a mensural and morphological study. *Journal of Anatomy,* 92**,** 236-60.

Hart, D. J., Wang, M. Y., Griffith, P. & Gordon Mccomb, J. 1976. Pediatric sacral fractures. *Spine,* 29**,** 667-70.

Hartmann, C. & Tabin, C. J. 2001. Wnt-14 plays a pivotal role in inducing synovial joint formation in the developing appendicular skeleton. *Cell,* 104**,** 341-351.

Hildebrand, T., Laib, A., Müller, R., Dequeker, J. & Rüegsegger, P. 1999. Direct three-dimensional morphometric analysis of human cancellous bone: microstructural

data from spine, femur, iliac crest, and calcaneus. *Journal of Bone and Mineral Research,* 14**,** 1167-1174.

Hildebrand, T. & Rüegsegger, P. 1997a. A new method for the model-independent assessment of thickness in three-dimensional images. *Journal of Microscopy,* 185**,** 67-75.

Hildebrand, T. O. R. & Rüegsegger, P. 1997b. Quantification of bone microarchitecture with the structure model index. *Computer Methods in Biomechanics and Biomedical Engineering,* 1**,** 15-23.

Hofbauer, L. C., Khosla, S., Dunstan, C. R., Lacey, D. L., Boyle, W. J. & Riggs, B. L. 2000. The roles of osteoprotegerin and osteoprotegerin ligand in the paracrine regulation of bone resorption. *Journal Of Bone And Mineral Research,* 15**,** 2-12.

Hofer, M. 2007. *CT Teaching Manual: A Systematic Approach To CT Reading,* Thieme.

Hoppa, R. D. 1992. Evaluating human skeletal growth: an anglo-saxon example. *International Journal of Osteoarchaeology,* 2**,** 275-288.

Houghton, P. 1974. The relationship of the pre-auricular groove of the llium to pregnancy. *American Journal of Physical Anthropology,* 41**,** 381-389.

Huang, R., Zhi, Q., Brand-Saberi, B. & Christ, B. 2000. New experimental evidence for somite resegmentation. *Anatomy and Embryology,* 202**,** 195-200.

Hughes, J. & Petit, M. 2010. Biological underpinnings of Frost's mechanostat thresholds: the important role of osteocytes. *Journal of Musculoskeletal and Neuronal Interaction,* 10**,** 128-135.

Huiskes, R. 2000. If bone is the answer, then what is the question? *Journal of Anatomy,* 197**,** 145-156.

Igarashi, Y., Uesu, K., Wakebe, T. & Kanazawa, E. 2005. New method for estimation of adult skeletal age at death from the morphology of the auricular surface of the ilium. *American Journal of Physical Anthropology,* 128**,** 324-339.

Inman, V. T., Ralston, H. J. & Todd, F. 1981. *Human Walking,* Williams & Wilkins.

Iuliano-Burns, S., Hopper, J. & Seeman, E. 2009. The age of puberty determines sexual dimorphism in bone structure: a male/female co-twin control study. *Journal of Clinical Endocrinology and Metabolism,* 94**,** 1638-43.

Ivarsson, J., Okamoto, M. & Takahashi, Y. 2013. Experimental injury biomechanics of the pediatric extremities and pelvis. *In:* Crandall, J. R., Myers, B. S., Meaney, D. F. & Zellers Schmidtke, S. (eds.) *Pediatric Injury Biomechanics.* Springer New York.

Jamieson, D. J. M. M. & STEEGE, J. F. M. 1996. The Prevalence of Dysmenorrhea, Dyspareunia, Pelvic Pain, and Irritable Bowel Syndrome in Primary Care Practices. *Obstetrics & Gynecology,* 87**,** 55-58.

Jang, I. G. & Kim, I. Y. 2008. Computational study of Wolff's law with trabecular architecture in the human proximal femur using topology optimization. *Journal of Biomechanics,* 41**,** 2353-2361.

Jaovisidha, S., Ryu, K. N., De Maeseneer, M., Haghighi, P., Goodwin, D., Sartoris, D. J. & Resnick, D. 1996. Ventral sacroiliac ligament. Anatomic and pathologic considerations. *Investigative Radiology,* 31**,** 532-41.

Ji, B. & Gao, H. 2004. Mechanical properties of nanostructure of biological materials. *Journal of the Mechanics and Physics of Solids,* 52**,** 1963-1990.

Jiang, Y., Zhao, J., White, D. & Genant, H. 2000. Micro CT and micro MR imaging of 3D architecture of animal skeleton. *Journal of Musculoskeletal and Neuronal Interaction,* 1**,** 45-51.

Johnson, R. L. & Tabin, C. J. 1997. Molecular models for vertebrate limb development. *Cell,* 90**,** 979-90.

Kampen, W. U. & Tillmann, B. 1998. Age-related changes in the articular cartilage of human sacroiliac joint. *Anatomy and Embryology,* 198**,** 505-513.

Kapandji, I. A. 1974. *The Physiology of the Joints: Annotated Diagrams of the Mechanics of the Human Joints,* Churchill Livingstone.

Karageanes, S. J. 2005. *Principles of Manual Sports Medicine,* Lippincott Williams & Wilkins.

Keaveny, T. M., Morgan, E. F., Niebur, G. L. & Yeh, O. C. 2001. Biomechanics of trabecular bone. *Annual Review of Biomedical Engineering,* 3**,** 307-333.

Keen, M. 1993. Early development and attainment of normal mature gait. *JPO: Journal of Prosthetics and Orthotics,* 5**,** 35/23-26/38.

Khan, I. M., Redman, S. N., Williams, R., Dowthwaite, G. P., Oldfield, S. F. & Archer, C. W. 2007. The development of synovial joints. *Current Topics in Developmental Biology,* 79**,** 1-36.

Koyama, E., Ochiai, T., Rountree, R. B., Kingsley, D. M., Enomoto-Iwamoto, M., Iwamoto, M. & Pacifici, M. 2007. Synovial joint formation during mouse limb skeletogenesis: roles of Indian hedgehog signaling. *Annals of the New York Academy of Sciences***,** 100-12.

Kristiansson, P., Svärdsudd, K. & Von Schoultz, B. 1996. Serum relaxin, symphyseal pain, and back pain during pregnancy. *American Journal of Obstetrics and Gynecology,* 175**,** 1342-1347.

Kubo, M. & Ulrich, B. D. 2006. Early Stage of Walking: Development of control in mediolateral and anteroposterior directions. *Journal of Motor Behavior,* 38**,** 229-237.

Lai, Y. M., Qin, L., Yeung, H. Y., Lee, K. K. H. & Chan, K. M. 2005. Regional differences in trabecular BMD and micro-architecture of weight-bearing bone under habitual gait loading—A pQCT and microCT study in human cadavers. *Bone,* 37**,** 274-282.

Lanham, S., Roberts, C., Hollingworth, T., Sreekumar, R., Elahi, M., Cagampang, F., Hanson, M. A. & Oreffo, R. O. 2010. Maternal high-fat diet: effects on offspring bone structure. *Osteoporosis International,* 21**,** 1703-1714.

Lanyon, L. & Skerry, T. 2001. Perspective: postmenopausal osteoporosis as a failure of bone's adaptation to functional loading: a hypothesis. *Journal of Bone and Mineral Research,* 16**,** 1937-1947.

Lanyon, L. E. 1974. Experimental support for the trajectorial theory of bone structure. *Journal of Bone & Joint Surgery, British Volume,* 56-B**,** 160-166.

Lanyon, L. E. 1993. Osteocytes, strain detection, bone modeling and remodeling. *Calcified Tissue International,* 53**,** S102-S107.

Lanyon, L. E., Goodship, A. E., Pye, C. & Macfie, J. 1982. Mechanically adaptive bone remodelling. *Journal of Biomechanics,* 15**,** 141-154.

Laslett, M., Aprill, C. N., Mcdonald, B. & Young, S. B. 2005. Diagnosis of Sacroiliac Joint Pain: Validity of individual provocation tests and composites of tests. *Manual Therapy,* 10**,** 207-218.

Last, R. J. 1978. *Anatomy, Regional and Applied / R.J. Last,* Edinburgh ; New York : New York, Churchill Livingstone ; distributed by Longman.

Laurenson, R. D. 1964. The primary ossification of the human ilium. *The Anatomical Record,* 148**,** 209-217.

Lee, T. C. & Taylor, D. 1999. Bone remodelling: Should we cry wolff? *Irish Journal of Medical Science,* 168**,** 102-105.

Leong, J. C., Lu, W. W., Zheng, Y., Zhu, Q. & Zhong, S. 1998. Comparison of the strengths of lumbosacral fixation achieved with techniques using one and two triangulated sacral screws. *Spine,* 23**,** 2289-94.

LeVeau, B. F. & Bernhardt, D. B. 1984. Effect of forces on the growth, development, and maintenance of the human body. *Physical Therapy,* 64, 1874-1882.

Lindahl, O. 1976. Mechanical properties of dried defatted spongy bone. *Acta Orthopaedica,* 47**,** 11-19.

Lombardi, G., Di Somma, C., Rubino, M., Faggiano, A., Vuolo, L., Guerra, E., Contaldi, P., Savastano, S. & Colao, A. 2011. The roles of parathyroid hormone in bone remodeling: prospects for novel therapeutics. *Journal of Endocrinological Investigation,* 34**,** 18-22.

Lovejoy, C. O. 1988. Evolution of human walking. *Scientific American,* 259**,** 82-89.

Lovejoy, C. O., Meindl, R. S., Pryzbeck, T. R. & Mensforth, R. P. 1985. Chronological metamorphosis of the auricular surface of the ilium: a new method for the determination of adult skeletal age at death. *American Journal of Physical Anthropology,* 68**,** 15-28.

Macdonald, G. R. & Hunt, T. E. 1952. Sacroiliac joints; observations on the gross and histological changes in the various age groups. *Canadian Medical Association Journal,* 66**,** 157-63.

MacLester, J & St. Pierre, P. 2008. A*pplied biomechanics: Concepts and connections: Concepts and Connections,* Cengage Learning.

Magee, D. J. 2008. *Orthopedic Physical Assessment,* Saunders Elsevier.

Mahato, N. K. 2010a. Morphometric analysis and identification of characteristic features in sacra bearing accessory articulations with L5 vertebrae. *The Spine Journal,* 10**,** 616-621.

Mahato, N. K. 2010b. Association of rudimentary sacral zygapophyseal facets and accessory and ligamentous articulations: implications for load transmission at the L5-S1 junction. *Clinical Anatomy,* 23**,** 707-711.

Mahato, N. K. 2010c. Trabecular architecture in human sacra: patterns observed in complete sacralisation and accessory articulation with the fifth lumbar vertebrae. *Journal of Morphological Sciences,* 27**,** 19-22.

Mahato, N. K. 2011. Relationship of sacral articular surfaces and gender with occurrence of lumbosacral transitional vertebrae. *The Spine Journal,* 11**,** 961-965.

Mahato, N. K. 2013. Trabecular bone structure in lumbosacral transitional vertebrae: distribution and densities across sagittal vertebral body segments. *The Spine Journal*.

Majumdar, S., Genant, H., Grampp, S., Newitt, D., Truong, V. H., Lin, J. & Mathur, A. 1997. Correlation of trabecular bone structure with age, bone mineral density, and osteoporotic status: in vivo studies in the distal radius using high resolution magnetic resonance imaging. *Journal of Bone and Mineral Research,* 12**,** 111-118.

Malashichev, Y., Christ, B. & Pröls, F. 2008. Avian pelvis originates from lateral plate mesoderm and its development requires signals from both ectoderm and paraxial mesoderm. *Cell and Tissue Research,* 331**,** 595-604.

Manolagas, S. C. 2000. Birth and Death of Bone Cells: Basic Regulatory Mechanisms and Implications for the Pathogenesis and Treatment of Osteoporosis. *Endocrine Reviews,* 21**,** 115-137.

Marcus, R., Feldman, D., Nelson, D. & Rosen, C. J. 2009. *Fundamentals of Osteoporosis,* Elsevier Science.

Martin, J. P. & Hurwitz, L. 1962. Locomotion and the basal ganglia. *Brain,* 85**,** 261-276.

Martini, F., Ober, W. C. & Welch, K. 2006. *Fundamentals of Anatomy and Physiology,* Pearson Education Canada.

Mathias, S. D., Kuppermann, M., Liberman, R. F., Lipschutz, R. C. & Steege, J. F. 1996. Chronic pelvic pain: prevalence, health-related quality of life, and economic correlates. *Obstetrics & Gynecology,* 87**,** 321-327.

Mcauley, J. P. & Uhthoff, H. K. 1990. The Development of the Pelvis. *The Embryology of the Human Locomotor System.* Springer Berlin Heidelberg.

Mccoll, D. J., Abel, R. L., Spears, I. R. & Macho, G. A. 2006. Automated method to measure trabecular thickness from microcomputed tomographic scans and its application. *The Anatomical Record Part A: Discoveries in Molecular, Cellular, and Evolutionary Biology,* 288A**,** 982-988.

Mcgrath, C., Nicholson, H. & Hurst, P. 2009. The long posterior sacroiliac ligament: A histological study of morphological relations in the posterior sacroiliac region. *Joint Bone Spine,* 76**,** 57-62.

Migeon, S., Weber, O., Faugeres, J. C. & Saint-Paul, J. 1999. Scopix: A new X-ray imaging system for core analysis. *Geo-Marine Letters,* 18**,** 251-255.

Mishra, S., Singh, P., Agrawal, A. & Gupta, R. 2003. Identification of sex of sacrum of Agra region. *Journal of Anatomical Society of India,* 52**,** 132-136.

Mittler, D. M. & Sheridan, S. G. 1992. Sex determination in subadults using auricular surface morphology: a forensic science perspective. *Journal of Forensic Science,* 37**,** 1068-75.

Moore, K. L., Dalley, A. F. & Agur, A. M. R. 2013. *Clinically Oriented Anatomy,* Wolters Kluwer Health.

Moore, K. L., Persaud, T. V. N. & Torchia, M. G. 2011. *The Developing Human: with STUDENT CONSULT Online Access,* Elsevier Health Sciences.

Mulder, L., Koolstra, J. H., Den Toonder, J. M. J. & Van Eijden, T. M. G. J. 2007. Intratrabecular distribution of tissue stiffness and mineralization in developing trabecular bone. *Bone,* 41**,** 256-265.

Mulhern, D. M. & Jones, E. B. 2005. Test of revised method of age estimation from the auricular surface of the ilium. *American Journal of Physical Anthropology,* 126**,** 61-65.

Müller, R., Koller, B., Hildebrand, T., Laib, A., Gianolini, S. & Rüegsegger, P. 1996. Resolution dependency of microstructural properties of cancellous bone based on three-dimensional μ-tomography. *Technology and Health Care,* 4**,** 113-119.

Mundlos, S. & Olsen, B. R. 1997. Heritable diseases of the skeleton. Part I: Molecular insights into skeletal development-transcription factors and signaling pathways. *The FASEB Journal,* 11**,** 125-32.

Murray, P. D. F. & Drachman, D. B. 1969. The role of movement in the development of joints and related structures: the head and neck in the chick embryo. *Journal of Embryology and Experimental Morphology,* 22**,** 349-371.

Nicholson, P., Müller, R., Cheng, X., Rüegsegger, P., Van Der Perre, G., Dequeker, J. & Boonen, S. 2001. Quantitative Ultrasound and Trabecular Architecture in the Human Calcaneus. *Journal of Bone and Mineral Research,* 16**,** 1886-1892.

Nordin, M. & Frankel, V. H. 2001. *Basic Biomechanics of the Musculoskeletal System,* Lippincott Williams & Wilkins.

Nuzzo, S., Meneghini, C., Braillon, P., Bouvier, R., Mobilio, S. & Peyrin, F. 2003. Microarchitectural and Physical Changes During Fetal Growth in Human Vertebral Bone. *Journal of Bone and Mineral Research,* 18**,** 760-768.

O'Rahilly, R. & Gardner, E. 1978. The embryology of movable joints. *The Joints and Synovial Fluid,* 1**,** 105-176.

O'Rahilly, R., Muller, F. & Meyer, D. B. 1980. The human vertebral column at the end of the embryonic period proper. 1. The column as a whole. *Journal of Anatomy,* 131**,** 565-75.

O'Rahilly, R., Muller, F. & Meyer, D. B. 1990. The human vertebral column at the end of the embryonic period proper. 4. The sacrococcygeal region. *Journal of Anatomy,* 168**,** 95-111.

O'Rahilly, R. 1957. The development of joints. *The Irish Journal of Medical Science,* 32**,** 456-461.

Odgaard, A. 1997. Three-dimensional methods for quantification of cancellous bone architecture. *Bone,* 20**,** 315-328.

Ogden, J. A., Conlogue, G. J., Bronson, M. L. & Jensen, P. S. 1979. Radiology of postnatal skeletal development. II. The manubrium and sternum. *Skeletal Radiol,* 4**,** 189-95.

Olsen, B. R., Reginato, A. M. & Wang, W. 2000. Bone development. *Annual Review of Cell and Developmental Biology,* 16**,** 191-220.

Olson, T. R. 1996. *Adam Student Atlas of Anatomy,* Lippincott Williams & Wilkins.

Olszta, M. J., Cheng, X., Jee, S. S., Kumar, R., Kim, Y.-Y., Kaufman, M. J., Douglas, E. P. & Gower, L. B. 2007. Bone structure and formation: A new perspective. *Materials Science and Engineering: R: Reports,* 58**,** 77-116.

Onyekwelu, I., Goldring, M. B. & Hidaka, C. 2009. Chondrogenesis, joint formation, and articular cartilage regeneration. *Journal of Cellular Biochemistry,* 107**,** 383-392.

Ortega, N., Behonick, D. J. & Werb, Z. 2004. Matrix remodeling during endochondral ossification. *Trends in Cell Biology,* 14**,** 86-93.

Pal, G. P. 1989. Weight transmission through the sacrum in man. *Journal of Anatomy,* 162**,** 9-17.

Pal, G. P. & Routal, R. V. 1987. Transmission of weight through the lower thoracic and lumbar regions of the vertebral column in man. *Journal of Anatomy,* 152**,** 93-105.

Palastanga, N. & Soames, R. 2012. *Anatomy and Human Movement,Structure and function,* Churchill Livingstone.

Papadimitriou, A. & Chrousos, G. P. 2005. Reconsidering the sex differences in the incidence of pubertal disorders. *Hormones and Metabolism Research,* 37**,** 708-10.

Paquin, J. D., Rest, M. V. D., Marie, P. J., Mort, J. S., Pidoux, I., Robin Poole, A. & Roughley, P. J. 1983. Biochemical and morphologic studies of cartilage from the adult human sacroiliac joint. *Arthritis & Rheumatism,* 26**,** 887-895.

Parfitt, A. M., Drezner, M. K., Glorieux, F. H., Kanis, J. A., Malluche, H., Meunier, P. J., Ott, S. M. & Recker, R. R. 1987. Bone histomorphometry: standardization of nomenclature, symbols, and units: report of the asbmr histomorphometry nomenclature committee. *Journal of Bone and Mineral Research,* 2**,** 595-610.

Parfitt, A. M., Mathews, C. H., Villanueva, A. R., Kleerekoper, M., Frame, B. & Rao, D. S. 1983. Relationships between surface, volume, and thickness of iliac trabecular bone in aging and in osteoporosis. Implications for the microanatomic and cellular mechanisms of bone loss. *Journal of Clinical Investigation,* 72**,** 1396-409.

Parfitt, A. M., Travers, R., Rauch, F. & Glorieux, F. H. 2000. Structural and cellular changes during bone growth in healthy children. *Bone,* 27**,** 487-494.

Parkinson, I. H., Badiei, A. & Fazzalari, N. L. 2008. Variation in segmentation of bone from micro-CT imaging: implications for quantitative morphometric analysis. *Australasian Physics and Engineering Science in Medicine,* 31**,** 160-4.

Pearson, O. M. & Lieberman, D. E. 2004. The aging of Wolff's "law": Ontogeny and responses to mechanical loading in cortical bone. *American Journal of Physical Anthropology,* 125**,** 63-99.

Pel, J. J. M., Spoor, C. W., Pool-Goudzwaard, A. L., Hoek Van Dijke, G. A. & Snijders, C. J. 2008. Biomechanical Analysis of Reducing Sacroiliac Joint Shear Load by Optimization of Pelvic Muscle and Ligament Forces. *Annals of Biomedical Engineering,* 36**,** 415-424.

Peretz, A. M., Hipp, J. A. & Heggeness, M. H. 1998. The Internal Bony Architecture of the Sacrum. *Spine,* 23**,** 971-974.

Phillips, A. T., Pankaj, P., Howie, C.R., Usmani, A.S. & Simpson, A.H. 2007. Finite element modeling of the pelvis: inclusion of muscular and ligamentous boundary conditions. *Medical Engineering and Physics*, 29 (7), 739–748

Pool-Goudzwaard, A., Hoek Van Dijke, G., Mulder, P., Spoor, C., Snijders, C. & Stoeckart, R. 2003. The iliolumbar ligament: its influence on stability of the sacroiliac joint. *Clinical Biomechanics,* 18**,** 99-105.

Pool-Goudzwaard, A. L., Kleinrensink, G. J., Snijders, C. J., Entius, C. & Stoeckart, R. 2000. The sacroiliac part of the iliolumbar ligament. *Journal of Anatomy,* 199**,** 457-463.

Ratib, O. & Rosset, A. 2006. Open-source software in medical imaging: development of OsiriX. *International Journal of Computer Assisted Radiology and Surgery,* 1**,** 187-196.

Reissis, D. & Abel, R. L. 2012. Development of fetal trabecular micro-architecture in the humerus and femur. *Journal of Anatomy,* 220**,** 496-503.

Rho, J.-Y., Kuhn-Spearing, L. & Zioupos, P. 1998. Mechanical properties and the hierarchical structure of bone. *Medical Engineering & Physics,* 20**,** 92-102.

Richardson, C. A., Snijders, C. J., Hides, J. A., Damen, L., Pas, M. S. & Storm, J. 2002. The relation between the transversus abdominis muscles, sacroiliac joint mechanics, and low back pain. *Spine,* 27**,** 399-405.

Riddle, D. L. & Freburger, J. K. 2002. Evaluation of the presence of sacroiliac joint region dysfunction using a combination of tests: a multicenter intertester reliability study. *Physical Therapy,* 82**,** 772-781.

Rissech, C. & Malgosa, A. 2005. Ilium growth study: applicability in sex and age diagnosis. *Forensic Science International,* 147**,** 165-174.

Robling, A. G., Hinant, F. M., Burr, D. B. & Turner, C. H. 2002. Improved bone structure and strength after long-term mechanical loading is greatest if loading is separated into short bouts. *Journal of Bone and Mineral Research,* 17**,** 1545-1554.

Rogol, A. D., Clark, P. A. & Roemmich, J. N. 2000. Growth and pubertal development in children and adolescents: effects of diet and physical activity. *The American Journal of Clinical Nutrition,* 72**,** 521s-528s.

Rosset, A., Spadola, L. & Ratib, O. 2004. OsiriX: an open-source software for navigating in multidimensional DICOM images. *Journal of Digital Imaging,* 17**,** 205-216.

Rubin, C. & Lanyon, L. 1985. Regulation of bone mass by mechanical strain magnitude. *Calcified Tissue International,* 37**,** 411-417.

Rüegsegger, P., Koller, B. & Müller, R. 1996. A microtomographic system for the nondestructive evaluation of bone architecture. *Calcified Tissue International,* 58**,** 24-29.

Ruff, C., Holt, B. & Trinkaus, E. 2006. Who's afraid of the big bad Wolff?: "Wolff's law" and bone functional adaptation. *American Journal of Physical Anthropology,* 129**,** 484-498.

Ryan, T. M. & Krovitz, G. E. 2006. Trabecular bone ontogeny in the human proximal femur. *Journal of Human Evolution,* 51**,** 591-602.

Sadler, T. T. W. 2010. *Langman's Medical Embryology,* Wolters Kluwer Health/Lippincott William & Wilkins.

Saga, Y. & Takeda, H. 2001. The making of the somite: molecular events in vertebrate segmentation. *Nature Reviews Genetics,* 2**,** 835-845.

Salsabili, N. & Hogg, D. A. 1991. Development of the human sacroiliac joint. *Clinical Anatomy,* 4**,** 99-108.

Salsabili, N., Valojerdy, M. R. & Hogg, D. A. 1995. Variations in thickness of articular cartilage in the human sacroiliac joint. *Clinical Anatomy,* 8**,** 388-390.

Sashin, D. 1930. A critical analysis of the anatomy and the pathologic changes of the sacro-iliac joints. *The Journal of Bone & Joint Surgery,* 12**,** 891-910.

Scherf, H. & Tilgner, R. 2009. A new high-resolution computed tomography (CT) segmentation method for trabecular bone architectural analysis. *American Journal of Physical Anthropology,* 140**,** 39-51.

Scheuer, L. & Black, S. 2000. *Developmental Juvenile Osteology,* Elsevier Science.

Schott, J. M. & Rossor, M. N. 2003. The grasp and other primitive reflexes. *Journal of Neurology, Neurosurgery & Psychiatry,* 74**,** 558-560.

Schunke, G. B. 1938. The anatomy and development of the sacro-iliac joint in man. *The Anatomical Record,* 72**,** 313-331.

Schutkowski, H. 1993. Sex determination of infant and juvenile skeletons: I. Morphognostic features. *American Journal of Physical Anthropology,* 90**,** 199-205.

Schwarzer, A. C., Aprill, C. N. & Bogduk, N. 1995. The sacroiliac joint in chronic low back pain. *Spine,* 20**,** 31-37.

Seeman, E. 2009. Bone modeling and remodeling. *Critical Reviews in Eukaryotic Gene Expression,* 19**,** 219-33.

Sekine, K., Ohuchi, H., Fujiwara, M., Yamasaki, M., Yoshizawa, T., Sato, T., Yagishita, N., Matsui, D., Koga, Y., Itoh, N. & Kato, S. 1999. Fgf10 is essential for limb and lung formation. *Nature Genetics,* 21**,** 138-141.

Shaw, C. N. & Ryan, T. M. 2012. Does skeletal anatomy reflect adaptation to locomotor patterns? cortical and trabecular architecture in human and nonhuman anthropoids. *American Journal of Physical Anthropology,* 147**,** 187-200.

Sherwood, L. 2010. *Fundamentals of Physiology,* Brooks/Cole, Cengage Learning.

Sinclair, D. & Dangerfield, P. 1998. *Human Growth after Birth,* Oxford, Oxford University Press.

Sinnatamby, C. S. 2006. *Last's Anatomy: Regional and Applied,* Churchill Livingstone.

Skedros, J. G. & Baucom, S. L. 2007. Mathematical analysis of trabecular 'trajectories' in apparent trajectorial structures: The unfortunate historical emphasis on the human proximal femur. *Journal of Theoretical Biology,* 244**,** 15-45.

Skedros JG, Sorenson SM, Hunt KJ, Holyoak JD. 2007. Ontogenetic structural and material variations in ovine calcanei: a model for interpreting bone adaptation. *The Anatomical Record,* 290, 284-300.

Slyper, A. H. 2006. The pubertal timing controversy in the USA, and a review of possible causative factors for the advance in timing of onset of puberty. *Clinical Endocrinology,* 65**,** 1-8.

Smith, S. A., Abitbol, J.-J., Carlson, G. D., Anderson, D. R., Taggart, K. W. & Garfin, S. R. 1993. The effects of depth of penetration, screw orientation, and bone density on sacral screw fixation. *Spine,* 18**,** 1006-1010.

Snell, R. S. 2008. *Clinical Anatomy by Regions,* Lippincott Williams & Wilkins.

Snijders, C. J., Ribbers, M. T. L. M., De Bakker, H. V., Stoeckart, R. & Stam, H. J. 1998. EMG recordings of abdominal and back muscles in various standing postures: validation of a biomechanical model on sacroiliac joint stability. *Journal of Electromyography and Kinesiology,* 8**,** 205-214.

Snijders, C. J., Vleeming, A. & Stoeckart, R. 1993a. Transfer of lumbosacral load to iliac bones and legs: Part 1: Biomechanics of self-bracing of the sacroiliac joints and its significance for treatment and exercise. *Clinical Biomechanics,* 8**,** 285-294.

Snijders, C. J., Vleeming, A. & Stoeckart, R. 1993b. Transfer of lumbosacral load to iliac bones and legs: Part 2: Loading of the sacroiliac joints when lifting in a stooped posture. *Clinical Biomechanics,* 8**,** 295-301.

Solonen, K. A. 1957. The sacroiliac joint in the light of anatomical, roentgenological and clinical studies. *Acta Orthopaedica Scandinavica Supplement,* 27**,** 1-127.

Sommerfeldt, D. W. & Rubin, C. T. 2001. Biology of bone and how it orchestrates the form and function of the skeleton. *European Spine Journal,* 10**,** S86-95.

Stewart, T. 1938. Accessory sacro-iliac articulations in the higher primates and their significance. *American Journal of Physical Anthropology,* 24**,** 43-59.

Strender, L.-E., Sjöblom, A., Sundell, K., Ludwig, R. & Taube, A. 1997. Interexaminer reliability in physical examination of patients with low back pain. *Spine,* 22**,** 814-820.

Sutherland, D. H., Olshen, R., Cooper, L. & Woo, S. L. 1980. The development of mature gait. *Journal of Bone and Joint Surgeryof American Volume,* 62**,** 336-53.

Sutter, R. C. 2003. Nonmetric subadult skeletal sexing traits: I. A blind test of the accuracy of eight previously proposed methods using prehistoric known-sex mummies from northern Chile. *Journal of Forensic Science,* 48**,** 927-35.

Taanila, A., Murray, G. K., Jokelainen, J., Isohanni, M. & Rantakallio, P. 2005. Infant developmental milestones: a 31-year follow-up. *Developmental Medicine & Child Neurology,* 47**,** 581-586.

Tague, R. G. 2007. Costal process of the first sacral vertebra: Sexual dimorphism and obstetrical adaptation. *American Journal of Physical Anthropology,* 132**,** 395-405.

Takeuchi, J. K., Koshiba-Takeuchi, K., Suzuki, T., Kamimura, M., Ogura, K. & Ogura, T. 2003. Tbx5 and Tbx4 trigger limb initiation through activation of the Wnt/Fgf signaling cascade. *Development,* 130**,** 2729-2739.

Tanck, E., Homminga, J., Van Lenthe, G. H. & Huiskes, R. 2001. Increase in bone volume fraction precedes architectural adaptation in growing bone. *Bone,* 28**,** 650-654.

Tanner, J., Whitehouse, R. & Cameron, N. 1983. *Assessment of Skeletal Maturity and Prediction of Adult Height*. London: Academic Press.

Tanner, J. M., Whitehouse, R., Hughes, P. & Vince, F. 1971. Effect of human growth hormone treatment for 1 to 7 years on growth of 100 children, with growth hormone deficiency, low birthweight, inherited smallness, Turner's syndrome, and other complaints. *Archives of Disease in Childhood,* 46**,** 745-782.

Tanner, J. M., Whitehouse, R. H. & Takaishi, M. 1966. Standards from birth to maturity for height, weight, height velocity, and weight velocity: British children, 1965. I. *Archives of Disease in Childhood,* 41**,** 454-71.

Thelen, E. 1981. Rhythmical behavior in infancy: An ethological perspective. *Developmental Psychology,* 17**,** 237.

Thomsen, J. S., Laib, A., Koller, B., Prohaska, S., Mosekilde, L. I. & Gowin, W. 2005. Stereological measures of trabecular bone structure: comparison of 3D micro

computed tomography with 2D histological sections in human proximal tibial bone biopsies. *Journal of Microscopy,* 218**,** 171-179.

Tickle, C. 2003. Patterning systems—from one end of the limb to the other. *Developmental Cell,* 4**,** 449-458.

Tile, M. 1988. Pelvic ring fractures: should they be fixed? *J Bone Joint Surg Br,* 70**,** 1-12.

Tortora, G. J. & Nielsen, M. 2009. *Principles Of Human Anatomy, 12th Edition*.

Trotter, M. 1940. A common anatomical variation in the sacro-iliac region. *The Journal of Bone & Joint Surgery,* 22**,** 293-299.

Trueta, J. 1963. The Role Of The Vessels In Osteogenesis. *Journal of Bone & Joint Surgery, British Volume,* 45-B**,** 402-418.

Twomey, L., Taylor, J. & Furniss, B. 1983. Age changes in the bone density and structure of the lumbar vertebral column. *Journal of Anatomy,* 136**,** 15-25.

Twomey, L. T. & Taylor, J. R. 1987. Age changes in lumbar vertebrae and intervertebral discs. *Clinical Orthopaedics and Related Research,* 224**,** 97-104.

Ulrich, D., Van Rietbergen, B., Laib, A. & Rüegsegger, P. 1999b. Load transfer analysis of the distal radius from in-vivo high-resolution CT-imaging. *Journal of Biomechanics,* 32**,** 821-828.

Ulrich, D., Van Rietbergen, B., Laib, A. & ŘUegsegger, P. 1999a. The ability of three-dimensional structural indices to reflect mechanical aspects of trabecular bone. *Bone,* 25**,** 55-60.

Valojerdy, M. R., Salsabili, N. & Hogg, D. A. 1989. Age changes in the human sacroiliac joint: Joint fusion. *Clinical Anatomy,* 2**,** 253-261.

Vleeming, A., Mooney, V. & Stoeckart, R. 2007. Preface. *In:* Andry, V., Phd, Vert, M., Md & Rob Stoeckart, P. (eds.) *Movement, Stability & Lumbopelvic Pain (Second Edition).* Edinburgh: Churchill Livingstone.

Vleeming, A., Pool-Goudzwaard, A. L., Hammudoghlu, D., Stoeckart, R., Snijders, C. J. & Mens, J. M. A. 1996. The function of the long dorsal sacroiliac ligament: its implication for understanding low back pain. *Spine,* 21**,** 556-562.

Vleeming, A., Schuenke, M. D., Masi, A. T., Carreiro, J. E., Danneels, L. & Willard, F. H. 2012. The sacroiliac joint: an overview of its anatomy, function and potential clinical implications. *Journal of Anatomy,* 221**,** 537-567.

Vleeming, A., Stoeckart, R. & Snijders, C. J. 1989. The sacrotuberous ligament: a conceptual approach to its dynamic role in stabilizing the sacroiliac joint. *Clinical Biomechanics,* 4**,** 201-203.

Vleeming, A., Vries, H. J. D., Mens, J. & Van Wingerden, J. P. 2002. Possible role of the long dorsal sacroiliac ligament in women with peripartum pelvic pain. *Acta Obstetricia et Gynecologica Scandinavica,* 81**,** 430-436.

Walker, J. M. 1992. The sacroiliac joint: a critical review. *Physical Therapy,* 72**,** 903-916.

Walker, P. L. 2005. Greater sciatic notch morphology: sex, age, and population differences. *American Journal of Physical Anthropology,* 127**,** 385-391.

Wang, X. & Puram, S. 2004. The Toughness of Cortical Bone and Its Relationship with Age. *Annals of Biomedical Engineering,* 32**,** 123-135.

Warden, S. J., Hurst, J. A., Sanders, M. S., Turner, C. H., Burr, D. B. & Li, J. 2005. Bone adaptation to a mechanical loading program significantly increases skeletal fatigue resistance. *Journal of Bone and Mineral Research,* 20**,** 809-816.

Weaver, D. S. 1980. Sex differences in the ilia of a known sex and age sample of fetal and infant skeletons. *American Journal of Physical Anthropology,* 52**,** 191-195.

Weise, M., De-Levi, S., Barnes, K. M., Gafni, R. I., Abad, V. & Baron, J. 2001. Effects of estrogen on growth plate senescence and epiphyseal fusion. *Proceedings of the National Academy of Sciences,* 98**,** 6871-6876.

Weisl, H. 1954. The ligaments of the sacro-iliac joint examined with particular reference to their function. *Cells Tissues Organs,* 20**,** 201-213.

Wellik, D. M. 2007. Hox patterning of the vertebrate axial skeleton. *Developmental Dynamics,* 236**,** 2454-2463.

Whelan, M. A. & Gold, R. P. 1982. Computed tomography of the sacrum: 1. normal anatomy. *AJR American Journal of Roentgenology,* 139**,** 1183-90.

White, T. D. & Folkens, P. A. 2005. *The Human Bone Manual*, Elsevier Science.

Whitley, A. S., Sloane, C., Hoadley, G. & Moore, A. D. 2005. *Clark's Positioning in Radiography 12Ed*, Taylor & Francis.

Widmer, K. H., Zurfluh, B. & Morscher, E. W. 2002. Load transfer and fixation mode of press-fit acetabular sockets. *The Journal of Arthroplasty,* 17**,** 926-935.

Williams, P. & Warwick, R. 1980. The sacroiliac joint. *Gray's Anatomy, 36th ed. Edinburgh: Churchill-Livingstone***,** 473-475.

Wingerden, J. P., Vleeming, A., Buyruk, H. M. & Raissadat, K. 2004. Stabilization of the sacroiliac joint in vivo: verification of muscular contribution to force closure of the pelvis. *European Spine Journal,* 13**,** 199-205.

Wu, L. P., Li, Y. K., Li, Y. M., Zhang, Y. Q. & Zhong, S. Z. 2009. Variable morphology of the sacrum in a Chinese population. *Clinical Anatomy,* 22**,** 619-626.

Wurff, V. D. P., Hagmeijer, R. H. M. & Meyne, W. 2000. Clinical tests of the sacroiliac joint: A systematic methodological review. Part 1: Reliability. *Manual Therapy,* 5**,** 30-36.

Xu, R., Ebraheim, N. A., Yeasting, R. A., Wong, F. Y. & Jackson, W. T. 1995. Morphometric evaluation of the first sacral vertebra and the projection of its pedicle on the posterior aspect of the sacrum. *Spine,* 20**,** 936-939.

Young, J. W., Burgess, A. R., Brumback, R. J. & Poka, A. 1986. Pelvic fractures: value of plain radiography in early assessment and management. *Radiology,* 160**,** 445-451.

Zelle, B. A., Gruen, G. S., Hunt, T. & Speth, S. R. 2004. Sacral fractures with neurological injury: is early decompression beneficial? *International Orthopaedics,* 28**,** 244-251.

Zheng, N., Watson, L. G. & Yong-Hing, K. 1997. Biomechanical modelling of the human sacroiliac joint. *Medical and Biological Engineering and Computing,* 35**,** 77-82.

Zheng, Y., Lu, W. W., Zhu, Q., Qin, L., Zhong, S. & Leong, J. C. 2000. Variation in bone mineral density of the sacrum in young adults and its significance for sacral fixation. *Spine,* 25**,** 353-357.

APPENDIX 1

Full raw dataset for juvenile sacra six trabecular parameters.

			VOI																									
No.	Specimen	Age	1s	1i	2s	2i	3s	3i	4s	4i	5s	5i	6s	6i	7s	7i	8s	8i	9s	9i	10s	10i	11s	11i	12s	12i	13s	13i	14s	14i
1	SC-262	neonate	22.7658	39.5685	54.2797	58.2833	37.3315	34.1393	42.2725	50.9582	37.4775	37.9197	24.1044	37.9368	40.61	40.0554	49.5344	38.8206	35.0774	38.0924	50.1323	51.9068	42.3495	50.6814	47.4539	47.8388	38.7478	48.7316	37.5032	44.3794
2	SC-021	5 months																					28.4459	29.4191	24.4632	27.8292	29.7989	32.1107	29.8761	31.3897
3	SC-023	1 year	32.44	23.5724	45.1702	31.9038	26.208	20.3454	46.4351	41.734	22.0548	24.6455	22.1741	29.2577	37.184	38.8651	30.3756	36.9831	24.9977	13.1357	45.7184	46.2766	43.138	39.4055	33.7736	24.6246	36.3623	33.0005	35.3509	34.4803
4	SC-067	1 yr 2/12	28.9041	24.2964	37.5785	33.3569	27.0611	22.181	33.9215	34.4938	18.6035	25.9517	17.4922	25.4581	32.9666	37.0196	26.8273	31.4229	29.7753	34.435	46.3011	50.26	36.7081	28.9158	30.5434	26.2923	34.8151	33.7518	32.7234	30.4633
5	SC-068	1 yr 3/12	40.6054	36.1029	44.9683	43.5524	28.4477	22.9006	32.2208	38.8234	13.2189	3.93761	15.3755	18.2956	28.3999	33.7669	20.5523	17.5548	22.0027	21.7148	54.5261	48.1611	43.1298	37.7066	43.8958	42.0814	49.565	39.6963	50.2859	45.7679
6	SC-069	1 yr 3/12	43.0225	33.3717	50.1958	36.084	25.8695	19.7204	49.0959	44.1295	23.1445	19.8638	22.8299	19.3528	41.9775	46.2757	18.8244	24.0549	33.0421	46.8659	55.0854	54.6668	42.6374	42.2173	35.2504	33.3234	42.0199	43.2544	35.397	38.7203
7	SC-070	1 yr 6/12	32.8958	17.202	38.857	29.7	20.3592	16.481	36.2793	27.6821	30.6916	26.202	25.0097	14.1323	36.6572	25.9424	43.4866	16.6122	38.3124	26.4683	50.5588	40.5005	50.1535	37.7535	42.4218	20.0577	48.1105	46.0878	46.5519	37.9582
8	SC-071	1 yr 11/12	24.9949	19.0579	29.5977	25.7209	24.96	28.0963	31.8751	28.3068	12.8061	12.3461	14.6713	13.0043	26.6085	23.2134	21.0444	11.2104	24.1147	26.1197	31.2399	35.8605	30.8095	36.1846	24.4459	33.2831	26.1783	38.0221	32.6728	33.7545
9	SC-137	1.5 - 2 years	26.1063	27.2075	28.002	33.5754	20.3947	19.4317	37.5346	36.8161	12.8689	16.5575	17.8145	17.4294	39.0987	16.1536	22.5949	39.1404	25.609	28.2355	55.6477	37.0972	33.3635	27.5988	33.0004	26.355	27.3478	30.1927	41.0221	31.3502
10	SC-024	2 years	26.1076	22.0963	40.1006	35.1328	21.3873	23.9955	39.5692	38.3561													35.538	33.2142	27.7369	23.728	37.1356	36.5223	34.5942	34.9838
11	SC-073	3 years	16.0722	15.6285	34.285	31.6136	25.9096	29.8911	32.2349	37.9023			11.8539	12.1696	29.8272	38.6557			41.7458	20.9399	37.4212	40.3141	23.3812	31.9257	22.6841	27.0057	25.2265	42.2252	25.6132	34.2919
12	SC-025	3 years	33.7416	27.4717	37.3766	40.8644	20.686	17.4875	37.1563	29.7859	18.6738	17.842	25.3878	23.9544	38.3676	35.8663	32.4718	25.1494	36.1681	28.2535	38.9259	44.3211	34.0015	35.3199	25.6042	21.6695	30.6545	36.4877	31.3353	34.526
13	SC-131	3 yrs 4/12	26.9639	11.6639	31.5273	27.1449	15.2781	17.7255	29.7617	16.6546	39.9281	17.6606	9.90586	10.9295	24.3945	36.4256	50.9518	27.1392	17.2943	16.5592	30.2949	37.1872	25.6601	23.3507	23.5533	9.96691	21.6396	27.2818	29.2898	19.7362
14	SC-074	3 yrs 6/12	15.3402	23.254	16.7525	26.6374	12.5167	16.9038	15.3659	12.7261			17.4764	18.0821	17.8685	22.1398			24.7435	16.6737	37.6734	42.7608	39.1109	27.9313	39.6804	17.1417	38.8588	29.1084	37.1461	29.1643
15	SC-026	4 years	37.1693	36.3361	33.7975	37.6561	26.0684	16.6615	32.9777	26.9145	23.3189	29.228	29.6096	26.2688	32.3303	35.3654	43.8446	34.7129	41.5352	31.4594	47.5114	52.5695	56.7938	45.9139	38.9057	28.433	58.8455	43.7347	47.5403	41.0309
16	SC-010	4 years	26.0827	18.4654	36.2035	29.7445	19.6425	22.5344	40.2497	31.3184	26.154	25.4622	19.23	27.4662	31.5005	35.0708	32.5528	35.5175	30.0194	30.0446	45.7068	41.6031	32.3193	31.7547	28.202	27.7393	31.2114	33.5717	33.9988	27.6862
17	SC-027	4-5 years	28.839	23.2216	40.9192	39.3957	31.5689	29.8718	44.5441	44.5963	30.1674	19.6326	26.7626	23.7005	48.3806	36.7119	37.799	36.7119	57.8707	36.0732	60.8127	72.1532	44.9904	55.2043	34.0234	44.461	59.3898	56.5912	51.1972	47.8377
18	SC-247	4-6 years	25.6124	23.6535	42.6076	29.5596	25.8908	21.9864	31.6039	18.9431	30.5106	30.7655	18.7293	28.3093	37.4119	30.607	21.6651	22.7348	21.859	23.1283	45.9597	50.2304	36.6132	24.1691	33.7902	22.9185	49.6942	45.3915	45.2798	32.763
19	SC-076	5 years	40.0698	30.5259	43.8911	43.0157	26.6175	28.3646	41.9797	47.9736	34.6119	25.083	31.7019	23.4836	50.1926	47.4347	35.7641	52.215	39.7547	30.6303	54.5592	44.8155	45.4184	44.9942	42.2011	28.9271	42.0119	38.9926	37.603	39.2189
20	SC-288	5-6 years	41.8268	29.7022	32.8744	24.9677	20.5035	21.9434	31.5139	25.8257	33.1636	21.8261	20.3208	21.0344	36.9604	26.7586	38.6287	30.3571	23.1525	24.7183	40.7843	32.5557	31.2408	28.9142	29.1515	23.8873	33.7126	36.9158	31.8439	35.3501
21	SC-019	5-6 years	15.2891	16.9686	32.8678	17.7974	19.5566	19.3756	26.991	23.6284			20.6035	20.6011	32.9252	30.0978			24.2502	37.5843	36.3097	45.6476	37.9115	28.7934	20.8113	21.445	30.1033	34.0985	28.8025	32.8672
22	SC-001	5-8 years	18.2794	18.1658	25.6668	24.0345	17.1807	17.697	23.8738	23.9437	20.1123	19.2651	15.081	23.2402	28.418	28.1016	28.8927	30.0804	29.2483	24.8537	41.1051	39.4872	32.8965	25.3807	28.4742	25.684	35.816	39.1663	38.5766	39.7611
23	SC-077	6 years	27.5698	21.1335	38.3517	27.3971	23.0986	28.8749	36.8596	33.0221	31.8183	27.3152	35.7775	25.4874	40.5332	41.1474	56.6106	28.6349	41.3913	34.2374	50.1077	48.0137	48.3922	45.3127	35.4355	29.4498	37.3993	49.4481	43.9422	40.6626
24	SC-078	6 years	14.2718	11.9522	21.7134	18.3917	12.3299	15.5923	24.0692	21.8869	28.8145	14.1583	10.7768	18.2244	24.5672	32.0649	15.9973	19.0149	21.4488	27.9958	34.1631	35.1828	33.7172	18.4526	17.4915	18.6761	24.2087	25.9909	26.5861	26.602
25	SC-081	6-8 years	31.9462	29.7095	35.971	31.2917	27.1385	21.5261	36.215	31.2237	23.639	24.5522	20.8748	26.247	30.0872	31.8073	30.0987	38.8748	41.6386	33.3493	47.5084	44.5601	35.4655	35.2077	26.5921	28.2147	33.1265	36.9808	34.8271	35.6981
26	SC-248	6-10 years	22.8658	20.4506	31.7817	28.9012	16.2999	14.256	25.4542	26.7358	20.2496	20.4094	18.35	20.3398	27.0529	32.1978	29.3357	28.4345	29.4101	28.9948	36.5541	38.1724	35.6223	26.4541	26.328	21.5295	28.8027	29.8044	32.468	28.2776

Full raw data set for each volume of interest within each individual specimen. Bone Volume Fraction (BV/TV) %

			VOI																									
No.	Specimen	Age	1s	1i	2s	2i	3s	3i	4s	4i	5s	5i	6s	6i	7s	7i	8s	8i	9s	9i	10s	10i	11s	11i	12s	12i	13s	13i	14s	14i
1	SC-262	neonate	0.17904	0.21205	0.1928	0.18024	0.16898	0.15724	0.17025	0.17153	0.1573	0.14517	0.15515	0.16977	0.15146	0.1693	0.17258	0.16203	0.1756	0.17815	0.19183	0.19792	0.16922	0.18383	0.20259	0.19269	0.16833	0.17267	0.17947	0.18286
2	SC-021	5 months																					0.23302	0.24007	0.23624	0.22426	0.22799	0.22301	0.23656	0.22936
3	SC-023	1 year	0.37797	0.38728	0.43311	0.38764	0.46703	0.36396	0.42687	0.42022	0.33911	0.3311	0.36178	0.40313	0.41568	0.43755	0.48856	0.51201	0.46405	0.39138	0.4409	0.40278	0.44954	0.39221	0.42094	0.38583	0.39195	0.38177	0.42624	0.39531
4	SC-067	1 yr 2/12	0.30565	0.27981	0.29124	0.26043	0.24889	0.22911	0.24605	0.24748	0.2148	0.21145	0.21605	0.22357	0.24592	0.2452	0.24916	0.23929	0.29971	0.26838	0.28933	0.29827	0.28557	0.25819	0.26224	0.23659	0.27356	0.25152	0.26706	0.2572
5	SC-068	1 yr 3/12	0.25756	0.27268	0.27809	0.29806	0.2425	0.22931	0.23268	0.24964	0.16473	0.14309	0.21442	0.23408	0.23679	0.25801	0.19165	0.19315	0.22824	0.24465	0.27905	0.25045	0.28839	0.28718	0.29785	0.28932	0.31438	0.27293	0.31784	0.29584
6	SC-069	1 yr 3/12	0.49997	0.44161	0.36986	0.32247	0.34845	0.31904	0.37213	0.37858	0.2453	0.23749	0.31475	0.3011	0.31757	0.33686	0.22628	0.22724	0.29472	0.3536	0.37961	0.34057	0.37157	0.34877	0.39003	0.36862	0.3571	0.36599	0.37546	0.43147
7	SC-070	1 yr 6/12	0.24184	0.2039	0.22089	0.2031	0.18701	0.18476	0.21255	0.18654	0.17681	0.19876	0.19764	0.1812	0.22675	0.19283	0.19561	0.1723	0.23892	0.23647	0.24431	0.22306	0.25652	0.23993	0.26621	0.21439	0.26721	0.24563	0.27879	0.24409
8	SC-071	1 yr 11/12	0.29442	0.2596	0.25259	0.24777	0.24081	0.23356	0.25321	0.23983	0.1622	0.18699	0.21619	0.22191	0.26648	0.24644	0.20644	0.1918	0.24255	0.25739	0.23856	0.29365	0.2721	0.28122	0.27055	0.29807	0.25033	0.28579	0.2818	0.28594
9	SC-137	1.5 - 2 years	0.31868	0.30998	0.2726	0.3157	0.28234	0.26769	0.2925	0.31495	0.27893	0.26229	0.30153	0.30115	0.35392	0.27564	0.37223	0.3898	0.38557	0.34956	0.40944	0.31226	0.29825	0.29692	0.32491	0.29455	0.29938	0.29938	0.59643	0.347
10	SC-024	2 years	0.32793	0.34059	0.35766	0.33445	0.31456	0.30147	0.36838	0.3718													0.34407	0.33133	0.33752	0.32215	0.39337	0.31824	0.37672	0.36692
11	SC-073	3 years	0.34173	0.36413	0.33891	0.32858	0.36559	0.46193	0.41342	0.38405			0.29941	0.31522	0.34025	0.38947			0.41655	0.38003	0.36919	0.39507	0.33172	0.33077	0.35557	0.3629	0.33902	0.37235	0.35057	0.36472
12	SC-025	3 years	0.44682	0.45272	0.37674	0.41585	0.39075	0.34587	0.38788	0.37416	0.35802	0.35328	0.36968	0.3861	0.44478	0.44489	0.4578	0.44112	0.44908	0.45235	0.41632	0.42071	0.41447	0.42072	0.38731	0.38625	0.38149	0.41821	0.41178	0.44604
13	SC-131	3 yrs 4/12	0.38627	0.28809	0.35048	0.35871	0.34643	0.29546	0.34206	0.33198	0.33589	0.34398	0.36633	0.34609	0.37268	0.36286	0.33052	0.3129	0.35953	0.38092	0.41092	0.38507	0.42992	0.43681	0.37816	0.31818	0.32569	0.31647	0.36642	0.35803
14	SC-074	3 yrs 6/12	0.4516	0.48058	0.3656	0.46991	0.44291	0.42979	0.36975	0.34016			0.4004	0.47451	0.37003	0.42146			0.39736	0.40152	0.47214	0.63481	0.43702	0.42034	0.49381	0.36634	0.49336	0.41377	0.46685	0.45837
15	SC-026	4 years	0.37817	0.38156	0.36299	0.43745	0.32483	0.30553	0.34789	0.35567	0.29746	0.33595	0.35305	0.35054	0.38600	0.50538	0.34389	0.36515	0.39058	0.38626	0.39085	0.5812	0.44591	0.37041	0.41607	0.32915	0.48421	0.37104	0.42529	0.3979
16	SC-010	4 years	0.29304	0.2893	0.28141	0.27419	0.23757	0.24368	0.28496	0.25691	0.25817	0.2322	0.26678	0.27127	0.30938	0.28566	0.29072	0.27683	0.36312	0.3088	0.33995	0.2966	0.25153	0.25063	0.2711	0.23316	0.24964	0.23469	0.26967	0.25082
17	SC-027	4-5 years	0.45054	0.38718	0.42972	0.44235	0.43479	0.42245	0.4515	0.44893	0.3165	0.28605	0.34819	0.347	0.59049	0.43393	0.29895	0.43393	0.47174	0.40897	0.53537	0.55466	0.44013	0.50333	0.39855	0.46211	0.5179	0.47469	0.50168	0.46829
18	SC-247	4-6 years	0.36021	0.33147	0.3736	0.34328	0.35957	0.32942	0.37018	0.29973	0.36842	0.32593	0.31007	0.37147	0.37186	0.37679	0.31627	0.3636	0.35132	0.35684	0.40418	0.43276	0.3551	0.31657	0.43654	0.32823	0.43173	0.40799	0.44723	0.43291
19	SC-076	5 years	0.38557	0.38335	0.37925	0.37965	0.3486	0.37699	0.37694	0.42268	0.35943	0.30609	0.36405	0.34042	0.47582	0.44498	0.33358	0.45178	0.41131	0.37452	0.47788	0.45886	0.40519	0.39625	0.39821	0.34375	0.43187	0.3618	0.41722	0.40059
20	SC-288	5-6 years	0.35452	0.31729	0.29426	0.27813	0.28198	0.29591	0.28264	0.26576	0.34085	0.30786	0.29688	0.33689	0.33994	0.30645	0.33076	0.34268	0.31129	0.33828	0.36109	0.36755	0.34062	0.27835	0.31417	0.28425	0.30868	0.31833	0.30852	0.31171
21	SC-019	5-6 years	0.35591	0.36578	0.37202	0.32129	0.35543	0.37021	0.34715	0.3488			0.34796	0.36602	0.39599	0.36491			0.36507	0.44441	0.38338	0.46852	0.40369	0.34757	0.35335	0.34174	0.37776	0.37013	0.37776	0.39075
22	SC-001	5-8 years	0.48983	0.46067	0.47786	0.45953	0.52529	0.42415	0.39699	0.41786	0.42091	0.40615	0.40576	0.45341	0.46893	0.50547	0.4471	0.46273	0.49706	0.51343	0.50186	0.47295	0.44012	0.39179	0.45346	0.38923	0.44587	0.46866	0.42589	0.48518
23	SC-077	6 years	0.38069	0.369	0.36534	0.35915	0.3204	0.39382	0.33314	0.35137	0.31049	0.32632	0.34525	0.3573	0.38667	0.40062	0.39828	0.32711	0.38074	0.3697	0.40715	0.43996	0.39917	0.36139	0.34928	0.33518	0.36268	0.36814	0.40116	0.36938
24	SC-078	6 years	0.36459	0.37403	0.35312	0.38672	0.32862	0.36293	0.35702	0.3727	0.37028	0.31328	0.2944	0.36256	0.36045	0.40489	0.30453	0.31723	0.3318	0.40655	0.37046	0.4174	0.37519	0.324	0.32746	0.34072	0.35817	0.35672	0.35605	0.37179
25	SC-081	6-8 years	0.41585	0.41621	0.36501	0.38284	0.44804	0.35425	0.34599	0.3309	0.34572	0.32809	0.33842	0.36071	0.32646	0.33928	0.3892	0.46636	0.49441	0.44898	0.40916	0.45065	0.34419	0.34793	0.32653	0.31714	0.34208	0.37239	0.35258	0.36338
26	SC-248	6-10 years	0.46094	0.48005	0.42471	0.47066	0.46818	0.43254	0.42251	0.44344	0.40877	0.42322	0.42213	0.41501	0.44334	0.44926	0.44777	0.46221	0.51419	0.4911	0.46264	0.56225	0.56641	0.46034	0.44181	0.45097	0.42281	0.50401	0.46177	0.43979

Full raw data set for each volume of interest within each individual specimen. Trabecular Thickness (Tb.Th) mm

No.	Specimen	Age	VOI 1s	1i	2s	2i	3s	3i	4s	4i	5s	5i	6s	6i	7s	7i	8s	8i	9s	9i	10s	10i	11s	11i	12s	12i	13s	13i	14s	14i
1	SC-262	neonate	0.52207	0.32615	0.2013	0.17799	0.23525	0.26014	0.23527	0.20154	0.19694	0.19956	0.33561	0.23813	0.21748	0.24543	0.20093	0.28609	0.3148	0.27903	0.23041	0.232	0.23615	0.22086	0.29364	0.25915	0.26796	0.20614	0.29601	0.24025
2	SC-021	5 months																					0.53955	0.60921	0.73318	0.55444	0.58137	0.49189	0.56729	0.58625
3	SC-023	1 year	0.583	0.76661	0.54984	0.65294	0.70985	0.68286	0.48162	0.55076	0.66267	0.63135	0.73798	0.64649	0.58185	0.54884	0.55467	0.64764	1.1294	1.27006	0.48939	0.5183	0.57246	0.54163	0.69935	0.65776	0.59845	0.55852	0.6548	0.61164
4	SC-067	1 yr 2/12	0.67541	0.6338	0.48609	0.51016	0.51704	0.57608	0.46444	0.44696	0.54199	0.45948	0.6793	0.50467	0.4501	0.40607	0.49269	0.45055	0.60018	0.47736	0.37951	0.34184	0.55859	0.64536	0.56332	0.60139	0.53272	0.53587	0.58041	0.56939
5	SC-068	1 yr 3/12	0.35769	0.43093	0.34957	0.40157	0.44326	0.44627	0.38832	0.34954	0.37101	0.49342	0.50339	0.55572	0.39239	0.38097	0.38453	0.40036	0.45587	0.49481	0.27000	0.28231	0.38392	0.50439	0.40429	0.40741	0.34152	0.38498	0.38095	0.39163
6	SC-069	1 yr 3/12	0.60009	0.77967	0.44217	0.45307	0.68779	0.72141	0.40549	0.52309	0.41548	0.47418	0.58952	0.61949	0.3654	0.34881	0.44429	0.40421	0.42163	0.40754	0.31038	0.30632	0.51496	0.52573	0.61536	0.71595	0.54681	0.53526	0.70998	0.67549
7	SC-070	1 yr 6/12	0.35534	0.49922	0.30339	0.36805	0.38022	0.40567	0.30874	0.33886	0.2667	0.33431	0.36469	0.49576	0.2974	0.35366	0.25842	0.39299	0.35944	0.40904	0.2641	0.27277	0.28583	0.34479	0.35155	0.47689	0.30494	0.29482	0.35777	0.35827
8	SC-071	1 yr 11/12	0.62758	0.50919	0.44366	0.48385	0.41526	0.40322	0.40967	0.40489	0.3999	0.41333	0.435	0.54586	0.42129	0.44353	0.37169	0.45671	0.41093	0.47035	0.38796	0.41416	0.45696	0.47103	0.55314	0.46524	0.46217	0.40005	0.48037	0.48085
9	SC-137	1.5 - 2 years	0.56656	0.57172	0.50012	0.6545	0.56887	0.56467	0.41988	0.45288	0.7051	0.56341	0.65542	0.64346	0.49657	0.60758	0.77336	0.51941	0.7019	0.61898	0.34288	0.40877	0.49265	0.57355	0.62674	0.53852	0.56739	0.54376	0.58818	0.57085
10	SC-024	2 years	0.74924	0.8443	0.49944	0.55314	0.60778	0.58595	0.47924	0.50387													0.52777	0.57945	0.68648	0.71425	0.56398	0.49703	0.67677	0.54475
11	SC-073	3 years	0.89617	1.084	0.51823	0.44917	0.66683	0.74872	0.60112	0.48063			0.74622	0.84392	0.53486	0.48371			0.48151	0.95475	0.46498	0.52911	0.56672	0.50401	0.86206	0.63868	0.61959	0.48595	0.67374	0.58941
12	SC-025	3 years	0.67341	0.76211	0.52613	0.62799	0.74456	0.79237	0.53394	0.65024	0.71947	0.68046	0.67122	0.68868	0.52975	0.57115	0.71061	0.74984	0.67192	0.93103	0.54243	0.50693	0.64557	0.75686	0.91421	0.98188	0.68401	0.59483	0.82616	0.68713
13	SC-131	3 yrs 4/12	0.61821	0.8288	0.58889	0.64438	0.74808	0.70298	0.53068	0.74028	0.43628	0.86716	1.05936	1.31955	0.5989	0.48415	0.36996	0.53023	1.1433	1.11403	0.61755	0.7186	0.66054	0.67735	0.84902	0.82548	0.6175	0.48278	0.62871	0.69107
14	SC-074	3 yrs 6/12	1.1024	0.86573	0.93353	0.8016	1.10798	0.8543	0.85208	0.95289			0.79201	0.91053	0.73392	0.77126			0.81409	0.88756	0.64595	0.7286	0.58487	0.67783	0.76906	0.82626	0.63428	0.67129	0.71724	0.79988
15	SC-026	4 years	0.54426	0.6028	0.59462	0.7403	0.58112	0.72325	0.54623	0.62762	0.49017	0.44029	0.65227	0.7015	0.61500	0.88004	0.40623	0.46926	0.5226	0.61021	0.50698	0.6188	0.46667	0.45864	0.77305	0.65024	0.49054	0.47698	0.63539	0.59786
16	SC-010	4 years	0.76501	0.9975	0.50002	0.71954	0.5905	0.62463	0.44256	0.51031	0.60096	0.50398	0.82475	0.5679	0.53993	0.46886	0.54795	0.43283	0.76222	0.66291	0.45814	0.43832	0.59677	0.63555	0.87845	0.58455	0.56065	0.49424	0.62012	0.74758
17	SC-027	4-5 years	0.88001	0.85985	0.56266	0.73416	0.70855	0.77084	0.52411	0.57552	0.53711	0.52979	0.71924	0.82205	0.57037	0.64168	0.42723	0.64168	0.44787	0.59909	0.45987	0.33797	0.54555	0.59793	0.79157	0.70132	0.51381	0.49819	0.67766	0.63276
18	SC-247	4-6 years	0.66642	0.66286	0.53588	0.60431	0.58038	0.55726	0.56712	0.61323	0.56809	0.508	0.67422	0.75207	0.48845	0.6849	0.59528	0.63986	0.64367	0.63935	0.45227	0.41846	0.49737	0.54559	1.0317	0.6677	0.51343	0.45708	0.66215	0.80517
19	SC-076	5 years	0.56354	0.68618	0.52898	0.5334	0.63077	0.61682	0.51832	0.48865	0.50175	0.56367	0.62348	0.79281	0.52236	0.50813	0.49425	0.45137	0.59241	0.685	0.44755	0.50102	0.59432	0.577	0.64277	0.69483	0.64086	0.53421	0.87036	0.67402
20	SC-288	5-6 years	0.44484	0.60005	0.51286	0.54928	0.55066	0.60345	0.495	0.50135	0.55365	0.8738	0.75762	0.66134	0.49516	0.53513	0.44881	0.59253	0.74377	0.9822	0.44638	0.46236	0.54288	0.53872	0.64807	0.66488	0.5337	0.4728	0.7058	0.57379
21	SC-019	5-6 years	1.0013	0.90878	0.62715	0.79993	0.82187	0.88585	0.62337	0.84575			0.79956	0.84444	0.69461	0.71951			0.6345	0.60539	0.57551	0.48484	0.57808	0.64661	0.90128	0.89058	0.64711	0.57049	0.73043	0.6833
22	SC-001	5-8 years	1.16549	1.37403	1.01177	1.11222	1.25149	1.15206	0.83428	0.97732	0.78925	0.79751	1.17013	0.98686	0.97757	1.01643	0.68809	0.679	0.90545	1.07921	0.69126	0.74022	0.75953	0.78409	0.94168	0.74474	0.70996	0.6839	0.73247	0.76652
23	SC-077	6 years	0.74233	1.16568	0.55294	0.93258	0.72969	0.72338	0.51507	0.69479	0.47406	0.53097	0.58064	0.84509	0.55042	0.58241	0.37604	0.46998	0.4692	0.53974	0.50294	0.56697	0.5008	0.51054	0.62836	0.7197	0.54922	0.47733	0.71991	0.58509
24	SC-078	6 years	1.04462	1.47685	0.77348	0.91446	0.92245	1.09642	0.76644	1.00676	0.63916	0.75402	0.92569	0.95556	0.69233	0.73154	0.66406	0.65043	0.67742	0.67917	0.57555	0.66236	0.62515	0.84353	1.03153	0.80992	0.69354	0.67061	0.73135	0.73529
25	SC-081	6-8 years	0.72942	0.79775	0.64302	0.77263	0.74145	0.7987	0.58624	0.63622	0.5656	0.59091	0.748	0.7277	0.61338	0.59227	0.54057	0.50349	0.6132	0.71404	0.51428	0.49159	0.60486	0.64708	0.80137	0.66419	0.68564	0.63468	0.67671	0.64732
26	SC-248	6-10 years	0.83428	1.1897	0.65434	0.87488	1.09865	1.12245	0.74203	0.75202	0.77785	0.82414	1.02287	0.96411	0.78048	0.76141	0.69957	0.76847	0.8975	0.90802	0.64717	0.71619	0.66714	0.81498	0.83032	0.82755	0.67626	0.69503	0.7842	0.73014

Full raw data set for each volume of interest within each individual specimen. Trabecular Separation (Tb.Sp) mm

			VOI																									
No.	Specimen	Age	1s	1i	2s	2i	3s	3i	4s	4i	5s	5i	6s	6i	7s	7i	8s	8i	9s	9i	10s	10i	11s	11i	12s	12i	13s	13i	14s	14i
1	SC-262	neonate	1.27152	1.86596	2.81532	3.23371	2.20923	2.17111	2.48296	2.97081	2.38255	2.61206	1.55361	2.23461	2.6812	2.36597	2.8703	2.39595	1.99754	2.13817	2.61336	2.62266	2.50259	2.75699	2.34237	2.48273	2.30191	2.82216	2.08967	2.4269
2	SC-021	5 months																					1.22074	1.22543	1.03551	1.24093	1.30701	1.43986	1.26294	1.36857
3	SC-023	1 year	0.85826	0.60867	1.04293	0.82303	0.56116	0.55901	1.08781	0.99316	0.65037	0.74435	0.61291	0.72576	0.89454	0.88824	0.62174	0.72231	0.53868	0.33563	1.03694	1.14892	0.95959	1.00471	0.80233	0.63822	0.92774	0.86441	0.82936	0.87224
4	SC-067	1 yr 2/12	0.94567	0.86832	1.29031	1.28086	1.08727	0.96813	1.37867	1.39382	0.86608	1.22735	0.80965	1.1387	1.34053	1.5098	1.07672	1.31317	0.99348	1.28306	1.6003	1.68505	1.28542	1.11993	1.16471	1.11132	1.27269	1.34189	1.22533	1.18442
5	SC-068	1 yr 3/12	1.57655	1.32402	1.61704	1.46117	1.17309	0.99866	1.38478	1.55517	0.80248	0.27519	0.71707	0.7816	1.19939	1.30872	1.07236	0.90888	0.96401	0.88758	1.95397	1.92297	1.49552	1.31302	1.47378	1.4545	1.5766	1.45445	1.58212	1.54705
6	SC-069	1 yr 3/12	0.86051	0.75568	1.35717	1.11898	0.74241	0.61812	1.31932	1.16567	0.94353	0.8364	0.72533	0.64274	1.32183	1.37374	0.83189	1.05859	1.12112	1.32538	1.45112	1.60518	1.1475	1.21046	0.90378	0.904	1.17668	1.18185	0.94277	0.8974
7	SC-070	1 yr 6/12	1.36022	0.84363	1.75913	1.46235	1.08867	0.89204	1.70684	1.48397	1.73583	1.31828	1.2654	0.77993	1.61665	1.34534	2.22313	0.96412	1.60354	1.11932	2.06942	1.81566	1.95516	1.57353	1.59353	0.93558	1.80045	1.87628	1.66977	1.55508
8	SC-071	1 yr 11/12	0.84895	0.73414	1.17179	1.03809	1.03651	1.20295	1.25885	1.18028	0.78951	0.66026	0.67864	0.58602	0.99853	0.94197	1.01938	0.58447	0.99421	1.01479	1.3095	1.22121	1.13227	1.28668	0.90355	1.1166	1.04574	1.33044	1.15942	1.18046
9	SC-137	1.5 - 2 years	0.8192	0.87773	1.02724	1.06353	0.72235	0.72591	1.28326	1.16896	0.46137	0.63126	0.59081	0.57876	1.10473	0.58604	0.60702	1.00411	0.66419	0.80774	1.35913	1.18801	1.11864	0.9295	1.01569	0.89475	0.91347	1.00851	0.68779	0.90346
10	SC-024	2 years	0.79614	0.64876	1.12121	1.05045	0.6799	0.79595	1.07413	1.03163													1.03286	1.00244	0.82179	0.73655	0.94404	1.14764	0.91831	0.95345
11	SC-073	3 years	0.47031	0.4292	1.01163	0.96212	0.7087	0.64709	0.77971	0.9869			0.3959	0.38606	0.87663	0.99251			1.00218	0.551	1.01359	1.02042	0.70486	0.96519	0.63796	0.74417	0.7441	1.13402	0.73062	0.94024
12	SC-025	3 years	0.75515	0.60681	0.99209	0.98268	0.52939	0.50561	0.95794	0.79608	0.52158	0.50504	0.68675	0.62041	0.86262	0.80618	0.7093	0.57013	0.80538	0.62459	0.93501	1.05348	0.82036	0.83952	0.66108	0.56102	0.80354	0.87247	0.76098	0.77405
13	SC-131	3 yrs 4/12	0.69805	0.40487	0.89955	0.75674	0.44101	0.59992	0.87006	0.50167	1.18872	0.51341	0.27041	0.3158	0.65457	1.00384	1.54158	0.86734	0.48102	0.43471	0.73725	0.96573	0.59686	0.53457	0.62285	0.31325	0.66442	0.86207	0.79935	0.55125
14	SC-074	3 yrs 6/12	0.33968	0.48387	0.45821	0.56686	0.2826	0.39331	0.41558	0.37412			0.43647	0.38107	0.48289	0.52532			0.6227	0.41527	0.79792	0.6736	0.89495	0.66449	0.80356	0.46791	0.78763	0.70349	0.79568	0.63626
15	SC-026	4 years	0.98286	0.95231	0.93108	0.86081	0.80253	0.54533	0.94793	0.75672	0.78393	0.87002	0.83869	0.74938	0.83757	0.69978	1.27496	0.95065	1.06342	0.81446	1.21559	0.9045	1.27365	1.23954	0.93507	0.86384	1.2153	1.1787	1.11782	1.03118
16	SC-010	4 years	0.89007	0.63829	1.2865	1.08483	0.8268	0.92476	1.41248	1.21903	1.01304	1.09657	0.72081	1.0125	1.0182	1.22772	1.11971	1.28299	0.8267	0.97295	1.34452	1.40269	1.28493	1.26698	1.04027	1.18972	1.25027	1.43049	1.26074	1.10382
17	SC-027	4-5 years	0.6401	0.59976	0.95223	0.8906	0.72607	0.7071	0.98657	0.99339	0.95316	0.68633	0.76862	0.68301	0.81932	0.84604	1.26437	0.84604	1.22675	0.88205	1.1359	1.30086	1.0222	1.09678	0.85368	0.96213	1.14675	1.19218	1.02051	1.02154
18	SC-247	4-6 years	0.71105	0.71358	1.14047	0.86109	0.72005	0.66743	0.85375	0.632	0.82815	0.94394	0.60404	0.76208	1.00606	0.81231	0.68502	0.62527	0.62219	0.64814	1.13711	1.1607	1.03107	0.76346	0.77404	0.69825	1.15106	1.11255	1.01245	0.75681
19	SC-076	5 years	1.03923	0.7963	1.15732	1.13303	0.76355	0.75241	1.1137	1.13499	0.96296	0.81946	0.87081	0.68985	1.05487	1.06599	1.07214	1.15575	0.96654	0.81786	1.1417	0.97667	1.12091	1.1355	1.05977	0.84152	0.9728	1.07775	0.90128	0.97902
20	SC-288	5-6 years	1.1828	0.94199	1.1237	0.90176	0.73287	0.74176	1.11411	0.97298	0.97454	0.71411	0.68251	0.62243	1.09299	0.87299	1.17162	0.89165	0.74287	0.73311	1.13476	0.89287	0.92165	1.03876	0.93266	0.84035	1.0902	1.15968	1.03187	1.13407
21	SC-019	5-6 years	0.43212	0.46321	0.88451	0.55391	0.55342	0.52198	0.78285	0.68419			0.59187	0.56032	0.83264	0.82154			0.66164	0.8457	0.95156	0.9743	0.94153	0.83264	0.59387	0.63287	0.80135	0.92488	0.76199	0.84121
22	SC-001	5-8 years	0.37317	0.39433	0.53712	0.52303	0.32707	0.41724	0.60137	0.57301	0.47783	0.47433	0.37167	0.51256	0.60601	0.55595	0.64622	0.65007	0.58843	0.48407	0.81906	0.83492	0.74745	0.64781	0.62793	0.65987	0.80328	0.8357	0.9058	0.81952
23	SC-077	6 years	0.72421	0.57273	1.04977	0.76283	0.72092	0.73321	1.10644	0.93982	1.02477	0.83706	1.03629	0.71333	1.04825	1.02709	1.42138	0.87539	1.08713	0.92608	1.23068	1.09132	1.21233	1.25385	1.01453	0.87862	1.03118	1.34318	1.09537	1.10082
24	SC-078	6 years	0.39145	0.31955	0.61491	0.47558	0.3752	0.42962	0.67418	0.58725	0.77818	0.45193	0.36606	0.50265	0.68157	0.79193	0.52531	0.5994	0.64644	0.68863	0.92217	0.84291	0.89868	0.56952	0.53415	0.54814	0.6759	0.7286	0.7467	0.7155
25	SC-081	6-8 years	0.76822	0.71381	0.98548	0.81735	0.60571	0.60766	1.04669	0.9436	0.68377	0.74834	0.61684	0.72765	0.92163	0.9375	0.77336	0.83357	0.84219	0.74277	1.16113	0.9888	1.03041	1.01191	0.81438	0.88966	0.96839	0.99306	0.98777	0.98239
26	SC-248	6-10 years	0.49606	0.42601	0.74831	0.61406	0.34815	0.32959	0.60245	0.60292	0.49538	0.48224	0.4347	0.49011	0.6102	0.71668	0.65516	0.61518	0.57197	0.5904	0.79012	0.67893	0.62891	0.57466	0.59592	0.4774	0.68122	0.59135	0.70312	0.64297

Full raw data set for each volume of interest within each individual specimen. Trabecular Number (Tb.N) mm^{-1}

			VOI																											
No.	Specimen	Age	1s	1i	2s	2i	3s	3i	4s	4i	5s	5i	6s	6i	7s	7i	8s	8i	9s	9i	10s	10i	11s	11i	12s	12i	13s	13i	14s	14i
1	SC-262	neonate	2.1037	1.5065	0.4454	0.5753	1.7289	1.7045	1.1966	0.7514	2.268	2.1756	2.3388	1.5885	1.5128	1.5327	1.4137	2.1985	1.714	1.6862	1.4185	1.4153	0.995	0.2341	0.1955	0.3238	1.0697	0.5313	1.1045	0.7589
2	SC-021	5 months																					1.4302	1.285	1.5023	1.3634	1.1846	1.1284	1.2208	0.9939
3	SC-023	1 year	2.0003	2.6113	1.3616	2.0076	2.5685	2.3789	1.2329	1.4577	2.3353	2.2056	2.2108	2.113	1.7162	2.0251	2.3911	2.4195	1.7789	2.2025	2.2061	1.264	1.6086	1.5311	1.7321	2.2537	1.5247	1.9381	1.5597	1.6541
4	SC-067	1 yr 2/12	1.6083	1.8534	1.2365	1.4171	1.7043	1.8049	1.3163	1.3119	2.0399	1.8403	1.8857	1.5701	1.3944	1.2328	1.8546	1.6781	1.6101	1.3103	0.813	0.771	0.9503	1.1252	1.246	1.3132	1.0077	1.0616	1.0453	1.1613
5	SC-068	1 yr 3/12	1.5558	1.4426	1.1621	1.4599	2.1531	2.2378	1.8126	1.581	2.6635	2.8992	2.5848	2.3544	2.1281	1.9446	2.3979	2.4157	2.2736	2.2167	1.2578	1.9892	1.0864	1.2293	1.2072	1.0874	0.8968	1.2155	0.731	1.0752
6	SC-069	1 yr 3/12	1.7269	1.7267	0.4593	1.7009	2.139	2.1498	0.7924	1.2379	2.3553	2.3481	2.4367	2.4105	1.7412	1.6102	2.3319	2.1497	1.8196	1.3976	1.8912	1.6134	1.0688	0.8339	1.7363	1.4692	0.6545	0.7194	1.0044	1.0472
7	SC-070	1 yr 6/12	1.8405	2.2843	1.2906	1.7947	2.3456	2.5851	1.4436	1.9916	2.0562	2.1233	1.9801	2.3925	1.7775	2.02	1.7	2.5417	1.5654	2.1052	0.879	1.7439	0.8706	1.3467	1.1482	2.1971	0.8914	0.9306	0.954	1.3058
8	SC-071	1 yr 11/12	2.022	2.4144	1.6165	2.0002	2.0596	1.8463	1.5497	1.7779	2.704	2.5573	2.5486	2.525	2.5444	2.2411	2.4694	2.6317	2.2443	1.9619	2.1283	1.9681	1.6234	1.1943	1.9282	1.556	1.8536	1.2834	1.5153	1.3788
9	SC-137	1.5 - 2 years	2.2129	1.8683	1.822	1.6996	2.3718	2.2985	1.2949	1.4896	2.5342	2.5292	2.4617	2.4663	1.3415	2.5634	2.4973	1.8976	2.3403	1.9143	1.1426	1.8861	1.4334	1.8102	1.347	1.9151	1.7683	1.6302	1.7004	1.6173
10	SC-024	2 years	1.9407	1.9917	1.3226	1.5715	2.3808	2.0473	1.5533	1.552													1.4849	1.4521	1.8289	1.9392	1.5095	1.5557	1.3101	1.5693
11	SC-073	3 years	2.5411	2.3977	1.8129	2.1641	2.3077	2.0915	2.1552	1.8659			2.7535	2.6539	2.1398	1.7697			1.7459	2.3147	1.7817	1.5837	2.2503	1.7612	1.978	2.0126	2.004	1.0329	1.9235	1.5017
12	SC-025	3 years	1.8204	2.238	1.359	1.1591	2.4467	2.3983	1.3117	1.7982	2.4401	2.5117	1.9992	2.2131	1.9148	2.0943	1.9729	2.4554	1.5993	2.1361	1.7697	1.5416	1.6093	1.286	1.8073	2.1463	1.5953	1.5244	1.3724	1.5431
13	SC-131	3 yrs 4/12	2.3076	2.7213	1.8221	2.3108	2.5873	2.428	1.9961	2.5119	1.7644	2.654	2.9796	2.4337	2.3356	1.8942	1.6444	2.2025	1.9686	2.3978	2.2949	1.6222	2.5866	2.7882	2.046	2.8971	2.4041	2.4665	1.8517	2.4273
14	SC-074	3 yrs 6/12	2.8019	2.8272	2.4665	2.614	2.9463	2.8154	2.422	2.647			2.5935	2.716	2.7647	2.3922			1.9553	2.6248	1.8015	1.6278	1.6434	2.4253	1.247	2.4621	1.8831	2.2317	1.3505	1.8492
15	SC-026	4 years	1.5951	1.6356	1.6609	1.9639	2.0348	2.3784	1.6291	2.0285	2.4182	2.3479	1.6342	1.8938	1.7729	1.6867	1.831	2.2126	1.4907	1.8711	1.2097	1.3649	0.5356	1.2818	0.8868	1.5936	0.6796	1.1751	0.4867	0.9749
16	SC-010	4 years	1.3473	1.743	1.036	0.9733	2.0813	1.8807	0.8571	1.3	1.5852	1.699	1.8501	1.5924	1.5598	1.2717	1.4571	1.2971	1.5503	1.4332	0.7318	0.8339	0.8628	0.7962	0.7568	1.1565	1.0361	0.8801	0.5797	0.9241
17	SC-027	4-5 years	1.6962	2.0704	1.2666	1.6203	1.9309	1.8868	1.1648	1.0493	2.206	2.6015	1.7692	1.7751	1.5915	1.7121	2.0314	1.7121	0.4948	1.7832	1.2179	1.2212	1.0162	0.5541	1.1175	0.6481	0.7909	0.7448	0.4596	0.58
18	SC-247	4-6 years	1.9551	2.018	0.9772	1.8454	2.193	2.2035	1.7925	2.4005	2.1116	2.0204	2.2574	1.6741	1.417	1.686	2.4079	2.465	2.3525	2.3942	0.9991	1.2291	1.4584	2.0324	1.2039	1.9735	0.7413	1.2277	0.7026	1.2555
19	SC-076	5 years	1.4894	1.6518	0.9424	0.9817	1.9992	2.0996	1.1441	0.8454	1.7259	2.0597	1.4529	1.8032	0.9719	1.0946	1.7239	1.1091	1.2392	1.8299	0.7014	1.5953	0.5215	0.7602	0.5607	1.4686	0.8607	1.3712	0.615	0.7794
20	SC-288	5-6 years	1.3261	1.6101	1.4301	2.0052	2.2408	2.1757	1.462	1.7495	1.9705	2.0158	2.011	2.2921	1.4748	1.8902	1.6326	1.7283	1.9701	1.7151	1.449	2.1037	1.5097	1.3955	1.2853	1.6135	1.1677	1.1192	1.1388	0.9935
21	SC-019	5-6 years	2.2373	2.2879	1.501	2.2459	2.1415	2.106	1.796	1.8543			2.1068	2.1069	1.6198	1.5877			2.3004	1.7247	2.042	2.2498	1.2743	1.6694	1.9684	1.931	1.7444	1.5085	1.6081	1.4184
22	SC-001	5-8 years	2.3334	2.0502	1.8502	1.8347	2.551	2.1484	1.83	1.7387	2.5564	2.5429	2.1591	1.9843	1.5604	1.842	2.209	2.1226	2.0605	2.0745	1.2042	1.3142	1.3423	1.7704	1.5372	1.7513	1.2518	1.0684	0.7948	0.8772
23	SC-077	6 years	1.7113	1.6423	0.9941	1.3688	1.7664	1.5398	1.0305	1.0118	1.9946	2.229	1.1127	1.7395	0.9783	0.973	0.937	2.3429	1.3917	1.5337	1.104	0.8773	0.5892	0.3813	0.9039	1.1821	1.1161	0.8683	0.6347	0.616
24	SC-078	6 years	2.3503	2.3548	1.9739	2.3197	2.5492	2.2608	1.8938	1.7862	2.0686	2.5691	2.5376	2.2598	1.9966	1.4914	2.5533	2.4669	2.0747	1.9238	1.4678	1.5294	1.2327	1.9236	1.9351	2.1284	2.0036	1.9274	1.6877	1.794
25	SC-081	6-8 years	1.7085	1.8898	1.1681	1.6893	2.3507	2.0603	1.1016	1.3549	2.5018	2.4373	2.1912	1.9268	1.6949	1.7007	2.4629	2.3237	2.0497	2.1242	1.2443	1.751	1.0221	1.0111	1.4011	1.4324	1.1526	0.9607	0.9817	1.0159
26	SC-248	6-10 years	2.3444	2.0887	1.7903	1.8696	2.5538	2.3843	1.9864	2.0664	2.3942	2.3334	2.2327	2.0763	1.9721	1.5138	1.957	1.94	1.9453	1.8198	1.4997	1.6972	1.8377	2.0036	1.8185	2.2895	1.8503	2.1837	1.3526	1.9202

Full raw data set for each volume of interest within each individual specimen. Structural Model Index (SMI).

			VOI																										
No.	Specimen	Age	1s	1i	2s	2i	3s	3i	4s	4i	5s	5i	6s	6i	7s	7i	8s	8i	9s	9i	10s	10i	11s	11i	12s	12i	13s	13i	14s	14i
1	SC-262	neonate	0.46964	0.57786	0.54391	0.61169	0.60731	0.76914	0.58433	0.67273	0.73194	0.53528	0.3829	0.4329	0.58809	0.55655	0.27094	0.4649	0.64571	0.59309	0.73449	0.60638	0.2962	0.38463	0.33685	0.49191	0.24267	0.43891	0.15283	0.3688
2	SC-021	5 months																					0.2824	0.27078	0.28728	0.40356	0.39975	0.42057	0.35959	0.41703
3	SC-023	1 year	0.37787	0.33205	0.55363	0.5665	0.53164	0.44014	0.71885	0.69306	0.50878	0.42008	0.40719	0.40467	0.52055	0.40883	0.7036	0.79128	0.66895	0.27721	0.77645	0.66914	0.3639	0.454	0.3815	0.52063	0.48003	0.48106	0.33617	0.43043
4	SC-067	1 yr 2/12	0.66065	0.526	0.35994	0.25048	0.52681	0.55907	0.41657	0.32335	0.27812	0.38809	0.31544	0.50383	0.45811	0.44216	0.4295	0.32577	0.54214	0.60464	0.32886	0.5163	0.17255	0.33176	0.1084	0.40067	0.30272	0.31964	0.17802	0.27766
5	SC-068	1 yr 3/12	0.58376	0.46704	0.33807	0.50518	0.57164	0.8428	0.23498	0.23832	0.8385	0.83546	0.51016	0.47000	0.37992	0.49987	0.56044	0.41869	0.92357	0.43106	0.94244	0.81206	0.28485	0.40788	0.18897	0.06203	0.36567	0.25396	0.23422	0.11155
6	SC-069	1 yr 3/12	0.46446	0.33664	0.49368	0.41733	0.57153	0.60256	0.51608	0.40502	0.47882	0.56287	0.55788	0.58302	0.55504	0.58621	0.60879	0.45044	0.8276	0.68986	0.66791	0.56847	0.20314	0.33864	0.36824	0.40504	0.30737	0.21543	0.27348	0.27971
7	SC-070	1 yr 6/12	0.80089	0.87643	0.86958	0.99623	0.71981	0.72198	0.67277	0.66499	0.60495	0.65354	0.78144	0.73019	0.79706	0.76525	0.75783	0.6922	0.98424	0.7003	0.87912	0.95894	0.68400	0.52095	0.55983	0.47333	0.61071	0.54224	0.58092	0.50955
8	SC-071	1 yr 11/12	0.28685	0.62951	0.39273	0.39054	0.30336	0.79391	0.50284	0.39027	0.48958	0.61288	0.79417	0.79991	0.50939	0.60712	0.45446	0.39895	0.89662	0.57147	0.64396	0.60301	0.35477	0.34046	0.20762	0.39916	0.33762	0.28325	0.25809	0.28951
9	SC-137	1.5 - 2 years	0.74822	0.58691	0.52079	0.59261	0.72088	0.67693	0.51493	0.41276	0.70393	0.55178	0.29566	0.41083	0.38757	0.36259	0.40633	0.33881	0.52631	0.4151	0.52259	0.3579	0.15817	0.21634	0.19808	0.32757	0.39275	0.37908	0.38625	0.37007
10	SC-024	2 years	0.64081	0.49284	0.90233	0.84697	0.96077	0.89479	0.6389	0.72556													0.4544	0.38964	0.37964	0.43475	0.43602	0.37673	0.43337	0.27042
11	SC-073	3 years	0.48741	0.6582	0.70101	0.66271	0.52134	0.68955	0.54697	0.69771			0.42564	0.43596	0.36951	0.3793			0.64145	0.70518	0.78638	0.57861	0.3192	0.17433	0.30598	0.20304	0.23949	0.31066	0.17686	0.28417
12	SC-025	3 years	0.46819	0.35228	0.42947	0.40229	0.27637	0.2982	0.44273	0.46663	0.27439	0.31969	0.40307	0.32489	0.51475	0.48128	0.24385	0.44735	0.50457	0.60732	0.85459	0.69109	0.24215	0.14116	0.20615	0.26784	0.35511	0.31959	0.17264	0.27527
13	SC-131	3 yrs 4/12	0.38395	0.58801	0.57691	0.36651	0.14451	0.39815	0.25467	0.27793	0.52736	0.68471	0.44611	0.55525	0.55818	0.53693	0.44129	0.60086	0.71697	0.55206	0.47659	0.99571	0.30961	0.13327	0.34871	0.26322	0.27684	0.19057	0.45971	0.38953
14	SC-074	3 yrs 6/12	0.5934	0.39588	0.63611	0.64742	0.8369	0.97518	0.74366	0.39347			0.72969	0.78932	0.76084	0.57268			0.82994	0.57734	0.59809	0.50856	0.60422	0.26945	0.23363	0.35408	0.22874	0.56626	0.33708	0.41792
15	SC-026	4 years	0.86496	0.70061	0.82688	0.60457	0.66495	0.50532	0.77826	0.52806	0.59812	0.61107	0.53395	0.48331	0.70869	0.51146	0.69958	0.71706	0.88215	0.59675	0.90275	0.88669	0.31704	0.28246	0.42254	0.30843	0.19959	0.50847	0.22993	0.16045
16	SC-010	4 years	0.63326	0.44175	0.29689	0.26843	0.5687	0.659	0.34662	0.23635	0.35891	0.27084	0.27328	0.335	0.47087	0.4845	0.15815	0.21307	0.49293	0.51965	0.74281	0.70739	0.16989	0.31608	0.24134	0.48845	0.40886	0.11391	0.32797	0.23808
17	SC-027	4-5 years	0.36859	0.24007	0.24468	0.39238	0.22575	0.30962	0.17971	0.31495	0.59295	0.6177	0.39559	0.6207	0.61603	0.61651	0.49894	0.61651	0.77283	0.62403	0.92069	0.87334	0.11145	0.18523	0.2599	0.35123	0.29739	0.34157	0.24872	0.23604
18	SC-247	4-6 years	0.61672	0.43595	0.41128	0.76236	0.58379	0.73554	0.21635	0.64158	0.81565	0.43179	0.4722	0.39479	0.51092	0.42667	0.73218	0.54032	0.9674	0.46838	0.6266	0.9723	0.11784	0.19896	0.24669	0.3912	0.35725	0.2137	0.23614	0.3072
19	SC-076	5 years	0.92257	0.73804	0.39807	0.6682	0.50695	0.79955	0.44241	0.6336	0.61719	0.56611	0.49937	0.39117	0.31617	0.77845	0.46515	0.70225	0.68125	0.65104	0.58004	0.74331	0.4674	0.30087	0.38178	0.30573	0.28324	0.23907	0.20799	0.39814
20	SC-288	5-6 years	0.48983	0.54001	0.47779	0.65401	0.61991	0.56799	0.59298	0.44979	0.51959	0.53192	0.48826	0.59443	0.49078	0.48608	0.51133	0.55915	0.83966	0.68932	0.99855	0.92219	0.38913	0.22974	0.4192	0.25101	0.26112	0.26818	0.29918	0.32953
21	SC-019	5-6 years	0.38575	0.25403	0.31023	0.31417	0.36909	0.33945	0.44789	0.35562			0.50238	0.46441	0.62931	0.62548			0.91285	0.79396	0.90781	0.73566	0.20108	0.18734	0.18413	0.37064	0.28143	0.27751	0.23715	0.32692
22	SC-001	5-8 years	0.85239	0.48206	0.27385	0.36978	0.77732	0.59653	0.5443	0.35501	0.45245	0.41259	0.4779	0.42326	0.62786	0.59598	0.36276	0.36469	0.77625	0.83114	0.93386	0.88233	0.28926	0.32284	0.29369	0.41114	0.47757	0.37281	0.41359	0.36782
23	SC-077	6 years	0.2527	0.30924	0.27778	0.32363	0.39981	0.30628	0.3179	0.35629	0.77275	0.94887	0.43538	0.71939	0.72003	0.56073	0.85076	0.87252	0.71572	0.46493	0.92141	0.99375	0.33616	0.22627	0.35749	0.26349	0.28197	0.17982	0.29539	0.24514
24	SC-078	6 years	0.21615	0.29364	0.27832	0.21348	0.35282	0.26912	0.38707	0.37916	0.52735	0.80375	0.35409	0.31451	0.55312	0.59982	0.489	0.55126	0.47941	0.47351	0.72882	0.93936	0.34991	0.4129	0.40614	0.44044	0.29456	0.18491	0.30593	0.22724
25	SC-081	6-8 years	0.21359	0.2058	0.30632	0.2163	0.50425	0.30972	0.39523	0.14962	0.53309	0.51699	0.35164	0.39304	0.55799	0.56382	0.50351	0.3588	0.77317	0.64851	0.63927	0.83283	0.25924	0.22535	0.18913	0.30795	0.28341	0.37069	0.22578	0.28982
26	SC-248	6-10 years	0.55907	0.5226	0.22126	0.32942	0.55142	0.35854	0.31508	0.33278	0.40241	0.44458	0.46823	0.54871	0.53777	0.7378	0.45583	0.46228	0.51296	0.50256	0.77351	0.99033	0.34784	0.17926	0.26179	0.35167	0.3656	0.34054	0.22711	0.30332

Full raw data set for each volume of interest within each individual specimen. Degree of Anisotropy (DA).

APPENDIX 2

Raw specimen data for juvenile ilia surface area measurement.

No.	Sample	Age	Au (A)	Post-Au (PA)	A + PA	Fossa (F)	Ilium (I)
1	IP	Neonate	76.24	100.23	176.47	547.42	723.89
2	NP2 R	Neonate	69.8	102.51	172.31	566.89	739.2
3	NP2 L	Neonate	76.54	103.42	179.96	589.78	769.74
4	P1 R	Neonate	74.02	85.42	159.44	542.52	701.96
5	P1 L	Neonate	77.72	87.77	165.49	597.08	762.57
6	SS2 R	4-6 months	85.23	120.66	205.89	681.84	887.73
7	SS2 L	4-6 months	86.82	125.36	212.18	677.00	889.18
8	P2	5 months	163.56	214.68	378.24	1133.72	1511.96
9	P4 R	1 year	174.55	246.42	420.97	1436.52	1857.49
10	P4 L	1 year	173.72	297.55	471.27	1458.33	1929.6
11	P5 R	2 years	267.26	393.53	660.79	1932.86	2593.65
12	P5 L	2 years	264.84	394.07	658.91	1930.49	2589.4
13	SS1 R	3-5 years	231.76	524.81	756.57	2273.89	3030.46
14	SS1 L	3-5 years	240.38	529.46	769.84	2259.39	3029.23
15	WK1 R	3 yrs 4 mnths	327.46	427.89	755.35	2511.16	3266.51
16	WK1 L	3 yrs 4 mnths	318.23	440.76	758.99	2424.76	3183.75
17	P7 R	4 years	335.25	493.6	828.85	2651.33	3480.18
18	P7 L	4 years	335.9	558.54	894.44	2602.31	3496.75
19	AET4 R	4 years	337.39	689.03	1026.43	2881.28	3907.71
20	AET4 L	4 years	351.6	679.25	1030.85	2926.44	3957.29
21	P8 R	4-5 years	290.6	544.09	834.69	2876.06	3710.75
22	P8 L	4-5 years	340.66	517.53	858.19	2924.47	3782.66
23	P9 R	6 years	402.1	580.82	982.92	3022.28	4005.2
24	P9 L	6 years	412.14	606.05	1018.19	3134.76	4152.95
25	STHB R	7 years	420.88	526.99	947.87	3628.81	4576.68
26	STHB L	7 years	425.86	600.4	1026.26	3465.62	4491.88
27	P10	8 years	506.5	701.97	1208.47	3993.51	5201.98
28	WK28 R	8 yrs 7 mnths	438.2	817.51	1255.71	3634.91	4890.62
29	WK28 L	8 yrs 7 mnths	464.34	817.7	1282.04	3637.49	4919.53
30	GS785 R	9 years	485.53	707.27	1192.80	3798.43	4991.23
31	GS785 L	9 years	491.9	719.37	1211.27	3905.12	5116.39
32	A7	10-12 years	346.27	916.77	1263.04	3515.12	4778.16
33	A8	11-13 years	429.72	892.33	1322.05	3876.82	5198.87
34	P11	11 years	532.08	756	1288.08	4170.63	5458.71
35	A6	12 years	404.54	712.28	1116.82	3221.87	4338.69
36	P12	12 years	542.38	786.84	1329.22	4546.57	5875.79
37	P13 R	12 years	607.3	1020.99	1628.29	5101.65	6729.94
38	P13 L	12 years	630.74	1059.57	1690.27	5246.05	6936.32
39	WK29 R	12 years	558.06	1273.06	1831.12	5471.67	7302.79
40	WK29 L	12 years	523.56	1248.41	1771.97	5326.05	7098.02

41	WK31 R	12 years	634.89	930.85	1565.74	6108.62	7674.36
42	WK31 L	12 years	640.67	938	1578.67	5790.18	7368.85
43	A12 R	12 years	597.88	1029.71	1627.61	4706.76	6334.37
44	A12 L	12 years	585.82	1005.29	1591.09	4206.62	5797.71
45	A13 R	12 years	590.34	1326.84	1917.18	4525.21	6442.39
46	A13 L	12 years	572.35	1068.79	1641.14	4796.72	6437.86
47	A9	11-14 years	819.69	1122.48	1942.17	5355.64	7297.81
48	A10	11-14 years	751.38	1237.36	1988.74	6085.95	8074.69
49	P14	14 years	591.58	1246.07	1837.65	6180.48	8018.13
50	A11	15 years	789.01	1602.90			
51	SC-302	15 years	768.53	1035.86			
52	A3	14-17 years	848.60	1621.81			
53	A14	14-17 years	1041.18	1926.96			
54	P15 L	17 years	1323.76	2374.68			
55	P15 R	17 years	1258.68	2072.79			
56	STHG R	Late adolescent	683.53	1477.94			
57	STHG L	Late adolescent	765.19	1694.81			
58	STHJ L	Late adolescent	756.35	1308.86			
59	STHJ R	Late adolescent	749.31	1187.84			
60	STHA L	Late adolescent	782.16	1154.02			
61	STHA R	Late adolescent	833.57	1124.95			
62	STHF L	Late adolescent	917.58	1731.86			
63	STHF R	Late adolescent	946.74	1489.9			
64	STHI R	Late adolescent	961.27	2523.42			
65	STHI L	Late adolescent	1165.41	2456.14			
66	STHD R	Late adolescent	1089.38	1701.97			
67	STHD L	Late adolescent	1332.61	1938.61			
68	STHE L	Late adolescent	1259.32	1329.44			
69	STHH L	Late adolescent	1343.05	1234			
70	SC-138 R	Late adolescent	1472.28	2028.29			
71	SC-138 L	Late adolescent	1452.89	2211.94			
72	P19 L	19 years	857.47	2438.28			
73	P19 R	19 years	799.75	2092.74			
74	P17 L	19 years	973.62	1738.74			
75	P17 R	19 years	911.22	1631.66			
76	P16 R	19 years	1025.99	2287.64			
77	P16 L	19 years	1136.92	2210.02			
78	P18 L	19 years	1226.84	1972.17			
79	P18 R	19 years	1517.65	1818.54			
80	SC-375	18-22 years	1278.68	2771.34			

APPENDIX 3

Peer reviewed publications in support of this thesis:

Yusof, N. A., Soames, R. W., Cunningham, C. A., & Black, S. M. (2013). Growth of the Human Ilium: The Anomalous Sacroiliac Junction. *The Anatomical Record* **296**, 1688-1694.

Conference presentations and abstract publications in support of this thesis:

Yusof NA, Soames RW, Black, SM, Cunningham CA (2012) Growth of the human ilium: relationship to key developmental milestones. *Clinical Anatomy* **25**, 543

Yusof N, Soames RW, Cunningham C, Black, SM (2014) The developing sacrum: a method of assessing relative bone density. *Clinical Anatomy* **27**, 273.

Yusof N, Soames RW, Cunningham C, Black, SM (2014) The developing sacrum: a new perspective on the relationship between internal architecture and weight transfer. *Clinical Anatomy* **27**, 273.